



Asphalt Research Consortium

Quarterly Technical Progress Report July 1 – September 30, 2009

October 2009

Prepared for
Federal Highway Administration
Contract No. DTFH61-07-H-00009

By
Western Research Institute
Texas A&M University
University of Wisconsin-Madison
University of Nevada-Reno
Advanced Asphalt Technologies

www.westernresearch.org
www.ARC.unr.edu

TABLE OF CONTENTS

INTRODUCTION	1
GENERAL CONSORTIUM ACTIVITIES	3
PROGRAM AREA: MOISTURE DAMAGE.....	5
Category M1: Adhesion.....	5
Category M2: Cohesion	12
Category M3: Aggregate Surface	20
Category M4: Modeling.....	30
Category M5: Moisture Damage Prediction System	36
PROGRAM AREA: FATIGUE.....	39
Category F1: Material and Mixture Properties	39
Category F2: Test Method Development.....	73
Category F3: Modeling	94
PROGRAM AREA: ENGINEERED MATERIALS.....	127
Category E1: Modeling.....	127
Category E2: Design Guidance.....	161
PROGRAM AREA: VEHICLE-PAVEMENT INTERACTION.....	187
Category VP1: Workshop	187
Category VP2: Design Guidance	187
Category VP3: Modeling	193
PROGRAM AREA: VALIDATION.....	201
Category V1: Field Validation.....	201
Category V2: Accelerated Pavement Testing	203
Category V3: R&D Validation	203
PROGRAM AREA: TECHNOLOGY DEVELOPMENT.....	215
PROGRAM AREA: TECHNOLOGY TRANSFER.....	217
Category TT1: Outreach and Databases	217

INTRODUCTION

This document is the Quarterly Report for the period of July 1 to September 30, 2009 for the Federal Highway Administration (FHWA) Contract DTFH61-07-H-00009, the Asphalt Research Consortium (ARC). The Consortium is coordinated by Western Research Institute with partners Texas A&M University, the University of Wisconsin-Madison, the University of Nevada Reno, and Advanced Asphalt Technologies.

The Quarterly Report is grouped into seven areas, Moisture Damage, Fatigue, Engineered Paving Materials, Vehicle-Pavement Interaction, Validation, Technology Development, and Technology Transfer. The format of the report is based upon the Research Work Plan that is grouped by Work Element and Subtask.

This Quarterly Report summarizes the work accomplishments, data, and analysis for the various Work Elements and Subtasks. This report is being presented in a summary form. The Quarter of July 1 to September 30, 2009 is the second quarter of the Year 3 contract year. Reviewers may want to reference the Year 3 Work Plan and perhaps the Revised Year 2 Work Plan in order to obtain background information on specific areas of research. The more detailed information about the research such as approaches to test method development, data collection, and analyses will be reported in research publications as part of the deliverables. The Year 3 Work Plan, the Revised Year 2 Work Plan, as well as many other documents including previous quarterly reports, are posted on the ARC website, www.ARC.unr.edu.

SUPPORT OF FHWA AND DOT STRATEGIC GOALS

The Asphalt Research Consortium research is responsive to the needs of asphalt engineers and technologists, state DOT's, and supports the FHWA Strategic Goals and the Asphalt Pavement Road Map. More specifically, the research reported here supports the Strategic Goals of safety, mobility, and environmental stewardship. By addressing the causes of pavement failure and thus determining methods to improve asphalt pavement durability and longevity, this research will provide the motoring public with increased safety and mobility. The research directed at improved use of recycled asphalt pavement (RAP), warm mix asphalt, and cold mix asphalt supports the Strategic Goal of environmental stewardship.

GENERAL CONSORTIUM ACTIVITIES

PROGRESS THIS QUARTER

ARC Asphalt Microstructural Modeling team members Mr. Troy Pauli, Dr. Michael Greenfield, and Dr. Linbing Wang attended and made presentations at The First International Workshop on Chemo-Mechanics of Bituminous Materials, which was held in Delft, the Netherlands in June 2009. Publication of the proceedings is anticipated and can be arranged by contacting Dr. Tom Scarpas at Delft.

ARC partners and team members participated and made presentations at the 46th Annual Petersen Asphalt Research Conference and Pavement Performance Prediction Symposium in Laramie, Wyoming, July 13 – 17, 2009.

Several ARC members attended and made presentations at the Fundamental Properties & Advanced Models, Binder, and Mix & Construction ETG meetings in San Antonio, Texas on September 15 – 18, 2009.

ARC members from Texas A&M University in collaboration with personnel from the Technological University Delft, Netherlands conducted a short course on Advanced Constitutive Modeling in College Station, Texas during the week of September 21, 2009.

WORK PLANNED FOR NEXT QUARTER

ARC members, Dr. Hussain Bahia, Dr. Elie Hajj, and Mr. Michael Harnsberger, are planning to attend the RAP Expert Task Group meeting in Seattle, Washington on December 16 & 17, 2009. ARC members may present an update on the construction of the RAP sections in Manitoba and the RAP research being conducted by the ARC.

An ARC advisory board meeting is planned for the next quarter, details to be determined. In conjunction with this meeting, it is planned to meet with AOTR's Dr. Jack Youtcheff and Mr. Eric Weaver to discuss planned contract deliverables.

PROGRAM AREA: MOISTURE DAMAGE

CATEGORY M1: ADHESION

Work Element M1a: Affinity of Asphalt to Aggregate (UWM)

Work Done This Quarter

The research group focused its efforts on development of a procedure for testing the pull-off strength of binder-aggregate systems using the PosiTest (Posi) digital adhesion tester. Preliminary relationships between the Pneumatic Adhesion Tensile Testing Instrument (PATTI) and Posi test results were established. Although the Posi device presents some difficulties in controlling the loading rate, a method proposed to improve sample preparation allows the research team to obtain more repeatable and meaningful test results that can be correlated to the properties obtained from other devices.

The Posi test evaluates the pull-off strength—commonly referred to as adhesion—of a coating system, or binder, from a substrate. The test determines the greatest perpendicular force, in tension, that a surface area can bear before a plug of material is detached from the substrate. The testing procedure follows the ASTM D 4541 (2009) standard. Materials used for this investigation are listed in table M1a.1.

Table M1a.1. Proposed materials used for the Posi tests.

Mineral Surfaces	Granite	
Binders	Two	64-22 unmodified
		CRM + 2% LSBS modified

LSBS = linear styrene-butadiene-styrene.

To control the film thickness of the binder, five plastic beads were used between the aggregate (granite) and the dolly, as shown in figure M1a.1. This procedure allows for the preparation of more consistent samples.

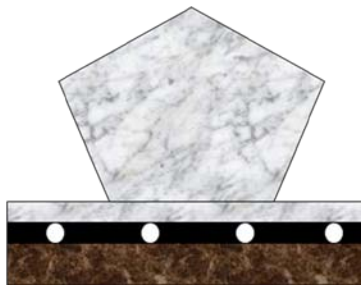


Figure M1a.1. Illustration. Sample preparation using beads to control film thickness.

The effect of loading rate and different operators on the pull-off strength obtained from the Posi test was investigated with a PG 64-22 binder on granite aggregate. Figure M1a.2 presents the probability distributions of the Posi test results for each condition (e.g., operator 1 and fast rate). Figure M1a.2 shows that there is a statistically significant difference between testing the specimens at slow (0-50 psi/sec) and fast (> 200 psi/sec) rates. On the other hand, no significant differences are observed between the results obtained from different operators.

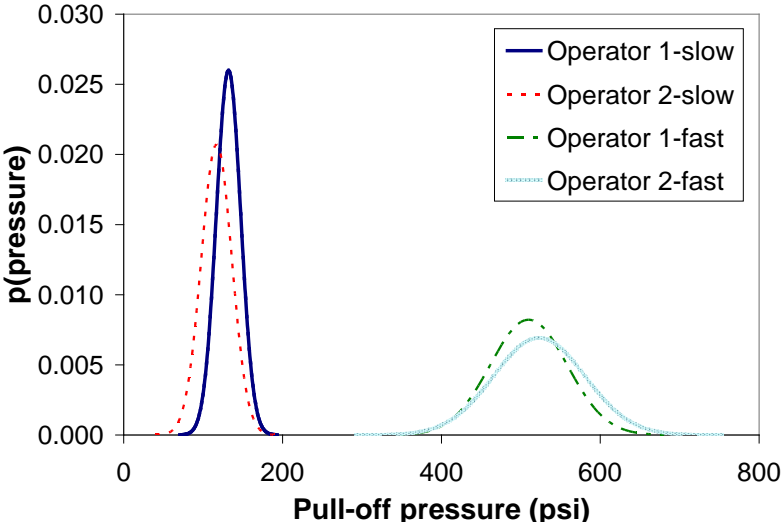


Figure M1a.2. Graph. Distributions of the Posi test results from two operators and two loading rates: slow (0-50 psi/sec) and fast (> 200 psi/sec).

After testing, it was observed that the failure surfaces of the slow and fast tests have different morphology, as shown in figure M1a.3.

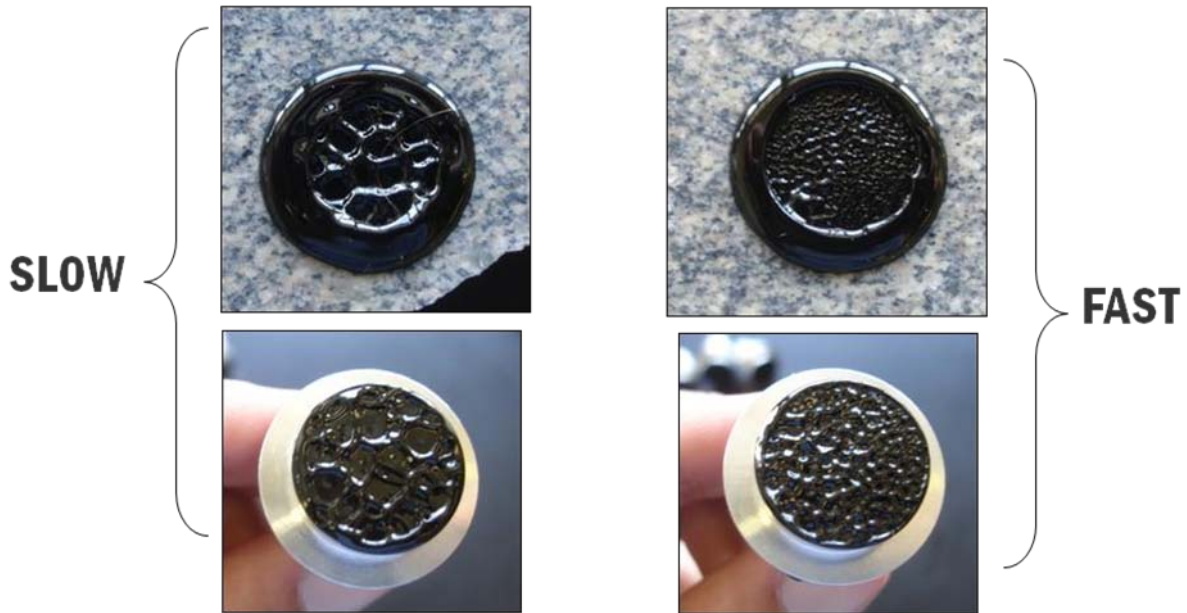


Figure M1a.3. Photographs. Illustration of the different surfaces obtained from two loading rates: slow (0-50 psi/sec) and fast (>200 psi/sec).

The average pull-off strength from the Posi device at different loading rates was compared to the corresponding pull-off strength from the modified PATTI test. Figure M1a.4 shows the probability distribution of the pull-off strength obtained from both devices. Figure M1a.4 indicates that there is a significant difference between the results obtained from these two methodologies. However, as shown in figure M1a.5, preliminary analysis indicates that Posi and PATTI test results can be correlated.

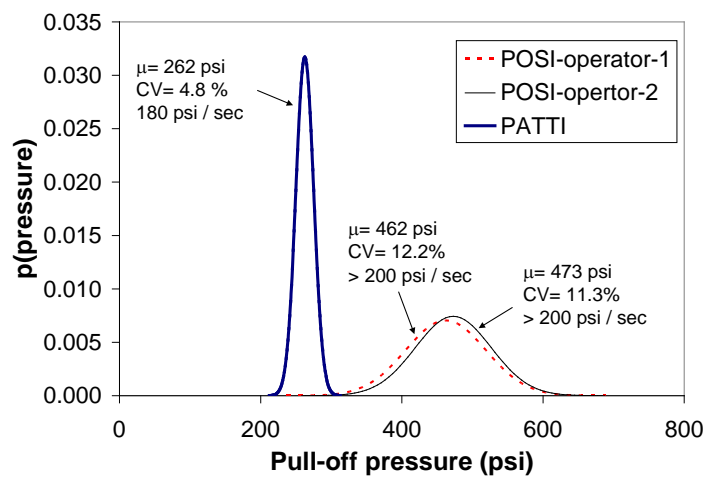


Figure M1a.4. Graph. Distributions of the Posi and PATTI test results.

Significant Results

The research team found that more consistent results in the Posi test could be obtained by using five plastic beads ($\phi = 0.5$ mm) during the sample preparation procedure. The beads are positioned between the aggregate and the dolly to maintain the binder film thickness as uniform as possible.

Another significant result is the good correlation observed between the pull-off strength values obtained from the Posi and PATTI tests, as shown in figure M1a.5.

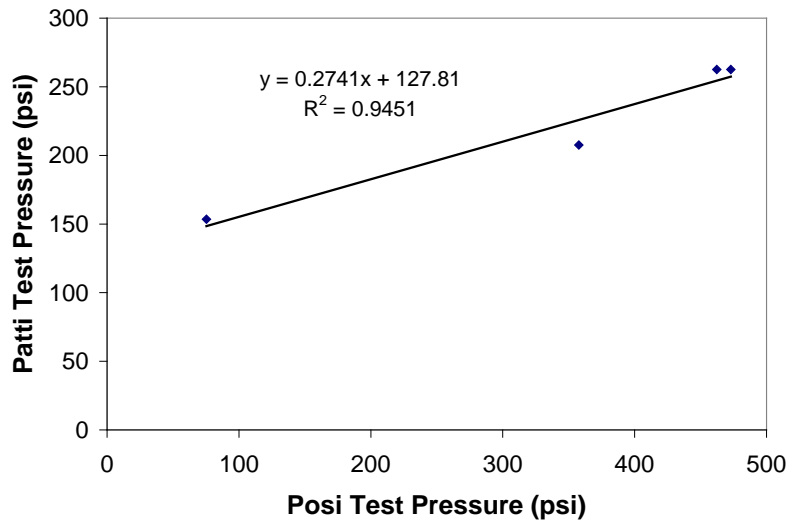


Figure M1a.5. Graph. Relation between pull-off strength obtained from Posi and PATTI tests.

Significant Problems, Issues and Potential Impact on Progress

Repairs and maintenance performed on the Dynamic Shear Rheometer during this quarter will delay completion of the experimental plan for stress sweep tests proposed in the previous quarterly report.

The Gantt chart has been updated to show the planned Presentation deliverables for subtasks M1a-3 and M1a-4 will be delivered in January 2010 and December 2009, respectively.

Work Planned Next Quarter

Next quarter, the research team will test binders in stress sweep according to the experimental plan. Results obtained from these tests will be correlated to the Bitumen Bond Strength (BBS) tests developed in work element M2c.

Further investigation of the correlation between the Posi and PATTI tests will include the effect of moisture (wet conditioning).

Cited References

ASTM, 2009, ASTM D 4541 - 09 Standard Test Method for Pull-Off Strength of Coatings Using Portable Adhesion Testers. American Society of Testing and Materials. West Conshohocken, PA.

Work Element M1b: Work of Adhesion Based on Surface Energy

Subtask M1b-1: Surface Free Energy and Micro-Calorimeter Based Measurements for Work of Adhesion (TAMU)

Work Done This Quarter

The main goal of this subtask is to provide material property inputs required in other work elements as required. Any data obtained from this subtask will be included in the material properties database.

Work Planned Next Quarter

Work on this subtask will be conducted in conjunction with and as required by other work elements.

Subtask M1b-2: Work of Adhesion at Nano-Scale Using AFM (WRI)

Work Done This Quarter

A digital high-speed camera has been ordered for use in this subtask.

Significant Results

None.

Significant Problems, Issues and Potential Impact on Progress

None.

Work Planned Next Quarter

The high-speed camera will be setup and preliminary testing with spin-casting of SHRP core asphalt samples will be begun.

Subtask M1b-3: Identify Mechanisms of Competition Between Water and Organic Molecules for Aggregate Surface (TAMU)

Work Done This Quarter

This sub task is investigating the mechanisms responsible for adhesion and debonding of model organic compounds (representing functional groups in asphalt binder) to minerals and representative aggregates. We are measuring the heat of reactions of the chemical mechanisms using a dual-mode flow adsorption calorimeter. Differences in molar heats of reaction of different organics bonding to the same absorbent are indicative of differences in the bonding strength of each absorbate with the absorbent of interest.

Work during this quarter focused on continued development of the instrument. We are currently conducting studies to validate the ability of the instrument to differentiate between bonding characteristics of materials produced under different conditions. These materials are known to have variable surface properties depending on the temperature of formation and other environment conditions. Currently we are evaluating the instrument ability to accurately measured changes in surface characteristics as a function of the pH of the aqueous environment.

Significant Results

There are no significant results for this quarter as we focused on aggregate characterizations.

Significant Problems, Issues and Potential Impact on Progress

There are no significant issues.

Work Planned Next Quarter

We plan on initiating flow through experiments to measure the molar heat of reaction of the adhesion of model organic compounds that represent asphalt to minerals and aggregates, as well as the molar heats of reactions of water adsorption to organic-coated minerals and aggregates. Adhesion will be modeled in the flow-through calorimeter by organic sorption from nonaqueous phase solvents. Experimental variables include the chemistry of the model organic, single versus mixtures of model organics, ionic salt content of the nonaqueous phase solvent, and the surface chemistry of the mineral or aggregate.

Competition of water and the model organics for the mineral or aggregate surfaces will be characterized through flow-through experiments that introduce small amounts of water to the systems created during the adhesion studies above.

Work Element M1c: Quantifying Moisture Damage Using DMA (TAMU)

Work Done This Quarter

A new method for preparing Fine Aggregate Matrix (FAM) specimens for the DMA testing was developed. This method aims at preparing FAM specimens that represent the composition and structure of the fine portion of the mixture. The method consists of preparing loose full asphalt mixtures and sieving into different sizes. Then, ignition oven is used to determine the binder content associated with the small size materials (passing on sieve #16). The sieve # 16 is used to separate fine aggregates from the coarse aggregates. Four different asphalt mixtures and three replicates from each mixture were evaluated. The binder content results from different replicates were consistent for a given mixture. FAM specimens were produced using binder content that was determined using the new method as well as the old one. The old method determines the binder content for the FAM mixture based on the binder content in the full mixture and the aggregate batch size. The FAM mixtures that were produced using new method were easily mixed, compacted and cored compared to the ones that were prepared using the old method. In some cases, the old method produces tender FAM specimens which are difficult to prepare. The common practice in the old method is to change the binder content until the FAM specimens become workable. Figure M1c-1 shows FAM specimens produced using the new method. Table M1c-1 presents the determined binder contents using the new and old methods.



Figure M1c-1. FAM specimens prepared using the new method

Table M1c-1: Binder Content

Mixture	Binder Content, %	
	Old method	New method
Limestone	10.7	8.0
Granite	12.0	7.0
Gravel	8.9	7.3
Texas	15.9	8.6

It should be pointed out that the FAM specimens produced using the new method are relatively stiffer. The current available DMA has limited torque capacity (0.20 N.m), so the test temperature in the new method is 30°C, which is higher than the room temperature that was used in the old method. It is planned to acquire a new DMA that has more torque capacity (5.6 N.m) by the beginning of the coming year. The FAM specimens can be tested at the room temperature using the new DMA.

Significant Results

The FAM specimen preparation and mixture design protocol is completed and the DMA tests are in progress.

Significant Problems, Issues and Potential Impact on Progress

None

Work Planned Next Quarter

Develop software to analyze the DMA data and provide the performance parameters developed under the ARC for the analysis of FAM fatigue resistance

CATEGORY M2: COHESION

Work Element M2a: Work of Cohesion Based on Surface Energy

Subtask M2a-1: Methods to Determine Surface Free Energy of Saturated Asphalt Binders (TAMU)

Work Done This Quarter

No activity was planned for this quarter.

Work Planned Next Quarter

Work on this task is anticipated to start in year 4 of the project.

Subtask M2a-2: Work of Cohesion Measured at Nano-Scale Using AFM (WRI)

Work Done This Quarter

During this quarter a preliminary series of ambient temperature AFM pull-off-force measurements was conducted. These measurements used a newly installed nano-positioning stage to control the motions associated with bringing the sample into initial contact with the probe tip and then applying a predefined loading and unloading cycle (as described last quarter).

The applied stage motions and resultant deflection of the AFM cantilever were recorded simultaneously using an independent data acquisition (DAQ) system connected to the stage position-sensor output and a photo-detector output on the AFM. Thin film samples of two SHRP core asphalts (AAA-1 and AAD-1) were prepared at nominal thicknesses of 0.25, 0.5, and 1 μm for this preliminary test series.

Significant Results

Figure M2a-2.1 shows a typical force curve as collected with the new system. The force curve shown was collected at ambient temperature using a silicon cantilever with a 10- μm glass bead tip and a nominal 0.95-N/m spring constant. The test sample was a 0.25- μm film of SHRP core asphalt AAA-1 on a glass microscope slide. For this particular force curve, the nano-positioning stage was programmed to ramp 1.5- μm from its starting position, hold this displacement for 60-seconds then ramp back to the starting position. The figure shows the output, in volts, recorded from the microscope (probe) and nano-stage (stage) plotted against time. The plot shows the same information as a typical AFM force curve as well as providing additional rate/time information that is not shown in the standard type plot. The DAQ-based plot also eliminates the trace-retrace format of typical AFM force curves to more clearly illustrate the relationship between the applied forces and the resultant response of the probe tip.

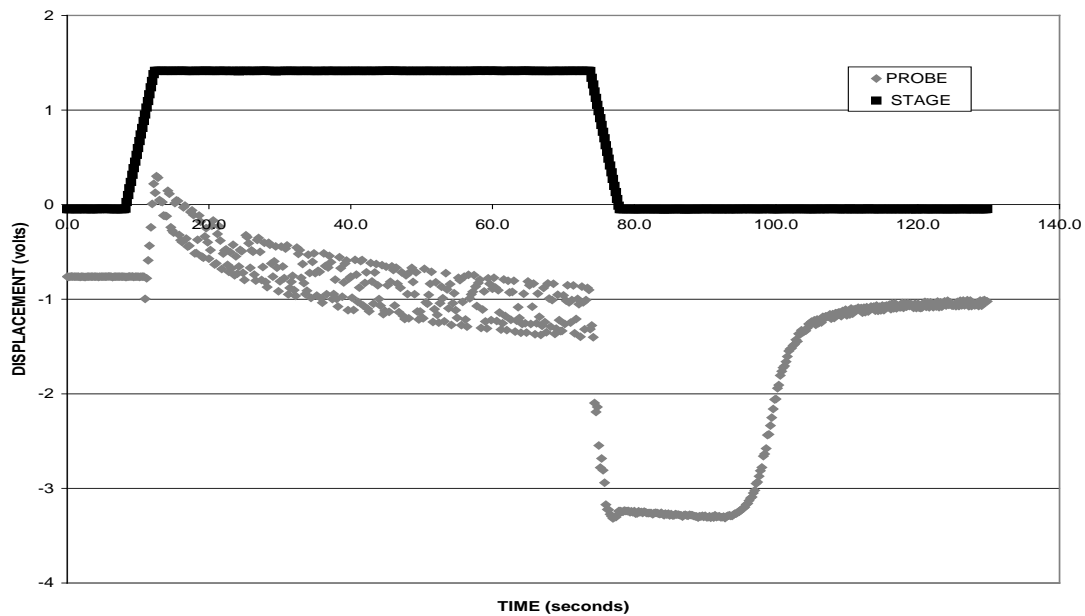


Figure M2a-2.1. Typical force curve showing output signals from AFM photo-detector and stage position sensors plotted against time.

Figure M2a-2.2 shows the same force curve with the voltage outputs converted to deflection, in μm , for the probe and stage relative to their respective starting positions.

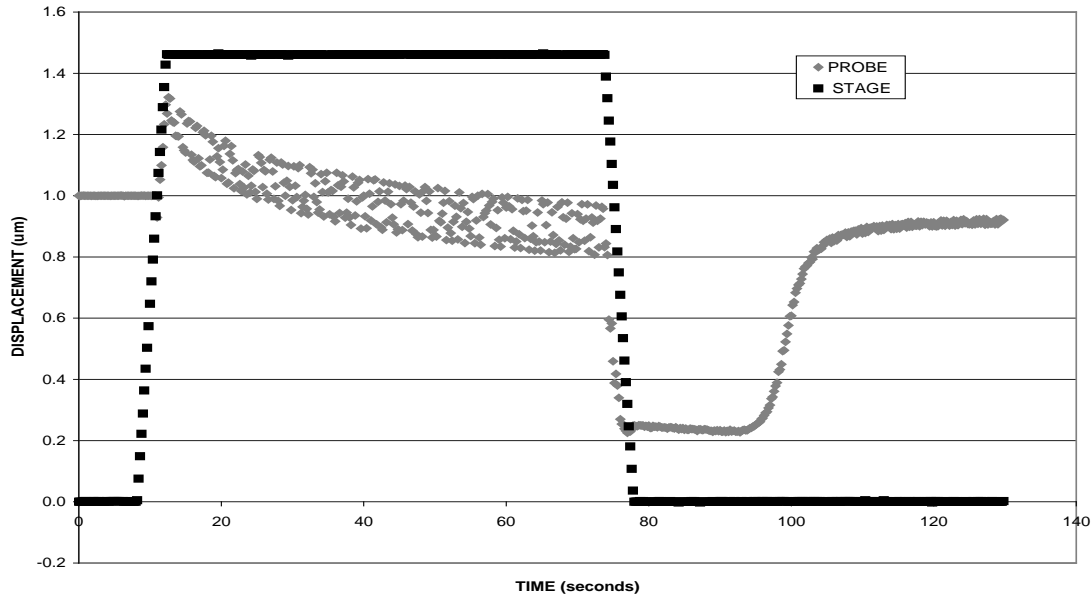


Figure M2a-2.2. Typical force curve showing relative positions of stage and probe plotted against time.

Figures M2a-2.3.a,b,c,d,e,f,g,h,i show a schematic representation of the relative tip and sample orientations at selected times during the load-unload cycle shown in figures M2a-2.1 and M2a-2.2. The tip and stage positions are shown with respect to their initial baseline (time 0) positions as well as with respect to each other. The figure also shows the approximate force exerted upon the probe tip by the cantilever spring at each of the selected times. The various times shown in the figure were selected to be representative of features commonly shown in AFM force/displacement (force curve) plots.

Figure M2a-2.3.a shows the relative positions of the probe and the sample surface at time 0 before the stage begins to ramp toward the probe tip. At this point the probe tip is approximately $1\text{-}\mu\text{m}$ above the sample surface. The cantilever is not deflected in any significant way by the sample surface with this large separation. This point corresponds to approximately -0.78 volts from the AFM detector output and is plotted as the beginning position of $+1\text{-}\mu\text{m}$ in figure M2a-2.2. Figure M2a-2.3.b shows the “snap-in” as the sample surface approaches the probe tip. At this point the tip is in contact with the sample and the cantilever is deflected so that the spring force is trying to pull the tip away from the surface as shown by the arrow in the figure. As the stage continues to advance toward the probe tip the direction of the force acting upon the probe tip by the cantilever spring quickly reverses so that the spring tends to push the probe into the surface (indent, loading force). Figure M2a-2.3.c shows the relative positions of the probe tip and the sample surface as the stage reaches its maximum translation ($+1.5\text{-}\mu\text{m}$). At this point the

cantilever spring is pushing the probe toward the surface with a force equal to the cantilever deflection times the cantilever spring-constant as shown by the arrow in the figure.

The loaded tip sinks into the sample surface until the force exerted by the cantilever spring is neutralized as shown in figure M2a-2.3.d. The tip then continues to be pulled toward the sample substrate due primarily to capillary wetting of the glass tip. The tip is attracted toward the sample substrate with a force great enough to overcome a counter-acting force applied by the cantilever spring as shown in figure M2a-2.3.e. It appears that the tip does not sink smoothly through the asphalt sample, but instead seems to move in a series of sudden incremental steps. The cantilever/laser detector system tends to over-respond to sudden motions resulting in the apparent wide band of position values as recorded in figures M2a-2.1 and M2a-2.2 for the probe tip as it sinks into the surface.

Figures M2a-2.3.f,g,h,i show the probe and sample positions through the unloading portion of the cycle. In figure M2a-2.3.f the stage has just retracted, the probe tip has moved with the retracting surface so that the cantilever spring is exerting a significant force trying to pull the tip away from the surface. In figure M2a-2.3.g the probe has detached from the sample substrate and is beginning to move under the influence of the force exerted by the cantilever spring. In figure M2a-2.3.h the probe has moved sufficiently to have detached from the surface. The fact that the probe tip is still strongly influenced by the sample indicates that the probe is deforming the surface and pulling up a “neck” of asphalt as the cantilever spring slowly pulls the tip away from the surface. In figure M2a-2.3.i the probe is well above the original asphalt surface, but it is clearly still attached sufficiently to resist the pull of the slightly deflected cantilever. For this system at ambient temperature, flow and plastic deformation could account for a significant fraction of the energy dissipation.

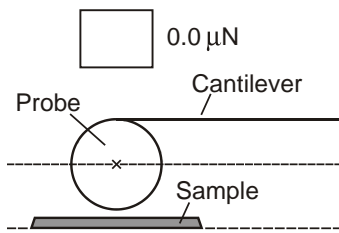


Figure M2a-2.3a.
Time 0 seconds.

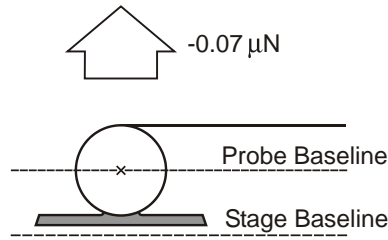


Figure M2a-2.3b.
Time 11 seconds.

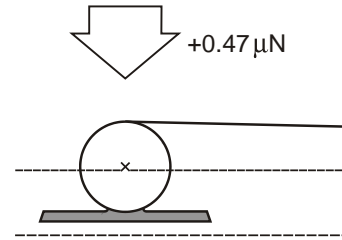


Figure M2a-2.3c.
Time 12.4 seconds.

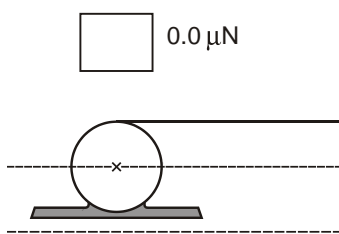


Figure M2a-2.3d.
Time 30 seconds.

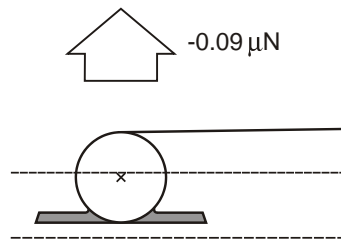


Figure M2a-2.3e.
Time 65 seconds.

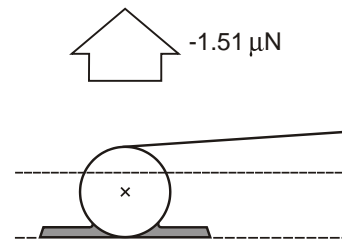


Figure M2a-2.3f.
Time 80 seconds.

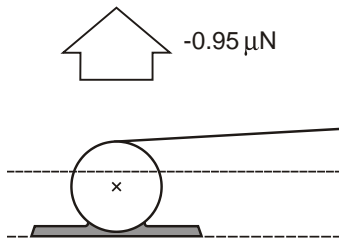


Figure M2a-2.3g.
Time 98 seconds.

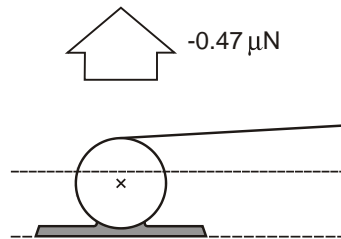


Figure M2a-2.3h.
Time 101 seconds.

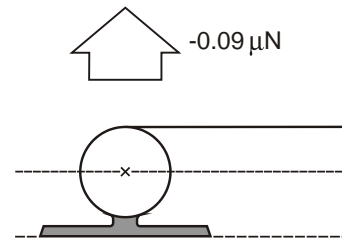


Figure M2a-2.3i.
Time 120 seconds.

Figure M2a-2.3.a,b,c,d,e,f,g,h,i. Schematic showing relative probe position and force applied by cantilever spring at various times in force curve cycle.

Work Planned Next Quarter

Work planned for next quarter will include analysis, using the mechanical models described in the previous quarterly report for this task (Quarterly Technical Progress Report, July 2009), of

force curve data collected this quarter. Additional force curve data will be collected for a wider selection of asphalt samples. Tests will be conducted to begin to address the effect of temperature and loading/unloading rates with respect to how “fracture” energy is dissipated as indicated by the various parts of the force curve measurements. These measurements should lead to a better understanding of the ductile-brittle transition that takes place as asphalt is cyclically heated and cooled.

Work Element M2b: Impact of Moisture Diffusion in Asphalt Mixtures

Subtask M2b-1: Measurements of Diffusion in Asphalt Mixtures (TAMU)

Work Done This Quarter

Tests related to the measurement of moisture diffusion using the FTIR, gravimetric measurements and hysteretic effect of moisture diffusivity has been completed using the FTIR. Three different asphalt binders were included in this study. Analysis of the results from the measurements of diffusivity using FTIR and gravimetric measurements is complete and the analysis of measurements related to the hysteretic effect are in progress.

Significant Results

The significant results on measurement of diffusivity using the FTIR were summarized in the form of a technical paper and submitted for consideration to be presented at the TRB annual meeting. The paper models the diffusion of moisture through thin films of asphalt binder using a dual mode diffusion model following Fick’s model for diffusion. Results from three different asphalt binders were presented. The results were found to be in the same order of magnitude as the measurements made at the FHWA TFHRC facility using an electron impedance spectroscopy. Results using the gravimetric analysis on sand-asphalt mortars for Fine Aggregate Matrix (FAM) were also modeled using a similar approach. Results from two different temperatures were used to estimate the rate at which diffusion can be accelerated by increasing temperature.

Work Planned Next Quarter

The work planned for next quarter is to complete the analysis on the hysteretic effect on moisture diffusivity. The results will be summarized in the form of two additional technical papers.

Subtask M2b-2: Kinetics of Debonding at the Binder-Aggregate Interface (TAMU)

Work Done This Quarter

Most of the work accomplished under subtask M2b-1 also directly relates to this subtask. The most significant difference in this subtask is that a portion of the binder-ATR window interface will be purposefully exposed to be in direct contact with the water. This will allow the water to diffuse through the film as well as propagate along the binder-ATR window interface.

Work Planned Next Quarter

Researchers plan to continue work with emphasis on M2b-1 before addressing the specifics of this subtask.

Work Element M2c: Measuring Thin Film Cohesion and Adhesion Using the PATTI Test and the DSR (UWM)

Work Done This Quarter

The research team investigated the effect of pressure rate and bonding temperature on the experimental results in the Bitumen Bond Strength (BBS) device. A standard testing protocol was developed and adopted based on the results obtained during this quarter.

Significant Results

Two bonding temperatures were selected: 65 °C and 135 °C. The tests revealed no significant difference between the materials' ranking provided by the two bonding temperatures. The one notable difference between the two temperature values was that the higher temperature tends to lead to the asphalt binder flowing from in between the test surfaces. Loss of sample geometry has been observed on softer binders when bonded at 135 °C. Due to the risk of overflowing the binder at the 135 °C bonding temperature, 65 °C was selected as the bonding temperature for all subsequent testing.

Next, the influence of the pressure increase rate over the BBS test results was investigated. Results indicate that there is minimal change of tensile strength for both neat and modified binders when using different rates. It is found that the maximum tensile strength exhibited by the binder increases with the faster rates. This is expected since the faster rates simulate testing at lower temperatures. However, the percentage of tensile strength loss was similar for all rates tested. These results lead the research team to conclude that the testing rate does not change ranking of the moisture susceptibility of asphalt binders, as detected by the BBS test device. Results representing the various testing conditions are summarized in tables M2c.1 through M2c.4.

Table M2c.1. Percentage of tensile stress loss.

FH 64-22, neat	70 psi/s	240 psi/s
Average pullout tension, dry	276	329.25
Average pullout tension, wet	195	230.67
Percentage of tensile loss	29.3%	29.9%

Table M2c.2. Percentage of tensile stress loss.

CRM 58-28+2% LSBS	70 psi/s	120 psi/s	180 psi/s
Average pullout tension, dry	208.72	253.14	262.54
Average pullout tension, wet	153.52	197.59	207.61
Percentage of tensile loss	26.4%	21.9%	20.9%

LSBS = linear styrene-butadiene-styrene.

The maximum tensile stress loss is given by the equation below:

$$\frac{(\text{maximum pullout tension in dry condition}) - (\text{maximum pullout tension in wet condition})}{(\text{maximum pullout tension in dry condition})}$$

Table M2c.3. Percentage of tensile stress loss.

FH 64-22+1% PPA	200 psi/s	100 psi/s
(dry-wet 1)/dry	32.81%	33.92%
(dry-wet 2)/dry	21.58%	18.47%

PPA = polyphosphoric acid.

Table M2c.4. FH 64-22+2% Sasobit, granite, rate of 70 psi/s.

FH 64-22+2% Sasobit	Run	Dry		Wet	
Maximum Pullout Tension [psi] Rate 70 psi/s	1	314	388	152	236
	2	382	366	138	238
	3	304	419	124	216
	Average	333.3	391.0	138	230
	Standard Deviation	42.4	26.6	14.0	12.2
	Coefficient of Variation	12.7%	6.8%	10.1%	5.3%

As a result of the work done during this quarter, a standard testing protocol for the BBS test has been finalized. The testing parameters are as follows:

- Bonding temperature = 65 °C.
- Conditioning time, both dry and wet = 24 hours.
- Water conditioning temperature = 40 °C.
- Pressure increase rate = 100 psi/sec.
- Data acquisition rate = approximately 60 Hz.

Significant Problems, Issues and Potential Impact on Progress

The journal paper for subtask M2c-3 as noted on the Gantt chart was moved to January 2010. The team is working on submitting an ASTM proposal for the test method, and the team needs to make additional adjustments to the testing procedure for this submission. A journal paper will be submitted for publication after enough data are collected. The team expects to have the necessary amount of data before the end of 2009.

Work Planned Next Quarter

Next quarter, the team will continue running experiments according to the experimental design and procedure.

CATEGORY M3: AGGREGATE SURFACE

Work Element M3a: Aggregate Surface Characterization (TAMU)

Work Done This Quarter

Physical and chemical properties of aggregates at the macro and molecular scale influence the performance of asphalt mixes. These properties control the nature and durability of the bond between aggregates and asphalt in wet and dry conditions and its resistance to moisture induced damage and fatigue cracking. Recent research by Little and colleagues have shown that surface energy of the aggregate-asphalt interface is a reliable predictor of engineering properties of the asphalt mixture. Current understanding of the aggregate and bitumen properties that control and shape surface energy is limited, limiting our ability to *a priori* predict surface energy of any given aggregate-asphalt combination.

Current tasks are organized around the (1) characterization of the chemical composition of the surfaces of reference minerals and aggregates through electron beam spectroscopes, including electron microprobe, backscatter electrons and electron-dispersive spectroscopy (EDS), (2) the characterization of the surface energies of reference minerals and aggregates through the universal sorption device and microcalorimetry, (3) quantification of surface (upper 14 nm) atomic species and chemical state with an x-ray photoelectron spectroscope (XPS), and (4) surface topography characterization with scanning electron microscopy (SEM). The results from these tasks will support the development of a predictive model of aggregate surface energies based upon the surface energies of the minerals that compose the aggregate.

Tasks completed this quarter include additional BSE imaging of the basalt (RK) in order to more accurately calculate modal mineralogy, quantitative WDS analyses of the SAz-2 montmorillonite and Georgia kaolinite, image processing of X-ray elemental distribution maps of the aggregates and reference mineral samples, and compilation and organization of the quantitative WDS analyses. Specific accomplishments are highlighted in the tables below.

Surface energy measurements for quartz, microcline, labradorite, biotite, andesine, microcline, albite, augite, hornblende, hematite, siderite, dolomite, and calcite have been collected using the universal sorption device. The components of surface energy were calculated on replicates of the samples.

Sample preparation and aggregate surface characterization tasks completed this quarter are shown in the table below.

Table M3a.1. Status of tasks associated with mineralogical and chemical characterization of aggregates.

SHRP	Name	Yr.Qtr	Thin Section Prep Status	Microprobe Analysis Status
RA	Lithonia Granite	08.1	1 aggr sample prepared, 2 more in progress	1 set of X-ray maps, 1 set of BSE images, 1 preliminary set of WDS quant analyses
		08.2	2 more aggregate samples prepared	2 sets of X-ray maps, BSE images are not needed because of grain size
		09.1		WDS quant analyses of major minerals completed
RC	Limestone (higher absorption)	08.1	2 aggr samples prepared	1 set of X-ray maps, 1 set of BSE images, 1 preliminary set of WDS quant analyses
		08.2	-	No additional analyses
RD	Limestone (low absorp.)	08.1	4 aggr samples prepared,	4 sets of X-ray maps, 1 set of BSE images, 1 preliminary set of WDS quant analyses
		08.2	-	No additional analyses
RK	Basalt	08.1	2 aggr samples prepared, 1 more in progress	2 sets of X-ray maps, 1 set of BSE images, 1 preliminary set of WDS quant analyses
		08.2	1 sample in progress	3 additional sets of X-ray maps, 13 set of BSE images, 1 set of WDS quant analyses for pyroxene, olivine, amphibole
		09.1		WDS quant analyses of feldspar, pyroxene and clay completed.
		09.2		Additional BSE images of thin sections RK1a and RK1b acquired; image processing of X-ray maps in progress
RL	Gulf Coast Gravel	08.1	5 aggr samples prepared, 9 more in progress	4 sets of X-ray maps, 1 set of BSE images, 1 preliminary set of WDS quant analyses
		08.2	9 more in progress	9 sets of X-ray maps
		09.1		WDS quant analyses of mineral grains in 9 gravel particles completed.
		09.2		Image processing of X-ray maps in progress
MM	MM Sandstone	09.1	One 25mm aggr mount prepared with > 20 fragments	1 sets of X-ray maps acquired

Sample preparation and mineral surface characterization tasks completed this quarter are shown in the tables below.

Table M3a.2. Status of tasks associated with mineralogical and chemical characterization of mineral components of aggregates.

Mineral	Group	Yr.Qtr	(1) Acquisition Status (2) Microprobe Mount Status	Microprobe Analysis Status
Quartz	Silica Mineral	08.1	(1) > 200 grams acquired (Arkansas, RNG specimen) (2) Polished microprobe mount in preparation	In progress
		08.2	In progress	In progress
Microcline	Alkali Feldspar	08.1	(1) > 160 grams acquired (G&G collection, B0434) (2) Preliminary polished mount prepared	Preliminary homogeneity and quantitative chemical analysis acquired.
		08.2	In progress	In progress
Albite	Plagioclase Feldspar	08.1	(1) > 100 grams acquired (G&G collection, B0469) (2) Polished mount to be prepared	In progress
		08.2	In progress	In progress
Oligoclase	Plagioclase Feldspar	08.3	> 100 grams acquired (G&G collection, 008)	In progress
Andesine	Plagioclase Feldspar	08.1	(1) > 65 grams acquired (G&G collection, B0513) (2) Preliminary polished mount prepared	Preliminary homogeneity and quantitative chemical analysis acquired.
		08.2	In progress	In progress
Labradorite	Plagioclase Feldspar	08.1	(1) > 160 grams acquired (Naim, Labrador; RNG specimen) (2) Preliminary polished mount prepared	Preliminary homogeneity and quantitative chemical analysis acquired.
		08.2	In progress	In progress
Anorthite	Plagioclase Feldspar	08.1	Samples to be acquired	NA
		08.2	NA	NA

Table M3.a 2. Status of tasks associated with mineralogical and chemical characterization of mineral components of aggregates (cont.).

Mineral	Group	Yr.Qtr	(1) Acquisition Status (2) Microprobe Mount Status	Microprobe Analysis Status
Hornblende	Amphibole	08.1	(1) > 70 grams acquired (G&G collection, Room 008) (2) Polished mount to be prepared	In progress
		08.2	In progress	In progress
		09.1	(2) Polished mount prepared	X-ray map acquired; WDS quant analyses completed.
Augite	Pyroxene	08.1	(1) > 0 (?) grams acquired (G&G collection, B1007) (2) Preliminary polished mount prepared	Preliminary homogeneity and quantitative chemical analysis acquired.
		08.2	In progress	In progress
Augite	Pyroxene	08.1	(1) > 80 grams acquired (G&G collection, Room 008) (2) Polished mount to be prepared	In progress
		08.2	In progress	In progress
		09.2		WDS quant analyses completed.
Forsteritic Olivine	Olivine	08.1	(1) > 280 grams acquired (San Carlos, AZ) (2) Polished mount to be prepared	In progress
		08.2	In progress	In progress

Table M3a.2. Status of tasks associated with mineralogical and chemical characterization of mineral components of aggregates (cont.).

Mineral	Group	Yr.Qtr	(1) Acquisition Status (2) Microprobe Mount Status	Microprobe Analysis Status
Muscovite	Mica	08.1	(1) > 65 grams acquired (G&G collection, Room 008) (2) Polished mount to be prepared	Preliminary quantitative chemical analysis acquired.
		08.2	In progress	In progress
		09.1	(2) Polished mount prepared	X-ray map acquired; WDS quant analyses completed.
Biotite	Mica	08.1	(1) > 175 grams acquired (G&G collection, B0857) (2) Polished mount to be prepared	In progress
		08.2	In progress	In progress
		09.1		WDS quant analyses completed.
Biotite	Mica	08.1	(1) > 150 grams acquired (G&G collection, Room 008) (2) Polished mount to be prepared	Preliminary quantitative chemical analysis acquired.
		08.2	In progress	In progress
Calcite	Carbonate	08.1	(1) > 100 grams acquired (Mexico; RNG specimen) (2) Polished mount to be prepared	In progress
		08.2	In progress	In progress
Dolomite	Carbonate	08.1	Samples to be acquired	NA
		08.2	NA	NA
		09.1	(2) Polished mount prepared	X-ray map acquired; WDS quant analyses completed.
Siderite	Carbonate	09.1		WDS quant analyses completed.
Rhodochrosite	Carbonate	09.4		
Cerussite	Carbonate	09.4		

Table M3a.2. Status of tasks associated with mineralogical and chemical characterization of mineral components of aggregates (cont.).

Mineral	Group	Yr.Qtr	(1) Acquisition Status (2) Microprobe Mount Status	Microprobe Analysis Status
Hematite	Iron Oxide	08.1	Samples to be acquired	NA
		08.2	NA	NA
		09.1	(2) Polished mount prepared	X-ray map acquired; WDS quant analyses completed.
Ilmenite	Iron Titanium Oxide	08.3	> 100 g sample (Ontario; RNG specimen)	NA
		09.1	(2) Polished mount prepared	X-ray map acquired; WDS quant analyses completed.
Kaolinite (KGA-1B)	Clay Mineral	08.3	Samples acquired	NA
		08.2	Samples acquired	In progress
Kaolinite (Georgia)	Clay Mineral	08.3	Samples acquired	NA
		08.2	Samples acquired	In progress
		09.2	Unpolished flat mount prepared	WDS quant preliminary analyses completed
Montmorillonite (SAz-2)	Clay Mineral	08.3	Samples acquired	NA
		08.2	Samples acquired	In progress
		09.2	Unpolished flat mount prepared	WDS quant preliminary analyses completed
Chlorite	Clay Mineral	08.3	Samples acquired; ~25 g Calumet and New Melones (RNG)	NA
		08.2	Samples acquired	In progress

Significant Results

Establishing a Surface Energy Predictive Model

One of the first goals will be to establish a model for predicting aggregate bulk surface energies based on mineralogical composition. Improved prediction of aggregate bulk properties pertinent to moisture damage susceptibility can lead to better methods to measure material properties and moisture damage susceptibility of asphalt/aggregate mixes. Development of a simple visual field

test of aggregate surface energy properties will aid in on-site evaluation of aggregate moisture damage susceptibility.

We expect the bulk/total surface energy of an aggregate to be a function of the component surface energies of its mineralogical constituents as:

$$Se_{aggregate} = \sum (Se_{Mineral} \cdot SA) + \sigma \quad (M3a.1)$$

where Se is surface energy, SA is surface area, and σ is the error term. A visual inspection of rock mineralogy based on percent of constituents can accurately predict total surface energy of the sample.

Methods –A Universal Sorption Device can be used to measure pure phase mineral surface energies by calculating the amount of a reference gas (water, hexane, and methylpropyl ketone in this case) sorbed to the mineral surface at various pressures. The adsorption isotherm for each reference gas is used to calculate equilibrium spreading pressure for each of the vapors along with the specific surface area (SSA) using the BET Equation. The equilibrium spreading pressure of each vapor is then used to calculate the three surface energy components using GvOC Equations. These values will then be used to establish an additive model of total surface energy for previously characterized rock samples based on percent of each constituent at the surface. The validity of the model will be tested by using the same Universal Sorption Device technique on the aggregate samples. A statistical analysis will be performed on the observed measurements versus predicted values.

Experiments – Although rock mineralogy has the capacity to be very complex it is dominated by a relatively small group of minerals of predictable variability in North America. The mineralogy of common aggregates used in hot asphalt mixes across America is outlined in the aggregate analysis data from the Strategic Highway Research Program’s (SHRP) materials reference library. Pure phase minerals are being collected by Dr. Ray Guillemette based on the findings of the SHRP. These minerals are the dominant constituents in all major aggregates of the study. The chosen minerals are listed in table M3a.2.

The surface energies of these pure phase minerals will be calculated using a Universal Sorption Device using three reference gases to determine spreading pressures. Each mineral will be crushed and passed through a number 10 sieve. Minerals will be washed with distilled water and heated for 24 hours at 80° Celsius in a Fisher Isotemp® Oven. Each reference gas will be used on a separate sample of each pure phase mineral. After the test is run each sample will be washed with distilled water and reheated at 80° C for future analysis.

After each of the pure phase mineral surface energies have been quantified the SHRP aggregate samples themselves will be crushed and analyzed on the Universal Sorption Device to statistically determine the linear additive model’s validity

Data- The data gained from this experiment will be in $erg / (cm)^2$ for each pure phase mineral and SHRP aggregate. In order to calculate mineral surface energy the isotherm for each

reference gas must be calculated. To obtain a full isotherm, the aggregate is exposed to ten equal increments of partial probe vapor pressure from vacuum to saturated vapor pressure. At each stage the adsorped mass is recorded after it reaches equilibrium. The adsorped mass of each stage is then used to plot the isotherm. The measured isotherm for hexane is then used to calculate the specific surface area (SSA) using the Branauer, Emmett, and Teller BET equation:

$$A = \left(\frac{N_m N_0}{M} \right) \alpha \quad (\text{M3a.2})$$

where N_0 =Avogadro's number; M =molecular weight of the probe vapor; α = projected area of a single molecule; and N_m =monolayer capacity of the aggregate surface. The specific surface area and each adsorption isotherm are then used to calculate three surface energy components using the GvOC equation:

$$W = 2\sqrt{\gamma_s^{lw}\gamma_v^{lw}} + 2\sqrt{\gamma_s^+\gamma_v^-} + 2\sqrt{\gamma_s^-\gamma_v^+} \quad (\text{M3a.3})$$

where g^{Total} = total surface energy of the material; g^{lw} = Lifhsitz–van der Waals or dispersive component; g^{AB} = acid-base component; g^+ = Lewis acid component, and g^- = Lewis base component.

Current Results

In order to use the Universal Sorbtion Device as an appropriate measuring device for surface energy, the reproducibility must first be known. In order to test the reproducibility one of the SHRP aggregates was chosen at random and the surface energy was measured on the sorption device. The aggregate was RD-7, a shaly limestone composed primarily of calcite. Hexane and methylpropyl ketone were run in triplicate and water vapor was tested four times. The results indicated that there was a good deal of internal consistency between the test runs, and the overall surface energy calculation was within a 95 percent confidence interval to previous study of the aggregate over two years ago. In total, testing of 21 minerals and two clays has either been completed or is in progress. All minerals will be tested in quadruplicate for each vapor. The results to date are included in table M3a.3.

Table M3a.3. Calculated surface energies and surface energy components of minerals and aggregates.

Mineral Surface Energy							
Mineral	SSA	Energy Components (ergs/cm ²)					Total
		LW	Electron Acceptor	Electron Donor	Polar Component	Fractional Polarity	
RD-7	0.23	49.98	0.47	469.22	29.69	0.37	78.67
MM Sandstone	0.99	45.24	2.02	310.96	50.07	0.53	95.31
RC Limestone	0.96	49.55	2.98	799.29	97.61	0.66	147.16
Quartz	0.06	50.33	0.02	365.00	5.04	0.09	55.37
Microcline	0.12	44.00	0.46	202.79	19.35	0.31	63.35
Calcite	0.35	34.94	0.40	85.16	11.60	0.25	46.54
Rhodochrosite	NA	0.00	0.00	0.00	0.00	#DIV/0!	0.00
Cerussite	NA	0.00	0.00	0.00	0.00	#DIV/0!	0.00
Biotite	0.06	52.51	0.07	809.97	14.90	0.22	67.41
Labradorite	0.27	46.21	1.81	186.54	36.71	0.44	82.92
Andesine	0.10	40.64	0.40	4953.93	89.24	0.69	129.88
Albite	0.05	51.57	0.22	501.69	21.22	0.29	72.79
Augite	0.04	52.67	8.69	6981.14	492.71	0.90	545.38
Siderite	0.07	61.39	1.59	789.63	70.80	0.54	132.18
Hematite	0.05	48.99	2.85	558.07	79.82	0.62	128.81
Dolomite	0.06	60.29	0.18	564.05	20.28	0.25	80.57
Muscovite	0.12	47.55	0.55	544.68	34.52	0.42	82.07
Olivine	0.28	44.17	1.55	57.52	18.87	0.30	63.04
Gypsum	0.37	41.78	1.08	60.58	16.16	0.28	57.94
Bassanite	0.48	38.27	0.30	3036.03	59.90	0.61	98.16
Montmorillonite	23.30	42.85	1.57	80.43	22.45	0.34	65.29
Kaolinite	10.53	30.48	5.01	80.00	40.02	0.57	70.51
Hornblende	0.09	51.92	0.91	1338.86	69.70	0.57	121.63
Ilmenite	NA	0.00	0.00	0.00	0.00	#DIV/0!	0.00

Significant Problems, Issues and Potential Impact on Progress

No significant problems at this time.

Work Planned Next Quarter

Work planned in the next quarter includes continued analysis of the aggregates and minerals, with specific reference to surface energies.

CATEGORY M4: MODELING

Work Element M4a: Micromechanics Model (TAMU)

Work Done This Quarter

Lattice Micromechanical Model

The reader is referred the work element F3b.

Cohesive Zone Micromechanical Model

Researchers at TAMU have used the coupled micromechanical model of moisture damage in asphalt mixtures that was developed and implemented a year ago in several different applications. Recalling, the model integrates the effects of moisture in the microstructure of asphalt mixtures by degrading the mechanical properties of two important components of this material: the asphalt matrix (also called Fine Aggregate Matrix, FAM) and the aggregate-FAM interface. The former represents cohesive degradation of the asphalt matrix while the later represents adhesive deterioration of the mixture. Adhesive fracture of the aggregate-FAM interfaces is achieved by introducing thin layers of interfacial elements between the aggregates and the adhesive zones. The Cohesive Zone Modeling (CZM) technique is used to represent fracture processes within these interfacial layers (herein called *adhesive zones*). The micromechanical model was implemented in Abaqus® using a diffusion-mechanical sequentially coupled technique. Specific details about the model can be found in previous reports.

In this quarter, the model was used to continue investigating the effect of the air void phase on the mechanical performance of asphalt mixtures subjected to moisture diffusion processes.

There exist two common approaches to include the air void phase in the micromechanical modeling of asphalt mixtures. The first approach consists of assuming that the air voids are uniformly distributed within the FAM. In this case, the FAM is assumed to be a continuum and it is assigned effective material properties. The second approach consists of considering the air voids as an independent phase of the mixture. Under this approach, the voids are directly included into the model and are assigned their own material properties. While the first approach was used in the sensitivity study reported in the first 2009 quarterly report, the second approach was used to investigate the role of air voids in the initiation and evolution of moisture-related mechanical performance of asphalt mixtures, as reported in the previous quarterly report. In such a study, it was demonstrated that air voids play a main role in the development of moisture-related deterioration processes in asphalt mixtures and that they should not be overlooked when modeling damage in asphalt mixtures.

In this opportunity, a new approach based on random field theory was used to indirectly include the effects of the air void phase on the moisture-related mechanical response of the mixtures. Random field theory is an efficient stochastic-based tool that has been widely used in other fields to map a parameter or variable of interest (e.g., the strength or porosity of soils) into a predefined space, after taking into consideration the spatial autocorrelation and variability of such a

parameter in the field. Discrete-Markovian random field theory was used to incorporate the effects of air voids on the material properties of the FAM. In order to do so, the FAM phase was divided into 100 equal-size sections and each section was assigned its own physical and mechanical material properties according to probable air void spatial variability and internal distributions.

Figure M4a.1 presents the 50mm by 50mm representative volume element (RVE) that was selected for the study. This microstructure contains a total of 231 coarse aggregates, and is the same as the one used in the work reported in the previous report.

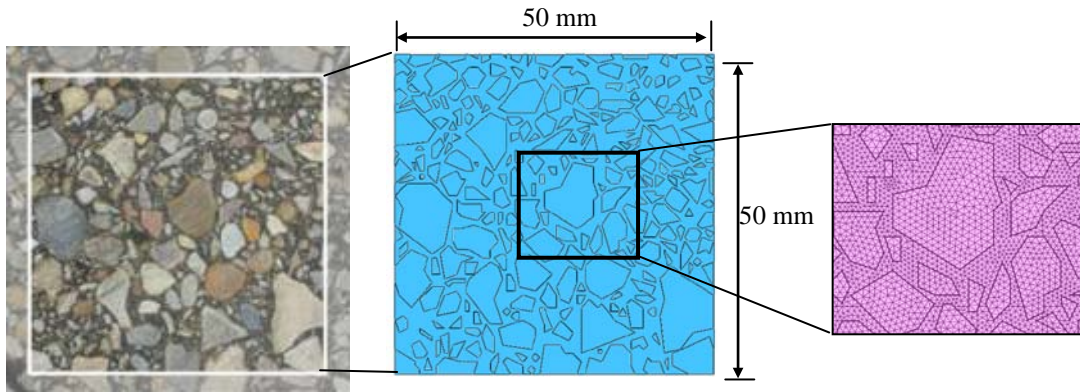


Figure M4a.1. Microstructure model used in the parametric analysis and its corresponding finite element implementation.

The stochastic technique was designed to account for two different levels of variability of the air void phase that are found in compacted asphalt layers in the field:

1. The spatial variability of the air voids within the asphalt layer (i.e., the difference among the total air voids content at different spatial locations at the asphalt layer), and
2. The internal distribution of the air voids within the microstructure of the mixture (i.e., internal air void distribution within a particular location).

The covariance decomposition technique introduced in 2000 by El-Kadi and Williams (El-Kadi and Williams 2000) was selected for the stochastic generation of the air voids within the microstructure model. According to this technique, the realization of the air void random field can be obtained from:

$$AV_n = S\varepsilon_n + \mu_n, \quad (M4a.1)$$

where AV is a [100x1] vector containing the air voids content of the 100 elements of the FAM, S is the [100x100] autocorrelation matrix, ε is a [100x1] vector containing standard normally distributed values (i.e., with mean 0 and standard deviation 1), μ is a [100x1] vector containing the mean values of the internal air voids distribution within a particular microstructure and the subscript n refers to the results for the n -th realization of the random field. The autocorrelation

matrix can be obtained from equation (M4a.2) after applying the Cholesky decomposition technique. In equation (M4a.2), C is the covariance matrix which, under anisotropic conditions, can be defined by equation (M4a.4).

$$C = SS^T \quad (M4a.2)$$

$$C_{i,j} = \sigma \exp \left[-\sqrt{\left(\frac{d_{i,j}^x}{L_x}\right)^2 + \left(\frac{d_{i,j}^z}{L_z}\right)^2} \right] \quad (M4a.3)$$

In equation (M4a.3) $C_{i,j}$ is the $(i^{\text{th}}, j^{\text{th}})$ position of the covariance matrix C , L_x and L_z are the autocorrelation lengths in the x (i.e., horizontal) and z (vertical) directions, respectively, $d_{i,j}^x$ and $d_{i,j}^z$ are the horizontal and vertical components of the distance between the points i and j and σ is the standard deviation of the air voids in the field. Due to the nature of the spatial distribution of the air voids in the field, it is expected that the air void content value assigned to a particular FAM division is somehow correlated with the air void content of the surrounding spatial divisions. The autocorrelation lengths are defined as the distance at which this similarity is expected (i.e., the length of influence of the value of air void content). In this study, it was assumed that the vertical and horizontal autocorrelation distances of the air void random field (L_z and L_x) are 10 mm and 35 mm, respectively.

Three different cases of air void content variability in the field were studied: asphalt layers with coefficient of variation (COV) of the air void content of 10%, 20% and 30%. According to the quality control requirements of most state transportation agencies, the air void content variability in the field is expected to be in a range of 10% to 15%, while a COV of 30% is an extreme-non desirable case of spatial air void variability. The mean value vector of the air void content, μ_n in equation (M4a.1), was randomly generated.

The stochastic technique was implemented in Matlab[®], and 15 realizations at each level of spatial variability (i.e., COV of field air voids of 10, 20 and 30%) were generated. Figure M4a.2 presents a typical realization of the air void random field. Moisture diffusion coefficients and linear viscoelastic material properties were assigned to each FAM division according to the amount of stochastically produced values of air void content. Material properties of the other two phases (i.e., aggregates and the portion of the FAM free of voids) were assigned to be the same as those used in the study reported in the previous quarter.

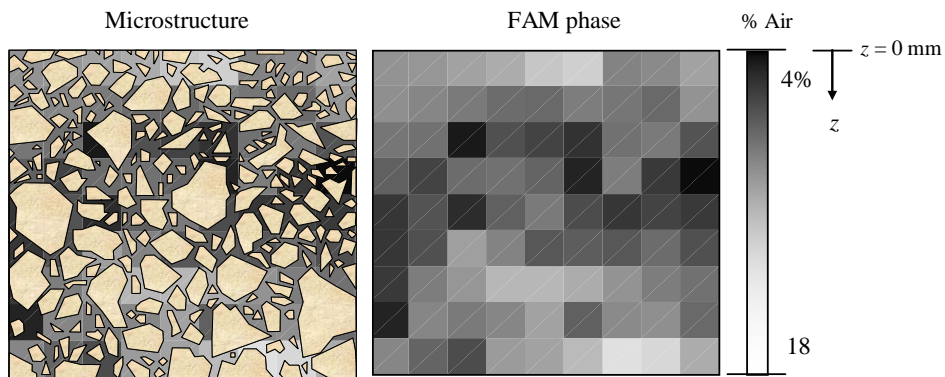


Figure M4a.2. Example of a stochastic realization of the air void random field within the FAM phase.

All microstructures were subjected to a 10-day moisture diffusion period after which a 30 s mechanical loading-controlled test was conducted at a rate of 0.28 N/s (monotonic loading and unloading). Figure M4a.3 shows the moisture content profiles at different stages of the moisture conditioning process. The total energy dissipated by the mixtures (DE in figure M4a.4) and its overall stiffness (K in figure M4a.4) were used as indicators of the mechanical performance of the mixtures.

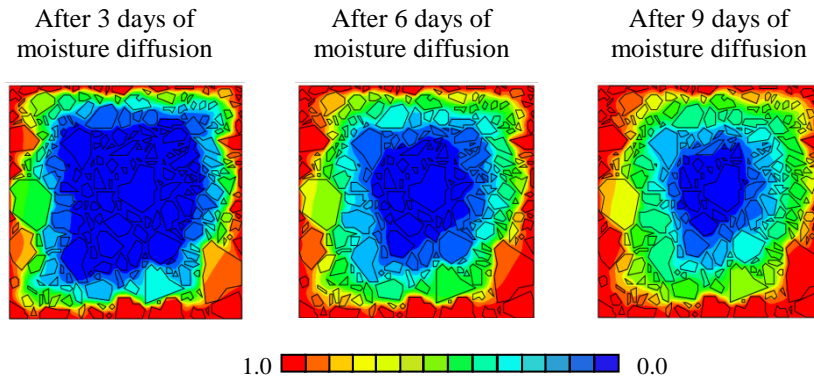


Figure M4a.3. Moisture diffusion profiles at different moments of the moisture conditioning process (in terms of normalized moisture content with respect to the maximum moisture saturation level).

As expected, an increase in the variability of the air voids content within the asphalt mixture in the field is associated with an increase in the variability of DE and K . In fact, it was observed that the COV of DE and K in the asphalt mixture is between 25% and 30% of the magnitude of the spatial variability of field air void contents. In other words, if the COV of the field air voids in an asphalt layer is, for example, 20%, the COV of the mechanical performance of the mixture is expected to be in a range of 5 to 6%. This range was found to be close to reported data on the

relationship between the air void variability and the expected mechanical response of the mixtures in the field.

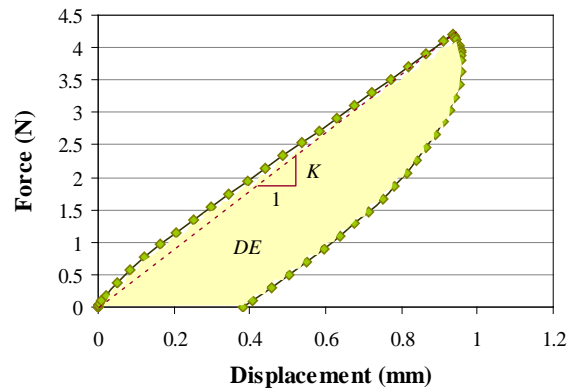


Figure M4a.4. Typical force-displacement curve obtained for a microstructure in which the material properties within the FAM change as a function of probable air void distributions

It was also found that Weibull probabilistic distributions provide a good representation of the mechanical performance of the moisture-conditioned mixtures. This information is useful to conduct probabilistic analysis on the expected response of an asphalt mixture layer that is characterized by certain spatial dispersion of the of air void phase.

Significant Results

Lattice Micromechanical Model

The reader is referred the work element F3b.

Cohesive Zone Micromechanical Model

In previous quarters, the micromechanical model was successfully applied to study the role of different physical and mechanical material properties of the mixture on its susceptibility to moisture damage. In this quarter, it was demonstrated that the coupled model can be efficiently used in combination with stochastic theory to incorporate the complexity of the internal air void structure in the micromechanical modeling of moisture damage in asphalt mixtures. A paper containing the main findings from this study (titled "Stochastic Micromechanical Modeling of Asphalt Mixtures Subjected to Moisture Diffusion Processes") was submitted for evaluation to the International Journal for Numerical and Analytical Methods in Geomechanics.

Significant Problems, Issues and Potential Impact on Progress

Lattice Micromechanical Model

The reader is referred the work element F3b.

Cohesive Zone Micromechanical Model

None

Work Planned Next Quarter

Lattice Micromechanical Model

The reader is referred the work element F3b.

Cohesive Zone Micromechanical Model

The researchers plan to use the micromechanical model to conduct a numerical study on the relationship that exists between the ideal and practical work of adhesive fracture in asphalt mixtures. This task is strongly related to the work conducted as part of the subtask F1a-4. The researchers will also evaluate the convenience of including special thermodynamic considerations to better describe moisture saturation processes occurring at the aggregate-FAM interfaces.

Cited References

El-Kadi, A.I., and S.A. Williams, 2000, Generating two-dimensional fields of autocorrelated, normally distributed parameters by the matrix decomposition technique. *Ground Water*, 38(4): 523-532.

Journal Papers

Caro, S., E. Masad, A. Bhasin, D. Little, and M. Sanchez-Silva, 2009a, Probabilistic Modeling of the Effect of Air Voids on the Mechanical Performance of Asphalt Mixtures Subjected to Moisture Diffusion. *Journal of the Association of Asphalt Paving Technologists (AAPT)* (submitted for evaluation).

Caro, S., E. Masad, M. Sanchez-Silva, and D. Little, 2009b, Stochastic Micromechanical Modeling of Asphalt Mixtures Subjected to Moisture Diffusion Processes. *The International Journal for Numerical and Analytical Methods in Geomechanics* (submitted for evaluation).

Work Element M4b: Analytical Fatigue Model for Mixture Design

The initial development of this work element is the same as Subtask F3c-1. The development of a method to separate the viscoelastic response from fatigue damage and the development of a model to analyze resistance to fatigue cracking under both dry and wet conditions is provided under subtask F1b-1. See the progress reported under Work Element F3c.

Work Element M4c: Unified Continuum Model

Work Done This Quarter

The reader is referred the work element F3c.

CATEGORY M5: MOISTURE DAMAGE PREDICTION SYSTEM




This area is planned to start later in the project.

Moisture Damage Year 3		Year 3 (4/09-3/10)												
		4	5	6	7	8	9	10	11	12	1	2	3	
Adhesion														
M1a	Affinity of Asphalt to Aggregate - Mechanical Tests													
M1a-1	Select Materials													
M1a-2	Conduct modified DSR tests													
M1a-3	Evaluate the moisture damage of asphalt mixtures												P	
M1a-4	Correlate moisture damage between DSR and mix tests												P	P
M1a-5	Propose a Novel Testing Protocol													P
M1b	Work of Adhesion													
M1b-1	Adhesion using Micro calorimeter and SFE							JP						
M1b-2	Evaluating adhesion at nano scale using AFM													
M1b-3	Mechanisms of water-organic molecule competition													
M1c	Quantifying Moisture Damage Using DMA													
Cohesion														
M2a	Work of Cohesion Based on Surface Energy													
M2a-1	Methods to determine SFE of saturated binders													
M2a-2	Evaluating cohesion at nano scale using AFM													
M2b	Impact of Moisture Diffusion in Asphalt													
M2b-1	Diffusion of moisture through asphalt/mastic films							JP					D	F
M2b-2	Kinetics of debonding at binder-aggregate interface													
M2c	Thin Film Rheology and Cohesion													
M2c-1	Evaluate load and deflection measurements using the modified PATTI test													
M2c-2	Evaluate effectiveness of the modified PATTI test for Detecting Modification													
M2c-3	Conduct Testing												JP	
M2c-4	Analysis & Interpretation												D	
M2c-5	Standard Testing Procedure and Recommendation for Specifications				D									
Aggregate Surface														
M3a	Impact of Surface Structure of Aggregate													
M3a-1	Aggregate surface characterization													
Modeling														
M4a	Micromechanics model development				2JP		JP							JP
M4b	Analytical fatigue model for use during mixture design													
M4c	Unified continuum model				JP		JP							JP
M5	Moisture Damage Prediction System													

LEGEND

Deliverable codes

- D: Draft Report
- F: Final Report
- M&A: Model and algorithm
- SW: Software
- JP: Journal paper
- P: Presentation
- DP: Decision Point
- [x]

-  Work planned
-  Work completed
-  Parallel topic

Deliverable Description


- Report delivered to FHWA for 3 week review period.
- Final report delivered in compliance with FHWA publication standards
- Mathematical model and sample code
- Executable software, code and user manual
- Paper submitted to conference or journal
- Presentation for symposium, conference or other
- Time to make a decision on two parallel paths as to which is most promising to follow through
- Indicates completion of deliverable x

Moisture Damage Year 2 - 5		Year 2 (4/08-3/09)				Year 3 (4/09-3/10)				Year 4 (04/10-03/11)				Year 5 (04/11-03/12)					
		Q1	Q2	Q3	Q4	Q1	Q2	Q3	Q4	Q1	Q2	Q3	Q4	Q1	Q2	Q3	Q4		
Adhesion																			
M1a	Affinity of Asphalt to Aggregate - Mechanical Tests																		
M1a-1	Select Materials		DP																
M1a-2	Conduct modified DSR tests		P		P														
M1a-3	Evaluate the moisture damage of asphalt mixtures				DP					P	P								
M1a-4	Correlate moisture damage between DSR and mix tests									P	P								
M1a-5	Propose a Novel Testing Protocol				P					P						JP, F			
M1b	Work of Adhesion																		
M1b-1	Adhesion using Micro calorimeter and SFE								JP					JP,F					
M1b-2	Evaluating adhesion at nano scale using AFM								JP					JP			JP, F		
M1b-3	Mechanisms of water-organic molecule competition				JP								JP	D	F				
M1c	Quantifying Moisture Damage Using DMA													JP	D	F			
Cohesion																			
M2a	Work of Cohesion Based on Surface Energy																		
M2a-1	Methods to determine SFE of saturated binders															JP			
M2a-2	Evaluating cohesion at nano scale using AFM								JP					JP			JP, F		
M2b	Impact of Moisture Diffusion in Asphalt																		
M2b-1	Diffusion of moisture through asphalt/mastic films								JP	D	F			JP	D	F			
M2b-2	Kinetics of debonding at binder-agreagte interface													JP	D	F			
M2c	Thin Film Rheology and Cohesion																		
M2c-1	Evaluate load and deflection measurements using the modified PATTI test	DP	JP	D	F														
M2c-2	Evaluate effectiveness of the modified PATTI test for Detecting Modification			D	DP,F														
M2c-3	Conduct Testing									JP									
M2c-4	Analysis & Interpretation				P					D			D, JP		F				
M2c-5	Standard Testing Procedure and Recommendation for Specifications					D								D	P,F				
Aggregate Surface																			
M3a	Impact of Surface Structure of Aggregate																		
M3a-1	Aggregate surface characterization																		
Models																			
M4a	Micromechanics model development				JP	2JP	JP			JP						M&A	D	DP	F, SW
M4b	Analytical fatigue model for use during mixture design																	M&A,D	F
M4c	Unified continuum model					JP	JP			JP						M&A	D	DP	F, SW
M5	Moisture Damage Prediction System																		

LEGEND

Deliverable codes

- D: Draft Report
- F: Final Report
- M&A: Model and algorithm
- SW: Software
- JP: Journal paper
- P: Presentation
- DP: Decision Point
- [x]

-  Work planned
-  Work completed
-  Parallel topic

Deliverable Description

- Report delivered to FHWA for 3 week review period.
- Final report delivered in compliance with FHWA publication standards
- Mathematical model and sample code
- Executable software, code and user manual
- Paper submitted to conference or journal
- Presentation for symposium, conference or other
- Time to make a decision on two parallel paths as to which is most promising to follow through
- Indicates completion of deliverable x

PROGRAM AREA: FATIGUE

CATEGORY F1: MATERIAL AND MIXTURE PROPERTIES

Work Element F1a: Cohesive and Adhesive Properties

Subtask F1a-1: Critical Review of Measurement and Application of Cohesive and Adhesive Bond Strengths (TAMU)

Work Done This Quarter

A draft journal paper summarizing the evidence from the literature on the differences between the ideal work of fracture to the practical work of fracture was completed. The paper also included findings from tests conducted on asphalt materials.

Significant Results

None

Significant Problems, Issues and Potential Impact on Progress

None

Work Planned Next Quarter

Improvements to this white paper will be made continually based on literature review. In addition, researchers plan to validate the findings from this paper in the context of bituminous materials by accomplishing the various subtasks in this work element.

Subtask F1a-2: Develop Experiment Design (TAMU)

Work Done This Quarter

The experiment design was completed and reported in the last quarterly report.

Work Planned Next Quarter

At this time, researchers do not anticipate any changes to this experiment design. However, as the work progresses in this subtask and in the area of modeling, some refinement to the proposed experiment design may be required in future.

Subtask F1a-3: Thermodynamic Work of Cohesion and Adhesion (Year 1 start)

Work Done This Quarter

The objective of this subtask is to provide the surface free energy of asphalt binders that will be used in other subtasks as a material property input or for the comparison with results from other test methods. Based on the requirements from other tasks, tests under this subtask will be ongoing through the remainder of this project.

Work Planned Next Quarter

Based on the requirements from other tasks, tests under this subtask will be ongoing through the remainder of this project.

Subtask F1a-4: Mechanical Work of Adhesion and Cohesion

Work Done This Quarter

A direct relationship between ideal and practical work of fracture was found using a pull-off test utilizing stainless steel substrate and thin asphalt films. The practical work of fracture was calculated as the area under the force-displacement curve. Through the use of image analysis, the ideal work of fracture, or effective ideal work of fracture, was calculated based on the percent adhesive and cohesive failure measured from each failed sample holder as seen in equation (F1a-4.1).

$$\text{Effective Ideal Work of Fracture} = P_a \times \text{Adhesive Energy} + P_c \times \text{Cohesive Energy} \quad (\text{F1a-4.1})$$

Where P_a is the percent adhesive failure, *Adhesive Energy* is the adhesive bond energy between the asphalt and substrate, P_c is the percent cohesive failure, and *Cohesive Energy* is the cohesive bond strength of the asphalt binder. Figures F1a-4.1 and F1a-4.2 display the relationship between practical work of fracture and effective ideal work of fracture.

The amount of energy dissipated (practical work of fracture) is affected by the loading rate of the test, the film thickness of the asphalt binder, the material properties of the substrate and thin film, the temperature the test is conducted at, and the moisture content at the interface between the asphalt film and substrate. In order to measure these variables and see their affect on the practical work of fracture, a new testing setup was developed. The new testing setup is less prone to vertical misalignments and will hopefully decrease the variability of the results. Instead of using stainless steel as the substrate, two different aggregates are being used to better simulate field conditions along with the three original asphalt binders.

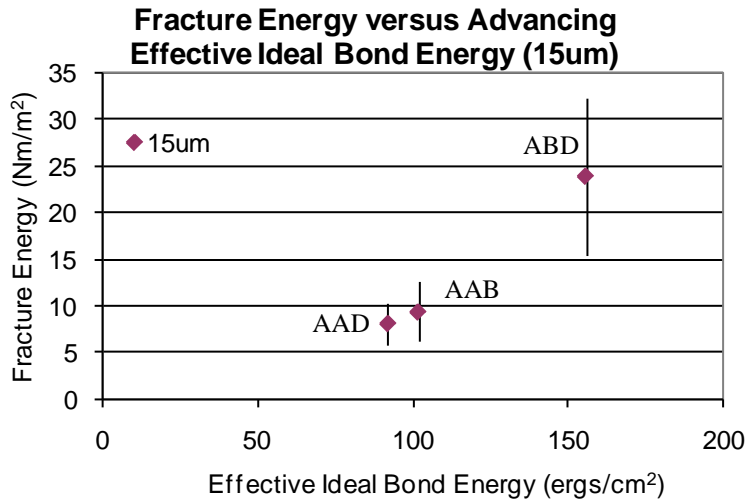


Figure F1a-4.1. Relationship between fracture energy (practical work of fracture) and effective ideal work of fracture at 40- μ m film thickness

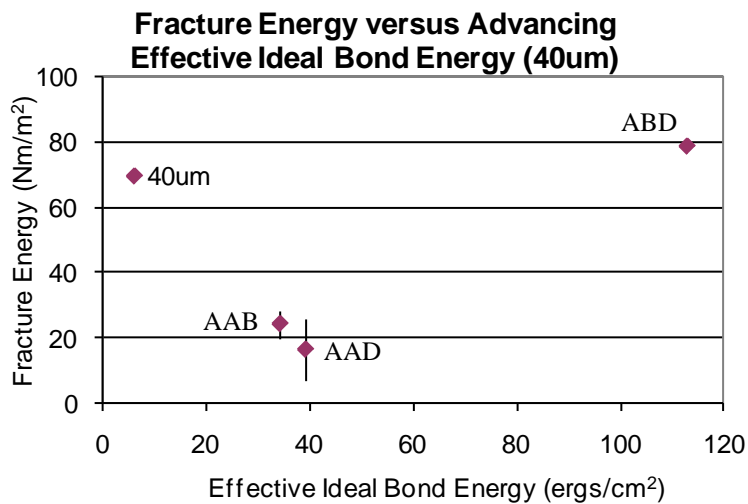


Figure F1a-4.2. Relationship between fracture energy (practical work of fracture) and effective ideal work of fracture at 40- μ m film thickness

Significant Results

Paper Submitted to AAPT: “Relationship of Ideal Work of Fracture to Practical Work of Fracture: Background and Experimental Results”

Significant Problems, Issues and Potential Impact on Progress

None

Work Planned Next Quarter

Researchers will begin testing aggregate-asphalt samples while alternating the following variables:

- Loading rate
- Film thickness
- Temperature
- Moisture content at the interface
- Material properties

The influence of these variables on the dissipated energy, and ultimately, on the practical work of fracture will be determined based on the results of the experiments that will be conducted in the coming quarter.

Journal Papers

Masad, E., J. Howson, A. Bhasin, S. Caro, and D. Little, 2009, Relationship of Ideal Work of Fracture to Practical Work of Fracture: Background and Experimental Results. *Journal of the Association of Asphalt Paving Technologists* (AAPT) (submitted for evaluation).

Subtask F1a-5: Evaluate Acid-Base Scale for Surface Energy Calculations

Work Done This Quarter

No activity was planned for this quarter.

Work Planned Next Quarter

Work on this subtask is planned in year 4 of this project.

Work Element F1b: Viscoelastic Properties (Year 1 start)

Subtask F1b-1: Separation of Nonlinear Viscoelastic Deformation from Fracture Energy under Cyclic Loading (TAMU)

Work Done This Quarter

The main objective of this task was to develop an approach to determine the following three main aspects of material response during cyclic loading:

- i) identify the limiting stress or strain amplitude that results in a nonlinear viscoelastic response without causing damage,
- ii) model and monitor the change in the nonlinear viscoelastic parameters with increasing number of load cycles, and
- iii) model and monitor the change in the nonlinear viscoelastic parameters within each cycle.

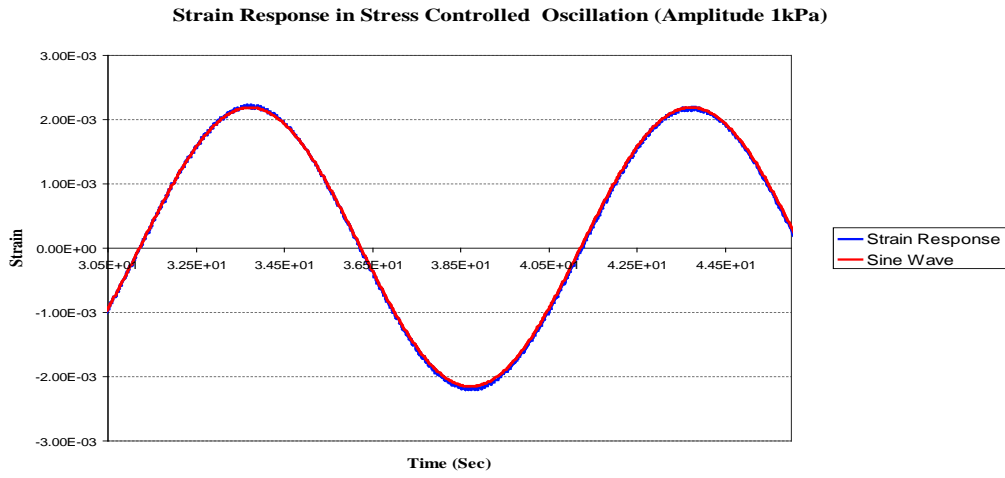
Researchers have made significant progress to achieve the first two steps that were reported in the previous quarterly reports. The last step is important because the researchers hypothesized that during each load cycle only specific portions of the load cycle contribute to damage. Also, in order to obtain accurate estimate of the dissipated energy due to fatigue damage, the non-linear viscoelastic response and response due to damage must be accurately modeled and discounted for at each and every point within the load cycle.

The modeling effort was primarily geared towards FAM. However, pending the fabrication of FAM specimens using the selected core materials researchers decided to evaluate the model using asphalt binder. In last quarter the mechanical response of binders subjected to cyclic loading at different amplitudes was investigated. Different types of binders were tested under torsion using the DMA. Binders with different PG grades were selected in order to ensure a broad spectrum of mechanical properties. Most of these binders were polymer modified and were tested in torsional shear using DMA. The cone and plate geometry was used in order to have a uniform stress-strain distribution.

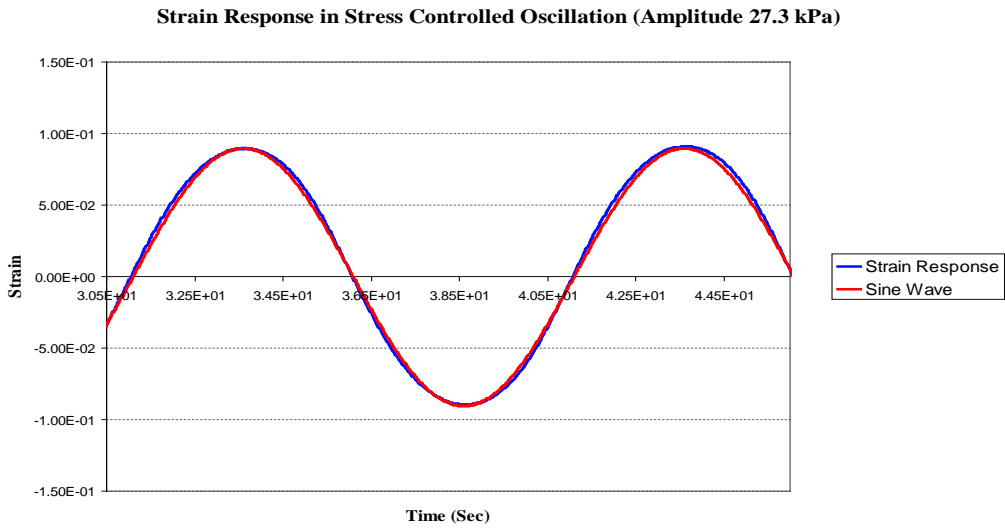
The hypothesis behind this effort is briefly described here. When a time dependent material is subjected to a cyclic sinusoidal load the steady state response also follows a sinusoidal response for a linear material. However, when the stress levels are high and the response is non-linear the steady state response deviated from a sinusoidal curve and there exists a non-uniform phase angle throughout the loading cycle. By conducting stress sweep test on binders, it was observed that the response at low stress levels exactly follows a sine wave, as expected (figure F1b-1.1a). However, when the amplitude was increased the strain response was symmetric but did not follow a sine wave (figure F1b-1.1b). A further increase in the stress amplitude resulted in an asymmetric response with an amplitude that changed with each load cycle (figure F1b-1.1c). In summary the following three stages could be observed:

1. At low stress levels the strain response perfectly followed a sinusoidal curve and the amplitude of the response did not change with increasing number of cycles.
2. At intermediate stress levels the strain response deviated from a sinusoidal curve (indicating non-linear behavior) but the amplitude did not change with increasing number of cycles.
3. At high stress levels the strain response deviated from a sinusoidal curve (indicating non-linear behavior) and the material response changed with increasing number of cycles (indicating significant change in the material properties with increasing number of cycles).

a)



b)



c)

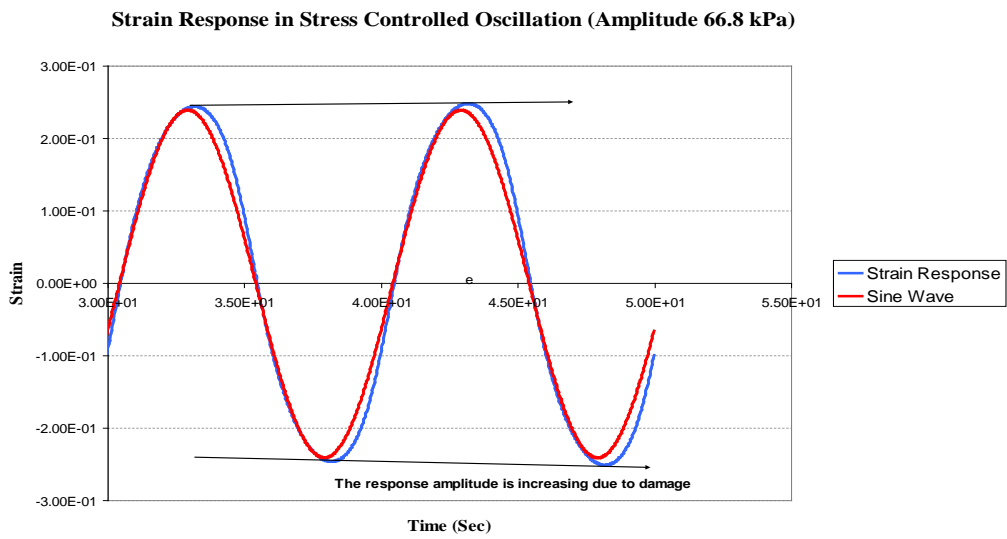


Figure F1b-1.1. Strain response under stress controlled oscillation.

It was speculated that the change in material response with increasing number of cycles could be due to plastic deformation resulting in hardening or softening of the material and the deviation from sine wave before going through damage is due to material nonlinearity. The next step was to model the nonlinear response using the model originally proposed by Schapery. In order to quantify nonlinearity in binder several creep and recovery tests at different stress levels were conducted. The stress levels were 0.1, 1, 5, 10, 20, 40, and 60 kPa and the number of replicates was three. The loading duration was 5 sec and recovery time was 500 sec. The test temperature was 40°C. The results from creep and recovery tests indicated that even at low strain levels there was some level of permanent deformation in the material. Consequently, the observed nonlinearity under cyclic loading was in fact due to change in material properties due to plastic deformation.

Further investigations showed that due to Weissenberg effect in non-Newtonian fluids, a normal force will be generated that will change the stress state of the material. Presence of any type of normal force will lead to interaction nonlinearity in which material will show less torsional stiffness due to effect of normal force rather than pure shear, figure F1b-1.2.

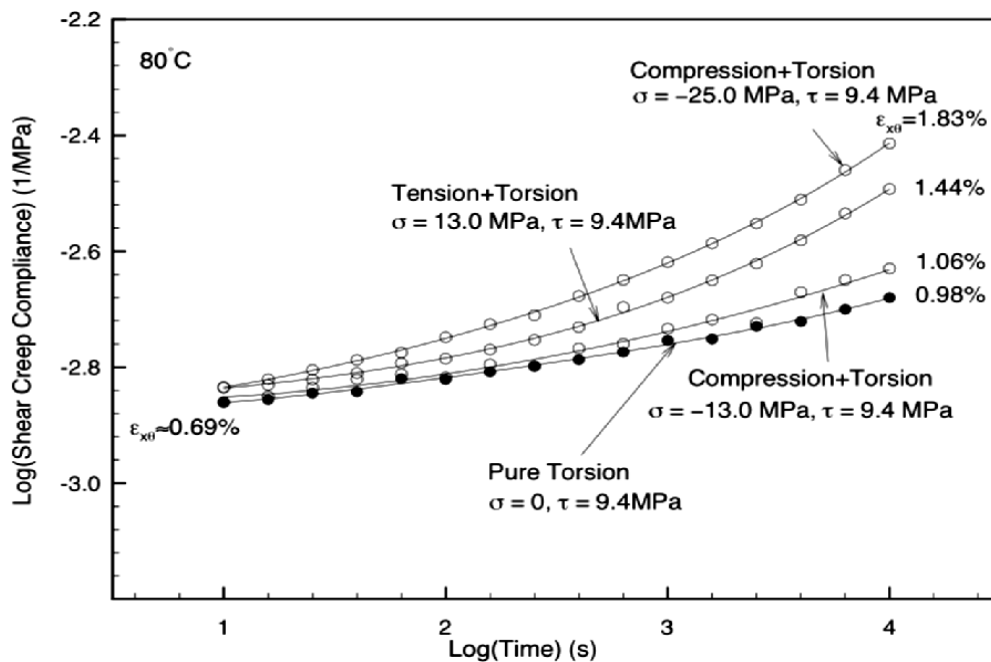


Figure F1b-1.2. Shear creep compliance curves for pure torsion and torsion with superimposed tension or compression for PMMA. Change in creep compliance with multiaxial load test illustrates interaction nonlinearity (Lu and Knauss 1999).

Work Planned Next Quarter

In the next quarter, we will conduct similar tests on typical FAM specimens. We will also try to model the plastic deformation and nonlinearity in the binder tests by including the effect due to the normal force acting from the specimen.

Subtask F1b-2: Separation of Nonlinear Viscoelastic Deformation from Fracture Energy under Repeated and Monotonic Loading

Work Done This Quarter

A technical paper, entitled “Distribution of Crack Size in Asphalt Mixtures”, was completed and submitted for presentation to The Transportation Research Board (TRB) 89th Annual Meeting, which will be held in Washington, D.C., January 2010. This paper details the Weibull distribution model for the air void/crack size in asphalt mixtures, which was developed based on the dissipated Pseudo Strain energy (DPSE) theory and was briefly summarized in Subtask F1b-2 of the last quarterly report. Preliminary results of this Weibull distribution model were presented in The 46th Petersen Asphalt Research Conference in Laramie, Wyoming, July 2009.

In this quarter, the DPSE theory was further developed to more accurately determine the Paris’ Law coefficients, A and n . This newly developed method of determining A and n made use of the test results from the Viscoelastic Characterization (VEC) test and the Repeated Direct Tension (RDT) test, which were presented in Work Element F2c of the previous quarterly reports. As a result, the relaxation modulus test and the tensile strength test could be avoided, which involved assumptions for simplicity and empirical curve fitting in the test data analysis (Si 2001; Arambula 2007). The nondestructive VEC test provides the properties of the undamaged intact asphalt mixtures; the destructive controlled-strain RDT test was conducted on the same asphalt mixture specimen to obtain the material properties at various numbers of loading cycles. As the number of loading cycles increased, the crack radius increased so the cross section of the specimen was losing area. As a result, there was less cross-sectional area to sustain the stress. In addition, the stress sustained by the intact material at the cross section was nonuniform since there was stress concentration at the crack tips. The mean of this nonuniform stress was defined as the “true stress”. The applied load divided by the whole cross-sectional area was defined as the “apparent stress”. The true stress was associated with the true complex modulus and true DPSE, while the apparent stress was associated with the apparent complex modulus and apparent DPSE. Based on the test data from the VEC test and the controlled-strain RDT test, the true complex modulus, apparent complex modulus, true DPSE, apparent DPSE and elastic pseudo strain energy (EPSE) were determined. The relation between the true DPSE and the apparent DPSE was used to calculate the ratio of true stress to apparent stress. After the stress ratio was determined, the true stress was computed as the mean of the nonuniform stress distribution in the intact material on the cross section. This calculation took into account the stress concentration at the crack tips and the nonuniform stress distribution close to the crack tips.

In the controlled-strain RDT test, both true DPSE and apparent DPSE were in fact accumulating as the damage accumulated in the specimen. More specifically, the DPSE reflected the damage accumulation from the undamaged state of the specimen to the current damaged state. This damage accumulation corresponded to crack growth from the initial air void size to the current crack radius. Similarly, the EPSE was also accumulated as the number of loading cycles increased in the RDT test. For a single loading cycle, N_i , the redistribution of the EPSE can be expressed in Equation F1b-2.1 with a crack increment of Δc_i :

$$\begin{aligned}
 \text{Measured EPSE} &= \text{EPSE of intact material} \\
 &\quad - \text{released EPSE due to growth of } \Delta c_i \\
 &\quad + \text{stored surface energy due to growth of } \Delta c_i
 \end{aligned}
 \tag{F1b-2.1}$$

At the loading cycle N , corresponding to the current crack radius c ($c = \sum_{i=1}^n \Delta c_i$), Equation F1b-2.1 needs to be revised as follows:

$$\begin{aligned}
 \text{Accumulated measured EPSE} &= \text{accumulated EPSE of intact material} \\
 &\quad - \text{released EPSE due to growth of } c \\
 &\quad + \text{stored surface energy due to growth of } c
 \end{aligned}
 \tag{F1b-2.2}$$

in which the accumulated measured EPSE is calculated by the measured EPSE of load cycle N multiplied by an energy accumulation ratio. Consequently, by solving Equation F1b-2.2, the average crack radius c can be expressed as a function of several measured variables as shown in Equation F1b-2.3:

$$c = f(\text{stress ratio, energy accumulation ratio, measured DPSE}) \tag{F1b-2.3}$$

As a result, the average crack radius of any arbitrary number of loading cycles, N , can be determined directly from the controlled-strain RDT test using Equation F1b-2.4. Plotting c versus N on the logarithmic scale generates a straight line as shown in figure 1b-2.1.

$$c = DN^e \tag{F1b-2.4}$$

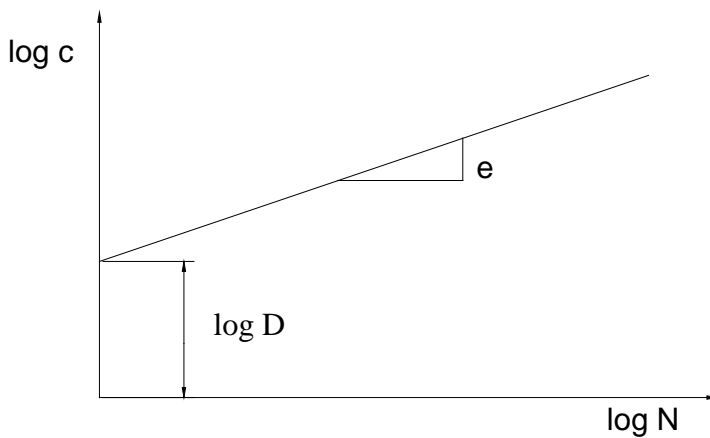


Figure F1b-2.1. Crack growth in controlled-strain RDT test.

Another expression for c was obtained using Paris' Law and was stated in the last quarterly report:

$$c = \left[(c_0)^{\frac{2n+1}{n+1}} + \left(\frac{2n+1}{n+1} \right) A^{\frac{1}{n+1}} \left(\frac{b}{4\pi M} \right)^{\frac{n}{n+1}} N \right]^{\frac{n+1}{2n+1}} \quad (\text{F1b-2.5})$$

Comparing Equations F1b-2.4 and F1b-2.5 yields the expressions for A and n as follows:

$$A = D^{(2n+1)} \left(\frac{n+1}{2n+1} \right)^{(n+1)} \left(\frac{4\pi M}{b} \right)^n \quad (\text{F1b-2.6})$$

$$n = \frac{1-e}{2e} \quad (\text{F1b-2.7})$$

Significant Results

The ability to characterize fatigue cracking using the controlled-strain RDT test protocol was extended by developing this analytical method for A and n . The values thus calculated matched well with other published values for asphalt mixtures using similar tests (Arambula 2007; Walubita 2006). In addition, the results were verified using Schapery's theory of crack growth for viscoelastic material. It was demonstrated that this method can produce accurate and realistic values for the Paris' Law fracture parameters.

Significant Problems, Issues and Potential Impact on Progress

The new MTS is still not ready to run tests. The software programming has not finished yet. It is expected that the new MTS will be ready in this quarter so more testing can be accomplished.

Work Planned Next Quarter

The newly developed analytical method for Paris' Law coefficients will be finalized and documented in a technical paper. The presentation slides will be prepared for the next TRB Annual Meeting if the paper is accepted for presentation.

A healing test protocol will be initiated to study the healing properties of asphalt mixtures.

References

Arambula, E., 2007, *Influence of Foundational Material Properties and Air Void Structure on Moisture Damage of Asphalt Mixes*. Ph.D. Dissertation, Texas A&M University, College Station, Texas.

Si, Z., 2001, *Characterization of microdamage and healing of asphalt concrete mixtures*. Ph.D. Dissertation, Texas A&M University, College Station, Texas.

Walubita, L.F., A. Epps Martin, C.J. Glover, and R.L. Lytton, 2006, Computation of Pseudo Strain Energy and Paris Law Fracture Coefficients from Surface Energy and Uniaxial Strain-Controlled Tension Test Data. *International Journal of Pavement Engineering*, 7(3): 167-178.

Work Element F1c: Aging

Subtask F1c-1: Critical Review of Binder Oxidative Aging and Its Impact on Mixtures (TAMU)

Work Done This Quarter

No significant literature reports were noted this quarter.

Significant Problems, Issues and Potential Impact on Progress

There are no problems or issues.

Work Planned Next Quarter

Review of literature and other work is an ongoing effort.

Subtask F1c-2: Develop Experimental Design (TAMU)

Work Done This Quarter

A draft experimental design was submitted last quarter. Final selection of materials (binder and aggregate) for testing has been determined.

Significant Results

The pilot experiment design was completed, and specimen fabrication (Subtask F1c-4) continued and was completed. Testing of the specimens has been delayed by equipment issues (Subtask F1c-4).

Significant Problems, Issues and Potential Impact on Progress

Further review of the core materials for use in the expanded experiment and of additional field sites for validation is needed.

Work Planned Next Quarter

Conducting the laboratory experiments of the experimental design that use the improved testing protocol (work element F2c) has been delayed by equipment difficulties but will begin in the next quarter. Also, additional field site cores for use in validation of the transport oxidation model and for evaluating the impact of binder oxidation on fatigue will be obtained from WRI.

Subtask F1c-3: Develop a Transport Model of Binder Oxidation in Pavements (TAMU)

Work Done This Quarter

Early results on laboratory measurements of diffusivity for neat binders are showing values of the order of 10^{-12} m²/s. This result is consistent with previous approximate measurements in our laboratories, but those early data provide a big target. Additional data will more precisely determine diffusivity values and their changes with binder oxidative hardening and the addition of aggregate fines. These values and effects are essential parameters for the transport oxidation model.

To assess the sensitivity of oxidation diffusivity values, pavement oxidation rate calculations were made over a wide range of diffusivities. From our previous results, binder diffusivity is related to viscosity (dynamic, low shear-rate at 60 °C, h_o^*) approximately according to $D = D_o h_o^{*B}$. Model calculations for a binder with known reaction kinetics parameters are shown in figure F1c-3.1. The calculations are for a specific location in Arizona and for a one-year time period for which temperature profiles were previously calculated, and for 20 mm below the pavement surface. Calculations for the diffusivity indicated as level M ($D_o = 4 \times 10^{-9}$ m²/s) is approximately 10^{-12} m²/s. Then, calculations for one order of magnitude greater and smaller values of D_o are shown, plus one for nine orders of magnitude higher. This latter calculation is shown as the limiting case of essentially no diffusion resistance in the binder. The other extreme condition, that of infinite diffusion resistance, would show very low oxidation, as only the binder at the very surface of the pores would oxidize. Thus, we see significant effects of diffusion resistance, but not at all to the point of eliminating binder oxidation at distances away from the pore surfaces.

Figure F1c-3.2 shows a similar plot at 160 mm below the pavement surface. Again, the effect of varying diffusion is clearly seen, but in each case, oxidation is significant. Future measurements of diffusivity and determinations of binder oxidation in pavements will provide improved information on the accuracy of these model calculations.

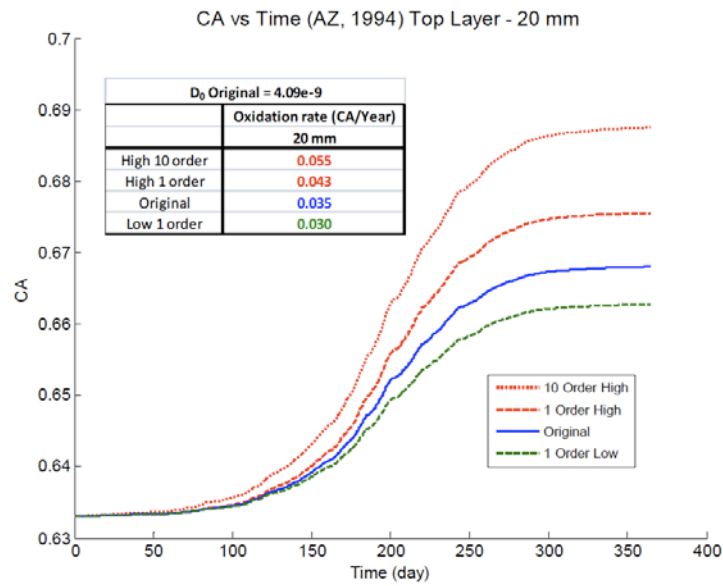


Figure F1c-3.1. The sensitivity of pavement binder oxidation calculations to variations in diffusivity, 20 mm below the pavement surface.

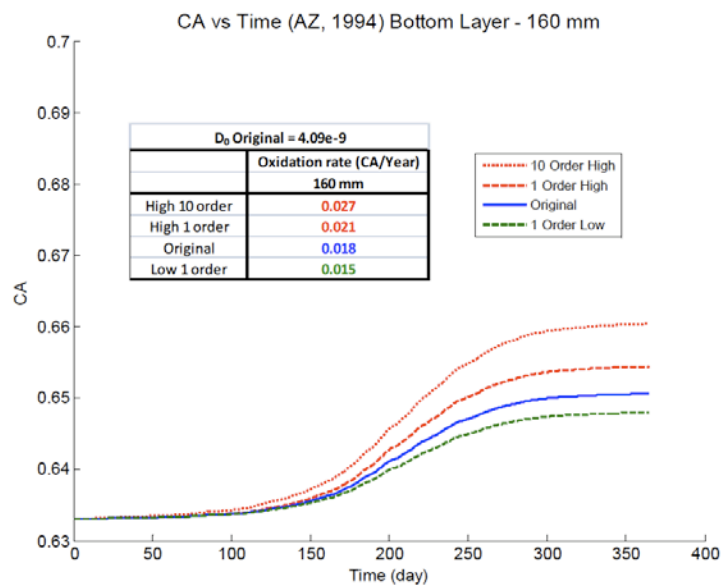


Figure F1c-3.2. The sensitivity of pavement binder oxidation calculations to variations in diffusivity, 160 mm below the pavement surface.

Significant Results

The ability to estimate binder oxidation in pavements as a function of time and depth, and in a full range of climates, has been demonstrated. These estimates also now include the full range of binder oxidation over both the fast-rate and constant-rate periods. These calculations are essential for providing a foundation for mixture model calculations that include binder (and thus pavement) changes over time due to binder oxidation and thus an improved understanding of pavement durability. At the same time, mixture models that include crack growth over time will provide changes to the binder oxidation model in the form of increasing numbers of pores (cracks) that can transport oxygen to the pavement interior.

Significant Problems, Issues and Potential Impact on Progress

Further binder oxidation model validation is needed. More actual pavement aging rates need to be compared to model calculations. Pending finalizing the mixture testing methods, pavement cores will be tested for physical properties (subtask F1c-4) in the next quarter. Also, air void characteristic data for the corresponding pavements will be measured.

Also, binders from field cores will be extracted, recovered, and tested to assess binder aging as a function of time and depth. Ideally, the physical properties of cores (fatigue, e.g.) will be measured before the destructive determination of air voids and extraction and recovery so that a complete set of matching data will be available for each core. The purpose of this specific protocol is to provide binder oxidation as a function of core age and depth on the very same cores as the mixture tests. In this way, the effects of binder oxidative hardening will be more closely matched to changes in the mixture physical properties due to this hardening. However, whether this protocol can be followed will depend upon the progress with mixture testing development.

Work Planned Next Quarter

Work the next quarter will proceed with field core tests to determine air voids and binder properties as a function of depth below the surface. Depending on mixture testing progress, these characterization tests will be done either following mixture testing (the preferred method) or on replicate cores without mixture testing.

Publications

Prapaitrakul, Nikornpon, Rongbin Han, and Charles J. Glover, 2009, A Transport Model of Asphalt Binder Oxidation in Pavements. *Road Materials and Pavement Design*, 10 (Special Issue): 95-113.

Submitted for Publication

Rongbin Han, Xin Jin, and Charles J. Glover. "Modeling Pavement Temperature for Use in Binder Oxidation Models and Pavement Performance Prediction," submitted July 2009 to *Journal of Materials in Civil Engineering*.

Presentations

Prapaitrakul, Nikornpon, Rongbin Han, Xin Jin, and Charles J. Glover. “Transport Model Calculations of Asphalt Binder Oxidation in Pavements,” presented at the 46th Annual Petersen Asphalt Research Conference, Laramie, Wyoming, July 14, 2009.

Prapaitrakul, Nikornpon, Rongbin Han, Xin Jin, and Charles J. Glover, “A Transport Model of Asphalt Binder Oxidation in Pavements,” presented at the 3rd International Conference on Asphalt Materials, Qingdao, Shandong Province, China, August 6, 2009.

Subtask F1c-4: The Effects of Binder Aging on Mixture Viscoelastic, Fracture, and Permanent Deformation Properties (TAMU)

Work Done This Quarter

In this quarter, a testing and data analysis method was developed to obtain the properties of the aged field asphalt mixtures. The field cores were cut into rectangular specimens for testing. The rectangular specimen was set up in the environmental chamber of the Material Testing System (MTS). Four vertical linear variable differential transformers (LVDTs) and two horizontal LVDTs were installed on the four surfaces of the test specimen in order to measure the vertical and horizontal deformations of the specimen. A monotonically increasing tensile load was applied to the specimen until the weakest side of the specimen had a strain of $80\mu\epsilon$. The number of $80\mu\epsilon$ was regarded as the fatigue endurance limit, under which the specimen would not be further damaged. The same test was conducted on the same specimen at three temperatures (10°C , 20°C and 30°C) in order to construct the master curves of the magnitude and phase angle of the complex modulus. Work Element E1a presents the details of this testing and data analysis method for characterizing aged field asphalt mixtures.

In addition to the measurement of the tensile properties of the aged asphalt mixtures, a testing and data analysis method was developed to characterize the anisotropic compressive properties of asphalt mixtures. Three nondestructive test scenarios were conducted on the same test sample: i) uniaxial compressive creep test, ii) uniaxial tensile creep test, and iii) indirect tensile creep test. The Universal Testing Machine (UTM) was used to run the compressive creep tests and the indirect tensile creep tests, and the Material Testing System (MTS) was utilized to conduct the tensile creep tests. These three tests were repeated on the same specimen at three temperatures (10°C , 20°C and 30°C) in order to construct master curves of the complex modulus. Equations F1c-4.1 and F1c-4.2 were used to model the master curves of the magnitude and phase angle of the complex modulus, respectively.

$$|E^*(\omega)| = \frac{E_g}{\left[1 + \left(\frac{\omega_c E}{\omega \cdot 10^{C(T-T_r)}} \right)^{R_E} \right]^{\frac{\log 2}{\log 2}} \frac{R_E}{\log 2}} \quad (\text{F1c-4.1})$$

where E_g = glassy modulus of the asphalt mixture, MPa; ω_{cE} = crossover frequency of the asphalt mixture, rad/sec; R_E = rheological index for modulus; and C = slope of temperature shift factor.

$$\varphi_E = \frac{\varphi_{mE}}{\left[1 + \frac{\log \left(\frac{\omega_{mE}}{\frac{C_1(T-T_r)}{\omega \cdot 10^{C_2+(T-T_r)}}} \right)}{R_{\varphi E}} \right]^2}^{\frac{m}{2}} \quad (F1c-4.2)$$

in which φ_{mE} = the maximum phase angle for modulus, degrees; ω_{mE} = the frequency where φ_{mE} occurs, rad/sec; $R_{\varphi E}$ = fitting parameters for modulus; T_r = reference temperature; and C_1 and C_2 = constants. The master curves of the magnitude and phase angle of the compressive complex modulus are shown in figures F1c-4.1 and F1c-4.2, respectively.

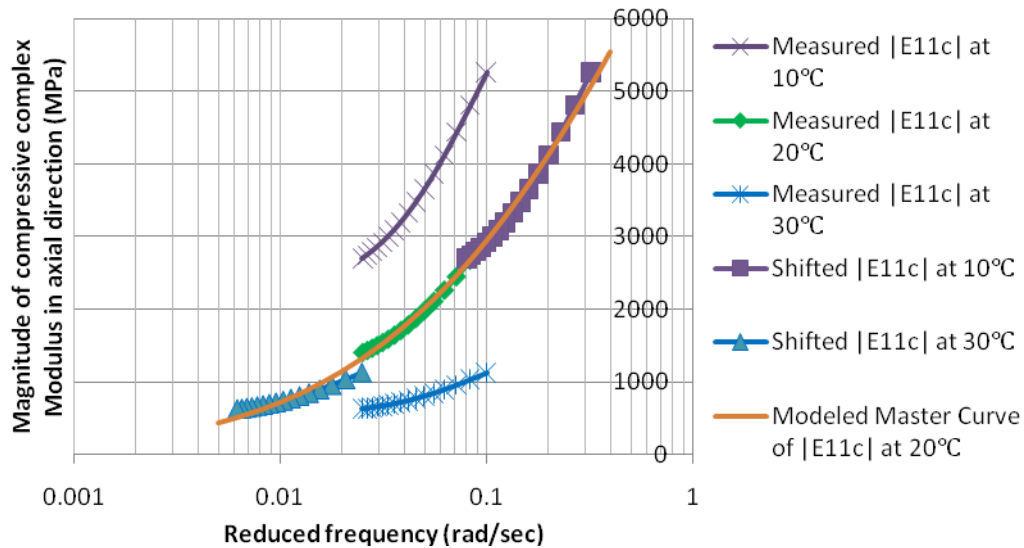


Figure F1c-4.1. Master curve of the magnitude of the compressive complex modulus at reference temperature 20°C.

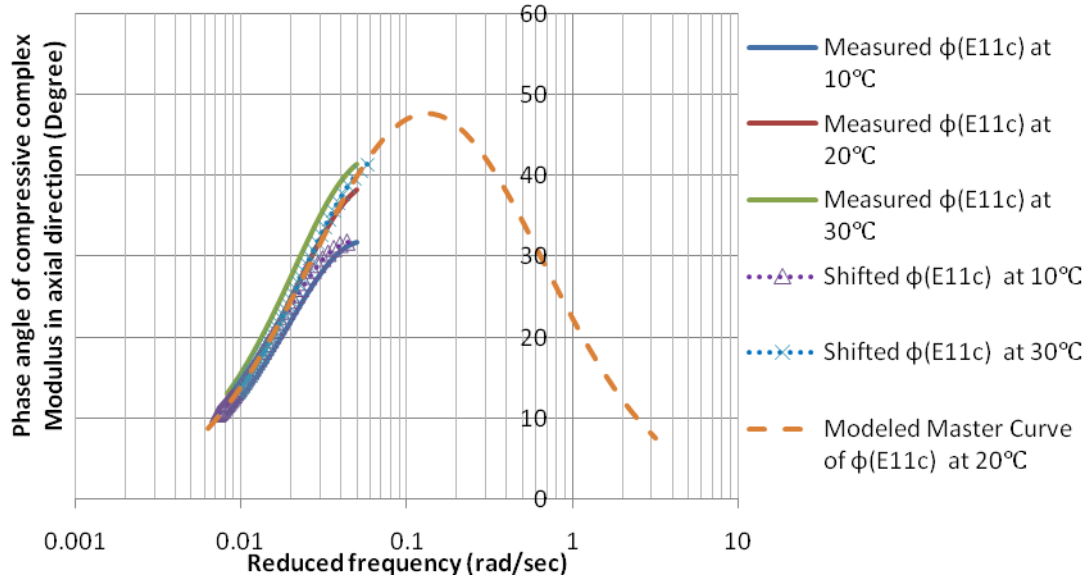


Figure F1c-4.2. Master curve of the phase angle of the compressive complex modulus at reference temperature 20°C.

The compressive complex Poisson’s ratio was also determined using the three test scenarios. The master curves of both magnitude and phase angle of the complex Poisson’s ratio were constructed at a reference temperature of 20°C. The master curves for Poisson’s ratio and the mathematical models are presented in Work Element F2c.

Significant Results

A testing and data analysis method was developed to characterize the tensile properties of aged field asphalt mixtures. The modulus of the field samples were found to be nonuniformly distributed with the pavement depth. The modulus gradient in the field mixture was determined using the Direct Tension Test. Based on the test data, a mathematical model was developed to predict the tensile modulus of the field mixture with the pavement depth.

The compressive properties of asphalt mixtures were characterized by three test scenarios. The test data of these three test scenarios were used to construct the master curves of the magnitude and phase angle of the compressive complex modulus and the complex Poisson’s ratio.

Significant Problems, Issues and Potential Impact on Progress

The software programming for the newly purchased MTS is not finished yet. As a result, the new MTS is still not ready to use. The necessary software is expected to be completely installed in the new MTS in the next quarter.

Work Planned Next Quarter

In the next quarter, more field samples will be tested. The master curves of the magnitude and phase angle of the tensile complex modulus will be constructed at various pavement depths to show the effect of aging of the asphalt mixture with depth below the pavement surface.

Subtask F1c-5: Polymer Modified Asphalt Materials (TAMU)

Work Done This Quarter

No activity this quarter.

Significant Results

No activity.

Significant Problems, Issues and Potential Impact on Progress

No activity.

Work Planned Next Quarter

During the next quarter, polymer modified binders will be obtained for testing.

Work Element F1d: Healing

Subtask F1d-1: Critically Review Previous Work on Healing under FHWA Contracts DTFH61-C-92-00170 and DTFH61-C-99-00022 (TAMU)

Work Done This Quarter

The literature review was continued in this quarter.

Work Planned Next Quarter

This is an ongoing subtask that will be continued through this project.

Subtask F1d-2: Select Materials with Targeted Properties (TAMU)

Work Done This Quarter

The test method to determine the intrinsic healing function was initially developed using neat asphalt binders. Pending the sampling and collection of the core binders that will form the basis of the main test program, we tried to evaluate the use of this test method on modified binders. Figure F1d-2.1 illustrates results showing intrinsic healing for two polymer modified binders.

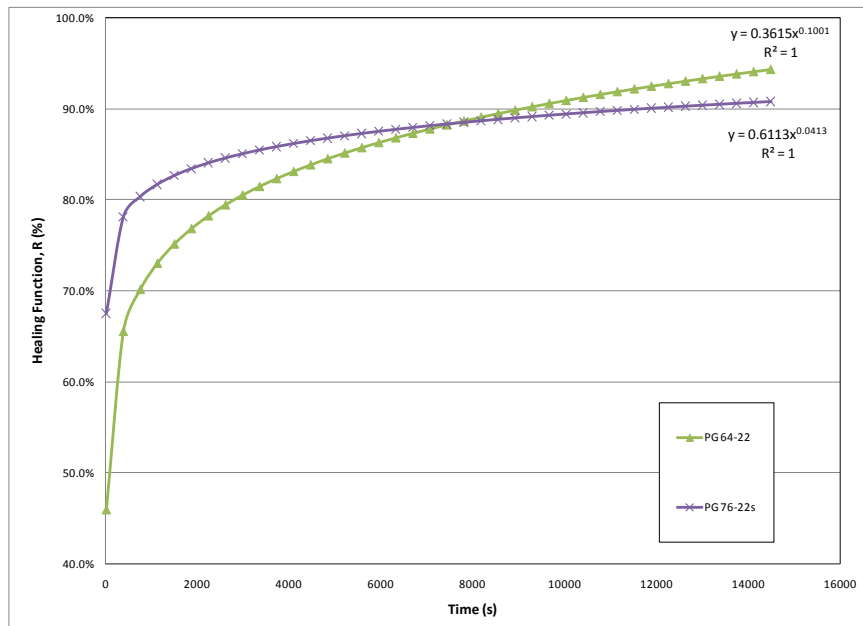


Figure F1d-2.1. Intrinsic healing healing function for polymer modified binders measured using the protocol identified earlier

Work Planned Next Quarter

For next quarter we plan to measure the properties related to the healing model for the core asphalt binders.

Subtask F1d-3: Develop Experiment Design (TAMU)

Work Done This Quarter

In the last quarter researchers proposed an experiment design to determine the wetting properties of the asphalt binder by testing FAM specimens. After an initial review of the experiment design with the consortium partners and some preliminary testing, the experiment design to determine the wetting function was slightly modified from the version reported in the previous quarterly report.

Work Planned Next Quarter

Modifications to the work plan, if required, will be made after obtaining initial results.

Subtask F1d-4&5: Investigate Test Methods to Determine Material Properties Relevant to Asphalt Binder Healing (TAMU)

Work Done This Quarter

The preliminary experiment design to validate the healing model was developed as described in F1d-3. Testing with asphalt binders following this test plan is underway.

Work Planned Next Quarter

The intrinsic healing function for different asphalt binders will be measured for different asphalt binders using the DSR and the normal force methods.

Subtask F1d-5: Testing of Materials for model validation* (TAMU)

Work Done This Quarter

No work planned.

Work Planned Next Quarter

Work in this subtask is planned for later after completion of Subtask F1d-4. Summarily, step 3 of the outline presented in F1d-3 is for validation of the healing model.

Subtask F1d-6: Evaluate Relationship Between Healing and Endurance Limit of Asphalt Binders (UWM)

Work Done This Quarter

Work focused on time sweep testing for calculation of endurance limits of the binders listed in table F1d-6.1. Previous quarterly reports have shown that endurance limits may be useful for binder characterization. A new method following the advancements in determining the healing of mixtures by Christensen and Bonaquist (2009) was described in the last quarterly report. Data for use of this methodology were generated this quarter. Mixture endurance limits from fatigue testing will be available for the binders listed in table F1d-6.1. This data set will allow for a direct comparison between the endurance limits of binders and mixtures.

Currently, work is under way by ARC partners at Texas A&M University to evaluate healing properties of binder at the macro- and micro-scales. This effort will be used to compare and validate the two approaches.

Table F1d-6.1. Binders for endurance limit estimation using time sweep tests.

Binder Identification
64-28 AI
64-28 PPA
64-34 SemMaterials
76-22 Citgo
64-22 12% GTR
64-28 AI 2% Latex

AI = Asphalt Institute. PPA = polyphosphoric acid. GTR = ground tire rubber.

Significant Results

Significant progress has been made toward completing the time sweep tests of the materials listed in table F1d-6.1. The experimental plan for the time sweep tests includes two replicates and two strain amplitudes: 5% and 7%.

Significant Problems, Issues and Potential Impact on Progress

The progress of this task has been delayed due to the research team's focus on other tasks related to developing a binder fatigue specification test. Some delays also occurred because one of the graduate students expected to begin work in July could not join the research team.

Work Planned Next Quarter

The following tasks are planned for the next quarter:

- Continue testing of the binders in table F1d-6.1. Compare binder and mixture endurance limit strains calculated using the reduced cycle approach.
- Investigate the relationship between the linear viscoelastic properties of the material with its healing properties by means of modeling the cyclic behavior of simplified mechanical models such as the Burgers and Maxwell models.

Cited References

Christensen, D. W., and R. Bonaquist, 2009, Analysis of HMA fatigue data using the concepts of reduced loading cycles and endurance limit. *Journal of the Association of Asphalt Paving Technologists*, 78.

Subtask F1d-7: Coordinate with Atomic Force Microscopic (AFM) Analysis (WRI)

Work Done This Quarter

Hypothesis

In the later stages of fatigue cracking, the failing sections of pavement are often observed to form distinct crack patterns (i.e., alligator crack pattern) usually localized in the traffic wheel path, and often occurring later in the life of the pavement. By comparison, in investigations relating to metal fatigue, pattern forming cracking has been successfully correlated to the microstructure which develops in these materials during casting [Cappelli et al. 2008, Bian and Taheri 2008] corresponding to grain boundaries at the meso, micron and nanometer scale. Occurrence of grain boundaries may be a result of the heterogeneous nature of a material [Cappelli et al. 2008; Bian and Taheri 2008]. Thus, this same idea (i.e., grain boundary formation) can be applied to paving materials if such pattern forming phenomena were to be observed [Robertson et al. 2005, 2006].

Experimental

Neat asphalts and SARA fractions separated from neat asphalts from the comparative performance sites at Rochester Minnesota and Arizona [*Fundamental Properties of Asphalts and Modified Asphalts, III Quarterly Report, September 2009*] were imaged with AFM (intermittent-contact mode). To briefly summarize, asphalts which were found to be the "lumpiest", when imaged by AFM as thin-films (500-nm to 1000-nm) with the exception of polymer modified asphalt, correlated reasonably well with, thermal and fatigue crack severity.

Figure F1d-7.1 depicts phase-contrast images of the four MN asphalts. The asphalt with the most phase-contrast poly-disperse domains showed more thermal cracking.

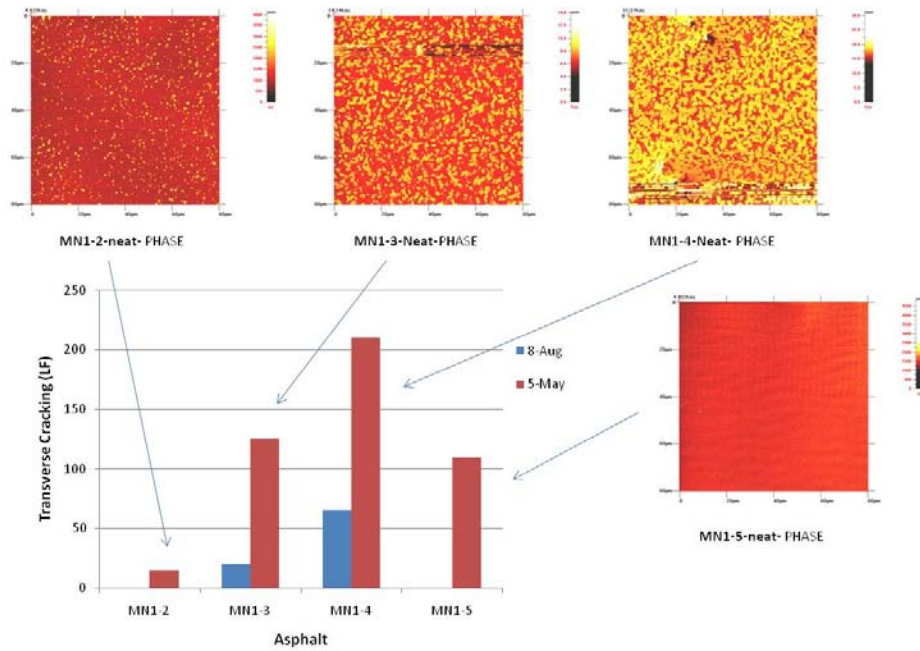


Figure F1d-7.1. AFM Phase-contrast images and a thermal crack severity plot, lowest-to-highest; MN1-2 (polymer), MN1-5, MN1-4, and MN1-4 (high wax).

Figure F1d-7.2 depicts both topography-profile (top-4) (left-to-right, top-to-bottom): MN1-4, MN1-5, MN1-2, and MN1-3; and phase-contrast (bottom-4), same order. Both the waxiest, and subsequently lowest in asphaltene content, and the polymer modified material are the lumpiest based on AFM topography and phase-contrast, MN1-5 is the smoothest, and MN1-3 is intermediate in wax content (phase-contrast), and intermediate, excluding the modified asphalt, in thermal crack severity.

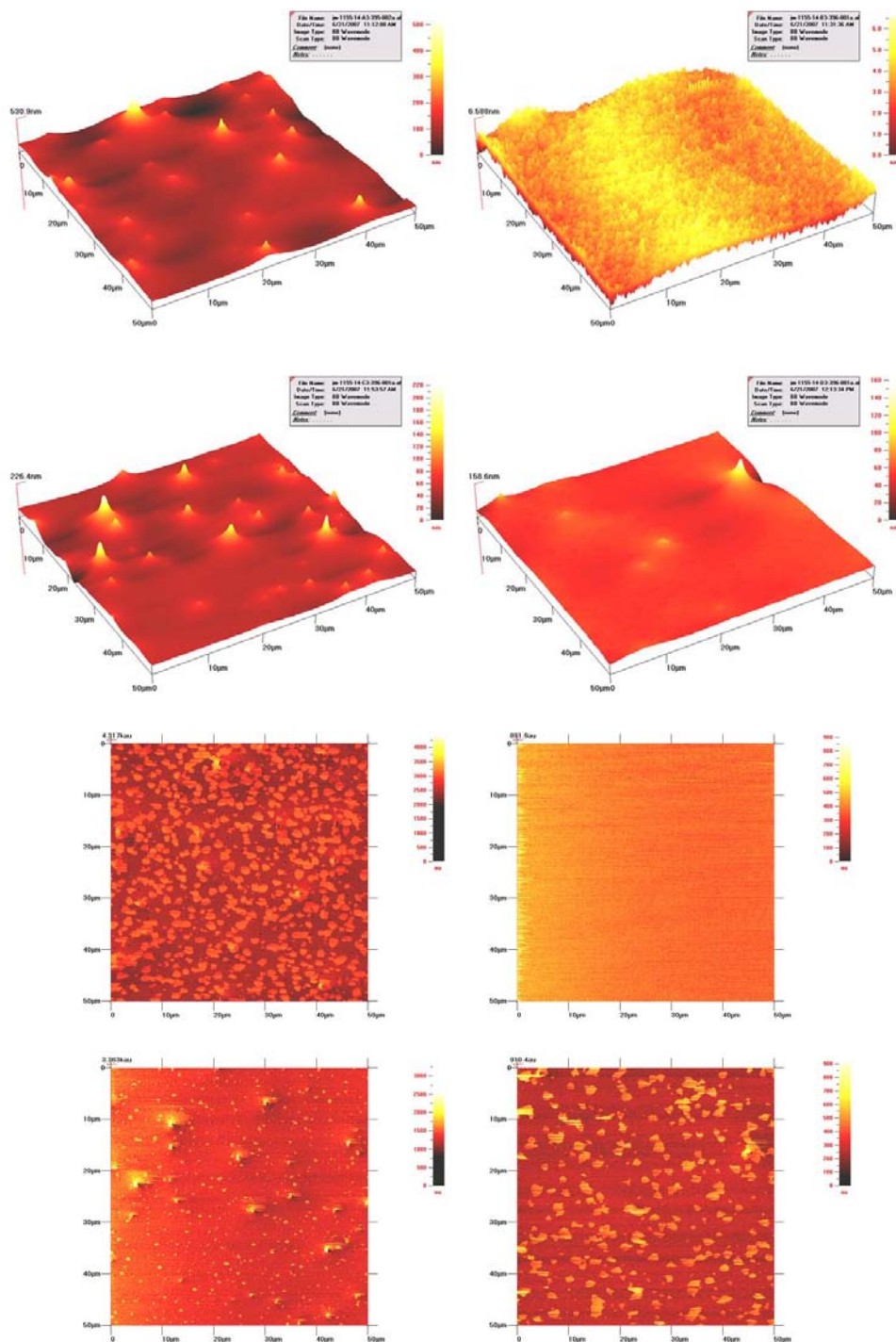


Figure F1d-7.2. Topography-profile (top-4) (Left-to-right, top-to-bottom): MN1-4, MN1-5, MN1-2, and MN1-3; and phase-contrast (bottom-4), same order. Images obtained under ambient conditions of pressure and temperature.

Closer inspection of the maltenes and SARA fractions of MN1-4 reveal by AFM (figure F1d-7.3) that pronounced micro/nano-structuring occurs with all fractions investigated. This figure depicts topography and phase-contrast images of isooctane soluble maltenes, SARA naphthene aromatics fraction, and polar aromatics fraction materials. The other three fractions from the other three asphalts (MN1-2, 1-3, and 1-5) remain to be studied.

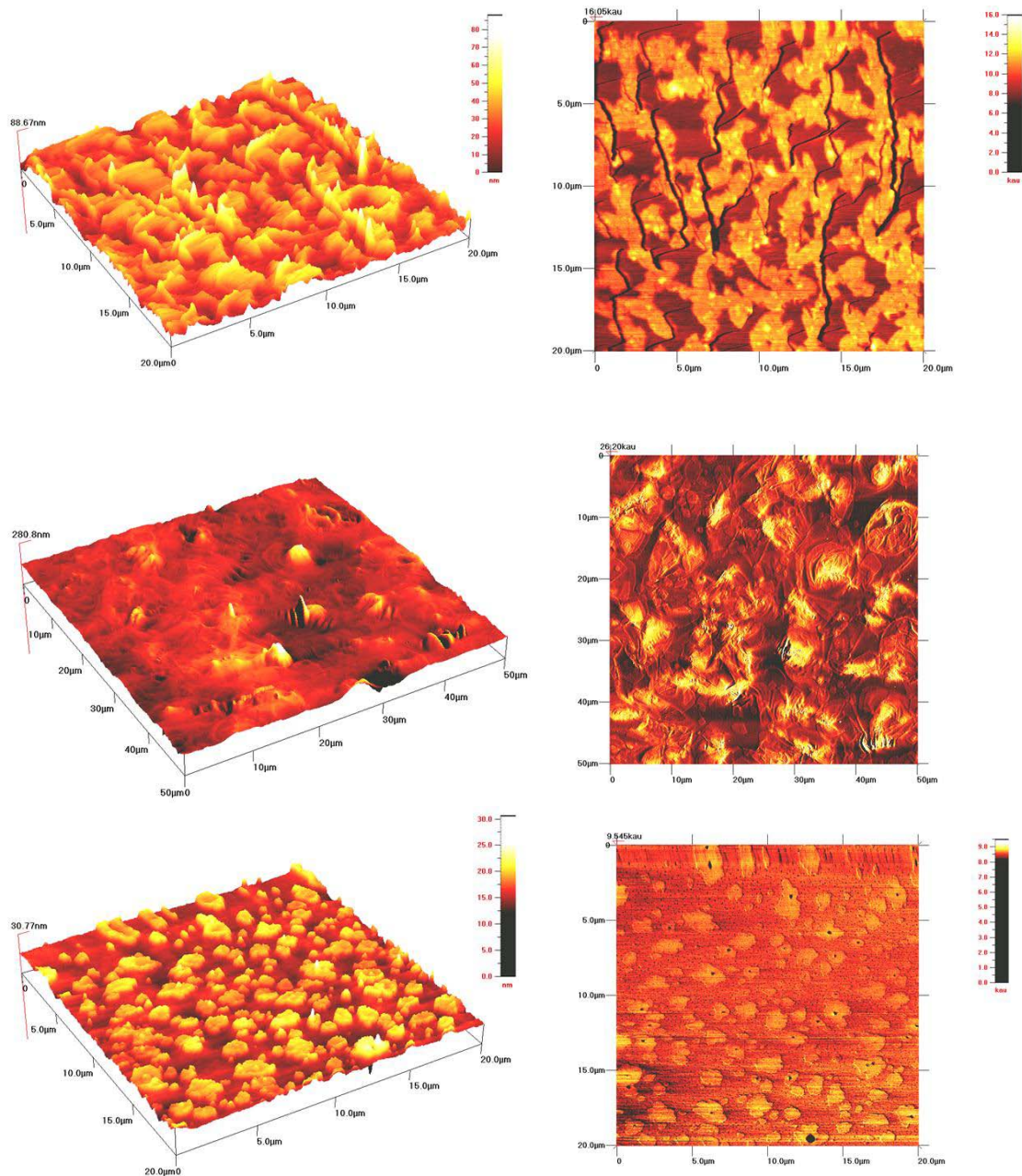


Figure F1d-7.3. Top-to-bottom (two image sets), topography (left), phase-contrast image (right) of MN1-4; maltenes, SARA naphthene aromatics fraction and polar aromatics fraction. Images obtained under ambient conditions of pressure and temperature.

The Arizona asphalts were then examined by the same film spin casting and AFM imaging techniques. Figures F1d-7.4 and F1d-7.5 depict topography and phase-contrast AFM images of the four Arizona asphalts, in order; AZ1-1, 2, 3, and 4, respectively.

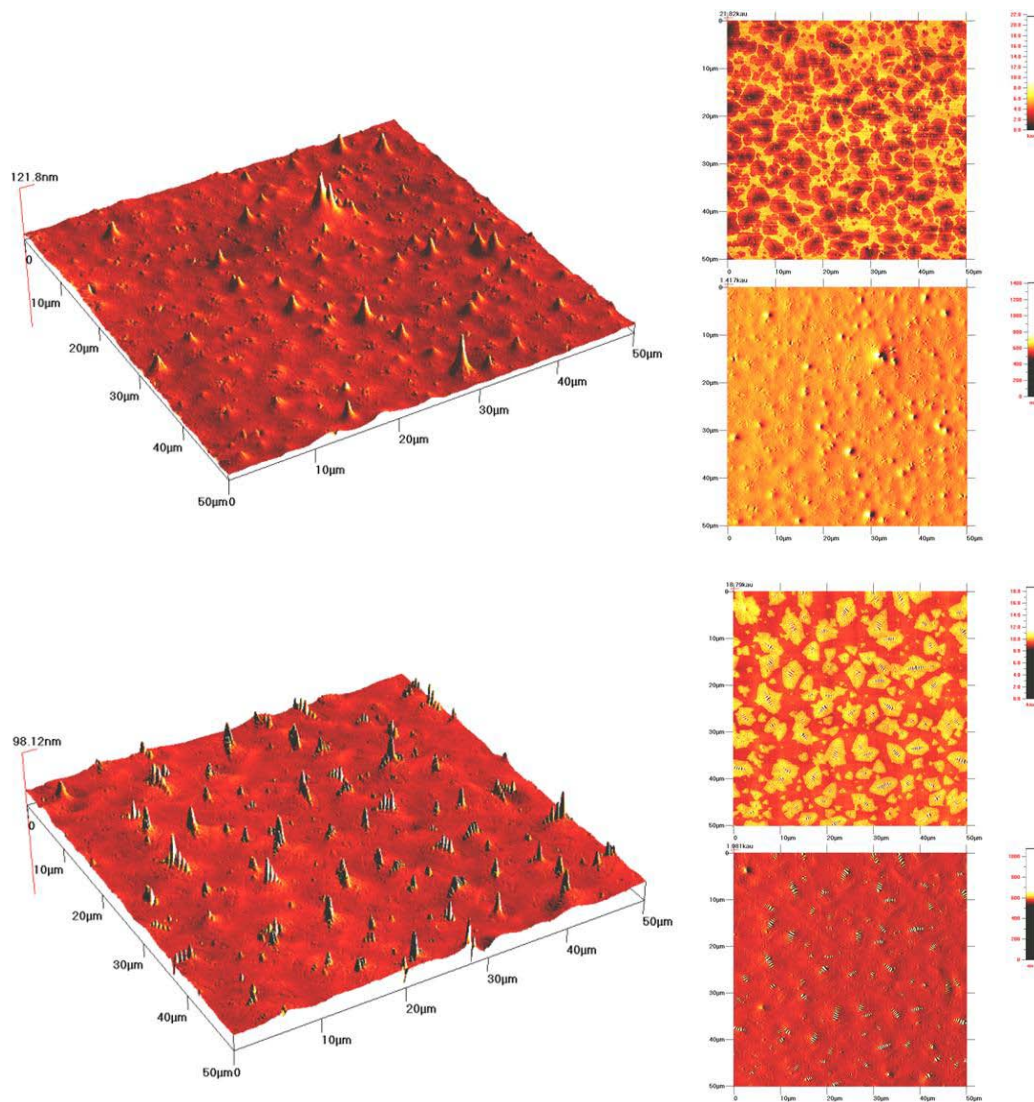


Figure F1d-7.4. Three image set, (left) topography, (upper-right) phase-contrast, (lower-right) error (derivative) of topography. Top set, neat asphalt AZ1-1 (film thickness = 729-nm), bottom set, neat asphalt AZ1-2 (film thickness = 744-nm). Images obtained under ambient conditions of pressure and temperature.

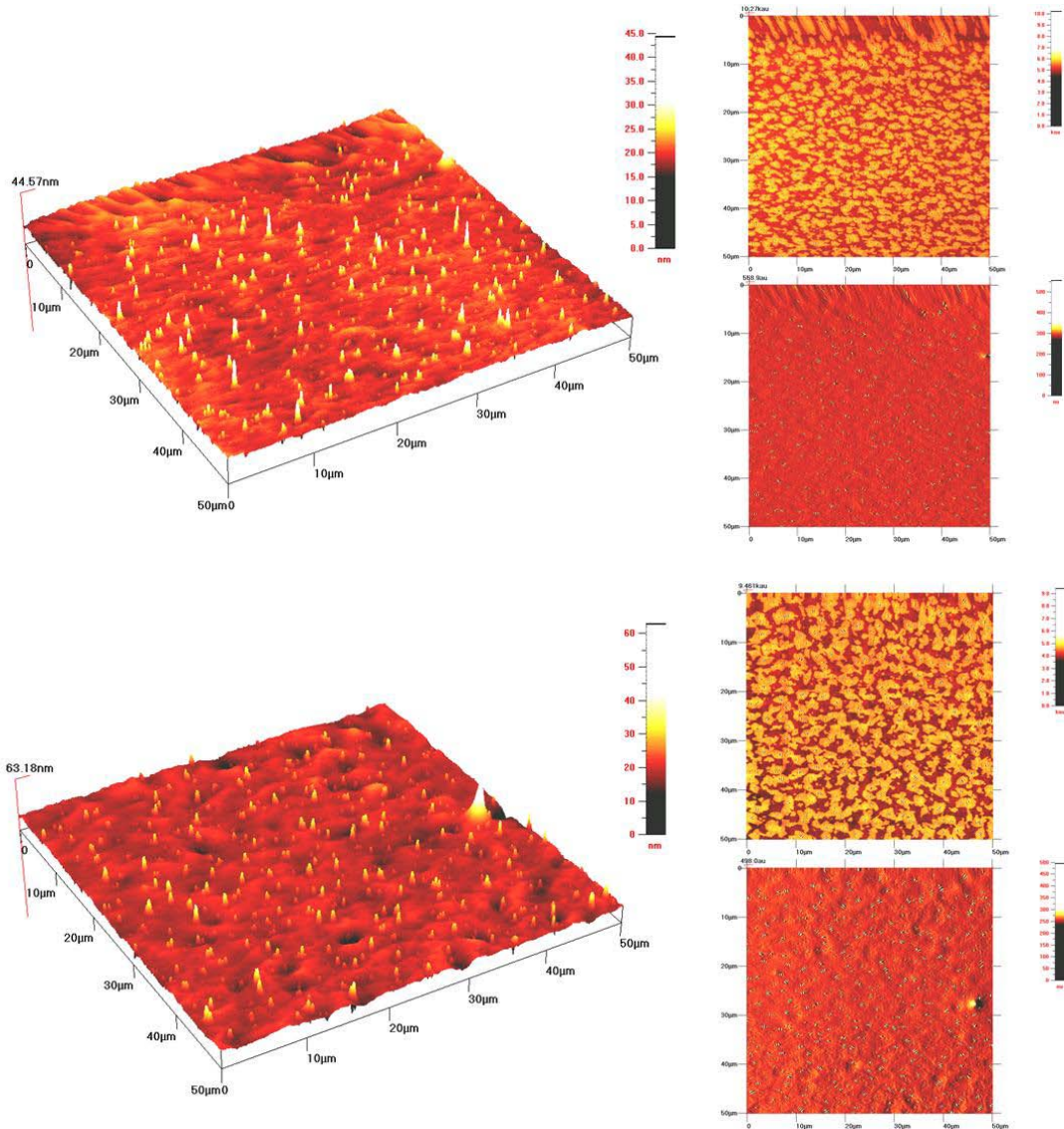


Figure F1d-7.5. Three image set, (left) topography, (upper-right) phase-contrast, (lower-right) error. Top set, neat asphalt AZ1-3 (film thickness = 644-nm), bottom set, neat asphalt AZ1-4 (film thickness = 737-nm). Images obtained under ambient conditions of pressure and temperature.

The "lumpiest" asphalt (as measured by height disparity and phase contrast differences), AZ1-1, figure F1d-7.4 (top), again showed more abundance of cracking in the field performance survey, specifically longitudinal cracking in the wheelpath and outside of the wheelpath. Table F1d-7.1 lists the distress survey data after five years of accumulated distress at the Arizona comparative performance sections (conducted in 2006). One method of numerically quantifying the "lumpiness" would be in terms of average cluster size and number per area in an AFM image.

Table F1d-7.1. Distress survey data after five years at the Arizona comparative performance sections (conducted in 2006).

Asphalt	Fatigue Cracking, m ²	Longitudinal Cracking Wheel path, m	Longitudinal Cracking non-Wheel path, m	Transverse Cracking, m
AZ1-1	1.9	58.4	205.2	12.6
AZ1-2	1.7	12	83.4	0.2
AZ1-3	12.2	10.2	8.3	0.5
AZ1-4	15.8	4.7	74.9	33.4

From the stand point of SHRP asphalts, for comparison

Over the past eight years this group has had the opportunity to conduct extensive studies of asphalt and chromatographic fractions of asphalt employing atomic force microscopy. In these studies the relationships between asphalt thin-film morphology and microstructure and material performance, specifically cracking and self-healing, were considered. It has been observed that both dynamic force microscopy, also referred to tapping mode (intermittent-contact) TM-AFM and friction or lateral force microscopy (FF-AFM) are both well suited for investigating asphalt thin-films at the micron and nanometer scale. In the discussion to follow, the results presented will only reflect images obtained in the TM-AFM imaging mode. Thus, TM-AFM provides compelling evidence for the existence of different phases in asphalt, particularly when prepared in varying thin-film thickness. In TM-AFM mode the scanning probe cantilever is oscillated at a resonance frequency of the cantilever above and in intermittent contact with soft material surfaces. The approach then provides a topography image of the morphological landscape of the surface of the material being probed. Furthermore, a unique feature of this approach is that the cantilever acts as a driven harmonic oscillator that experiences variations in energy dissipation due to dampening as the cantilever tip encounters domains of different hardness and/or adhesive properties in the sample [Bhushan 2005]. Generally speaking, hard domains next to softer domains will transition from darker to lighter profiles in phase contrast images produced during a sample scan providing information relating to the composition of the material phases.

Figure F1d-7.6 depicts AFM (WaveMode) phase contrast images obtained for eight SHRP “core” asphalts. Table F1d-7.2 provides rheological and compositional property data measured for these same asphalts. Specifically, the images in this figure represent spin-cast, 1-micron thick thin-films initially prepared as 0.1-g/mL solutions in cyclohexane, where samples were subsequently stored in an inert gas purged (N₂) dry box while awaiting analysis by AFM. Images were obtained within a few days after film preparation. Of the more interesting observation that may be noted in terms of similarities in structure and patterning are as follows; Asphalts AAB-1, AAC-1, AAD-1, and AAF-1, and to a lesser degree, AAG-1 and AAM-1 all depict a two-phase pattern. Asphalt AAA-1 depicts the least amount of structure, while AAG-1 simply depicts a small amount of patchy structures. AAB-1 and AAC-1 both show similar size, shape and patterning of structures (phases), while both AAD-1 and AAF-1 depict oblong (American football) shaped structures, where AAD-1 displays more, but smaller structures, while structures observed in AAF-1 phase images are larger and more well defined in terms of resembling the

shape of the “football” shape. AAM-1 simply displays very small spots. Finally AAK-1 does not depict the two phase characteristic pattern observed in most of the remaining samples, but both it, AAD-1 and AAF-1 do depict Loeber’s bees [Loeber, et al., 1996, 1998]. More specifically, Loeber’s bumble bees, at least in two cases; AAD-1 and AAF-1, constitute the laces of the footballs. Although this is not the case for asphalt AAK-1, similar structures for AAK-1, (i.e., footballs with laces) have been observed [Masson et al. 2007], this is also the case for six of the other eight asphalts considered here, but always with the exception of asphalt AAA-1, where bees have never been observed. Thus, if the observations previously discussed are considered in relation to the data listed in table F1d-7.2, it is reasonable to suggest that the percent crystalline material best correlates with the relative degree/extent of structuring observed among this set of eight asphalts.

Table F1d-7.2. Rheological and compositional properties measured for eight SHRP asphalts.

Asphalt SHRP Designation	Dynamic Viscosity, η^* , Pa·s	Rheological Phase Angle, δ , °	VPO Number Average Molecular Weight, M_n , Daltons	Isooctane asphaltene mass fraction χ_{iso-C8}	Percent Crystalline Material (DSC)
AAA1	37020	73	690	0.22	0.1
AAB1	118600	70	880	0.22	2.5
AAC1	90100	75	910	0.16	2.9
AAD1	57280	69	630	0.27	1.0
AAF1	381700	76	830	0.19	2.4
AAG1	248900	84	690	0.10	0.2
AAK1	251700	68	729	0.25	1.3
AAM1	364400	67	1400	0.11	3.7

NOTE: Dynamic shear viscosity and phase angle measurements of neat asphalts determined at 25°C at a frequency of 0.1 rad/sec (approximating a “zero” state of shear), and crystalline fraction determined by differential scanning calorimetry (DSC) [Robertson et al. 2001]. VPO number average molecular mass reported in [Branthaver et al. 1993].

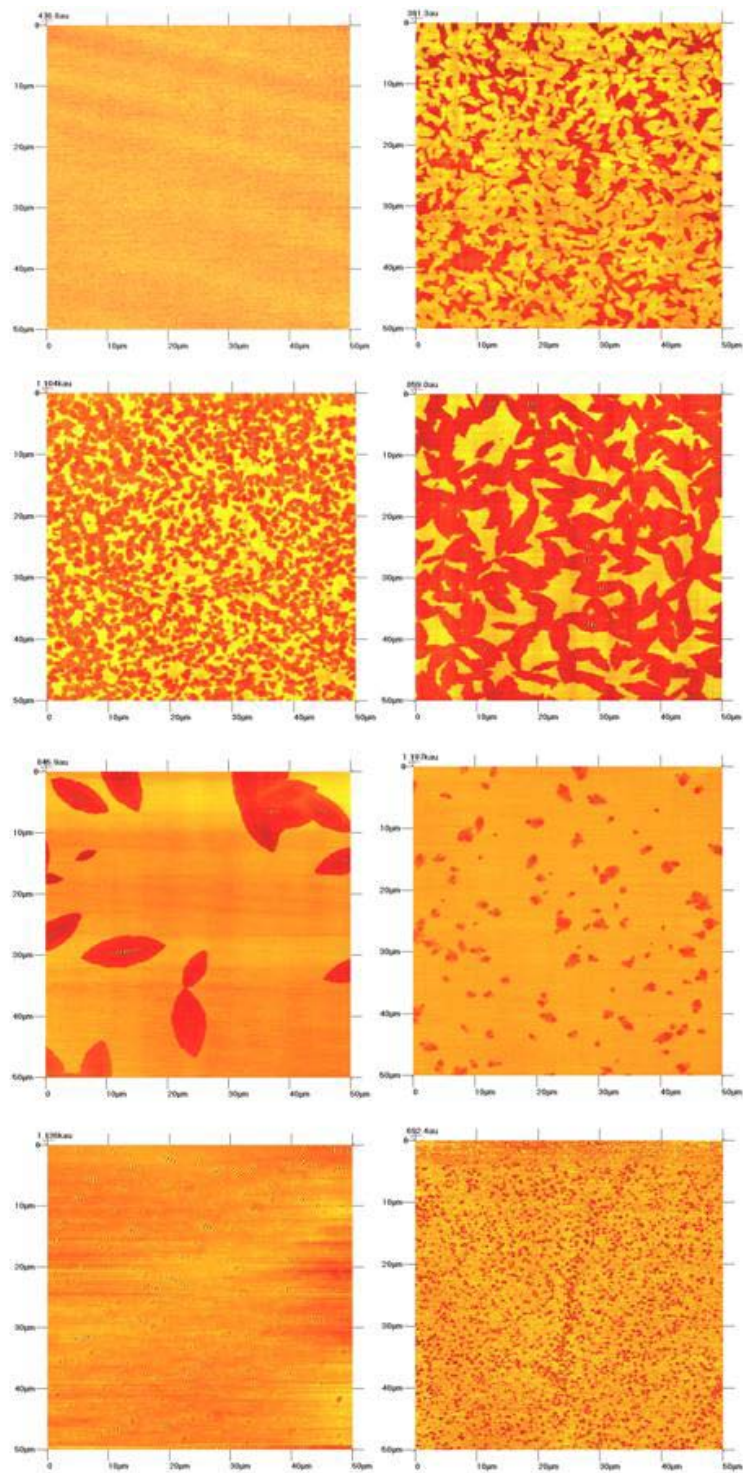


Figure F1d-7.6. SHRP asphalt phase (a.u. arbitrary units) images, 1- μ m thick films spin-cast from cyclohexane solution (0.1 g/mL concentration), from left to right proceeding down; AAA-1, AAB-1, AAC-1, AAD-1, AAF-1, AAG-1, AAK-1, and AAM-1.

AFM Imaging of IEC Fractions

In order to test the hypothesis that the structures/patterns observed in our asphalt samples were somehow associated with the presence of wax, studies were conducted to investigate “surface” structuring in maltenes and IEC (ion-exchange) and SARA (Saturates, Aromatics, Resins, Asphaltenes) chromatographic fractions. In these investigations, the eight SHRP asphalts were fractionated into asphaltenes and maltenes using both n-heptane and iso-octane as flocculation solvents. Iso-octane maltenes were subsequently fractionated into saturates, naphthene aromatics and resins (polar aromatics) fractions by SARA chromatography. Finally, whole "neat" asphalts were fractionated into total acidic, total basic, and neutral materials by ion-exchange chromatography. Thin-films of these fractions were then prepared for AFM analysis. In virtually all cases, sample thin-films were prepared by either dabbing a small amount of heat-softened material on a spatula followed by smearing (buttering) of the material onto a glass microscope slide to produce a thin translucent film, approximated to be several microns (5-ish) in thickness, and/or developed as solvent spin-cast films, which were much better controlled in film thickness (+/- 20nm) from 200-nm to 3000-nm. Asphaltenes most always precipitate as a brown to black, friable, powdery solid. Maltenes resemble lighter "dull-black" heavy crude oils, total acids, total bases, and resins (polar aromatics) resemble a friable crystalline solid, where finally, saturates are a clear to clear waxy oil, and naphthene aromatics and neutrals resemble yellow to red translucent to waxy oils, even something like a grease. Publications are presently being prepared reporting on this topic.

For now, figure F1d-7.7 depicts AFM topography images of IEC neutral fractions separated from the six asphalts which contained at least 1% wax by mass of asphalt. It is then interesting to note the similarities in shape of wax “single crystals” for AAD-1 and AAK-1, and AAB-1, AAC-1 and AAF-1. Structures in AAM-1 then appear to be quite different from either of these two sets. The data listed in table F1d-7.2 may lend insight as to why AAM-1 differs. It has been commonly observed that this asphalt has a higher average molecular mass compared to many other SHRP asphalts. This particular asphalt often deviates from trends when compositional properties are correlated with their rheological properties [Branthaver et al. 1993; Robertson et al. 2001], possibly due in part to an aberrantly high molecular weight (see table F1d-7.2).

As early as 1931, Ferris et al. [1931] observed, among other shapes, diamond shaped wax crystals extracted from petroleum similar in shape to those depicted in figure F1d-7.7, although orders of magnitude larger in size. By comparison, in terms of actual size, Lu et al. [2005] have observed wax crystals directly in asphalts using polarized light microscopy (PLM), confocal laser scanning microscopy, (CLSM), and transmission electron microscopy. The structures this group has observed are precisely of the same shape and size to the structures reported here.

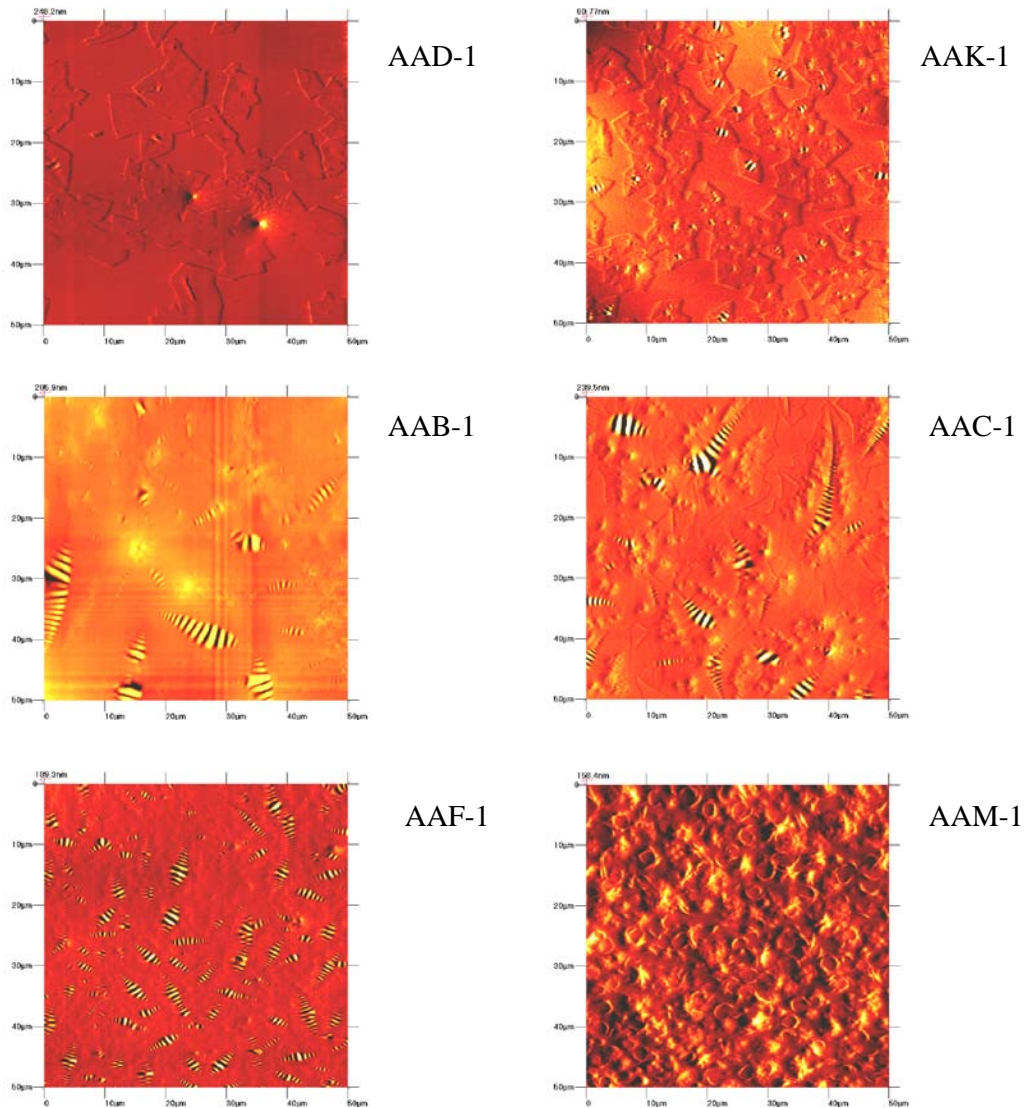


Figure F1d-7.7. AFM tapping WaveMode scans (surface topography) IEC neutral fractions originally separated from six of the eight SHRP core asphalts.

Significant Results

Micro- and nano-"lumps" in asphalt thin films may be discontinuities in asphalt due to microcrystalline and dendrite-like (bee) wax crystals. It is speculated that asphalts with higher concentrations of microcrystalline wax form microstructural discontinuities (grain boundaries) possibly in synergy with other material phases, and thus, tend to crack more, thermal, fatigue or otherwise.

Significant Problems, Issues and Potential Impact on Progress

A temperature and gas environmental control chamber is presently being fabricated around the AFM instrument to control oxygen and moisture influences upon thermal-cycle imaging and nano-mechanics experiments.

Work Planned Next Quarter

Analysis of existing data will continue in the next quarter. In these analyses, morphological features observed in asphalt and asphalt chromatographic fraction thin films prepared from validation site asphalts will be compared to performance data of the field site pavements. Image analysis of AFM scans will be developed to define a roughness “lumpiness” index.

Cited References

Bian, L., and F. Taheri, 2008, Fatigue Fracture Criteria and Microstructures of Magnesium Alloy Plates. *Materials Science and Engineering A*, 48774–85.

Bhushan, B. 2005, *Nanotribology and Nanomechanics An Introduction*. Springer-Verlag, Berlin Heidelberg, Germany.

Branthaver, J. F., J. C. Petersen, R. E. Robertson, J. J. Duvall, S. S. Kim, P. M. Harnsberger, T. Mill, E. K. Ensley, F. A. Barbour, and J. F. Schabron, 1993, SHRP-A-368, *Binder Characterization and Evaluation, Volume 2: Chemistry*. Strategic Highway Research Program, National Research Council, Washington, DC.

Cappelli, M. D., R. L. Carlson, and G. A. Kardomateas, 2008, The Transition Between Small and Long Fatigue Crack Behavior and its Relation to Microstructure. *International Journal of Fatigue*, 30: 1473–1478.

Ferris, S. W., H. C. Cowles, Jr., and L. M. Henderson, 1931, Composition and Crystal Form of the Petroleum Waxes, *Industrial and Engineering Chemistry*, 23(6), 681-688.

Loeber, L., O. Sutton, J. Morel, J.-M. Valleton, and G. Muller, 1996. New Direct Observation of Asphalts and Asphalt Binders by Scanning Electron Microscopy and Atomic force Microscopy. *Journal of Microscopy*, 182(1), 32-39.

Loeber, L., G. Muller, J. Morel, and O. Sutton, 1998. Bitumen in Colloid Science: A Chemical, Structural and Rheological Approach. *Fuel*, 77(13), 1443-1450.

Lu, X., M. Langton, P. Olofsson, and P. Redelius. 2005. Wax Morphology in Bitumen. *Journal of Materials Science*, 40, 1893-1900.

Masson, J-F., V. Leblond, J. Margeson, and S. Bundale-Perc, 2006. Low-Temperature Bitumen Stiffness and Viscous Paraffinic Nano- and Micro-Domains by Cryogenic AFM and PDM. *Journal of Microscopy*, 227(3), 191-202.

Robertson, R. E., K. P. Thomas, P. M. Harnsberger, F. P. Miknis, T. F. Turner, J. F. Branthaver, S-C. Huang, A. T. Pauli, D. A. Netzel, T. M. Bomstad, M. J. Farrar, J. F. McKay, and M. McCann. “Fundamental Properties of Asphalts and Modified Asphalts II, Final Report, Volume I: Interpretive Report,” Federal Highway Administration, Contract No. DTFH61-99C-00022, Chapters 1-4 submitted for publication, November 2005.

Robertson, R. E., K. P. Thomas, P. M. Harnsberger, F. P. Miknis, T. F. Turner, J. F. Branthaver, S-C. Huang, A. T. Pauli, D. A. Netzel, T. M. Bomstad, M. J. Farrar, D. Sanchez, J. F. McKay, and M. McCann. “Fundamental Properties of Asphalts and Modified Asphalts II, Final Report, Volume I: Interpretive Report,” Federal Highway Administration, Contract No. DTFH61-99C-00022, Chapters 5-7 submitted for publication, March 2006.

Robertson, R. E., J. F. Branthaver, P. M. Harnsberger, J. C. Petersen, S. M. Dorrence, J. F. McKay, T. F. Turner, A. T. Pauli, S.-C. Huang, J.-D. Huh, J. E. Tauer, K. P. Thomas, D. A. Netzel, F. P. Miknis, T. Williams, J. J. Duvall, F. A. Barbour, C. Wright, 2001, *Fundamental Properties of Asphalts and Modified Asphalts, Volume I: Interpretive Report*, FHWA-RD-99-212. U. S. Department of Transportation, Federal Highway Administration, McLean, VA.

Subtask F1d-8: Coordinate Form of Healing Parameter with Micromechanics and Continuum Damage Models (TAMU)

Work Done This Quarter

In this task, a continuum-based constitutive model for damage healing in asphaltic materials will be developed. This healing model will be coupled with the already developed continuum damage mechanics constitutive equations. The development will be based on introducing another natural configuration besides the damage and effective (undamaged) configurations. This additional natural configuration is the “healing configuration.” Based on this concept, one can write the stress evolution in the healing configuration in terms of the nominal stress, σ , the damage variable, ϕ , and the healing variable, h , such that:

$$\bar{\bar{\sigma}} = \frac{\sigma}{(1-\phi)(1+h)} \quad (\text{F1d-8.1})$$

where $\bar{\bar{\sigma}}$ is the stress in the healing configuration, and σ is the stress in the damaged configuration. The damage parameter ϕ has a range from 0 (no damage) to 1 (fracture). On the other hand, the healing variable h has a range between 0 (no healing) and $\phi/(1-\phi)$, where this limit is based on that the healing area cannot exceed the damaged area.

In order to enhance the coupling between healing and viscoelasticity and viscoplasticity, the effective stress in the healing configuration, Eq. F1d-8.1, will replace the nominal stresses in the viscoelasticity and viscoplasticity constitutive equations. Therefore, any healing occurrence will affect the amount of viscoelastic and viscoplasticity deformations. Moreover, this will allow

strong coupling between healing and damage due to mechanical or environmental loading conditions. The damage density ϕ includes damage due to mechanical loading conditions, ϕ^m , and damage due to adhesive and cohesive moisture induced damage, such that:

$$\phi = 1 - (1 - \phi^m)(1 - \phi^{aM})(1 - \phi^{cM}) \quad (\text{F1d-8.2})$$

where ϕ^{aM} is the adhesive moisture-damage, and ϕ^{cM} is the cohesive moisture-damage.

The focus of the current research activities is on using the micromechanical mechanisms that drive healing in asphaltic materials to develop a phenomenological evolution equation of the healing variable h . This evolution equation will be driven by the surface energy, temperature, stress field, and resting period. This damage variable will include micromechanical mechanisms that drive short-term as well long-term healing evolution.

Work Planned for Next Quarter

Using the approach described above we have begun to include healing into the continuum damage model. The micromechanical model of healing as described in previous quarterly reports as well as in refereed publications continues to be validated through laboratory experiments. We are working vigorously to make sure that coupling of the function that represents healing in the continuum damage model is as close a representation of the convolution mechanistic model of healing as possible. In the next quarter team members who focus on the micromechanical model and the function used to represent healing in the continuum damage model will work closely together to refine the approach. This is a critical stage.

CATEGORY F2: TEST METHOD DEVELOPMENT

Work Element F2a: Binder Tests and Effect of Composition (UWM)

Work Done This Quarter

The research team continued testing the materials included in the approved testing matrix. New materials were included in an effort to obtain a more detailed picture of the effects of composition on fatigue.

One base binder and several modifiers are included in this study. The base binder is a PG 64-22 binder from Flint Hills. All modifications to this binder have been performed in the lab following the modifier's guidelines. Each asphalt was tested after aging in the pressure aging vessel (PAV) following the AASHTO R28 standard procedure.

The modifiers used in this study are styrene-butadiene-styrene (SBS), Elvaloy and PPA. They cover a broad range of the modifier spectrum by including reactive and nonreactive elastomers, cross-linked and uncross-linked polymeric additives, and a low molecular weight acid modifier. Two levels of modification are selected for every polymer modifier used. This leads to a total of

seven modified binders and one unmodified base binder included in this study, as shown in table F2a.1.

Table F2a.1. Materials derived from the Flint Hills base binder.

Material	Grade
Neat	PG 64
2% LSBS	PG 70
2% LSBS XLK	PG 70
4% LSBS	PG 76
4% LSBS XLK	PG 82
0.7% Elvaloy	PG 70
1.5% Elvaloy	PG 76
1% PPA	PG 70

LSBS = linear styrene-butadiene-styrene. XLK = cross-linking. Elvaloy = Elvaloy terpolymer.
PPA = polyphosphoric acid.

Dynamic Shear Rheometer (DSR) elastic recovery tests are performed at intermediate temperatures. The testing temperatures are chosen such that the materials are investigated under equal stiffness conditions. Both strain rate (2.32% per second) and maximum strain values (278% strain) were calculated based on the geometry and deformation values required in the standard elastic recovery test, as described by AASHTO T301. The main difference between the two tests is that, while the DSR-run elastic recovery is performed in shear, the test described by the AASHTO T301 procedure is run in uniaxial tension. The continuous grade for intermediate temperatures is chosen as the determining criteria for selecting the testing temperatures, which are presented in table F2a.2.

Table F2a.2. Temperatures for equal-stiffness conditions: $G^* = 18$ MPa.

Flint Hills	Continuous Grade Temperature
Neat	21.3 °C
2% LSBS	24.6 °C
2% LSBS XLK	21.7 °C
4% LSBS	24.5 °C
4% LSBS XLK	21.9 °C
0.7% Elvaloy	22.9 °C
1.5% Elvaloy	21.7 °C
1% PPA	22.3 °C

Time sweep experiments were performed at temperatures that ensure equal stiffness among the materials tested. A minimum of two stress levels are chosen for each sample. By plotting the N_{p20} values against the dissipated energy (W_i) results obtained from the time sweep tests, a simple fatigue power law, given by equation F2a.1, was used to fit the data.

$$N_{p20} = K_1(W_i)^{K_2} \quad (\text{F2a.1})$$

where K_1 and K_2 are model coefficients.

Using the model, one can then predict the failure point (N_{p20}) of each binder at the dissipated energy values of 10 kPa and 30 kPa, which are assumed to be good representations of typical pavement structure conditions. The 10 kPa and 30 kPa dissipated energy values are representative for strong and weak pavement structure conditions, respectively.

Binder Yield Energy Test (BYET) was also performed at equal stiffness conditions at the same temperatures selected for time sweep and elastic recovery tests. The yield energy (YE) values presented are calculated as the area under the curve up to the peak stress if a single peak is present. In the case of materials exhibiting two peaks, the YE calculations were performed using the maximum of the second peak. This was done to account for the influence of the polymer modifiers—influence that in most cases is not clearly identified if the second peak is ignored. The strain rate imposed for the YE tests was 1% per second.

Significant Results

One notable result of the work performed during this quarter is the development of a new testing method aimed at improving how elastic properties of binders are measured. This new testing method will allow the research team to investigate the relationship between elasticity and fatigue resistance of binders. A paper was submitted to TRB for publication and is available for review upon request.

Conclusions and recommendations from this paper are as follows:

- Elastic recovery data measured with a new protocol in the DSR at intermediate temperatures show good correlation with elastic recovery results collected in the ductility bath following the AASHTO T301 procedure. This finding suggests that the T301 standard can be replaced with a simple test in the DSR. The DSR test procedure mimics the T301 procedure, in which a constant rate of deformation is imposed until a certain strain is reached, after which load is removed to allow for recovery.
- The new test in the DSR is believed to be more effective because its temperature, loading and unloading can be much better controlled than with the T301 procedure. In addition, a much smaller sample is needed, and the test can be done in standard DSR devices.
- Among the advantages the research team foresees in running DSR tests in place of elastic recovery are smaller sample size, shorter testing time and more information—such as toughness, tenacity and elastic recovery—all from one instrument.

- The elastic recovery values could not be correlated to fatigue results of binders. Therefore, the question of relevance of the elastic recovery to pavement performance remains unanswered. It is critical that this question be answered because, if elastic recovery cannot be found to relate to performance, it should not be used in selecting binders.
- This study also compared the YE of binders measured with a recently developed protocol called BYE test with fatigue and elastic recovery. Using the same testing temperatures, no correlation could be found between fatigue and YE, but a fairly good correlation could be found between YE and elastic recovery.
- BYET results and DSR elastic recovery offer valuable insight on type and level of modification. It is thus strongly recommended that if knowledge of existence of modifiers is needed, the use of the elastic recovery test in the DSR is a better choice than the ductility procedure specified in the AASHTO T301.
- MSCR data collected at intermediate temperatures for percent elastic recovery values could not be used to compare with either fatigue or YE numbers due to the data's narrow range.

Significant Problems, Issues and Potential Impact on Progress

None.

Work Planned Next Quarter

The research team will continue to test the materials according to the approved plan. In parallel, the team will also continue developing and validating this new test by including more samples and work toward proposing an ASTM standard for this method.

Cited References

AASHTO, 2009, AASHTO R28 Standard Practice for Accelerated Aging of Asphalt Binder Using a Pressurized Aging Vessel (PAV). American Association of State Highway and Transportation Officials. Washington, D.C.

AASHTO, 2003, AASHTO Designation T301-99 Elastic Recovery Test of Asphalt Materials by Means of a Ductilometer. American Association of State Highway and Transportation Officials. Washington, D.C.

Work Element F2b: Mastic Testing Protocol (TAMU)

Work Done This Quarter

Improvements to the test protocol to determine fatigue-cracking resistance of FAM specimens using the DMA were made in Subtask F1b-1. Further work on this subtask will be carried out in

coordination with the technology development area. The tentative protocol was presented to the mixture ETG at the semi-annual meeting in Reno, NV in September 2008.

Work Planned Next Quarter

Researchers will coordinate with the technology development work area to further develop the test protocols.

Work Element F2c: Mixture Testing Protocol (TAMU)

Work Done This Quarter

A technical presentation, entitled “Viscoelastic Behavior of Asphalt Mixtures under Repeated Tensile Loading”, was made in the 46th Petersen Asphalt Research Conference in Laramie, Wyoming, July 2009.

A technical paper, entitled “Anisotropic Viscoelastic Properties of Undamaged Asphalt Mixtures under Compressive Loading”, was completed and submitted to the *Journal of Transportation Engineering* (Zhang et al. 2009). This paper summarized the test protocols and data analysis methods that were newly developed to characterize the anisotropic viscoelastic properties of undamaged asphalt mixtures using four parameters in compression and two parameters in tension. These six parameters were obtained by three nondestructive test scenarios: i) uniaxial compressive creep test, ii) uniaxial tensile creep test, and iii) indirect tensile creep test. These tests were conducted at a single temperature (20°C) so the compressive properties of the asphalt mixtures were obtained at 20°C only.

In this quarter, the same test scenarios were conducted on asphalt mixture specimens at three temperatures (10°C, 20°C and 30°C). The Universal Testing Machine (UTM) was utilized to run the compressive creep tests and the indirect tensile tests; the Material Testing System (MTS) was used to conduct the tensile creep tests. Raw data were analyzed to obtain the magnitude and phase angle of complex modulus as well as Poisson’s ratio for both compressive and tensile loading conditions at the three different temperatures. A mathematical model shown in Equation F2c.1 was chosen to construct the master curve of the magnitude of the complex modulus in compression and tension, respectively.

$$|E^*(\omega)| = \frac{E_g}{\left[1 + \left(\frac{\omega_{cE}}{\omega \cdot 10^{C(T-T_r)}} \right)^{R_E} \right]^{\frac{\log 2}{\log 2}} \frac{R_E}{\log 2}} \quad (\text{F2c.1})$$

where E_g = glassy modulus of the asphalt mixture, MPa; ω_{cE} = crossover frequency of the asphalt mixture, rad/sec; R_E = rheological index for modulus; and C = slope of temperature shift factor. Figures F2c.1 and F2c.2 illustrate the master curves of the magnitude of the complex modulus at a reference temperature of 20°C in compression and tension, respectively.

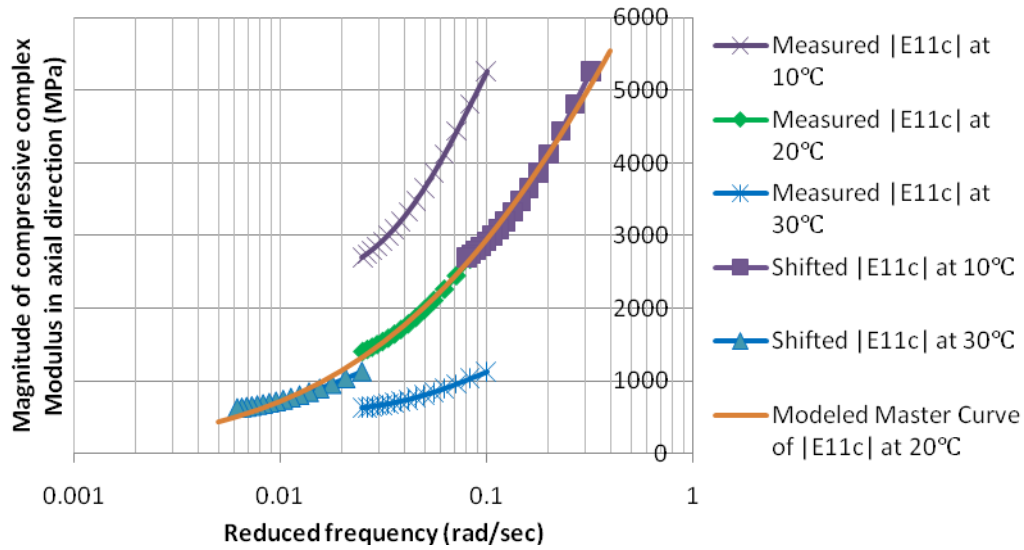


Figure F2c.1. Master curve of the magnitude of the compressive complex modulus at a reference temperature of 20°C.

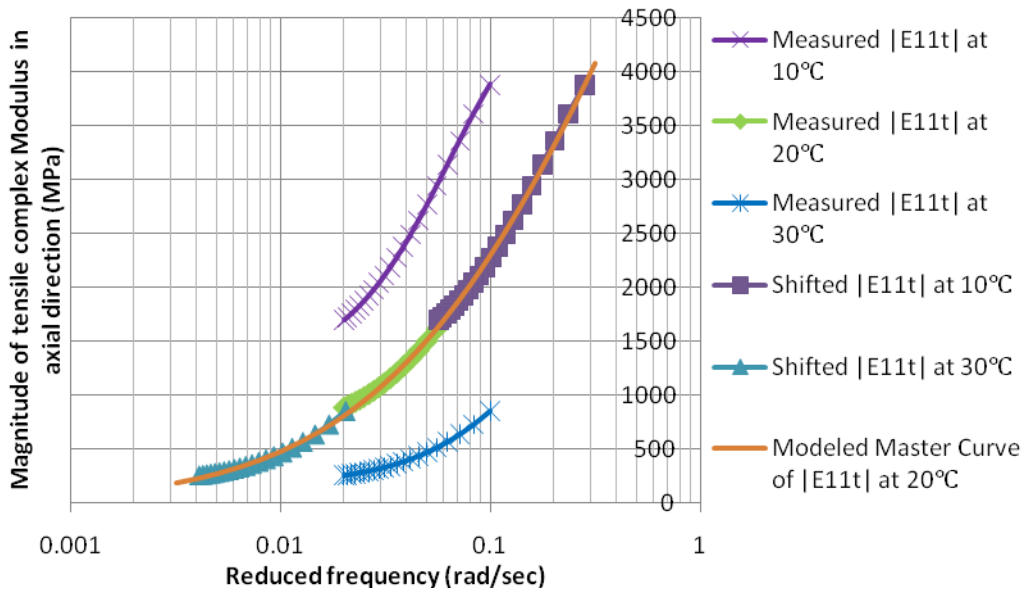


Figure F2c.2. Master curve of the magnitude of the tensile complex modulus at a reference temperature of 20°C.

Another model shown in Equation F2c.2 was employed to construct the master curves of the phase angle of the complex modulus in compression and tension, respectively. The models used for the magnitude and phase angle are found in the reference (Luo and Lytton 2009).

$$\varphi_E = \frac{\varphi_{mE}}{\left[1 + \frac{\log \left(\frac{\omega_{mE}}{\omega \cdot 10^{\frac{C_1(T-T_r)}{C_2+(T-T_r)}}}}{R_{\varphi E}} \right) \right]^2}^{\frac{m}{2}} \quad (\text{F2c.2})$$

in which φ_{mE} = the maximum phase angle for modulus, degrees; ω_{mE} = the frequency where φ_{mE} occurs, rad/sec; $R_{\varphi E}$ = fitting parameters for modulus; T_r = reference temperature; and C_1 and C_2 = constants. Figures F2c.3 and F2c.4 show the master curves of the phase angle of the complex modulus at a reference temperature of 20°C in compression and tension, respectively.

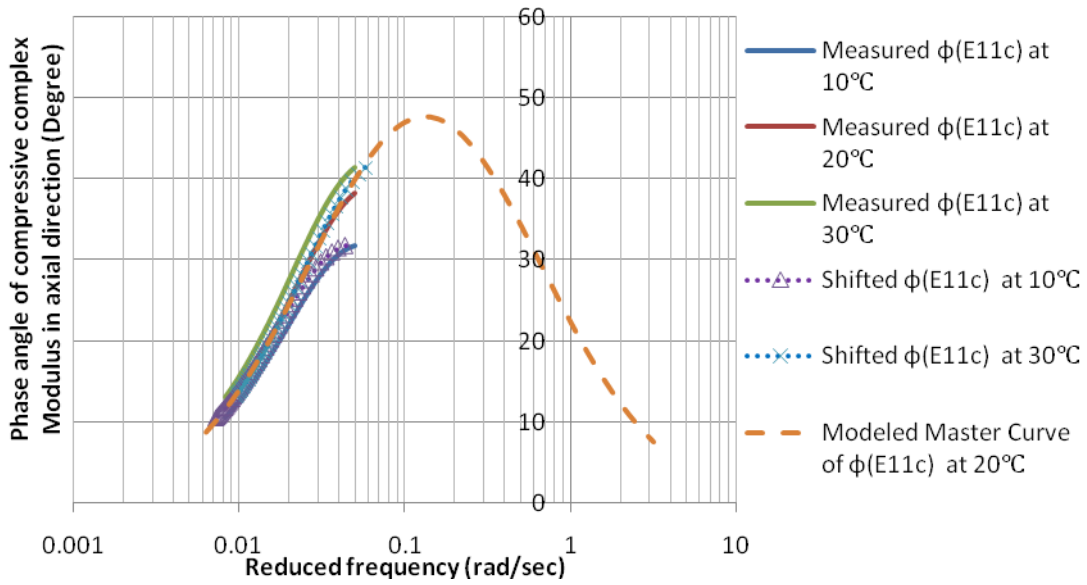


Figure F2c.3. Master curve of the phase angle of the compressive complex modulus at a reference temperature of 20°C.

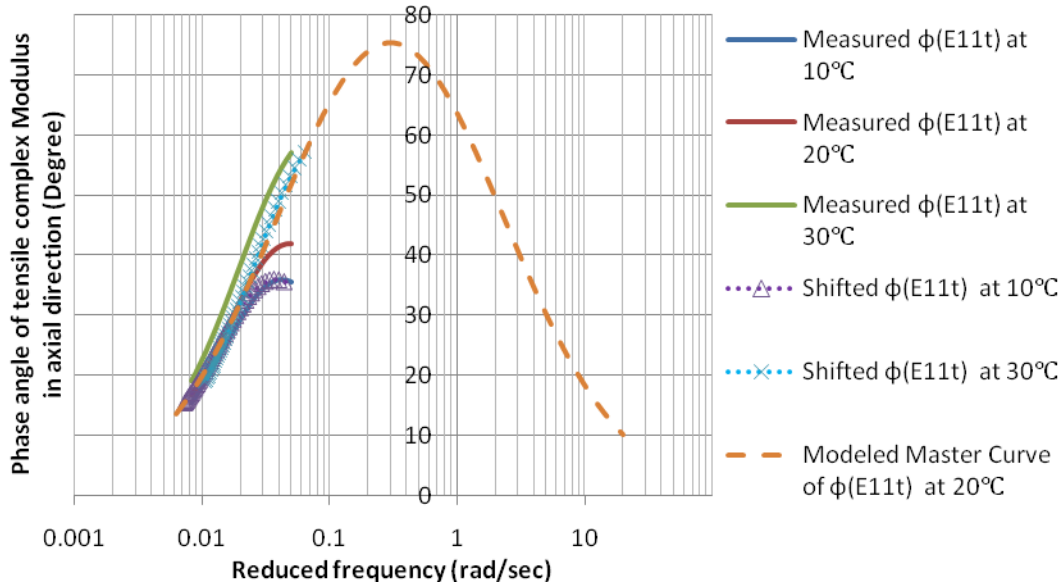


Figure F2c.4. Master curve of the phase angle of the tensile complex modulus at a reference temperature of 20°C.

Significantly different results were discovered on the master curves of the magnitude and phase angle of complex modulus in compression and tension. The magnitude of the compressive complex modulus is greater than that of the tensile complex modulus at a reference temperature of 20°C, while the peak phase angle of the tensile complex modulus is about 75 degrees which is significantly higher than the peak phase angle of the compressive complex modulus, which is approximately 46 degrees.

Equation F2c.3 is an empirical formula which is used to fit the S-shape master curve of the magnitude of the complex Poisson's ratio; Equation F2c.4, which is similar to Equation F2c.2, is utilized to construct the master curve of the phase angle of the complex Poisson's ratio.

$$|v^*(\omega)| = \frac{\alpha}{1 + \beta e^{k[\omega \cdot 10^{C(T-T_r)}]}} \quad (\text{F2c.3})$$

$$\varphi_v = \frac{\varphi_{mv}}{\left[1 + \frac{\log \left(\frac{\omega_{mv} \frac{C_1(T_r - T)}{C_2 + (T_r - T)}}{R_{\varphi_v}} \right)}{R_{\varphi_v}} \right]^2 \frac{m}{2}} \quad (\text{F2c.4})$$

where α , β , and k are fitting parameters; φ_{mv} = the maximum phase angle for Poisson's ratio, degrees; ω_{mv} = the frequency where φ_{mv} occurs, rad/sec; R_{φ_v} = fitting parameters for Poisson's ratio; T_r = reference temperature; and C , C_1 and C_2 = constants. Figures F2c.5 and F2c.6 show the master curves of the magnitude and phase angle of the complex compressive Poisson's ratio at a reference temperature of 20°C, respectively.

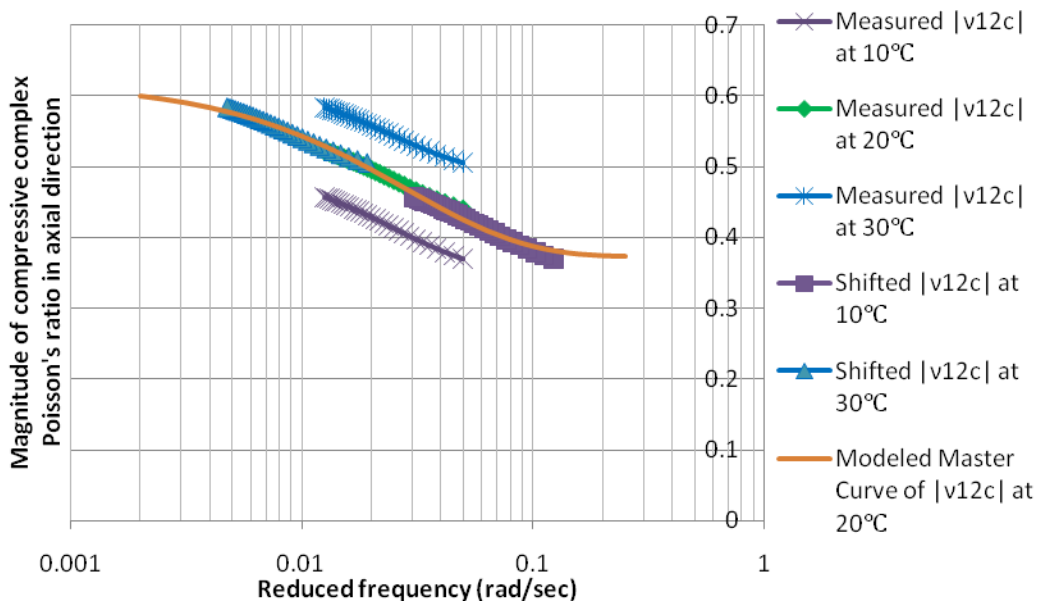


Figure F2c.5. Master curve of the magnitude of the compressive complex Poisson's ratio at reference temperature of 20°C.

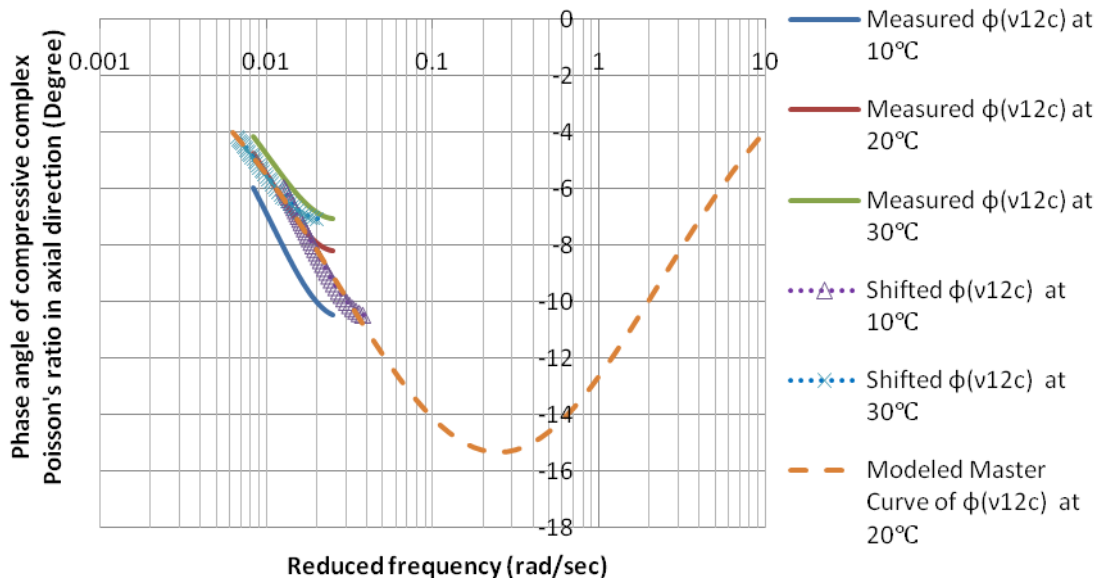


Figure F2c.6. Master curve of the phase angle of the complex compressive Poisson's ratio at a reference temperature of 20°C.

Significant Results

The test protocols were conducted at three different temperatures (10°C, 20°C and 30°C), and the magnitude and phase angle of the complex modulus were calculated using the proposed data analysis method using six parameters indicating the anisotropy of undamaged asphalt mixtures at each temperature. The master curves at 20°C of the magnitude and phase angle were constructed for the complex modulus in compression and tension, respectively. The master curves indicated that the undamaged asphalt mixture exhibited significant anisotropic properties under compressive loading. Specifically, the magnitude of the compressive complex modulus in the axial direction was greater than the magnitude of the compressive complex modulus in the radial direction. The master curve also showed that the undamaged asphalt mixture had different properties in compression from those in tension. The phase angle of the tensile complex modulus was significantly larger than that of the compressive complex modulus.

Significant Problems, Issues and Potential Impact on Progress

Test results indicated that the magnitude of the tensile Poisson's ratio might increase or decrease as the frequency increases depending on different temperatures and stress levels. It was also found in references that the viscoelastic Poisson's ratio does not vary monotonically with loading time (Lakes and Wineman 2006). The master curve of the magnitude of the tensile complex Poisson's ratio might not have an S-shape curve like that of the complex modulus. Thus, the models for master curves of complex modulus could not be used in constructing the master curves of the magnitude and phase angle of the tensile complex Poisson's ratio. New models need to be developed to construct the master curve of the complex Poisson's ratio. The complex Poisson's ratio needs to be further investigated so as to construct reasonable master curves for the magnitude and phase angle of the complex Poisson's ratio.

Work Planned Next Quarter

Further research will be conducted on the master curves of the magnitude and phase angle of the tensile complex Poisson's ratio. New models are going to be developed to address the complex Poisson's ratio. Then the complex Poisson's ratio in the axial direction and radial direction will be estimated and compared to find the anisotropy of the asphalt mixture.

Cited References

Lakes, R., and A. Wineman, 2006, On Poisson's Ratio in Linearly Viscoelastic Solids. *Journal of Elasticity*, 85(1): 45-63.

Luo, R., and R.L. Lytton, 2009, Characterization of the Tensile Viscoelastic Properties of an Undamaged Asphalt Mixture. *Journal of Transportation Engineering, American Society of Civil Engineers (ASCE)*, Accepted for Publication.

Zhang, Y., R. Luo, and R.L. Lytton, 2009, Anisotropic Viscoelastic Properties of Undamaged Asphalt Mixtures under Compressive Loading. *Journal of Transportation Engineering, American Society of Civil Engineers (ASCE)*, Submitted for review.

Work Element F2d: Tomography and Microstructural Characterization (TAMU)

Work Done This Quarter

Asphalt's microstructure consists of different domains with different viscoelastic properties (Masson et al. 2006). Nano-indentation using the AFM is a useful method to measure the distribution of the viscoelastic properties over these domains. For this purpose, a protocol was developed to systematically measure the creep and recovery of deformation during indentation of asphalt surface at specific locations.

Sample preparation:

For the preparation of asphalt solution, a known weight of asphalt was taken in a vial. A corresponding amount of toluene was then added to the vial so that the solution would have an asphalt concentration of 90.91 mg/cc. The mixture was allowed to sit for 24 hrs so that the asphalt completely dissolves in toluene. The obtained solution was coated on standard microscope glass slides using a **Laurell WS-650S spin processor at 1000 rpm.**

Experimental procedure:

The atomic force used for this study is Agilent Technology's 5400 Atomic Force Microscope. The cantilevers used for the experiment are the PPP-NCL cantilevers manufactured by Nanosensors. These cantilevers have a resonant frequency of 175 kHz on an average and have the stiffness ranging between 21-98 N/m. The cantilever tip is pyramidal in shape. All measurements were done using closed-loop scanning for obtaining accurate measurements of the vertical movement of the cantilever.

Initially, the sample was scanned in tapping mode to obtain the topography and phase image. Figure F2d.1 shows a typical phase image of the surface of AAD asphalt. The figure shows two phases - one dark colored and the other being light colored in the phase image.

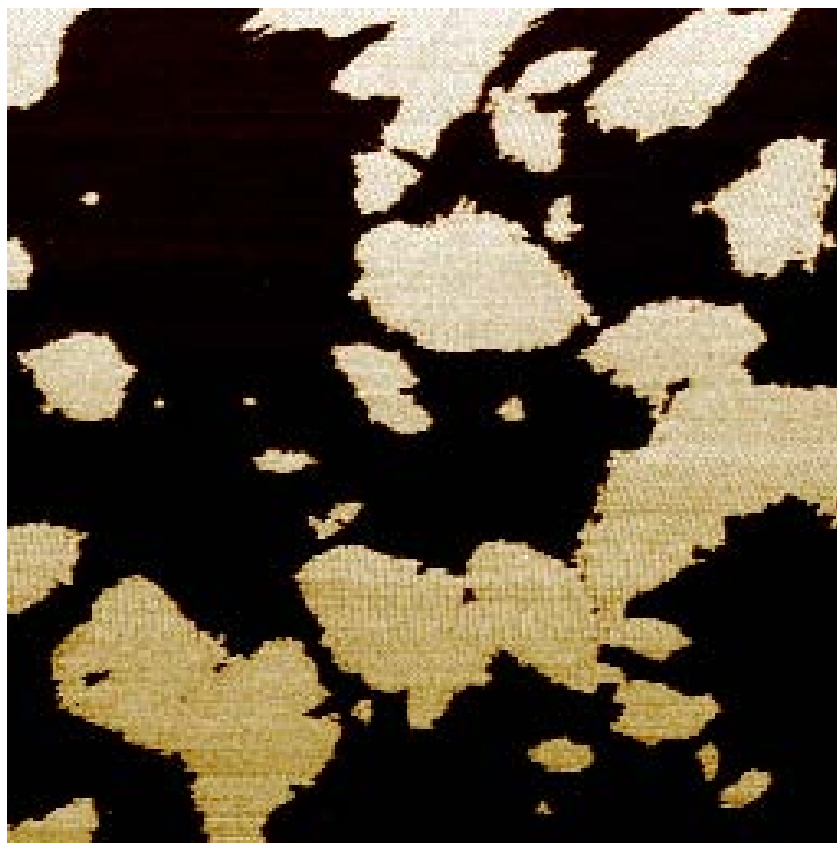


Figure F2d.1. Phase image of AAD asphalt.

The control was then changed to contact mode to perform indentation experiments on the sample. The tip was positioned over the point where the indentation response is needed. The force setpoint was increased slowly until the deflection error signal of the cantilever becomes 0.003 ± 0.001 V. The feedback control of the AFM brings moves the cantilever downwards until the deflection error signal reduces to 0 V. The above procedure ensures that the cantilever tip is just in contact with the surface before we conduct an indentation experiment.

The Picoview 1.6 software that comes with the AFM has features to conduct custom indentation experiments using the AFM. Using this feature, the setpoint was increased from the current value by 0.1 V in 0.02 sec and was held there for 1 sec. During this time, the deflection of the surface would increase showing a creep-like behavior. The setpoint was then decreased to its original value in 0.02 sec and then held at this point for another 1 sec to record the recovery of the deflection. The entire input is shown in figure F2d.2 as setpoint vs. time.

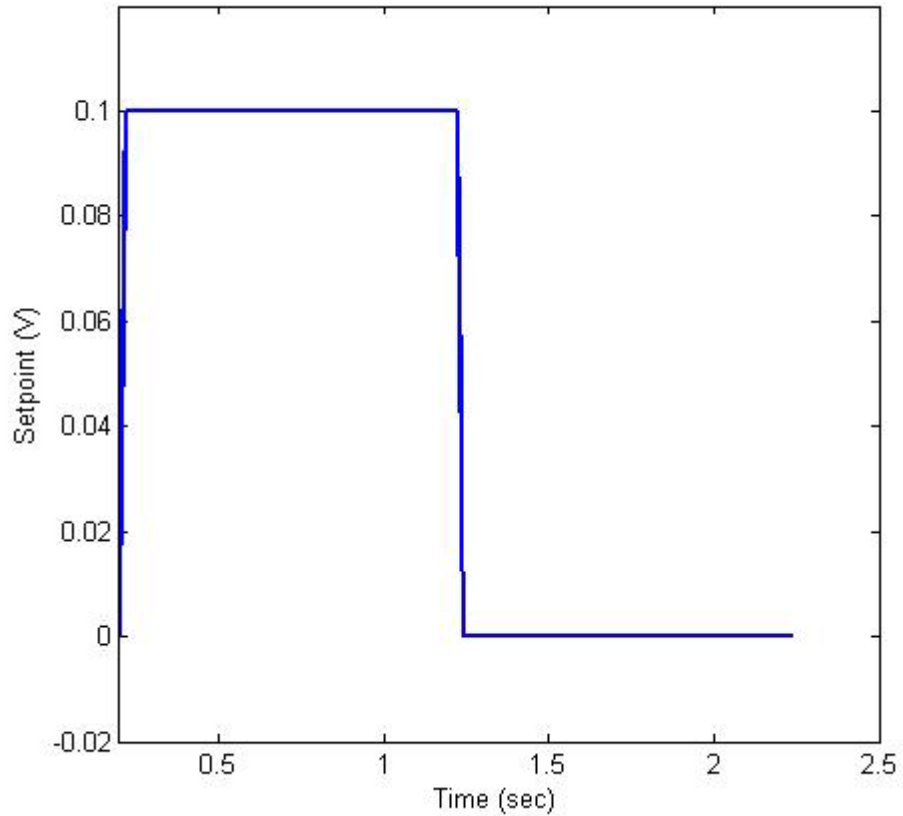


Figure F2d.2. Setpoint vs. time that is given as input to obtain the creep response.

In this manner, five such creep and recovery experiments were conducted on both the light phase and the dark phase. The results are shown in figure F2d.3. There is a significant difference between the creep and recovery response of the two phases. The results show that the light phase has a lower “stiffness” compared to the dark phase. This suggests that the AAD asphalt is a gel-type asphalt.

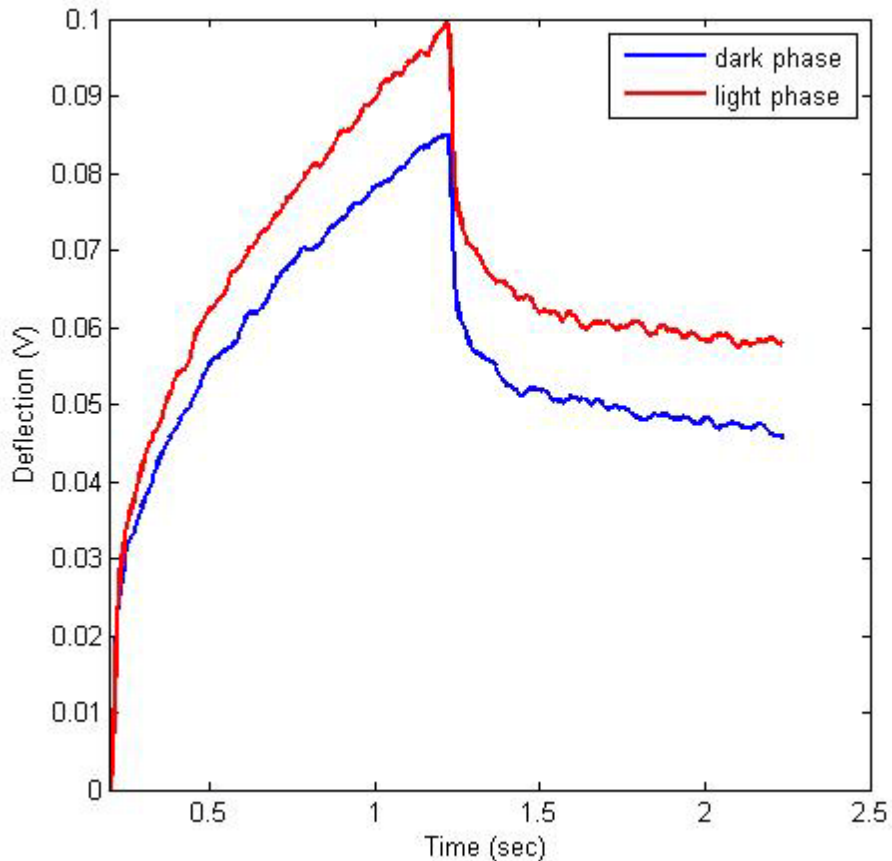


Figure F2d.3. Deflection vs. time obtained as a response from the indentation experiments.

Significant Problems, Issues and Potential Impact on Progress

The hardware problem related to the thermal K feature of the AFM still persists. Alternative methods for finding the stiffness of the cantilever are being explored.

Work Planned Next Quarter

Tests will be conducted on different asphalts to determine the distribution of viscoelastic properties in different asphalts. A method for determining the stiffness of the AFM cantilevers with reasonable accuracy will be chosen from the literature and employed for the creep and recovery experiments.

Texas A&M University is working under a memorandum of understanding with the Centre for Transportation and Infrastructure Excellence (CTIE) at the University of Saskatchewan to use the Synchrotron located at the university. This synchrotron is a world class instrument that allows us to use selected regions of the electromagnetic spectrum to investigate matter at the nano or even sub-nano scale. Details regarding the synchrotron at the University of Saskatchewan are provided under the website: lightsource.ca.

Texas A&M and the CTIE under the direction of Professor Curtis Berthelot have agreed begin with two experiments to investigate the mechanisms of microcrack and nanocrack healing. The first experiment investigates the intrinsic healing of asphalt binders across an artificially created crack interface. The second investigates the impact of moisture on the healing process as the moisture layer may interfere with the healing process. The basic objectives of each experiment are described below.

Experiment #1:

Intrinsic healing in asphalt binders across an artificially created crack interface.

The objective of this experiment is to determine the rate at which intrinsic healing occurs across an artificially created crack interface. The integrity of the material and amount of healing is quantified in terms of the mass density of the material. The hypothesis here is that the mass density at the interface of a crack would be zero (point of singularity). However, as the material heals over time the average mass density across the interface should approach a value that is similar to the bulk mass density.

Two specimens of the asphalt binder can be prepared on solid substrates (figure 1). These faces of these two specimens will be used to represent two faces of an ideally fractured bulk material. These two faces will be brought into intimate contact with each other and the mass density will be monitored across the interface over time (figure 2).

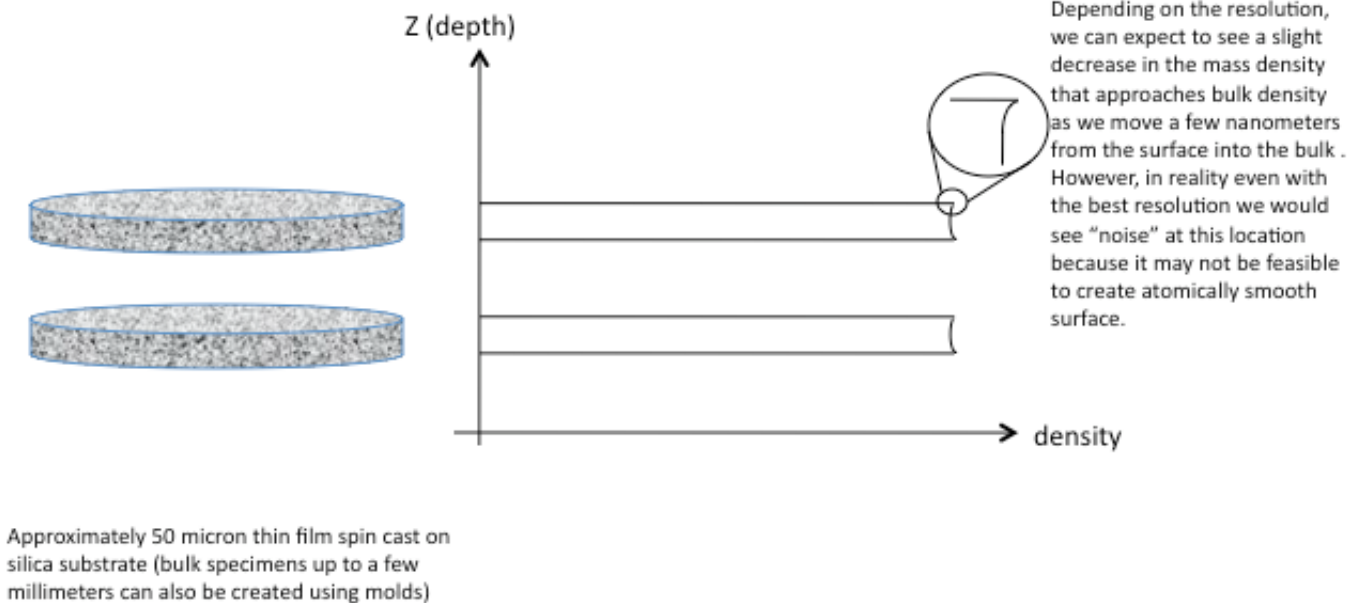


Figure 1. Schematic of the specimens and expected density profile.

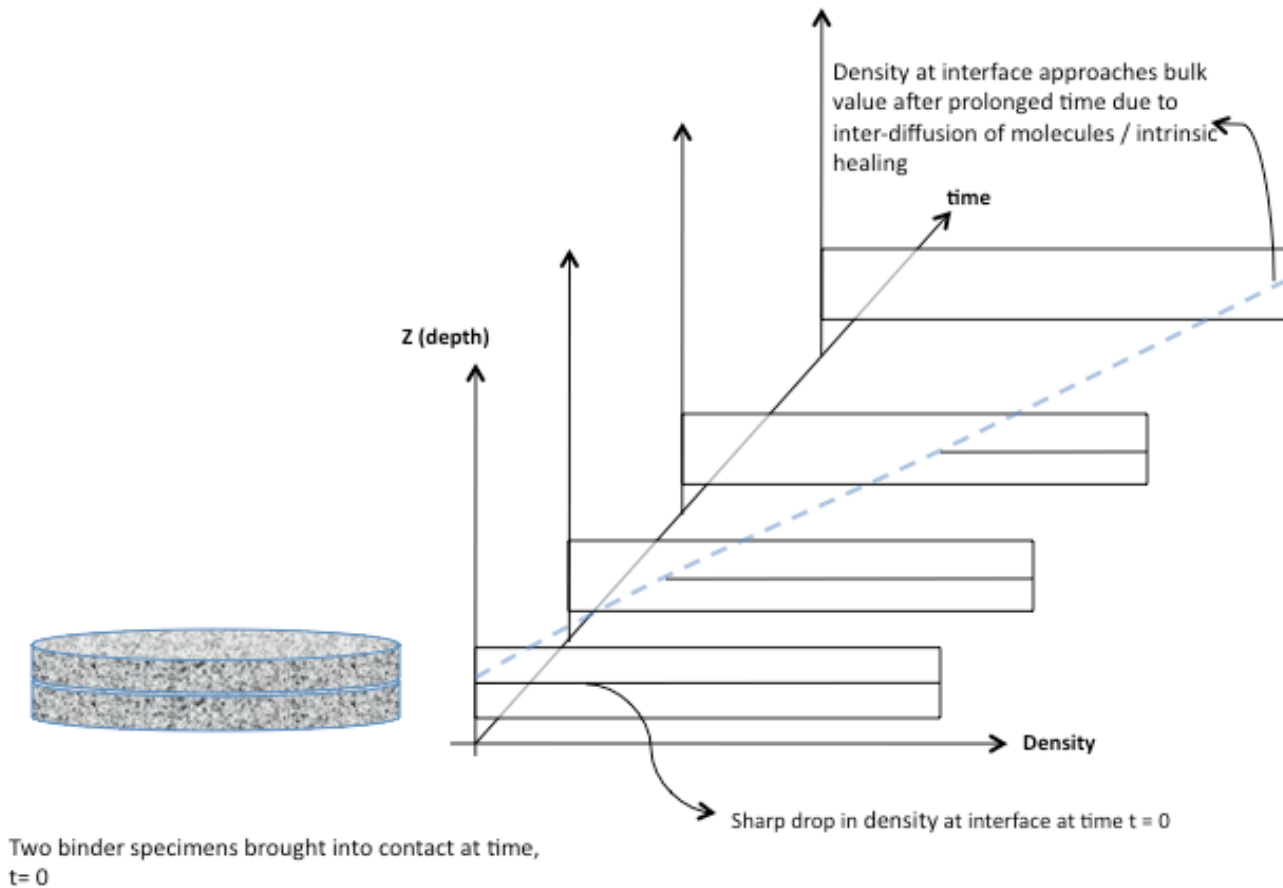


Figure 2. Measurement of density across the interface over time.

Experiment #2:

Adhesive failure at the binder-mineral interface due to moisture intrusion.

This experiment is very similar to experiment 1 with the following main differences.

The objective in this case is to determine the diffusion of moisture across the binder-mineral interface. The same experiment as above will be repeated with the exception that a smooth mineral surface and binder interface will be the subject of investigation (figure 3). The hypothesis in this case is that over time, moisture will displace the asphalt binder from its interface with the aggregates. The rate of displacement is a function of the thermodynamic properties of the asphalt binder.

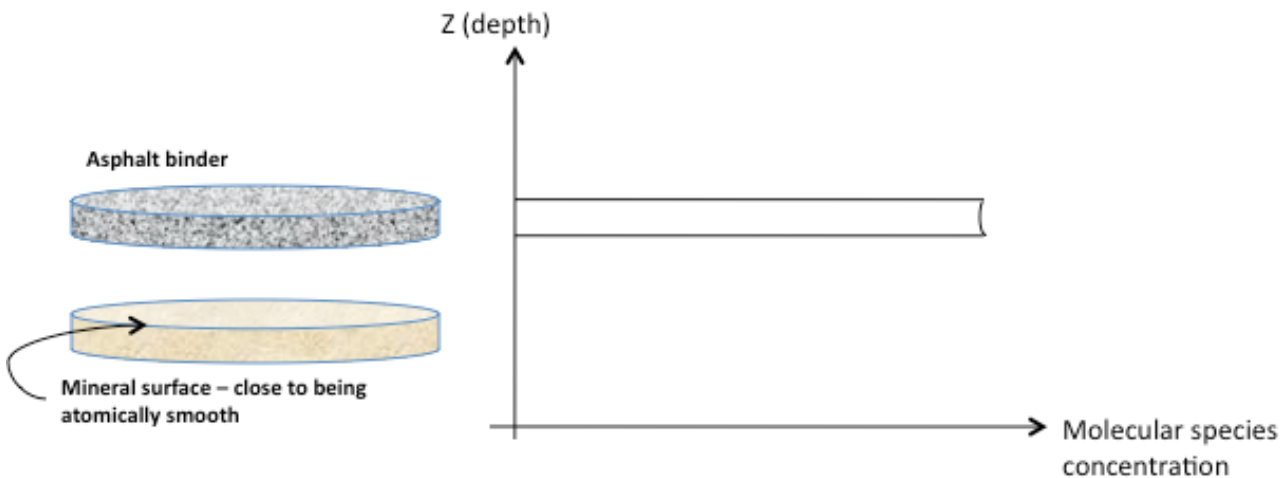


Figure 3. Set up for the failure at the binder-mineral interface due to moisture intrusion.

Cited References

Masson, J., V. Leblond, and J. Margeson, 2006, Bitumen morphologies by phase-detection atomic force microscopy. *Journal of Microscopy*, 221(1): 17-29.

Work Element F2e: Verification of the Relationship between DSR Binder Fatigue Tests and Mixture Fatigue Performance (UWM)

Work Done This Quarter

The research team evaluated the fatigue performance of binders selected in the previous quarter. Significant progress was made regarding the interpretation and modeling of the experimental data obtained using the framework of viscoelastic continuum damage (VECD).

Previous quarterly reports have shown that modeling damage from the Binder Yield Energy Test (BYET) with VECD works well for unmodified binders, but is not appropriate to model the response of modified binders due to the strain hardening (i.e., double peak) behavior of this material. For the case of modified binders, the measured stress curves with damage show more resistance to deformation than the predicted undamaged curves and, therefore, will result in an estimation of negative damage. BYET may still be useful for evaluating effects of polymer modification on binder properties and as a possible surrogate for force ductility tests. It is important to note that strain-hardening is difficult to include in the constitutive models necessary for VECD analysis; therefore, another test methodology such as amplitude sweep may be a better candidate for binder fatigue characterization.

The cyclic amplitude sweep tests did not show the phenomenon of strain-hardening. Cyclic tests are more indicative of fatigue-type failure; therefore, a refinement of amplitude sweep procedure

that allows for easier application of damage modeling using VECD was implemented this quarter. The new proposed methodology is based on strain sweep test with linear ramping and the calculation of damage growth based on dissipated energy. The amplitude sweep test results were compared to the standard time sweep tests. The time and strain sweep tests do not give the same VECD curve, as shown in figure F2e.1. Differences observed are most likely due to nonlinearity at high strains during the strain sweep. However, it appears that the VECD curve fit parameters from time and strain sweep data may be related.

If the VECD curves in figure F2e.1 are fit to a simple numeric equation:

$$\left|G^*\right| \sin \delta = C_0 - C_1 D^{C_2} \quad (\text{F2e.1})$$

then the fatigue life of the binder can be predicted using:

$$N_f = \frac{f(D_f)^k}{k \left(\pi \frac{I_D}{|G^*|} C_1 C_2 \right)^\alpha} |G^*|^{-\alpha} (\gamma_{\max})^{-2\alpha} \quad (\text{F2e.2})$$

where $k = 1 + (1 - C_2)\alpha$

The fatigue life equation F2e.2 can be further simplified in the form of the common fatigue law:

$$N_f = A(\gamma_{\max})^B \quad (\text{F2e.3})$$

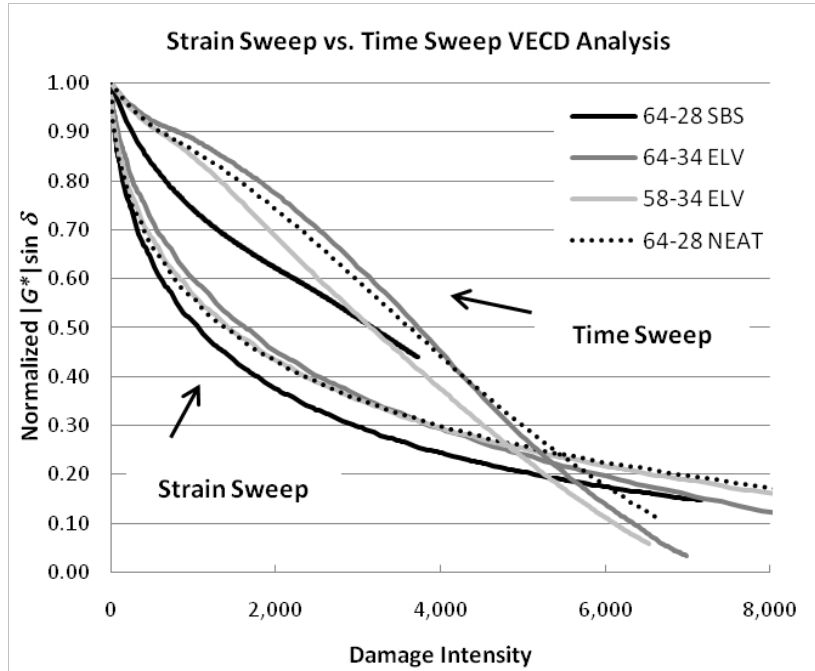


Figure F2e.1. Graph. Damage curve for time and strain sweep tests. (SBS = styrene-butadiene-styrene; ELV = Elvaloy.)

Fatigue life (N_f) and Parameters A and B were determined from strain and time sweep results. Figures F2e.2 and F2e.3 show a comparison between the fatigue parameters obtained from strain and time sweep tests. Significant correlation is observed between the fatigue life and the Parameter A obtained from strain and time sweep tests.

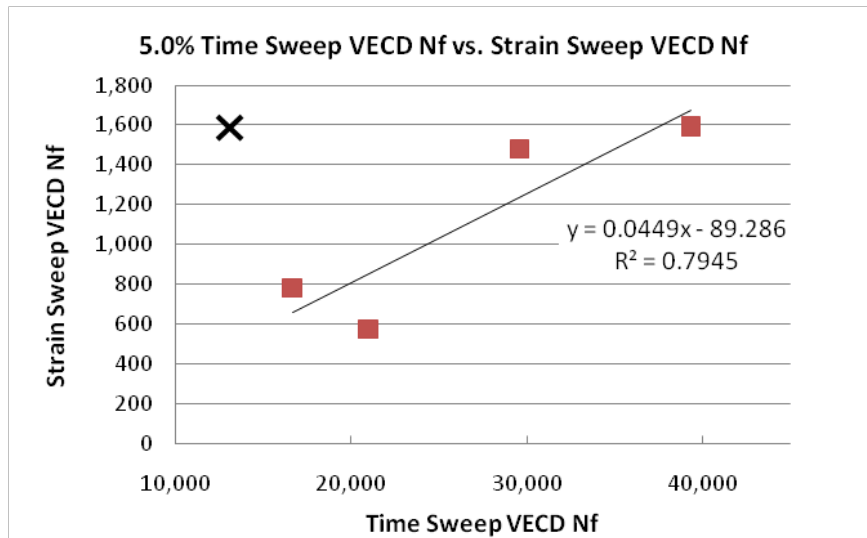


Figure F2e.2. Graph. Comparison of number of cycles to failure from time and strain sweep.

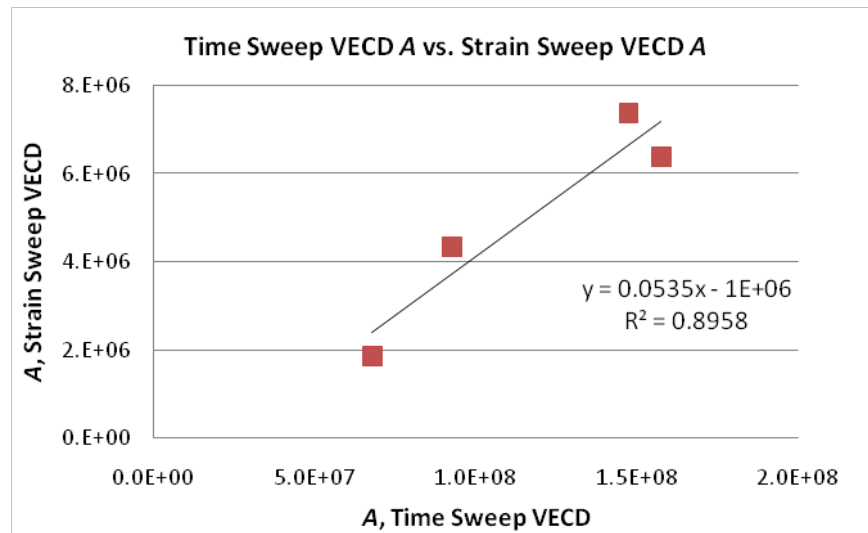


Figure F2e.3. Graph. Time and strain sweep comparison.

Work has also started to coordinate the activities of this work element with FHWA's Turner-Fairbank Highway Research Center (TFHRC) research on fatigue and cracking. A number of conference calls were conducted and a plan was developed to share materials, exchange ideas and compare results.

Significant Results

The amplitude sweep tests combined with VECD modeling can be used for fatigue characterization of asphalt binders. The following proposed accelerated fatigue procedure was developed during this quarter:

- Determine the value of the factor α to be used in equation F2e.2.
- Perform the amplitude sweep at continuous intermediate temperature (IT) grade temperature.
- Calculate damage intensity to build VECD curve.
- Determine curve fit coefficients to calculate A and B.
- Predict number of cycles to failure using appropriate strain level and local calibration.

A presentation was given at the Binder ETG meeting in September and very useful feedback was received. The research team proposed that an AASHTO draft procedure be developed for both the BYET and the Linear Amplitude Sweep. The ETG agreed that such standards will be useful. The research team has drafted the standards and will deliver them to the ETG early next quarter.

Significant Problems, Issues and Potential Impact on Progress

To reflect the actual progress of this research, the Gantt chart has been updated to show extended progress and completion dates for subtasks F2e-1 and F2e-2. The Gantt chart has also been updated to show the planned Draft Report deliverable for subtask F2e-2 will be delivered in December 2009 and the planned Final Report in March 2010.

Work Planned Next Quarter

Current binder fatigue specifications lack the ability to characterize damage of the material. The amplitude sweep procedure is currently being investigated to improve fatigue specifications. However, the ability of this procedure to accurately indicate mixture fatigue performance needs to be verified.

The work planned for next quarter includes continuing to test the full experimental matrix with the amplitude sweep method and validation of the binder fatigue characteristics to mixture fatigue performance. The evaluation of LTPP materials using the proposed method will also continue during next quarter.

Joint work with the TFHRC Working Group will continue, with special focus on running the Double-Edge Notched Tension (DENT) testing.

CATEGORY F3: MODELING

Work Element F3a: Asphalt Microstructural Model (WRI, URI, VT)

Work Done This Quarter

The main work in the July–September 2009 quarter was to establish the big picture for a multiscale chemo-mechanical model of asphalt. The current thinking is described in a contribution to the Proceedings of the First International Workshop on Chemo-Mechanics of Bituminous Materials, which was held in Delft, the Netherlands in June 2009 (Greenfield 2009). In that paper, we described a broad framework for how coupling must occur across length and time scales. The key idea is for a simultaneous “push” (from smaller scales to larger) and “pull” (from larger scales to smaller) within models. Arrows indicating possible “pushes” and “pulls” are shown in figure F3a.1, which was also shown at the September 2009 ETG meeting. The pale arrows in the lower left indicate how molecule-scale simulations can be conducted to yield results for larger lengths at short times, shorter lengths at longer times, or some combinations (“push”). Guidance from rheology and phase structure models (“pull”, darker arrow pointing down and to the left) is necessary to formulate the kinds of statistical averaging and simulation that can yield usable parameters. In other words, “pulls” from above help to recognize the “pushes” from below that yield functions and parameters that are found within and/or are useful for the larger scale models.

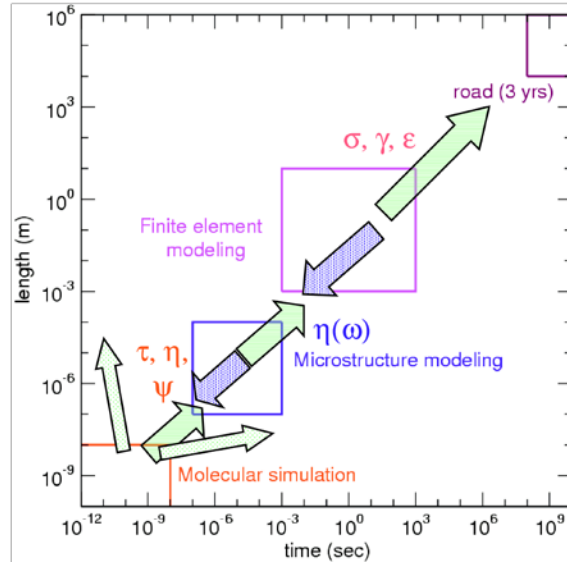


Figure F3a.1. “Push” and “pull” across length and time scales in modeling of asphalt chemical and mechanical properties across wide ranges of length and time scales.

Not all “pulls” are viable. For example, rheology data can be described within a number of different parameterized models. Some of the models are based on well-defined molecular concepts, such as distributions of relaxation times, while others are described more as resembling curve fits. Only the approaches based on solid fundamentals provide a pathway to connect molecular-scale dynamics results to the rheology model parameters. Another example is that a phase field model can be devised to work (as in many formulations) with a simple double-well potential. Averaging over true molecular-scale simulations doesn’t yield such simple results, however. Instead, a means of averaging the thermodynamics function that is simplified into a double-well free energy potential must be found. **Summarizing, the “pull” that can be obtained on the molecular scale as a feed “push” into the mesoscale is important to identify.**

A fresh analysis of prior asphalt simulation data with a perspective towards chemo-mechanics was also initiated this quarter. It was found that single-molecule self diffusion coefficients within model asphalt systems were qualitatively similar in magnitude to the overall self diffusion coefficient measured by the Delft group (Scarpas et al.) via spin-echo neutron scattering. This result is not yet published. Further findings are described in the Significant Results section.

In-person discussions this quarter:

- Follow-ups to the International Workshop on Chemo-Mechanics (Delft; June 2009)
- Petersen Conference (Laramie, WY; July 2009)
- Models ETG meeting (San Antonio; September 2009)

Presentations this quarter:

- Petersen Conference (Laramie, WY; July 2009): fundamental approaches to rheology modeling and its connections to chemo-mechanics

- Models ETG meeting (San Antonio; September 2009): molecular contributions to chemo-mechanical properties of asphalts (presentation specifically requested by ETG)
- International Workshop on Chemo-Mechanics (Delft, the Netherlands; June 2009 in prior quarter): molecular contributions to chemo-mechanical properties of asphalts (*costs not charged to this project*)
- Thermodynamics 2009 (London, UK; September 2009): contributions of individual molecules to overall asphalt relaxation and viscosity (*costs not charged to this project*)

Significant Results

A significant finding occurred when reanalyzing prior simulation results. The presence of a straight-chain C₂₂ ordering effect (i.e. **spontaneous wax crystallization**) was recognized in a first-generation model asphalt (Zhang and Greenfield 2007a) at 298 and 358 K but not at 400 and 443 K (0 and 85°C but not 127 or 170°C). The ordering occurred over times of 5 to 10 ns (1 ns ≡ 10⁻⁹ s) within a bulk model asphalt. (Surfaces had been precluded via periodic boundary conditions.) Preliminary information about this exciting event was shared at the Models ETG meeting. Further study is required to understand the crystallizations in detail.

Significant Problems, Issues and Potential Impact on Progress

A URI graduate student was not found for the project for the fall 2009 semester. This personnel issue is not expected to cause adverse effects on the overall project. It is expected that a graduate student will be available for the spring 2010 quarter.

Work Planned Next Quarter

The next quarter will focus on two areas: (1) next-generation model asphalts and (2) molecular/phase model connections. Dissemination efforts will continue concerning the wax crystallization event as well.

Sub-subtask F3a-1.1, *Next Generation Model Asphalts*. The first and second generation model asphalts need further improvements for accurate chemo-mechanical modeling. The three-component first generation asphalts (Zhang and Greenfield 2007a) contained too much saturate (59 mass%) and too few heteroatoms, but they described viscosity well (Zhang and Greenfield 2007b). The second generation model asphalts (Zhang and Greenfield 2008) provided a better density match due to improved alkane/aromatic balance and heteroatom concentrations, but the large number of polar resin molecules that were too small in size led to viscosities that were low compared to asphalt viscosities known from experiment. Next generation model asphalts will seek to improve further on the heteroatom concentration and alkane/aromatic balance while using model compounds of higher molecular weight for the resins and saturates. NMR and infrared spectroscopy data from the literature and from recent experiments at WRI will provide guidance about heteroatom concentration, alkane/aromatic ratio, and SARA balance. Data on size exclusion chromatography (SEC) will be sought from WRI and the literature since they are very useful for describing molecular weight. Additional asphaltene molecular structures will be considered as well. The choice of compounds will be pursued jointly by URI and WRI.

Sub-subtask F3a-1.2, *Molecular simulation “push” and phase model “pull”*. Additional formulation work is required to identify the detailed path for incorporating molecular simulation outputs into phase field model inputs. The possibility of using an equation of state, such as the Self Associating Fluid Theory (SAFT), will be studied in detail this quarter. This will include a literature study of SAFT applied to asphalt-like and/or asphaltene-containing systems.

Cited References

Greenfield, M. L., 2009, Bitumen at the Molecular Level: Molecular Simulations and Chemo-Mechanics, submitted to *Proceedings: International Workshop on Chemo-Mechanics of Bituminous Materials*, Delft, the Netherlands.

Zhang, L. and M. L. Greenfield, 2007a, Analyzing properties of model asphalts using molecular simulation. *Energy Fuels*, 21:1712-1716.

Zhang, L. and M. L. Greenfield, 2007b, Relaxation time, diffusion, and viscosity analysis of model asphalt systems using molecular simulation. *J. Chem. Phys.*, 127:194502.

Zhang, L. and M. L. Greenfield, 2008, Effects of polymer modification on properties and microstructure of model asphalt systems. *Energy Fuels*, 22:3363-3375

Work Element F3b: Micromechanics Model (TAMU)

Subtask F3b-1: Model Development

Subtask F3b-2: Account for Material Microstructure and Fundamental Material Properties

Cohesive Zone Model

Work Done This Quarter

During this quarter we have mainly progressed towards two activities:

- Implementation of a computational framework for extrinsic cohesive zone (CZ) models into an in-house finite element code to investigate numerical issues of each model (intrinsic and extrinsic) on the prediction of fracture;
- Development of testing accessories to completely set up the semi-circular bending (SCB) fracture test which is being used to identify CZ fracture properties of FAM phase by integrating experimental results with numerical simulations;

Work progress and significance of each activity can be summarized as follows.

- Implementation of a computational framework for extrinsic CZ models into an in-house finite element code;

As exemplified in figure F3b-1.1, CZ models can be postulated in different forms but mostly in two groups: intrinsic or extrinsic. In the intrinsic CZ models, the traction-separation ($T_i-\Delta_i$) relation is such that with increasing separation, the traction reaches a maximum, then decreases and eventually vanishes, indicating a complete decohesion (separation). In contrast, the extrinsic CZ models do not display the initial ascending trend by assuming that separation occurs when cohesive zone traction reaches the cohesive strength (T_{max}) of the material. The intrinsic model is typically easier to implement into a numerical framework, while cohesive elements in the extrinsic models are often adaptively inserted into the mesh, which leads to a much more complicated mesh updating scheme due to the renumbering of nodes and elements as fracture continues. However, the extrinsic model is considered representing the reality better, since it avoids the artificial compliance effect that is typically present in the intrinsic model. The artificial compliance effect can be significant and results in an adverse numerical impact such as non-convergence, when CZ elements are embedded in a large area in the object and/or when the initial ascending slope is not sufficiently steep. Furthermore, the intrinsic model requires much more computational costs than the extrinsic cases because of pre-embedded cohesive elements, where some of them are not really necessary.

The intrinsic cohesive zone models, such as the bilinear (linear hardening followed by linear softening) model presented in figure F3b-1.1(a) have been completely implemented in the recent version of ABAQUS (version 6.8). Therefore, ABAQUS was used to simulate fracture processes by the bilinear intrinsic CZ model. As a parallel step, an in-house finite element code, MULTIMECH, where the extrinsic CZ models have been developed and implemented, was used to compare simulation results from two different fracture modeling strategies (i.e., extrinsic vs. intrinsic). For a more equivalent comparison with the bilinear CZ model, a linear (softening) model presented in figure F3b-1.1(b), was implemented and used. Numerical issues of each CZ model on the prediction of fracture are investigated and compared by using the same set of meshes presented in figure F3b-1. 2.

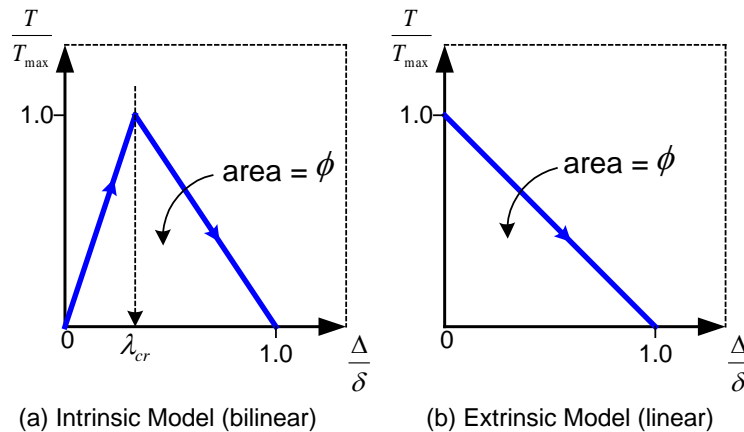


Figure F3b-1.1. Two primary groups of CZ models.

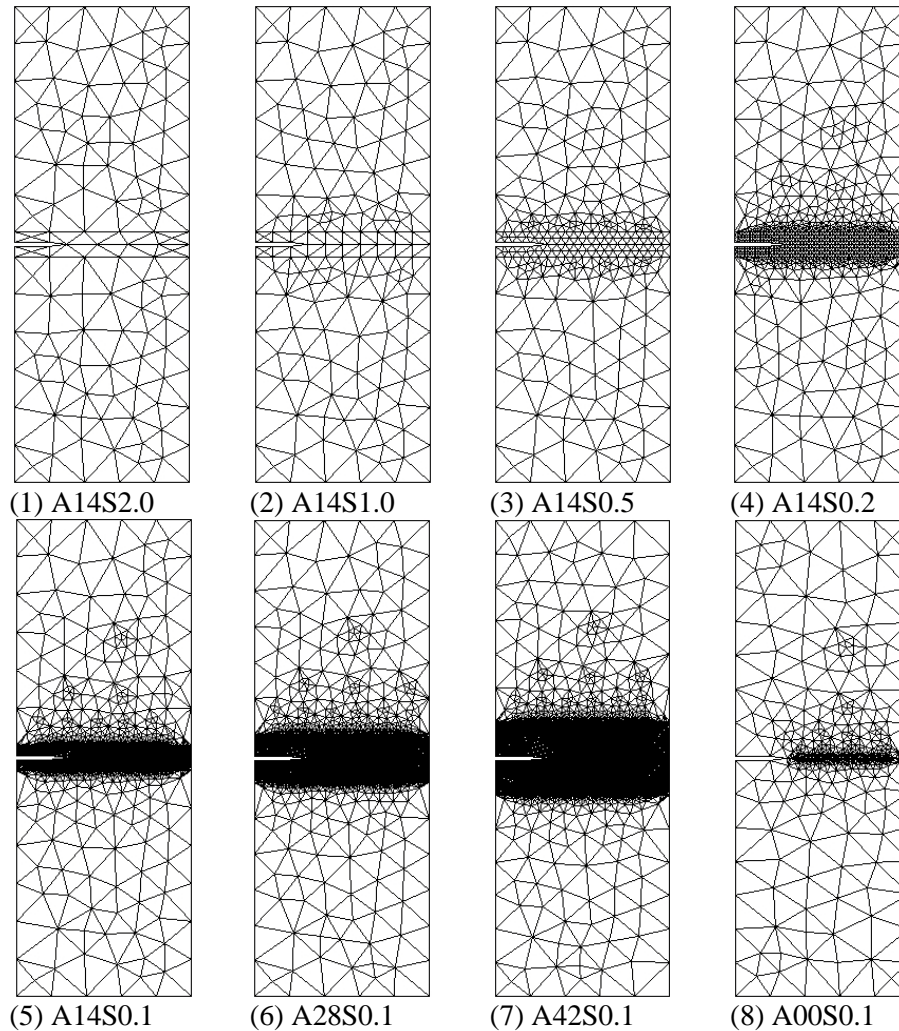


Figure F3b-1.2. Finite element meshes of the SENT specimen.

A total of eight meshes on a single-edge-notch tensile (SENT) specimen (10-cm wide and 27.4-cm tall) was generated. The ID of each mesh represents its characteristics based on the area where CZ elements are embedded, and the level of mesh refinement in that area, when the intrinsic bilinear CZ model is used. For example, the ID A14S0.1 indicates that 14 cm² in the middle of the specimen was discretized with an average CZ element of 0.1-cm size. For simulations with the extrinsic linear softening model, as mentioned earlier, CZ elements were not initially embedded in the same mesh but adaptively inserted as the stress states vary in the body during the fracture process. Comparing simulation results between the intrinsic model and the extrinsic model obtained from mesh ID No. (1) to (5), one can notice the effects of mesh refinement (i.e., size of CZ element) on the overall fracture behavior of the specimen simulated by two different CZ models. Similarly, by comparing results from mesh ID No. (5) to (8), any differences between two CZ models can be noticed, when the number of CZ elements varies with the same size of CZ elements.

The intrinsic CZ models inherently produce artificial compliance due to a pre-peak region described in the cohesive zone model. However, the artificial compliance can be significantly reduced by using the bilinear CZ model, since it can adjust initial slope in the model, as a result, the intrinsic model can be close to the extrinsic linear softening model. Figure F3b 3 clearly demonstrates how the artificial compliance can be reduced by increasing the pre-peak slope (K -value). Figure F3b-1.3 only presents simulation results from the mesh ID A28S0.1, but all other cases generally demonstrated an identical trend which implies that the numerical convergence can be met when the pre-peak slope is greater than 5.0×10^{12} .

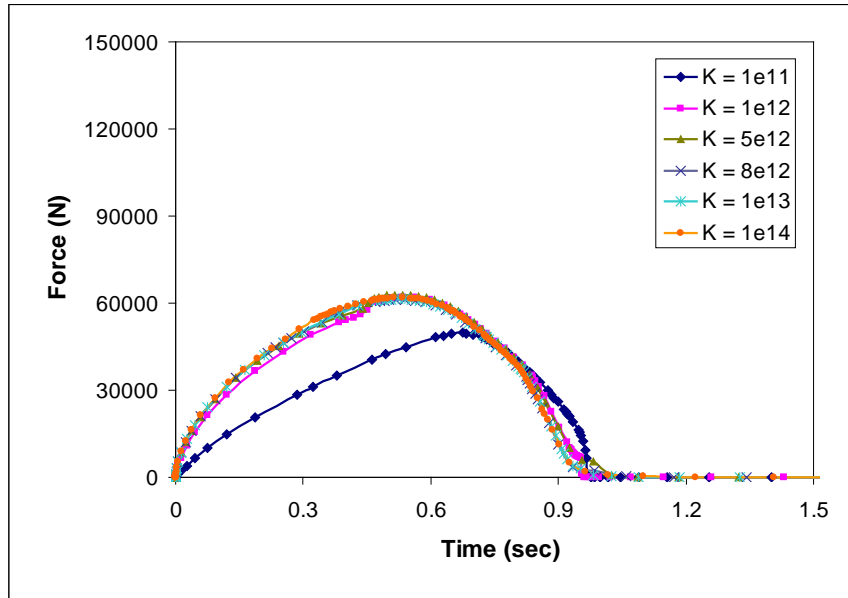
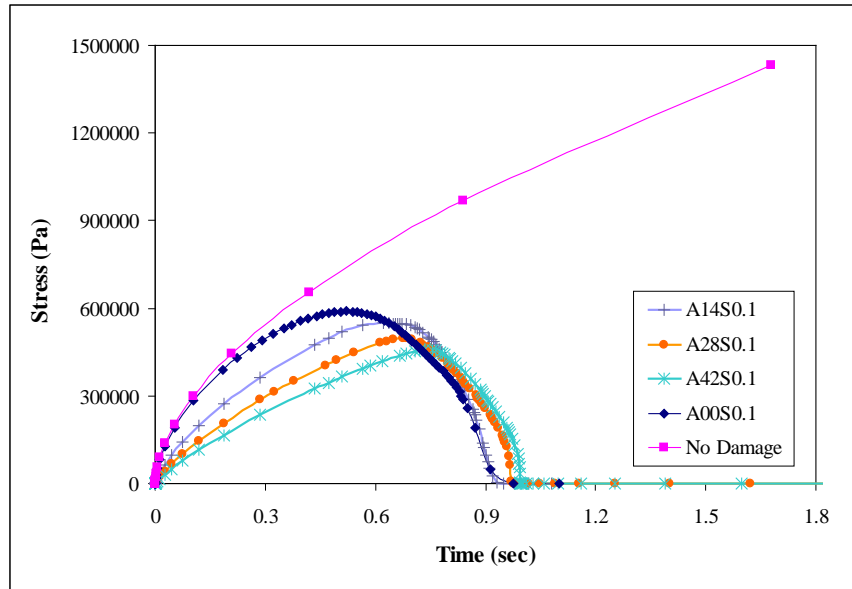
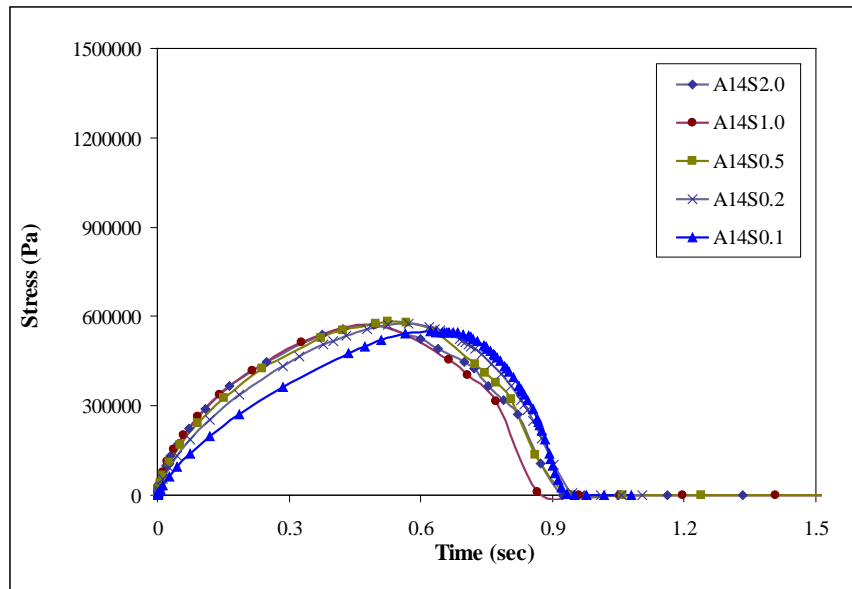


Figure F3b-1. 3. Simulation results from the mesh A28S0.1 at different K -values.

The artificial compliance effects of pre-peak slope are further demonstrated in figures F3b-1. 4 and 5. When the lower K -value such as 1.0×10^{11} is used, the influence of the pre-peak slope on the overall specimen fracture behavior is noteworthy. It is clearly observed from figure F3b-1. 4 that as the number of CZ elements increases (by changing the area or the level of refinement), the compliance likewise increases. This is expected, because as the number of CZ elements increases, the contribution of the CZ elements in terms of energy dissipation likewise increases. When the pre-peak slope is steep enough (K -value of 5.0×10^{12} as shown in figure F3b-1.5), the artificial compliance among meshes is not significantly sensitive any longer, although it is still recommended to minimize the number of CZ elements, if possible.

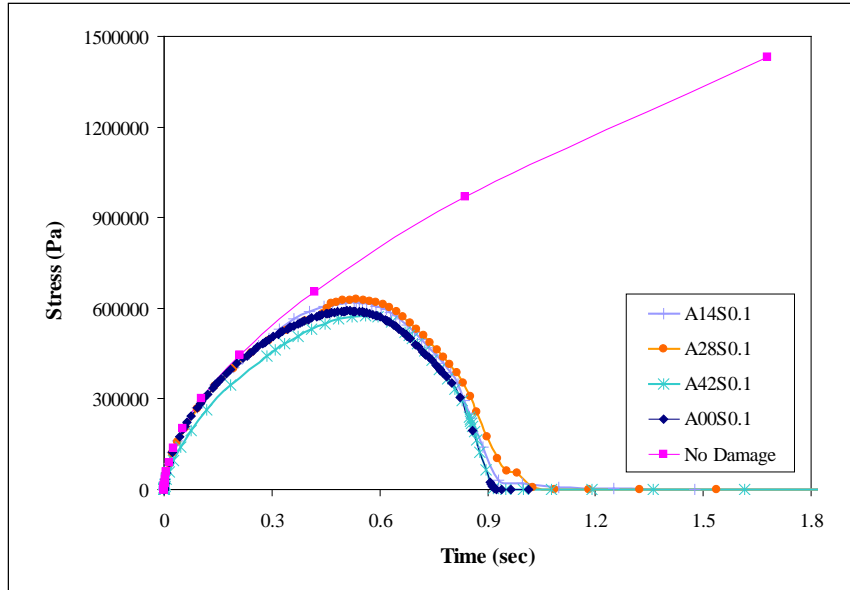


(a) meshes with different area for CZ elements

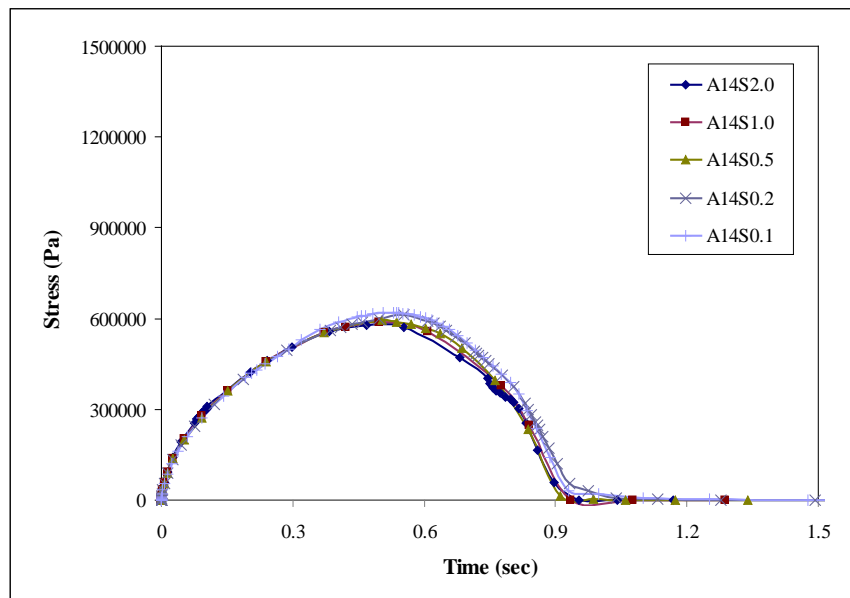


(b) meshes with different level of refinement

Figure F3b-1.4. Simulation results obtained at the pre-peak slope of $1.0 \cdot 10^{11}$.



(a) meshes with different area for CZ elements

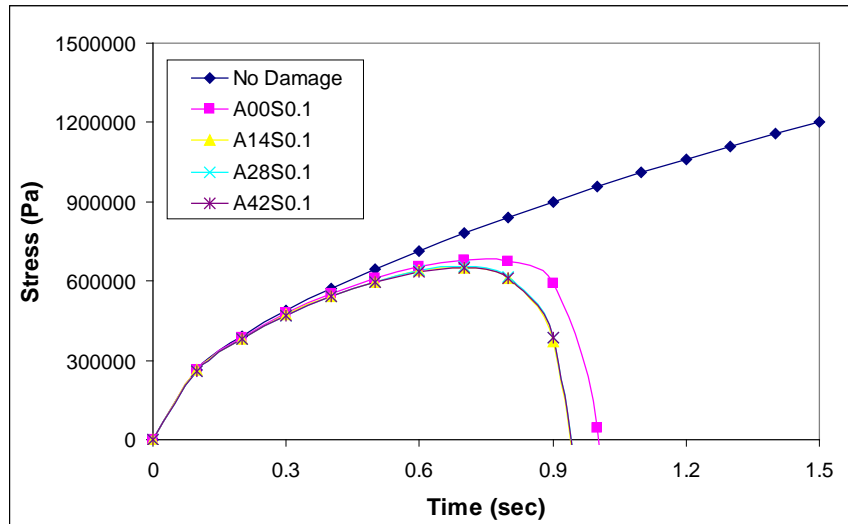


(b) meshes with different level of refinement

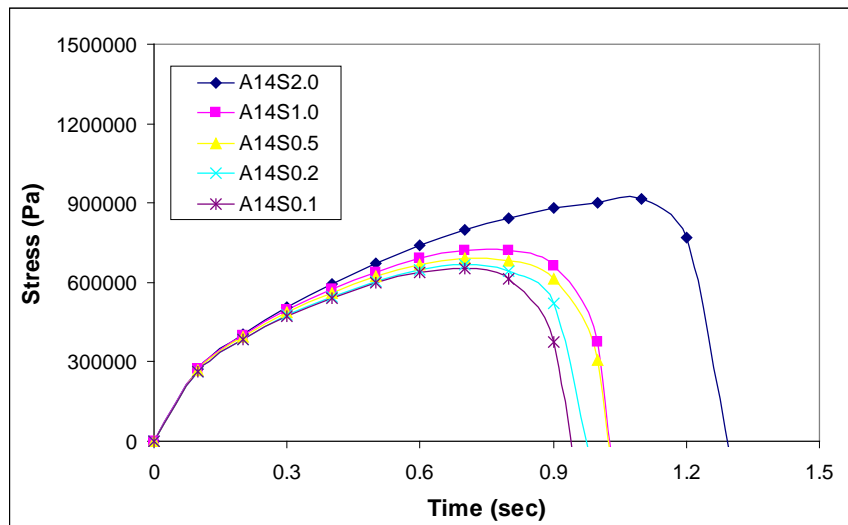
Figure F3b-1.5. Simulation results obtained at the pre-peak slope of $5.0 \cdot 10^{12}$.

On the contrary to the cases using the intrinsic bilinear CZ model, figure F3b-1.6 presents simulation results when the extrinsic linear softening model incorporated with the adaptive insertion scheme was applied. Clearly, simulation results converge and become stable as the mesh is finer with an appropriate size of region for the fracture process. This is expected in a sense that the adaptive insertion of CZ elements is governed by stress states in the body, and the

stress state is influenced by the local mesh refinement when using the finite element technique because of the discrete characteristics of geometry, however the fine mesh does not necessarily be applied to regions where cracks are not likely involved. Consequently, simulation results of all three cases (A14S0.1, A28S0.1, and A42S0.1) in figure F3b-1.6(a) were very similar, which infers that energy dissipation due to cracking of all three cases was independent of finite element meshes.



(a) meshes with different area of cohesive zone elements



(b) meshes with different level of refinement

Figure F3b-1.6. Simulation results using the extrinsic CZ model.

Based on the simulation results and corresponding outcomes, figure F3b-1.7 compares results from the intrinsic case (using the mesh A00S0.1) to the extrinsic case (using the mesh A14S0.1). The figure also includes the case when cohesive elements are not used: no damage. As can be seen in the figure, all cases match well from the initial stage of loading to a certain level before the peak stress. Then, the cases with damage degraded and deviated from the case without damage due to the fracture process induced by CZ elements. No huge difference was observed between the intrinsic model and the extrinsic model. The difference observed at the later stage of loading between two CZ modeling approaches is not surprising, considering that the way of simulating fracture process is quite different.

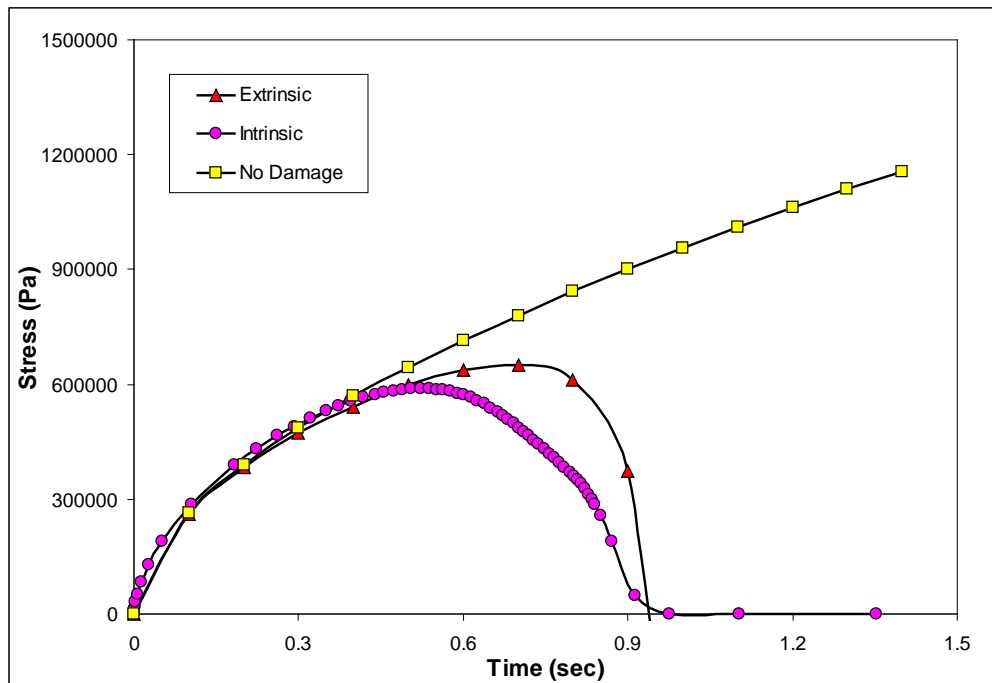


Figure F3b-1.7. Comparison between intrinsic model and extrinsic model.

- Development of testing accessories to completely set up the semi-circular bending (SCB) fracture test;

The experimental work for this quarter was related to the design and development of various accessories and to the purchase of a clip gauge to measure crack mouth opening displacements (CMOD) of semi-circular bending (SCB) testing specimens. These efforts are expected to enhance the quality and efficiency of the SCB testing to identify the CZ fracture properties of FAM phase. The SCB specimens are subjected to constant displacement rate loading condition to the top center line of the specimens. The parts and tools shown in figure F3b-1.8 facilitate the specimen positioning in the SCB fixture and eliminate any loading eccentricity that could have occurred if the specimens are positioned manually. Figure F3b-1.8 presents all the units developed or purchased for the testing, and figure F3b-1.9 shows a SCB specimen ready to be tested.

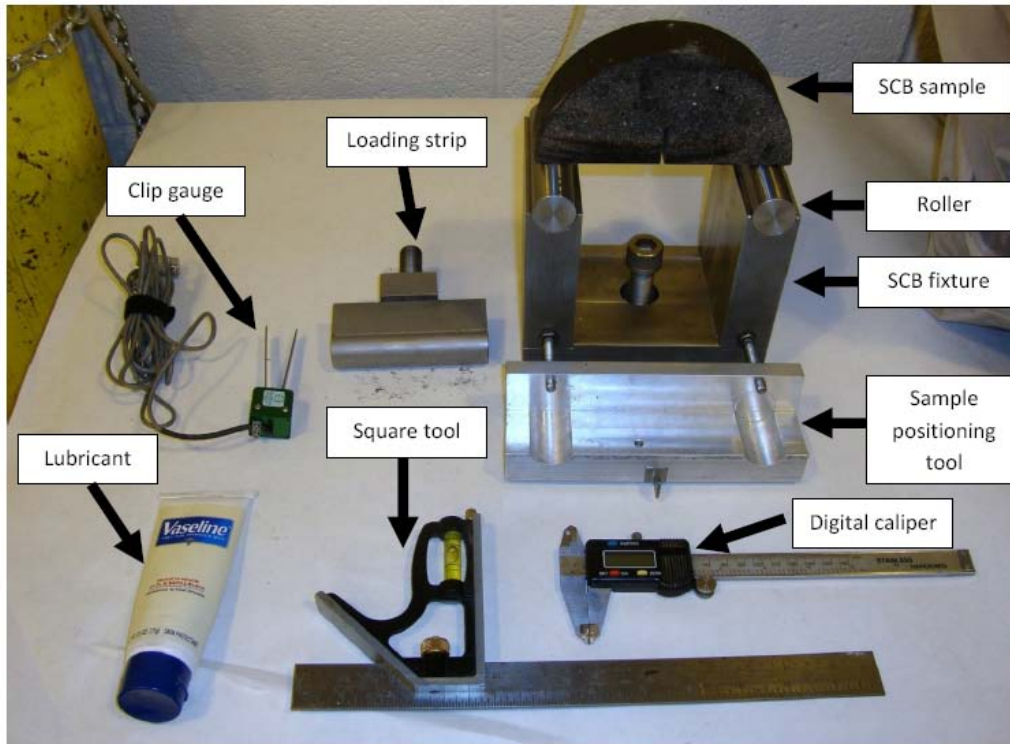


Figure F3b-1.8. Accessories designed, fabricated, and purchased for the SCB testing.

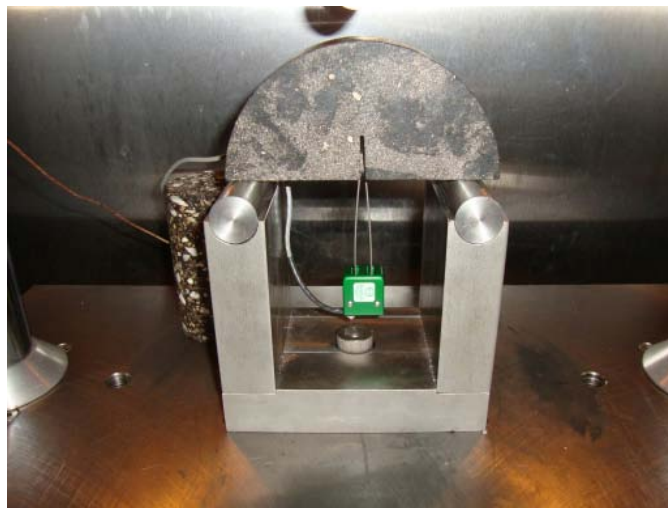


Figure F3b-1.9. SCB testing set-up.

With the aforementioned improvements on the experimental set-up, several SCB specimens were fabricated by slicing a single Superpave gyratory compacted (SGC) sample. A mechanical notch of 2-mm wide and 25-mm deep was generated in each specimen using a small diamond-blade table saw. Each specimen was placed inside of the chamber of a mechanical testing machine (UTM-25kN) at least four hours before testing for temperature conditioning. The testing temperature was set at 23°C. As an example, figure F3b-1.10 shows test results from two replicates subjected to a loading rate of 100 mm/min. Testing repeatability has improved from the initial set-up reported in the last quarter.

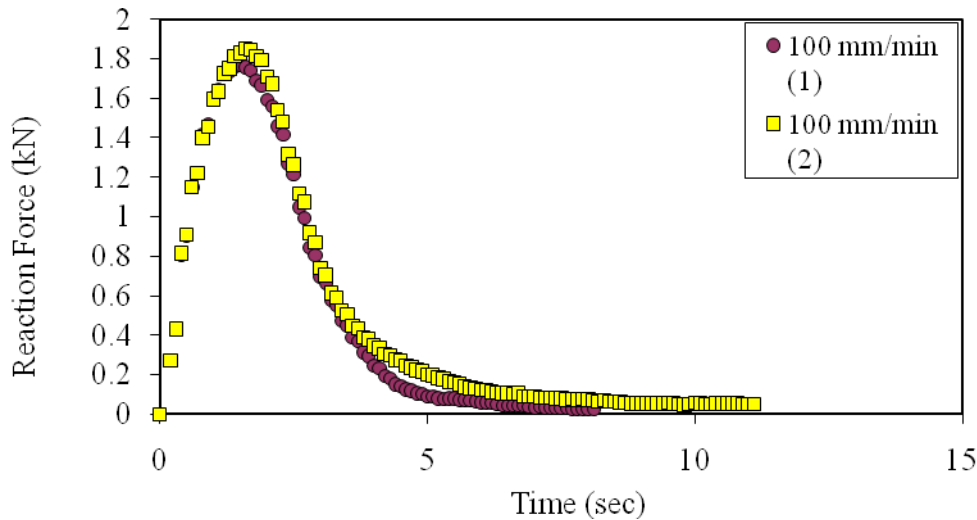


Figure F3b-1.10. SCB test results from two replicates at 100 mm/min.

Significant Problems, Issues and Potential Impact on Progress

None.

Work Planned Next Quarter

Using the improved SCB fracture testing system, we will perform tests at different loading rates with specimens fabricated with different thicknesses. This effort will provide any meaningful insights into the effects of specimen geometry and loading rates on fracture characteristics of FAM specimens, so that we can better identify cohesive zone model properties to be used for simulating asphalt concrete mixture fracture.

Another primary task we will focus for the next quarter is the implementation of the testing-analysis protocol that we have developed during the last quarters for mixing, compaction, and production of FAM specimens. The proper level of density (compaction) in the FAM phase will be determined in the next quarter. This task is to develop a more articulate and scientific protocol in mixing and compaction of the FAM phase which will produce key material properties (viscoelastic properties and cohesive zone properties of matrix phase) to accomplish

the micromechanical modeling. Advanced tomography analysis techniques and finite element computational simulations will be incorporated with mechanical tests to finally develop the best protocol to fabricate the FAM specimen. The tomography analysis will be conducted by researchers at the University of Texas-Austin.

Lattice Micromechanical Model

Work Done This Quarter

In the previous quarter, the efficiency of the multi-scale virtual fabrication and lattice modeling software (MS-VFLM) was further increased, with main focus on the efficiency of modeling viscoelastic fracture. The efficiency of the viscoelastic fracture algorithm was increased by incorporating the correspondence principle instead of conventional state variable approach. The current quarter's efforts focused on the characterization of the quantitative aspects of the model. A new postprocessor has been designed in order to facilitate the process of comparison of several test results obtained from MS-VFLM.

The postprocessor is capable of showing the damaged pattern of each specimen on the microstructure along with the stress-strain curve. It can also animate the process of crack formation along with the propagation of the crack inside specimen. Another feature of this postprocessor is statistical analysis resulting in the probability distribution of strength and stiffness of different specimens in the same scale. Example snapshots of the postprocessor are shown in the following two figures (figures F3b-1.11 and F3b-1.12).

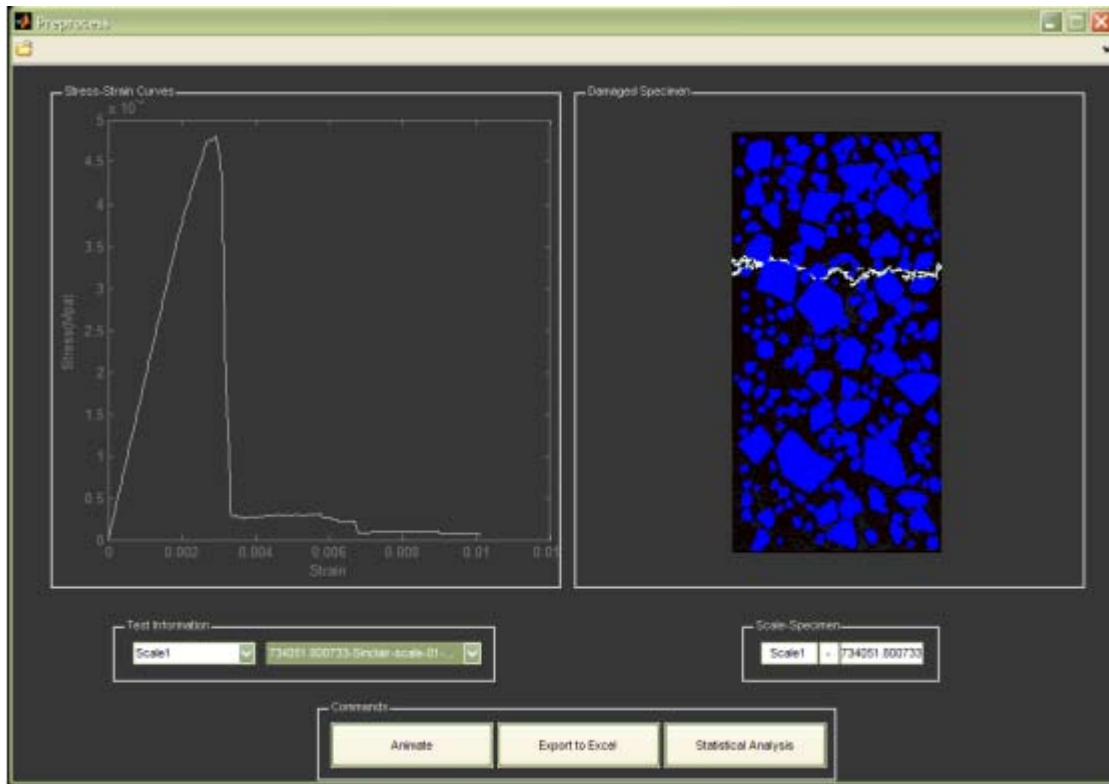


Figure F3b-1.11. Postprocessor designed for MS-VFLM.

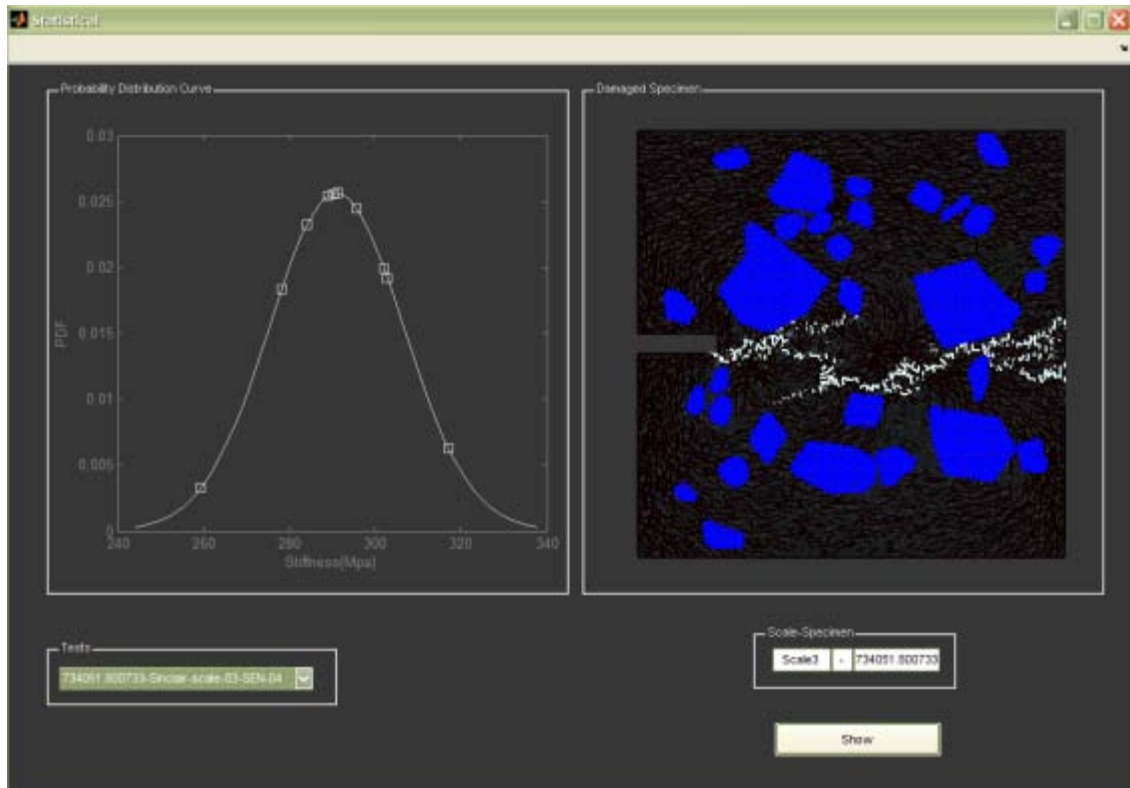
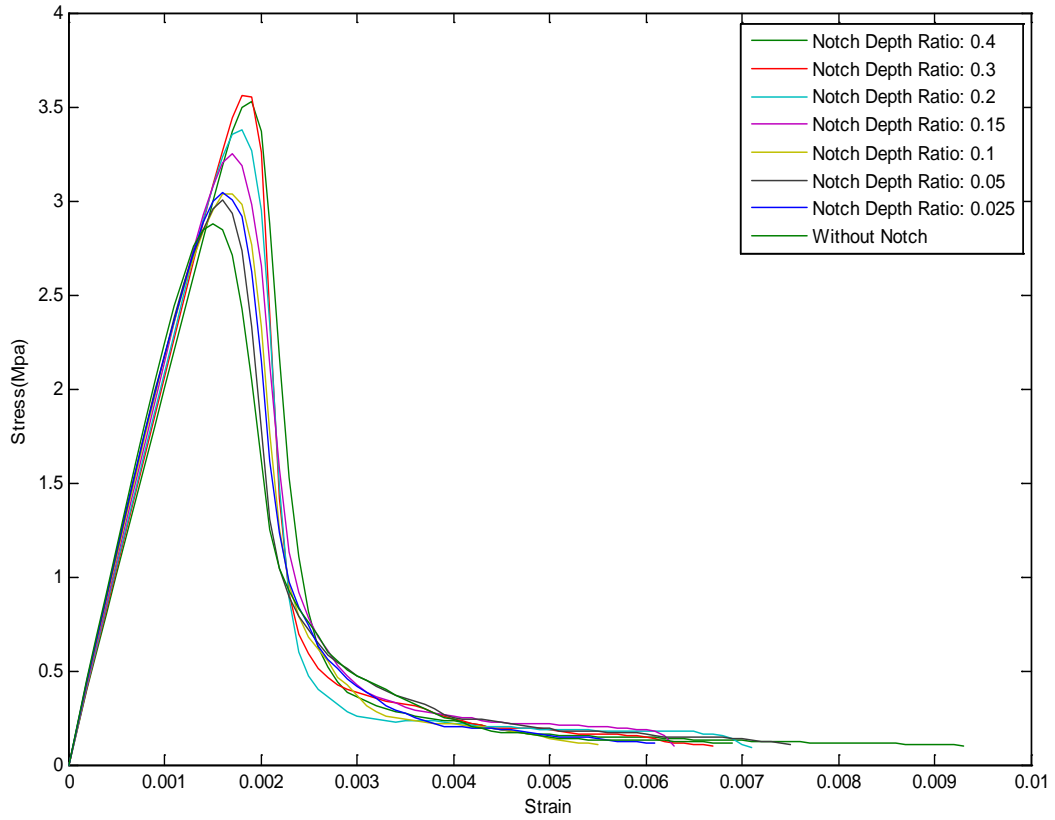
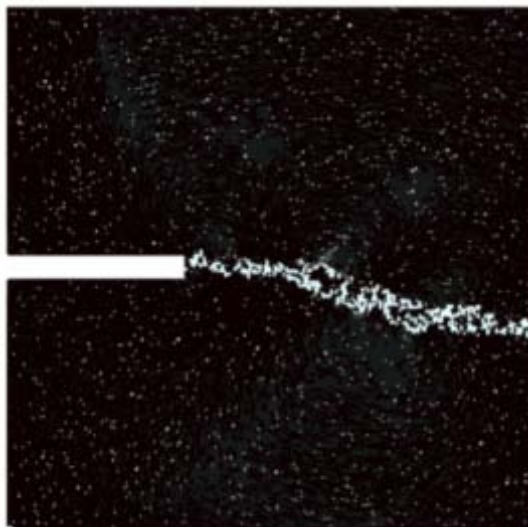


Figure F3b-1.12. Postprocessor-statistical analysis of the results.

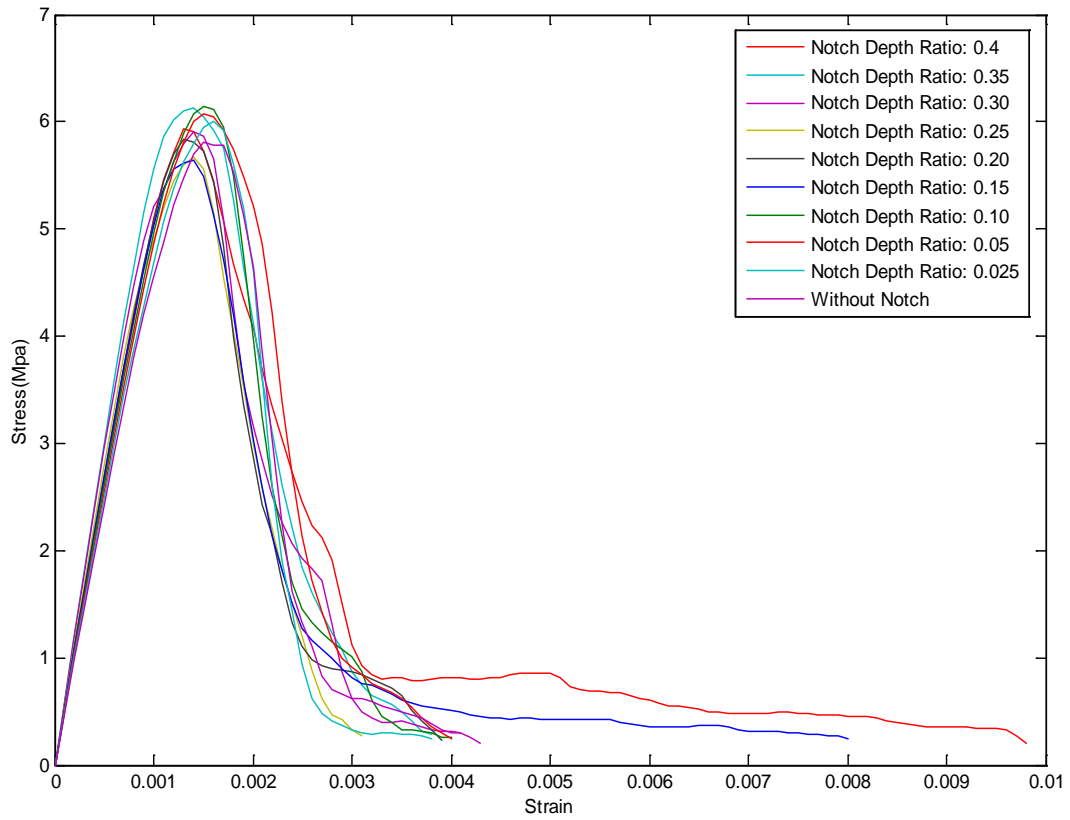
The new viscoelastic implementation requires accurate stress-strain curves from previous scale to be fed to the next scale as input. Any difference from real stress-strain curves may soften or harden the viscoelastic behavior in the next upper scale. Since the stress-strain curves from lower scales in MS-VFLM are obtained by performing single notch tests (SEN tests), the effect of notch size on stress-strain curve of each scale has been investigated. In other words, since all the scales are analyzed through the new viscoelastic implementation, there had been a suspicion that the notch size or even existence of a notch in viscoelastic analysis may change the behavior of stress-strain curve in each scale. The following figures (figures F3b-1.13 through F3b-1.16) show the effect of notch size on stress-strain curve in homogeneous and heterogeneous media.



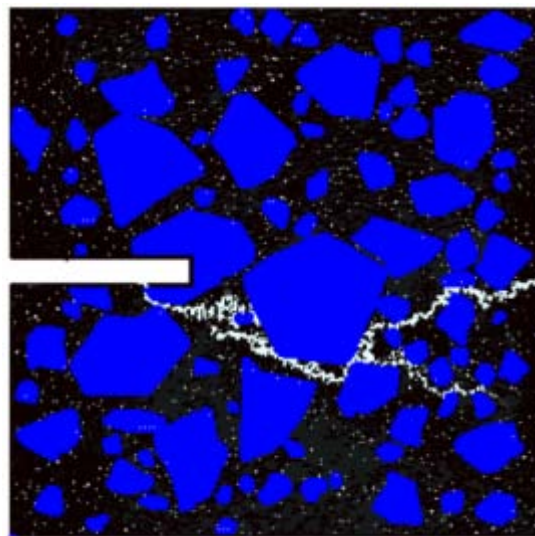
F3b-1.13. Notch size effect on stress-strain curve in homogeneous media.



F3b-1.14. Typical crack pattern observed for a homogeneous single notched specimen.

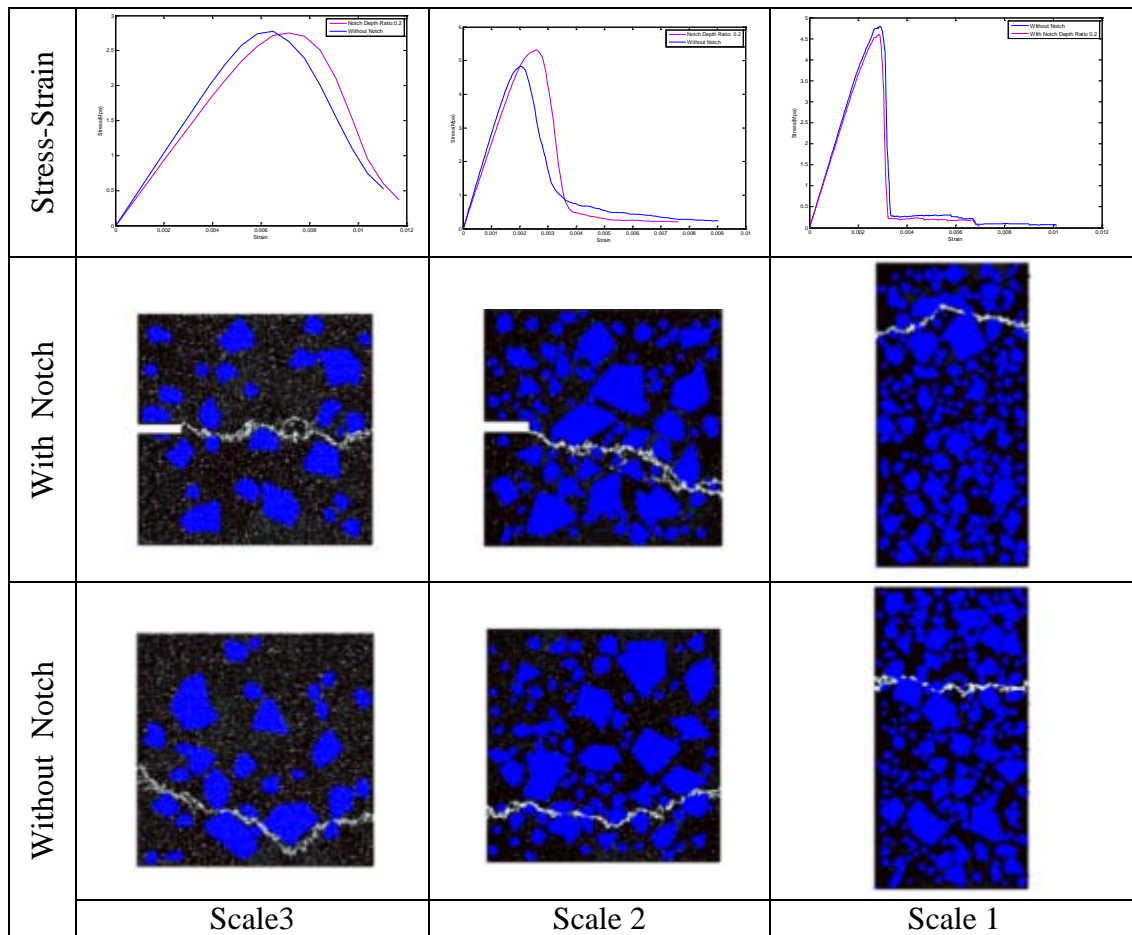


F3b-1.15. Notch size effect on stress-strain curve in heterogeneous media.



F3b-1.16. Typical crack pattern observed for a heterogeneous single notched specimen.

Specimens with the same microstructure but different notch sizes were subjected to SEN test. The notch sizes range from 0 to 0.4 times the size of the specimen. It is observed that in homogeneous media notch size affects the behavior of stress-strain curve while heterogeneous media shows little sensitivity to the notch size, indicating that the including a notch may not be critical for the proposed multi-scale modeling approach. To confirm this, we investigated the effect of notch size in the current multi-scale frame work. Specifically, we compared the behavior of specimen at different scales with and without notch (multiple specimens have been tested in each scale). The figure below (figure F3b-1.17) shows the stress-strain curves and crack patterns obtained from each set of specimens (one crack pattern for each scale is shown here as an example). The results show that the behavior of material is not very sensitive to notch size, indicating that a specimen without notch may be sufficient to obtain the stress strain curve. Further investigations are underway to finalize this strategy.



F3b-1.17. Multi-scale analysis of specimen with and without notch.

Within this quarter, the software development aspect of lattice modeling is concluded. Further work will focus on quantitative model refinement; work in the next quarter will focus on the following issues:

- a. An important factor that changes the strength of the material is the rate of loading. The current implementation of viscoelastic fracture does not incorporate this aspect and appropriate models will be developed to tackle this issue.
- b. Material characteristics fed to the lowest scale is the most important factor in determining the characteristics all other scales. We intend to use experimental data at mastic and mixture levels to confirm the validity of our up-scaling approach.
- c. Presence of air voids appears to affect the specimen strength significantly and their incorporation into lattice modeling will be investigated.

Significant Results

None

Significant Problems, Issues and Potential Impact on Progress

None

Work Planned Next Quarter

- Effect of rate dependency will be investigated and added to the model.
- Appropriate experimental results will be used to verify the accuracy of MS-VFLM.
- Preliminary implementation of air voids in lattice modeling software will begin.

Continuum Damage to Fracture

Work Done This Quarter

Work is underway in quantitatively defining micromechanical characteristics of damage, specifically under cyclic loading. This understanding is expected to eventually facilitate linking continuum damage model to localization and fracture.

Work Planned Next Quarter

Work will continue on quantitative, micromechanical characterization of damage, specifically under cyclic loading.

Work Element F3c: Development of Unified Continuum Model (TAMU)

Work Done This Quarter

Comparison of Different Loading Model for Wheel Tracking Test

The constitutive model that has been developed under ARC in the past three years has been incorporated in a three dimensional finite element structural model, which is subjected to a moving load. The challenge so far in using this three-dimensional structural model is that it takes long time to model a large number of cycles as occurs in pavements. Hence, it is necessary to find the optimum modeling approach which yields reasonable results and at the same time allows modeling the large number of loading cycles. In this study the effect of structure geometries (e.g. 2D simulation, and 3D simulation), and loading models (e.g. equivalent loading, pulse loading, moving loading etc.) on rutting performance of the pavements is investigated.

In order to study the effect of two-dimensional (2D) plane strain and three-dimensional (3D) analysis, a 2D and 3D finite element model were constructed to simulate a Wheel Tracking Test. The geometry of Wheel Tracking Test is sketched in figure F3c.1. The wheel tracking test consists an asphalt slab of dimensions 305mm, 280mm and 100mm in length, width and depth, respectively. The wheel loading area is 20mm*50mm and the wheel speed is set at 40 passes per minute over a wheel path 230mm. The finite element model can be reduced to half a slab due to the symmetry in width of slab by fixing the horizontal direction on the vertical edge of the mesh to represent the middles of slab. The 3D and 2D finite element model are shown in figures F3c.2 and F3c.3, respectively.

A comprehensive study in the effect of different loading model was conducted by comparing the rutting from different models. The rutting is calculated using equation (F3c.1) and compared at the center of test slab (Location A in figure F3c.1).

$$u^{per} = \sum_{i=1}^k \varepsilon_{vp}^k * h^k \quad (F3c.1)$$

Where u^{per} is the permanent deformation (Rutting), ε_{vp}^k is the viscoplastic strain at k^{th} layer and h^k is the element length in depth at k^{th} layer.

The first and second loading models are applied one wheel loading area on the center of slab with pulse and equivalent loading mode, respectively, shown in figure F3c.4. The equivalent loading mode is to accumulate the total loading time and apply a step loading on the surface. The third and fourth loading models are applied the loading over whole wheel path with pulse and equivalent loading mode, respectively. The fifth loading model is the moving loading by shifting the load at different positions over the whole wheel path. The loading models are summarized in table F3c.1. The rutting comparison between different loading models is shown in figure F3c.5. The results show that the pulse and equivalent loading modes essentially have the comparable rutting after a large number of cycles. Moreover, the loading applied on the whole wheel path results more rutting compare with only applied the loading on one wheel area. The rutting simulated by moving loading model is closer to loading model 1 and 2.

Table F3c.1. Summary of loading models.

Loading model	Loading area	Loading mode
Model 1	One wheel area	Pulse
Model 2	One wheel area	Equivalent
Model 3	Whole wheel path	Pulse
Model 4	Whole wheel path	Equivalent
Model 5	One wheel area	Moving

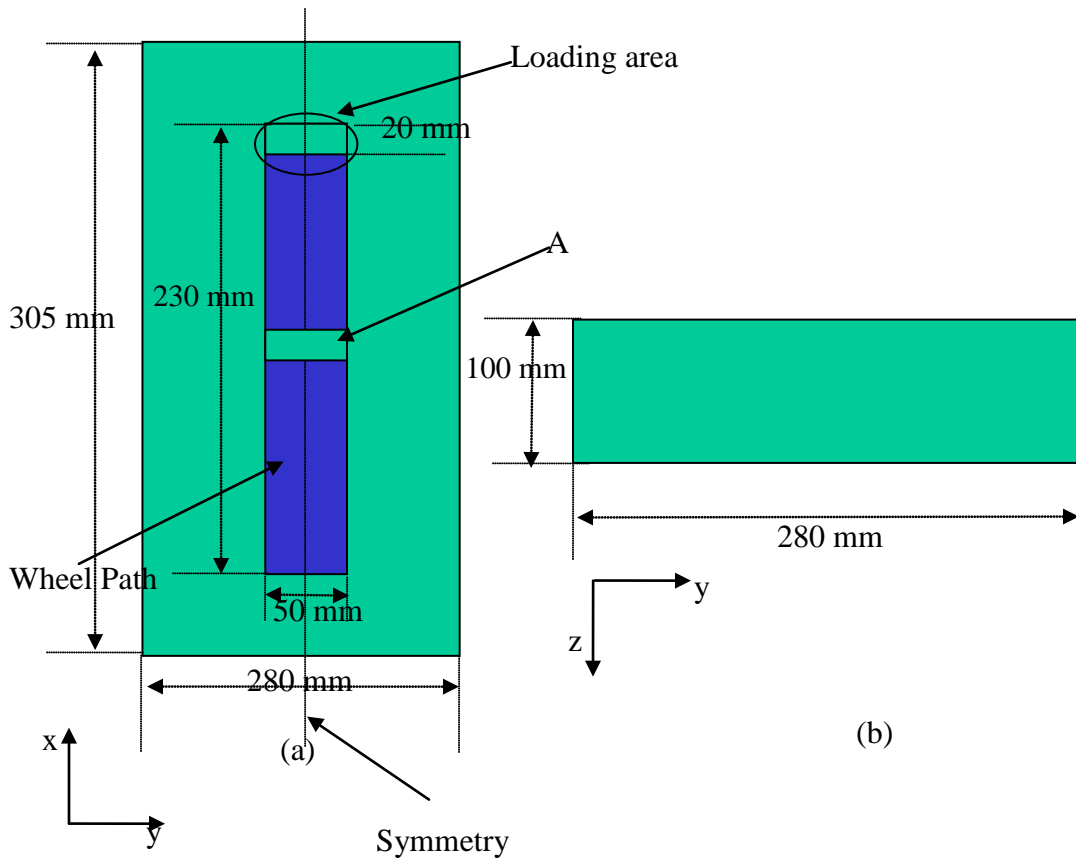


Figure F3c.1. The sketch of wheel tracking slab.

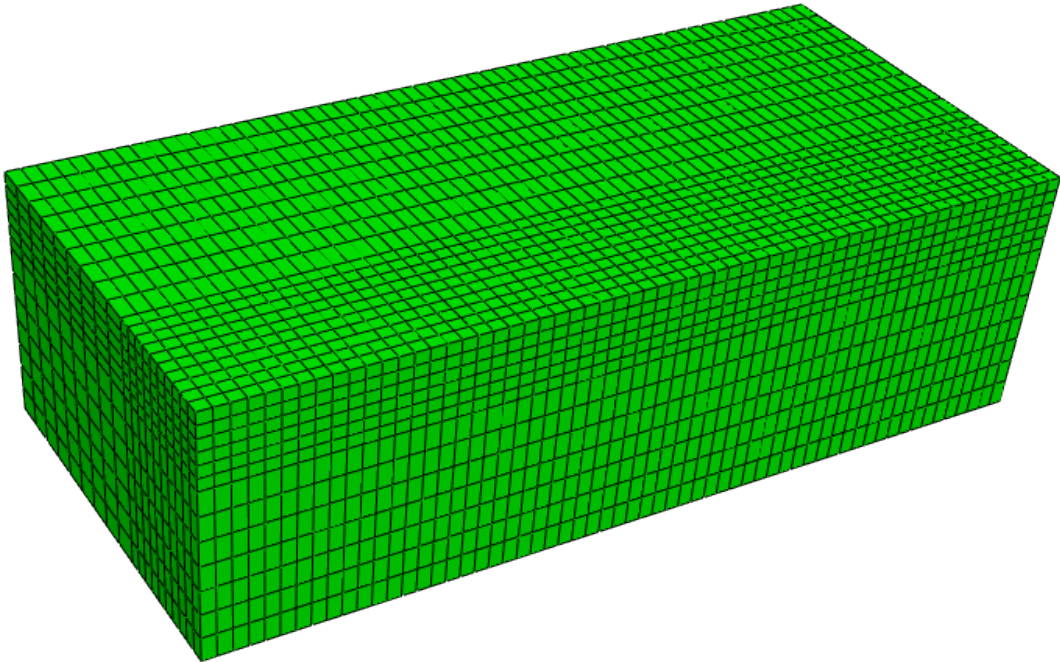


Figure F3c.2. The 3D finite element mesh.

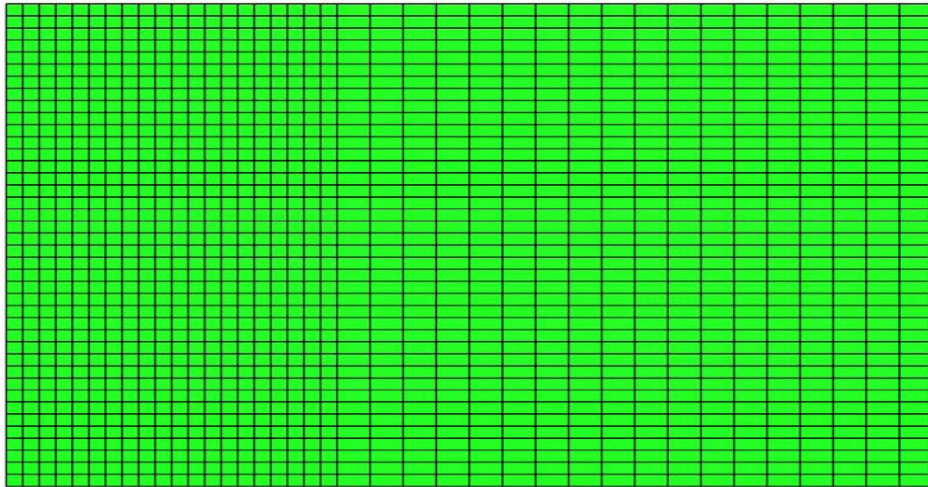


Figure F3c.3. The 2D finite element mesh.

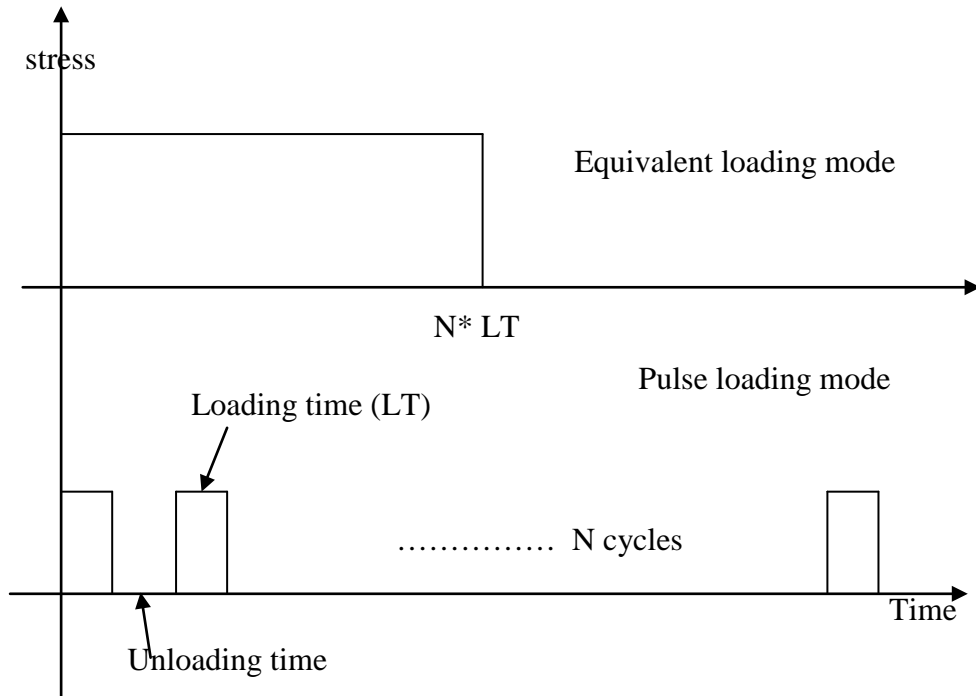


Figure F3c.4. The sketch of equivalent and pulse modes

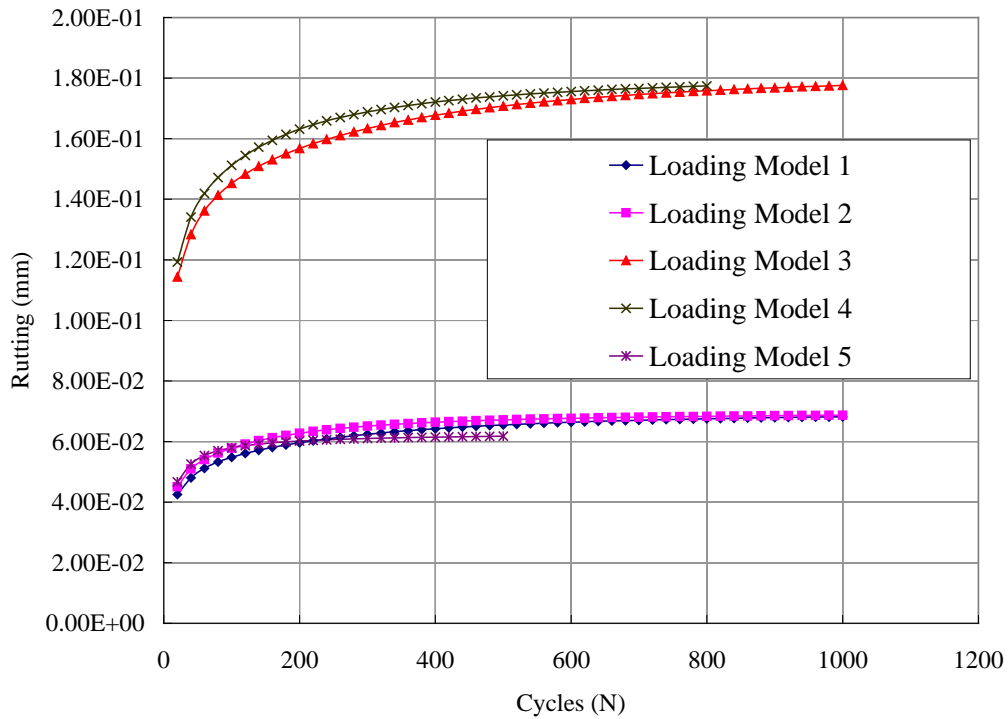


Figure F3c.5. The 3D comparison of rutting between different loading models.

In order to compare the effect of 2D and 3D analysis, this study conducted a 2D plane strain simulation using loading model 1 and 2. The 2D rutting simulation is shown in figure F3c.6. The results also show that the rutting does not have significant difference between equivalent and pulse loading mode after huge cycles. Figures F3c.7 and F3c.8 are the comparison between 2D and 3D simulation for equivalent and pulse loading, respectively. Since the 2D plane strain loading condition is more similar the loading model 3 and 4 in 3D simulation, only loading models 3 and 4 in 3D are compared with 2D simulation. The results show that under low cycles the rutting calculated by 2D is higher than 3D simulation, and the rutting rate calculated by 2D is higher than 3D calculation as well. Since the dimension of tested slab is 305mm in length, it is not long enough to assume plane strain in 2D. However, after 600 cycles the rutting does not have significant difference between 2D and 3D simulations. The error at 1000 cycles between 2D and 3D simulation is around 2%.

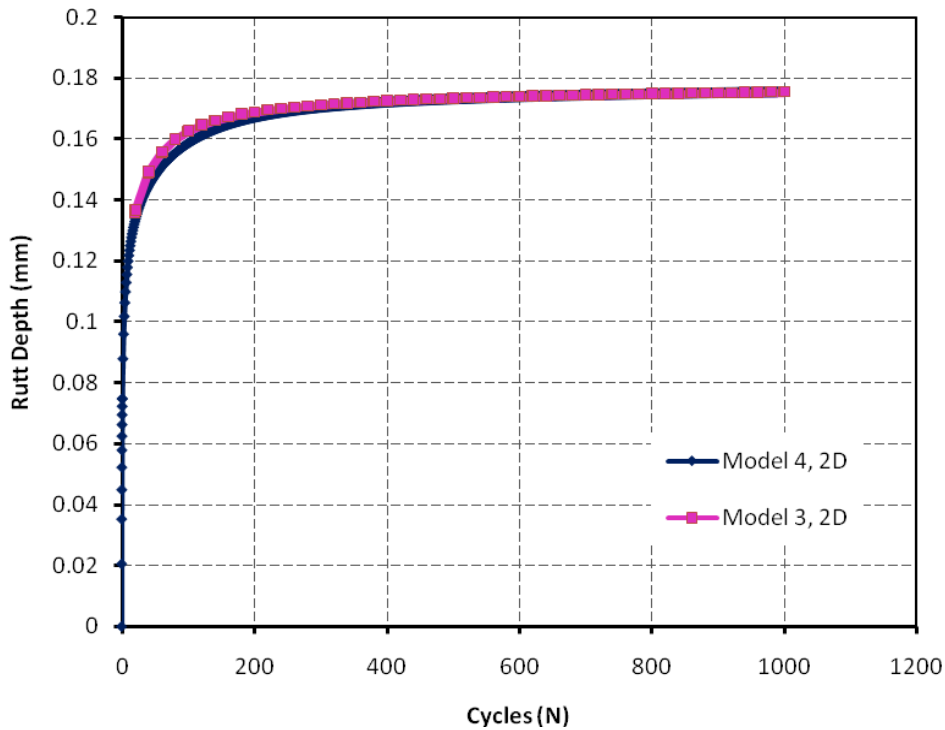


Figure F3c.6. The 2D comparison of rutting between different loading models.

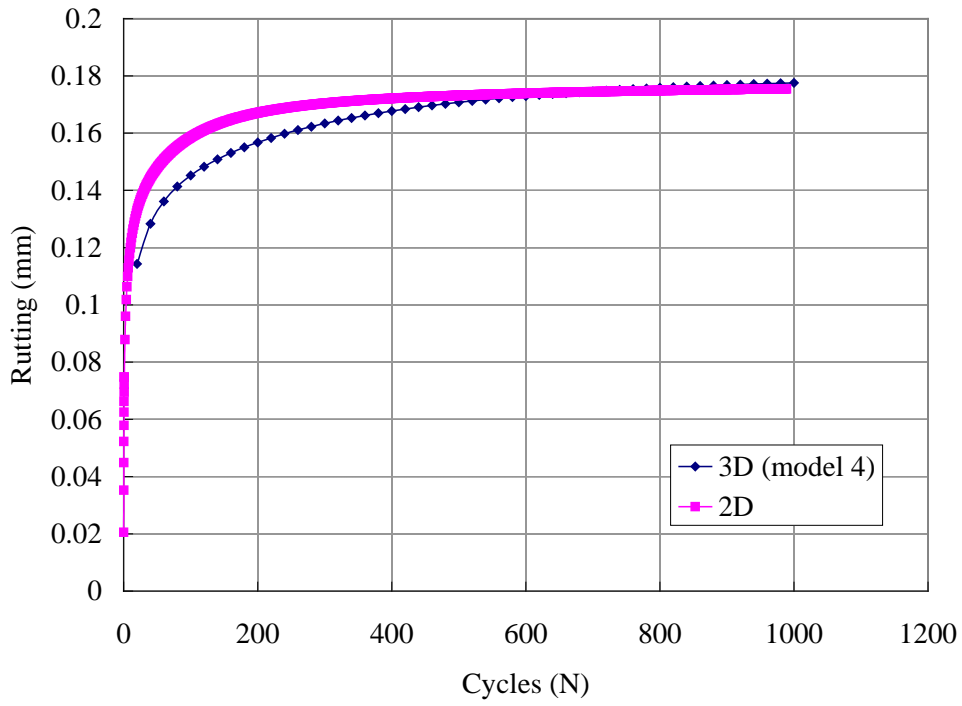


Figure F3c.7. The comparison between 2D and 3D simulation for equivalent loading.

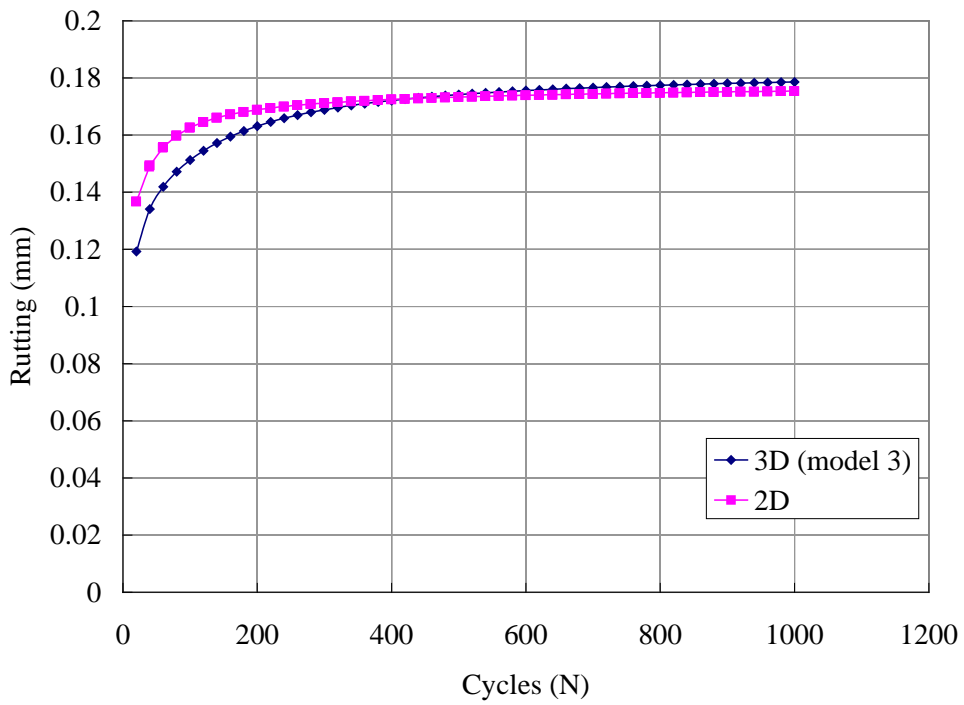


Figure F3c.8. The comparison between 2D and 3D simulation for pulse loading.

Extrapolation of 3D analysis based on 2D simulation

Since using 3D FE to simulate huge loading cycles is time consuming, this section conducts the extrapolation analysis based on 2D plane strain simulation to predict the rutting in 3D moving loading simulation. The extrapolation equation is expressed as:

$$Ruttung^{3D,N} = \frac{Ruttung^{3D,N_{ref}}}{Ruttung^{2D,N_{ref}}} * Ruttung^{2D,N} \quad (F3c.2)$$

where, $Ruttung^{3D,N}$ is the extrapolated rutting at N cycles for 3D moving loading, $Ruttung^{3D,N_{ref}}$ and $Ruttung^{2D,N_{ref}}$ is the 3D and 2D calculated rutting at reference cycles, respectively. The reference cycles are chosen as 20, 100, 200, 300, 400 and 500 for comparison. $Ruttung^{2D,N}$ is the 2D calculated rutting at N cycles.

The 2D simulation is simulated up to 1000 cycles; while the 3D moving loading simulation is only up to 500 cycles. Figure F3c.9 shows that using reference rutting at N=20 and 100 to extrapolate the 3D calculated rutting up to 500 cycles do not have accurate prediction compared with the 3D calculated rutting up to 500 cycles. However, using reference rutting at N=300~500 has good predictions. Figure F3c.10 is the extrapolation of 3D calculated rutting up to 1000 cycles. The results show that the extrapolated rutting using reference rutting at N=200, 300, 400 and 500 does not have significant difference. Hence, using 2D simulation results seems to be a promising method to extrapolate the 3D calculated rutting to predict the rutting for huge loading cycles.

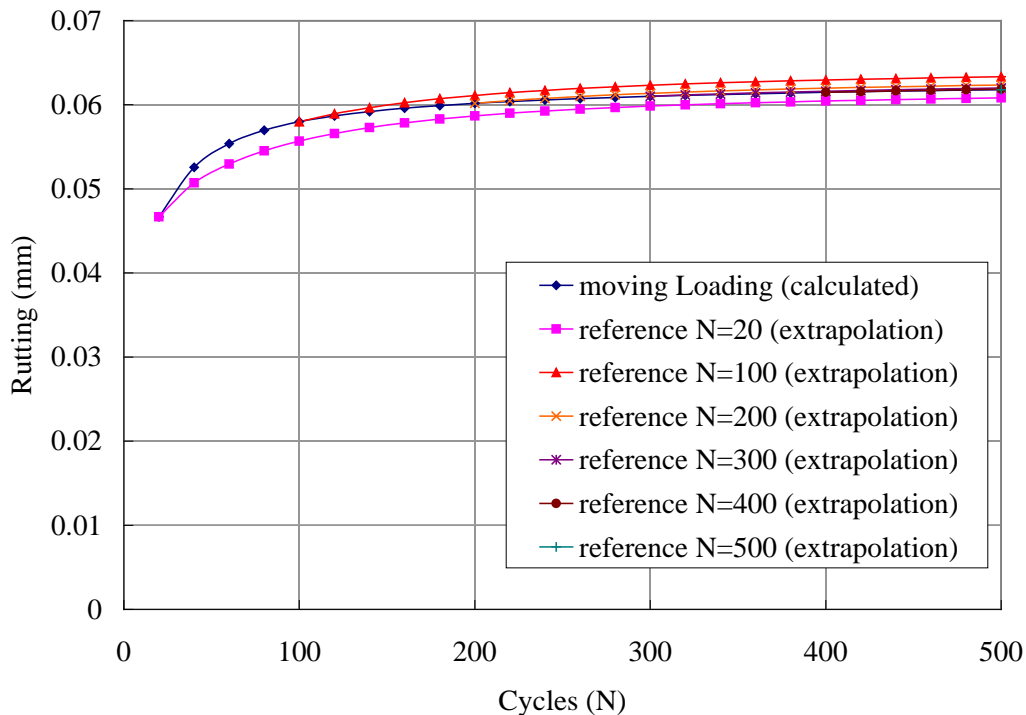


Figure F3c.9. The extrapolation of rutting for 3D moving loading up to 500 cycles.

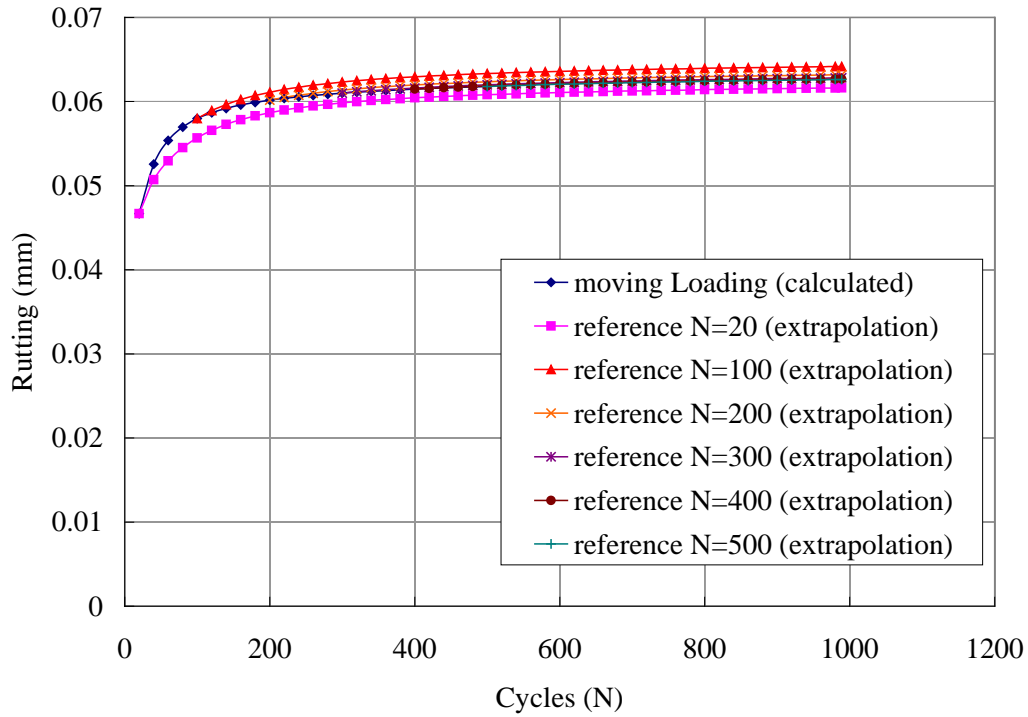


Figure F3c.10. The extrapolation of rutting for 3D moving loading up to 1000 cycles.

Improvement of Thermo-Viscodamage Model

Due to the fact that the changes in the material's microstructure during deformation cause HMA materials to experience a significant amount of micro-damage (micro-cracks and micro-voids) under service loading conditions, a temperature-, and rate- dependent damage law is coupled to the temperature-dependent viscoelasticity and temperature-dependent viscoplasticity models to model the highly nonlinear response of HMA under different loading conditions (e.g., different applied stresses, and strain rates), and different temperatures.

Damage is implemented using the effective (undamaged) configuration concept. The superimposed “-“ in the following equations designated the effective configuration. Temperature is coupled to the Schapery's nonlinear viscoelasticity theory (equation F3c.3), and Perzyna's viscoplasticity theory (equation F3c.4) to model the viscoelastic and viscoplastic responses of HMA, respectively:

$$\varepsilon^{nve,t} = g_0(\bar{\sigma}^t, T^t) D_0 \bar{\sigma}^t + g_1(\bar{\sigma}^t, T^t) \int_0^t \Delta D(\psi^t - \psi^\tau) \frac{d(g_2(\bar{\sigma}^\tau, T^\tau) \bar{\sigma}^\tau)}{d\tau} d\tau \quad (\text{F3c.3})$$

$$\dot{\varepsilon}_{ij}^{vp,\psi} = \Gamma \left(\frac{f(\bar{\sigma}_{ij}^\psi, \varepsilon_e^{vp,\psi})}{\sigma_y^0} \right)^N \frac{\partial g^\psi}{\partial \bar{\sigma}_{ij}^\psi} \quad (\text{F3c.4})$$

The evolution law for the viscodamage model is shown in equation (F3c.5).

$$\dot{\phi} = \Gamma^\varphi \exp(k\varepsilon_{eff}^{Tot}) \quad (\text{F3c.5})$$

where Γ^φ is a damage viscosity parameter, ε_{eff}^{Tot} is the effective total strain, and k is a material parameter. However, time of rupture in creep test and peak point in the stress-strain diagram for the constant strain rate test are highly stress dependent. As a result, one may assume the following power law:

$$\Gamma^\varphi = \Gamma_0^\varphi \left(\frac{Y}{Y_0} \right)^q \quad (\text{F3c.6})$$

where q is the stress dependency parameter, Γ_0^φ and Y_0 are the reference damage viscosity parameter and reference damage force obtained at a reference stress for a creep test, and Y is the damage driving force in the nominal (damaged) configuration.

Also, assuming the damage viscosity parameter to be a function of the damage force, Y , in the nominal (damaged) configuration instead of the effective (undamaged) configuration allows one to include damage history effects. Moreover, the damage density evolution highly depends on temperature. In this work, the proposed damage evolution law is coupled with temperature through a damage temperature function $G(T)$ as follows:

$$\dot{\phi} = \Gamma_0^\varphi \left[\frac{\bar{Y}(1-\phi)^2}{Y_0} \right]^q \exp(k\varepsilon_{eff}^{Tot}) G(T) \quad (\text{F3c.7})$$

Model predictions are compared with the experimental measurements for different loading conditions (creep, and constant strain rates), different stress levels, strain rates and temperatures. Figures F3c.11, and F3c.12 show model predictions and experimental measurements for the creep test at two temperatures. Comparisons of model prediction and experimental measurements for the constant strain rate test at different temperatures and strain rates are depicted in figures F3c.13 and F3c.14. These comparisons show that the model is able to predict the HMA response under different loading conditions, temperatures, and stress levels.

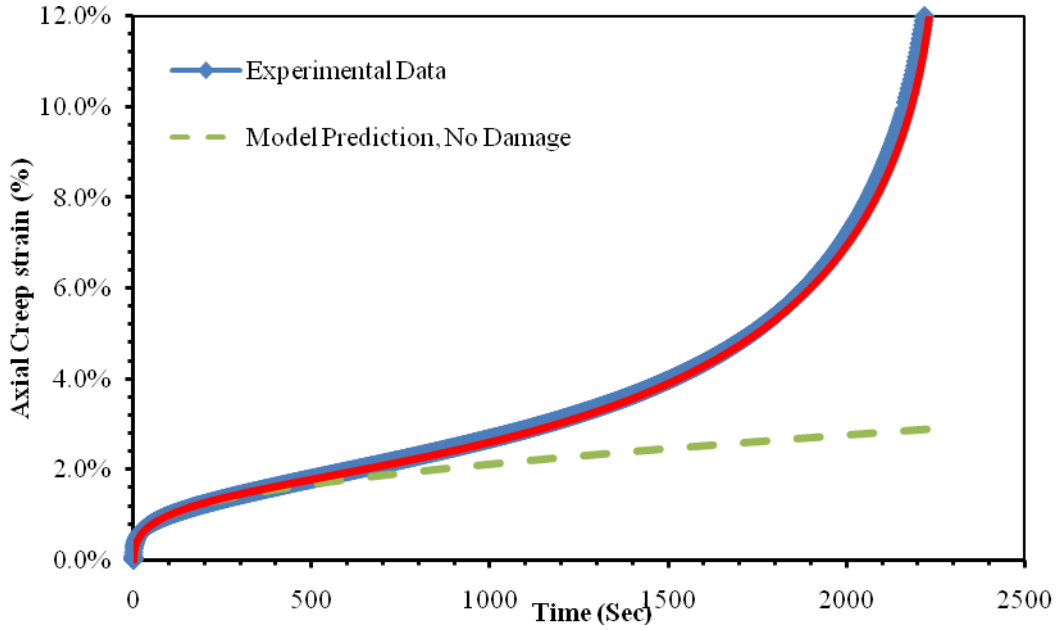


Figure F3c.11. Experimental measurement and model predictions of total strain for creep test ($T = 20^\circ$, $\sigma = 1000kPa$).

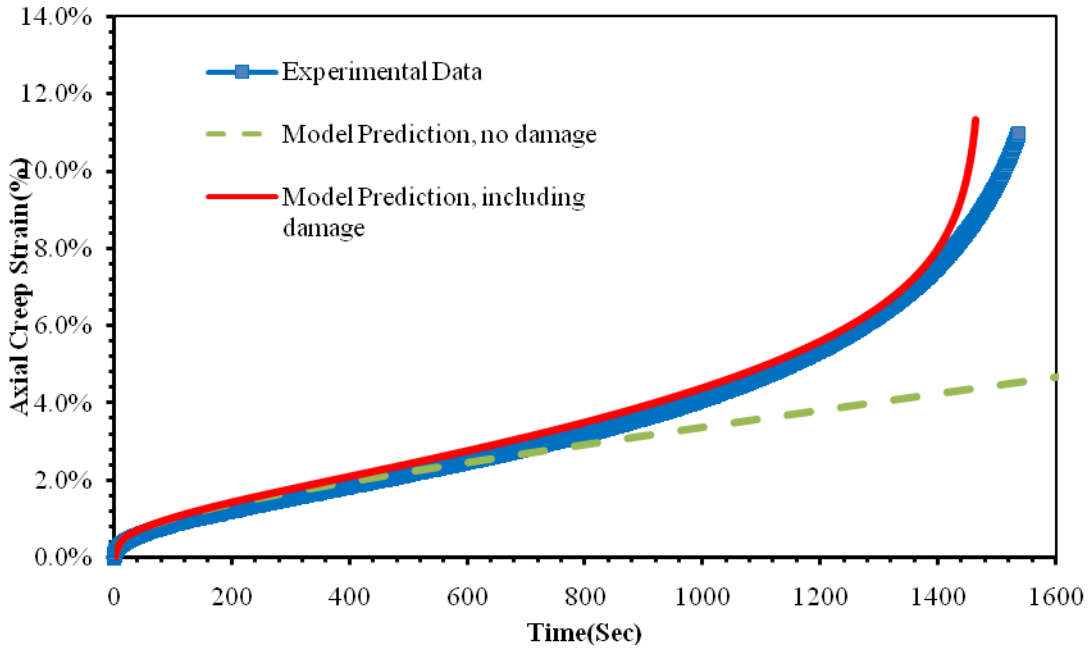


Figure F3c.12. The comparison of the creep response between experimental measurements and model predictions at $T = 10^\circ C$ and stress level of $\sigma = 2500kPa$

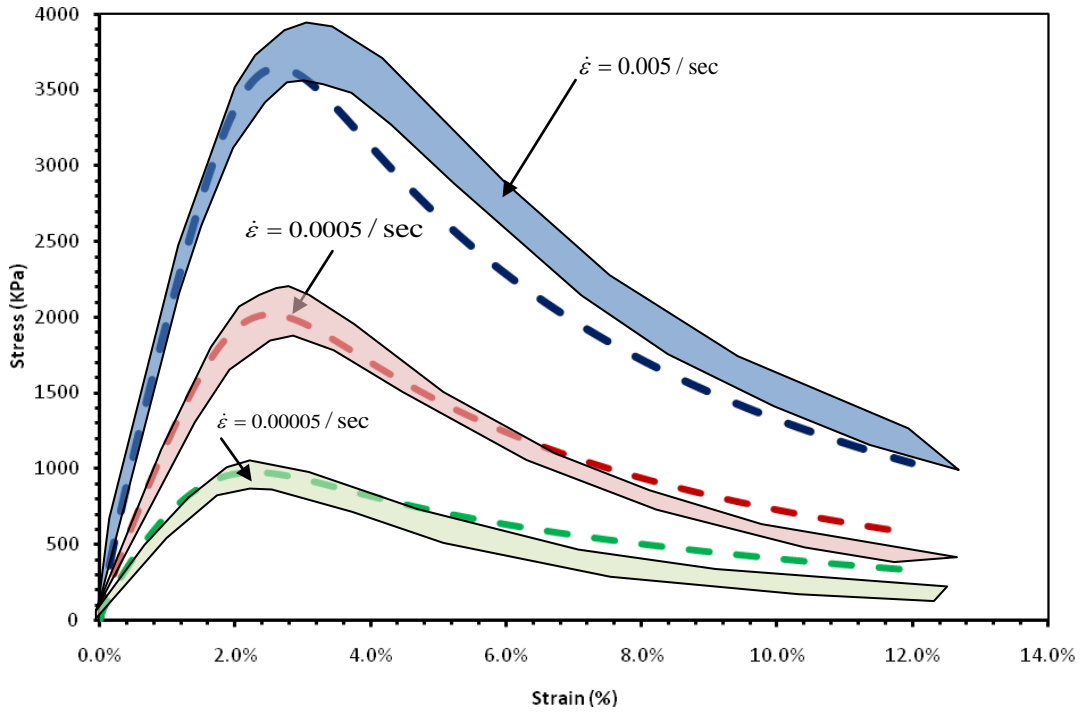


Figure F3c.13. The comparison of stress-strain diagram between the experimental measurements and the model predictions for the constant strain rate test at the reference temperature $T = 20^{\circ}C$ and for different strain rates.

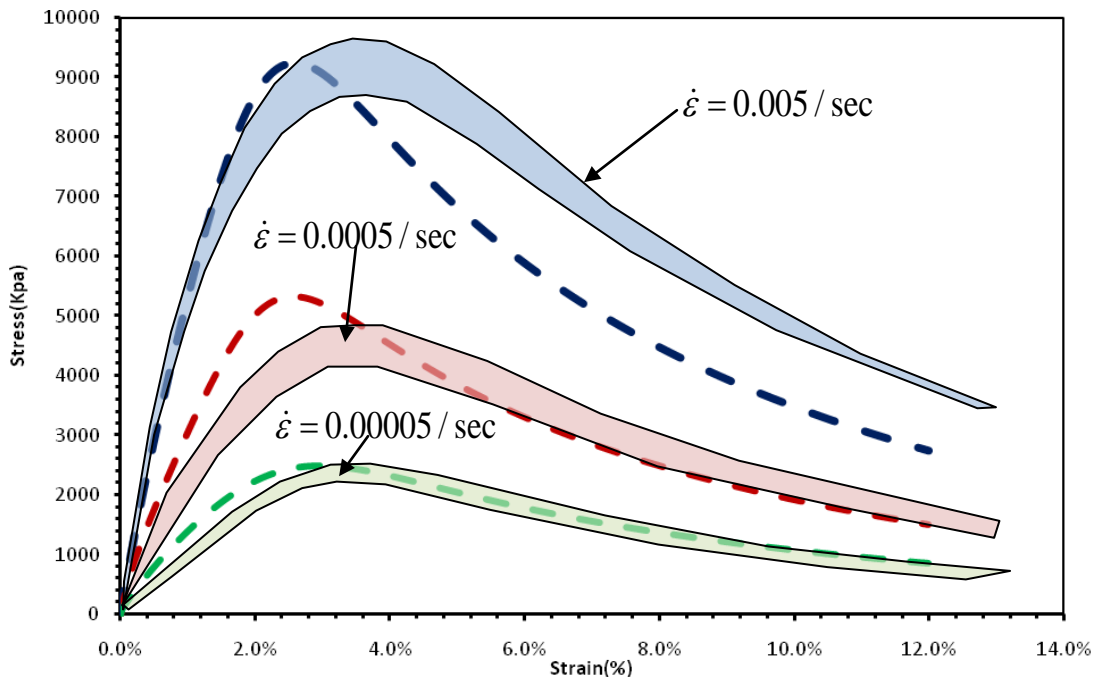


Figure F3c.14. The comparison of stress-strain diagram between the experimental measurements and the model predictions for the constant strain rate test when $T = 10^{\circ}C$ and for different strain rates.

Significant Results

A rate-, time-, and temperature-dependent damage model is coupled with the viscoelasticity and viscoplasticity model. The model is validated through the comparison of model predictions and experimental data for different loading conditions and over a range of temperature, strain rate, and stress levels.

The comprehensive study in the effect of different loading model using 2D plane strain and 3D FE analysis is conducted. The results provide a significant concept of simulation of wheel tracking test. A method to extrapolate the 3D rutting results based on 2D simulation is provided. The results show this is a promising method for predicting 3D rutting for a large number of loading cycles.

Significant Problems, Issues and Potential Impact on Progress

None

Work Planned Next Quarter

The ALF data will be analyzed during the coming quarter and the simulations of the ALF tests will be conducted.

Journal Papers

Darabi, M., R. Abu Al-Rub, E. Masad, C. W. Huang, and D. Little, 2009, A Thermo-Viscoelastic-Viscoplastic-Viscodamage Constitutive Model for Asphaltic Materials. *International Journal of Solids and Structures* (In Review).

Huang, C. W., R. Abu Al-Rub, E. Masad, and D. Little, 2009, Three-Dimensional Simulations of Asphalt Pavement Permanent Deformation Using a Nonlinear Viscoelastic and Viscoplastic Model. *Journal of Materials in Civil Engineering*, ASCE (Accepted for Publication).

Work Element F3d: Calibration and Validation

This work element is planned to start later in the project.

Fatigue Year 3		Year 3 (4/09-3/10)											
		4	5	6	7	8	9	10	11	12	1	2	3
Material Properties													
F1a	Cohesive and Adhesive Properties												
F1a-1	Critical review of literature												
F1a-2	Develop experiment design												
F1a-3	Thermodynamic work of adhesion and cohesion												
F1a-4	Mechanical work of adhesion and cohesion			JP				JP			D		F
F1a-5	Evaluate acid-base scale for surface energy calculations												
F1b	Viscoelastic Properties												
F1b-1	Separation of nonlinear viscoelastic deformation from fracture energy under cyclic loading												JP
F1b-2	Separation of nonlinear viscoelastic deformation from fracture energy under monotonic loading			P, JP									JP
F1c	Aging												
F1c-1	Critical review of binder oxidative aging and its impact on mixtures												
F1c-2	Develop experiment design		F										
F1c-3	Develop transport model for binder oxidation in pavements						P, JP					P, JP	D
F1c-4	Effect of binder aging on properties and performance										D		F
F1c-5	Polymer modified asphalt materials											P	D
F1d	Healing												
F1d-1	Critical review of literature												
F1d-2	Select materials with targeted properties												
F1d-3	Develop experiment design												
F1d-4	Test methods to determine properties relevant to healing												JP
F1d-5	Testing of materials												
F1d-6	Evaluate relationship between healing and endurance limit of asphalt binders				DP			JP			DP		
F1d-7	Coordinate with AFM analysis												
F1d-8	Coordinate form of healing parameter with micromechanics and continuum damage models												
Test Methods													
F2a	Binder tests and effect of composition												
F2a-1	Analyze Existing Fatigue Data on PMA												
F2a-2	Select Virgin Binders and Modifiers and Prepare Modified Binder												
F2a-3	Laboratory Aging Procedures												
F2a-4	Collect Fatigue Test Data							P					P
F2a-5	Analyze data and propose mechanisms										P		
F2b	Mastic testing protocol												
F2b-1	Develop specimen preparation procedures												
F2b-2	Document test and analysis procedures in AASHTO format												
F2c	Mixture testing protocol												
F2d	Tomography and microstructural characterization												
F2d-1	Micro scale physicochemical and morphological changes in asphalt binders							JP					
F2e	Verify relationship between DSR binder fatigue tests and mixture fatigue performance												
F2e-1	Evaluate Binder Fatigue Correlation to Mixture Fatigue Data												
F2e-2	Selection of Testing Protocols				DP						D		F
F2e-3	Binder and Mixture Fatigue Testing												
F2e-4	Verification of Surrogate Fatigue Test												
F2e-5	Interpretation and Modeling of Data						JP					P	
F2e-6	Recommendations for Use in Unified Fatigue Damage Model												
Models													
F3a	Asphalt microstructural model												
F3b	Micromechanics model												
F3b-1	Model development												
F3b-2	Account for material microstructure and fundamental material properties												
F3c	Develop unified continuum model												
F3c-1	Analytical fatigue model for mixture design												
F3c-2	Unified continuum model				JP						JP		
F3c-3	Multi-scale modeling												

LEGEND

Deliverable codes

- D: Draft Report
- F: Final Report
- M&A: Model and algorithm
- SW: Software
- JP: Journal paper
- P: Presentation
- DP: Decision Point
- [x]

-  Work planned
-  Work completed
-  Parallel topic

Deliverable Description

- Report delivered to FHWA for 3 week review period.
- Final report delivered in compliance with FHWA publication standards
- Mathematical model and sample code
- Executable software, code and user manual
- Paper submitted to conference or journal
- Presentation for symposium, conference or other
- Time to make a decision on two parallel paths as to which is most promising to follow through
- Indicates completion of deliverable x

Fatigue Year 2 - 5		Year 2 (4/08-3/09)				Year 3 (4/09-3/10)				Year 4 (04/10-03/11)				Year 5 (04/11-03/12)				
		Q1	Q2	Q3	Q4	Q1	Q2	Q3	Q4	Q1	Q2	Q3	Q4	Q1	Q2	Q3	Q4	
Material Properties																		
F1a	Cohesive and Adhesive Properties																	
F1a-1	Critical review of literature			JP														
F1a-2	Develop experiment design																	
F1a-3	Thermodynamic work of adhesion and cohesion																	
F1a-4	Mechanical work of adhesion and cohesion					JP	JP	D	F									
F1a-5	Evaluate acid-base scale for surface energy calculations														JP			
F1b	Viscoelastic Properties																	
F1b-1	Separation of nonlinear viscoelastic deformation from fracture energy under cyclic loading			D,JP	M&A, F				JP	JP		P		JP, M&A, D		F		
F1b-2	Separation of nonlinear viscoelastic deformation from fracture energy under monotonic loading			JP	M&A, F	P,JP			JP	JP		P		JP, M&A, D		F		
F1c	Aging																	
F1c-1	Critical review of binder oxidative aging and its impact on mixtures																	
F1c-2	Develop experiment design			D	F													
F1c-3	Develop transport model for binder oxidation in pavements		P		P, JP	P, JP			P, JP		P		P, JP			D, M&A	F	
F1c-4	Effect of binder aging on properties and performance				JP, P				D	F					JP	D	F	
F1c-5	Polymer modified asphalt materials										P					D	F	
F1d	Healing																	
F1d-1	Critical review of literature																	
F1d-2	Select materials with targeted properties																	
F1d-3	Develop experiment design																	
F1d-4	Test methods to determine properties relevant to healing				JP				JP	D	F							
F1d-5	Testing of materials								JP					M&A, D	JP, F			
F1d-6	Evaluate relationship between healing and endurance limit of asphalt binders	DP				DP	JP	DP			JP		P		JP	D	F	
F1d-7	Coordinate with AFM analysis																	
F1d-8	Coordinate form of healing parameter with micromechanics and continuum damage models											JP				JP, D	F	
Test Methods																		
F2a	Binder tests and effect of composition																	
F2a-1	Analyze Existing Fatigue Data on PMA		DP															
F2a-2	Select Virgin Binders and Modifiers and Prepare Modified Binder		DP															
F2a-3	Laboratory Aging Procedures																	
F2a-4	Collect Fatigue Test Data		P		JP	P			P					JP, D, F				
F2a-5	Analyze data and propose mechanisms				P				P			P			P	D	F	
F2b	Mastic testing protocol																	
F2b-1	Develop specimen preparation procedures		D															
F2b-2	Document test and analysis procedures in AASHTO format		D															
F2c	Mixture testing protocol		D, JP	F														
F2d	Tomography and microstructural characterization																	
F2d-1	Micro scale physicochemical and morphological changes in asphalt binders						JP				JP	M&A, D	F					
F2e	Verify relationship between DSR binder fatigue tests and mixture fatigue performance																	
F2e-1	Evaluate Binder Fatigue Correlation to Mixture Fatigue Data								D	F								
F2e-2	Selection of Testing Protocols					DP												
F2e-3	Binder and Mixture Fatigue Testing																	
F2e-4	Verification of Surrogate Fatigue Test												D	F, DP				
F2e-5	Interpretation and Modeling of Data		JP		P		JP		P		JP		M&A					
F2e-6	Recommendations for Use in Unified Fatigue Damage Model															D	F	
Models																		
F3a	Asphalt microstructural model								JP					JP			M&A	F
F3b	Micromechanics model																	
F3b-1	Model development				JP				JP				M&A	D	DP	F, SW		
F3b-2	Account for material microstructure and fundamental material properties										JP			D		F		
F3c	Develop unified continuum model																	
F3c-1	Analytical fatigue model for mixture design															M&A, D	F	
F3c-2	Unified continuum model				JP		JP		JP				M&A	D	DP	F, SW		
F3c-3	Multi-scale modeling											JP	M&A	D		F		

LEGEND

Deliverable codes

- D: Draft Report
- F: Final Report
- M&A: Model and algorithm
- SW: Software
- JP: Journal paper
- P: Presentation
- DP: Decision Point

- [x] Work planned
- [] Work completed
- [] Parallel topic

Deliverable Description

- Report delivered to FHWA for 3 week review period.
- Final report delivered in compliance with FHWA publication standards
- Mathematical model and sample code
- Executable software, code and user manual
- Paper submitted to conference or journal
- Presentation for symposium, conference or other
- Time to make a decision on two parallel paths as to which is most promising to follow through
- Indicates completion of deliverable x

PROGRAM AREA: ENGINEERED MATERIALS

CATEGORY E1: MODELING

Work element E1a: Analytical and Micro-mechanics Models for Mechanical Behavior of Mixtures (TAMU)

Work Done This Quarter

A technical presentation, entitled “Absorption of Asphalt Binder by Aggregates”, was made in the 46th Petersen Asphalt Research Conference in Laramie, Wyoming, July 2009. This presentation summarized the major findings on the aggregate absorption investigated in last quarter.

In this quarter, a testing and data analysis method was developed to obtain the properties of the aged field asphalt mixtures. After the measurement on field mixtures, the asphalt binder will be extracted from the mixtures to be tested for its aged properties, which will be reported under Work Element F1c. By measuring the properties of both aged mixture and aged binder, the aggregate properties in the aged field mixture can be predicted using the inverse and forward self-consistent micromechanics models that were developed in previous quarters. Preliminary results on the measurement of the field mixture properties were reported in the last quarterly report under Subtask F1c-4. It has been found that the modulus of the field mixture is not uniform with the pavement depth. Instead, there is a modulus gradient because the pavement surface has a higher level of aging than the asphalt layer beneath the pavement surface. The newly developed method uses the Viscoelastic Characterization (VEC) Test to obtain the complex modulus at the top and bottom of the field sample as well as the modulus gradient with the field sample depth.

As reported in the last quarterly report, the field cores were cut into test samples in a rectangular shape. The rectangular sample was set up in the environmental chamber of the Material Test System (MTS) as shown in figure E1a.1. Four vertical linear variable differential transformers (LVDTs) and two horizontal LVDTs were installed on the four surfaces of the test sample in order to capture the vertical and horizontal deformations in all surfaces. A monotonically increasing tensile load was applied to the specimen until the weakest side of the specimen reached a strain of approximately $80\mu\epsilon$. The threshold of $80\mu\epsilon$ was regarded as a fatigue endurance limit, under which it was assumed that the specimen was not further damaged in the VEC Test. The same test was conducted on each sample at three different temperatures (10°C , 20°C and 30°C) in order to construct the master curve of the complex modulus using the time-temperature superposition principle.



Figure E1a.1. Test configuration of rectangular field sample.

Because of the modulus gradient in the field samples, there was significant strain oscillation in the VEC Test, as reported in the last quarterly report. When analyzing the oscillating strain data, the strain distribution with depth was assumed as a linear function, and Equation E1a.1 was used to characterize the modulus gradient with depth in the rectangular field sample:

$$E(z) = E_d + (E_0 - E_d) \left(\frac{d-z}{d} \right)^n \quad (\text{E1a.1})$$

in which:

$E(z)$ = complex modulus at depth of z ;

E_d = complex modulus at the bottom of the field sample;

E_0 = complex modulus at the top of the field sample;

n = a parameter indicating the rate of change in complex modulus with sample depth; and

d = thickness of field sample.

The complex modulus at the bottom of the field sample was calculated using Equation E1a.2:

$$s\overline{E}_d(\omega) = \frac{\overline{P}(\omega)}{A \left\{ \overline{\varepsilon}_0(\omega) \left[\frac{1}{2} + \frac{(k-1)}{(n+2)} \right] + \overline{\varepsilon}_d(\omega) \left[\frac{1}{2} + \frac{(k-1)}{(n+1)(n+2)} \right] \right\}} \quad (\text{E1a.2})$$

where \overline{E}_d is the Laplace transform of E_d ; \overline{P} is the Laplace transform of applied load, s is the Laplace transform variable; the parameter k is defined as: $sE_0(\omega) = k \cdot sE_d(\omega)$; A is the cross-sectional area of the sample; $\overline{\varepsilon}_0$ is the Laplace transform of the strain on the top surface; and $\overline{\varepsilon}_d$ is the Laplace transform of the strain on the bottom surface of the sample.

When a field sample was relatively thick (approximately 3 in), the modulus of the top surface was found to be significantly different from that at the bottom of the field sample. The magnitude of the complex modulus at the top and bottom of the sample was reported in the last quarterly report. The gradient of the magnitude of the complex modulus with the pavement depth is illustrated in figure E1a.2.

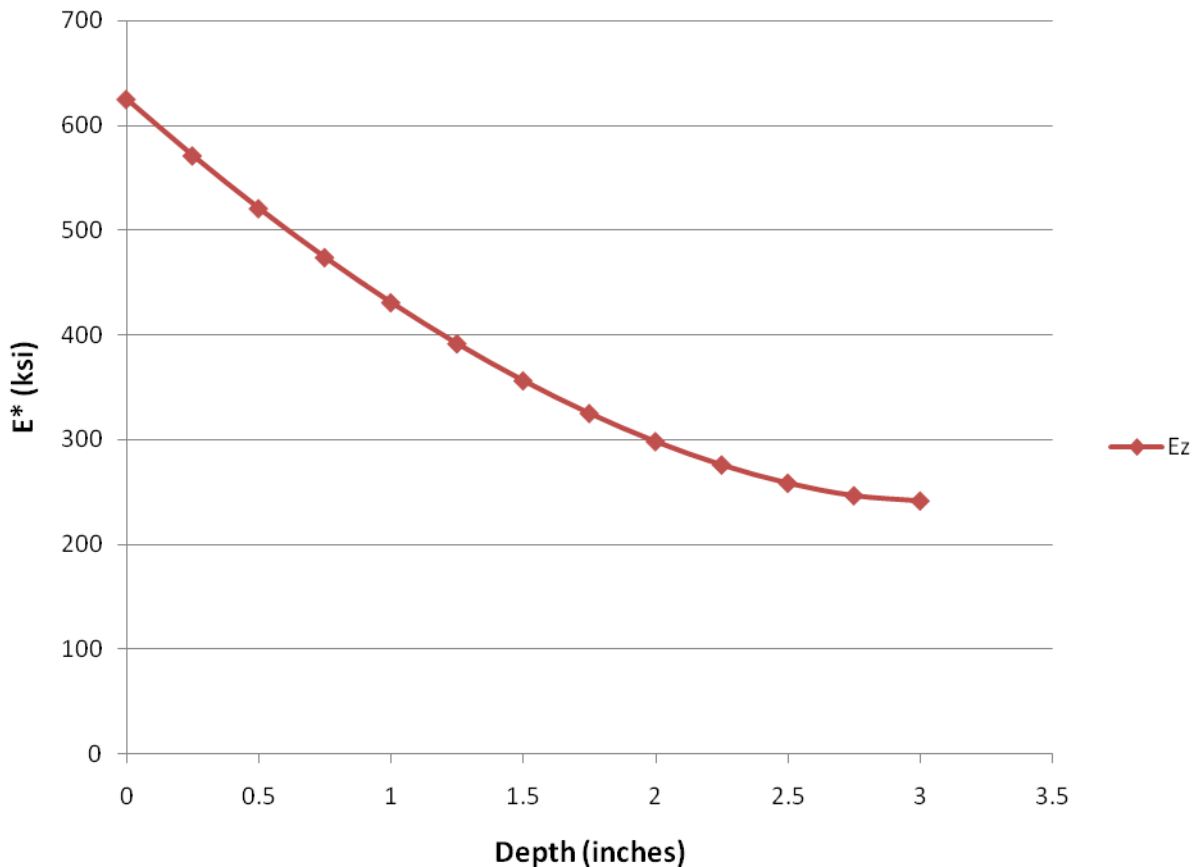


Figure E1a.2. Magnitude gradient of complex modulus of 3 in thick field sample with pavement depth.

If the field sample was relatively thin (approximately 1.5 in), the modulus at the top surface was found to be similar to that at the bottom surface. A master curve was constructed for the average modulus of the thin sample using the method developed in previous quarters (Luo and Lytton 2009). Figure E1a.3 shows the master curve of the magnitude of the complex modulus at a reference temperature of 20°C.

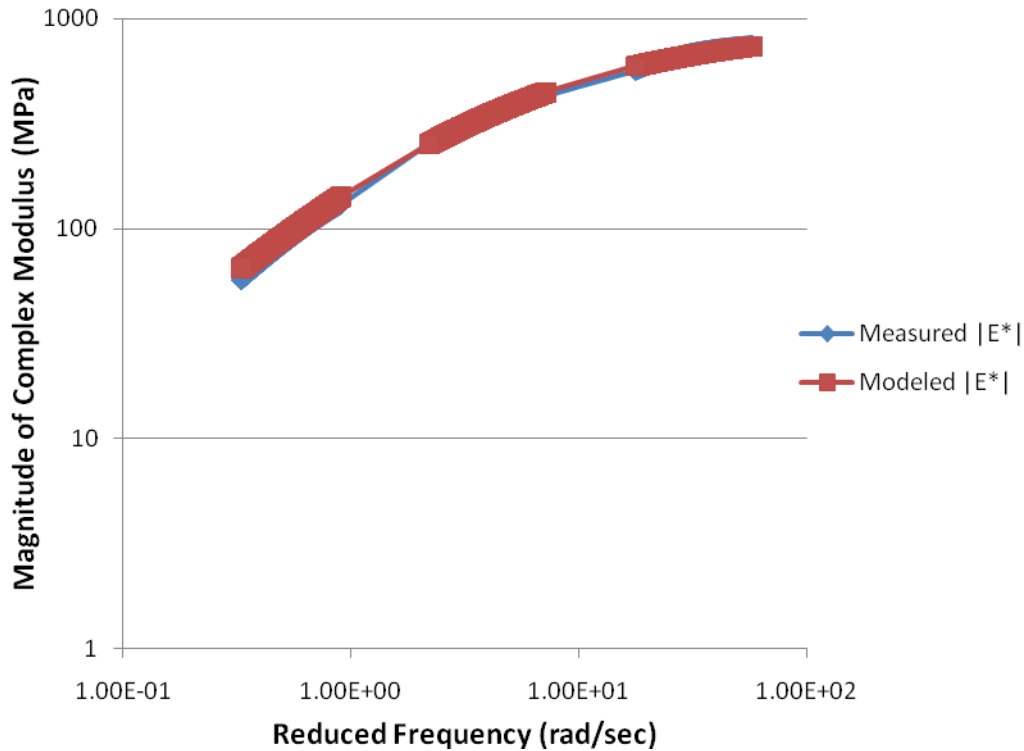


Figure E1a.3. Master curve of average complex modulus of 1.5 in thick field sample.

Significant Results

A testing and data analysis method was developed to characterize the field asphalt mixtures. The complex modulus was found to vary with the depth of the pavement. The gradient of the magnitude of the complex modulus was determined based on the test data from the VEC Test on the field sample. A master curve was constructed of the magnitude of the average complex modulus of a 1.5 in thick field sample, whose complex modulus at the top surface was similar to that at the bottom surface.

Significant Problems, Issues and Potential Impact on Progress

The newly purchased MTS is still not ready for testing because the software has not been completely installed. This issue delayed the testing schedule.

Work Planned Next Quarter

More field samples will be cut and tested. The phase angle of the complex modulus will be determined, and a master curve of the phase angle will be constructed. The Poisson's ratio will be further investigated. The relation of the modulus gradient to the in-place air voids content will be explored. Where there is a significant modulus gradient, the master curves of the magnitudes and phase angles of the top surface modulus, the bottom surface modulus and their Poisson's ratios will be constructed.

Cited Reference

Luo, R., and R. L. Lytton, 2009, Characterization of the Tensile Viscoelastic Properties of an Undamaged Asphalt Mixture. *Journal of Transportation Engineering, American Society of Civil Engineers (ASCE)*, Accepted for Publication.

Work element E1b: Binder Damage Resistance Characterization (DRC) (UWM)

Subtask E1b-1: Rutting of Asphalt Binders

Work Done This Quarter

Binder and Mastic Testing

Multiple Stress Creep and Recovery (MSCR) testing was conducted on two modified binders and four mastics. One binder was modified with an elastomer to have high elasticity, as measured by percent recovery (%R), and the other was modified with a plastomer to have a very low elasticity, as measured by %R. The purpose of this selection is to study the effect of elasticity, or %R, on rutting performance of mastics and mixtures.

The mineral fillers combined with binders to produce mastics included granite and hydrated lime. Two binders were mixed with each filler individually to yield a total of four mastics. The MSCR testing was performed at two temperatures—64 °C and 46 °C. At 64 °C, testing included stress levels of 0.1, 3.2 and 10 kPa; at 46 °C, the MSCR testing included stress levels of 0.1, 3.2, 10 and 20 kPa. Testing was conducted using the 25-mm-diameter parallel-plate geometry system in the Dynamic Shear Rheometer (DSR). It should be mentioned that cone-and-plate geometry was tried in the past and did not give reliable results. Analysis of data included calculating the average nonrecoverable creep compliance (J_{nr}) and the average %R of 10 cycles at each combination of stress and temperature levels.

Mixture Testing

Repeated Creep and Recovery (RCR) testing was conducted on mixtures prepared with the mastics described above. The mix consisted of a coarse blend of granite aggregates. The granite filler used in the mastics is the native filler of the aggregate used in the mixtures. The mixtures were generated after washing the aggregate to control the precision of filler. Mixture testing was

conducted on cylindrical specimens of 4-inch diameter and 6-inch height. Testing was conducted in uniaxial mode using a haversine loading pattern where the load period lasted for 0.1 second and the rest period lasted for 0.9 seconds. Analysis of data included estimating the flow number (FN) and the permanent strain accumulated at the loading cycle corresponding to the FN. Testing was conducted at stress levels of 50, 100 and 150 psi (0.435, 0.689 and 1.03 MPa, respectively). All mixture testing was conducted at 46 °C.

Significant Results

Binder and Mastic MSCR Results

Binders and mastics were tested using the MSCR protocol. Testing was conducted at multiple stresses and temperatures to evaluate the sensitivity to these parameters. Figures E1b-1.1 and E1b-1.2 show the measured Jnr at 46 °C and 64 °C for the binders and mastics tested thus far.

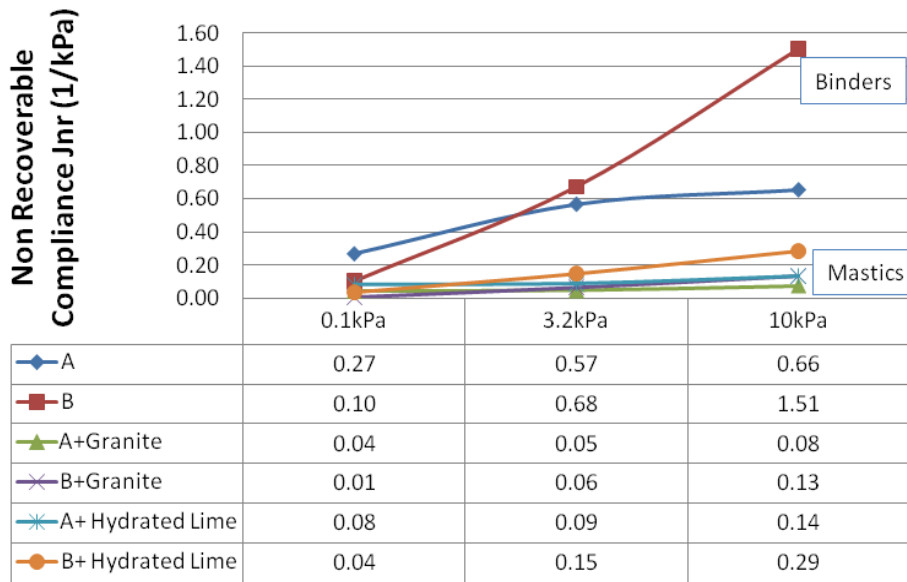


Figure E1b-1.1. Graph. Stress sensitivity of Jnr for binders and mastics at 64 °C. (Binder A = elastomer-modified. Binder B = plastomer-modified.)

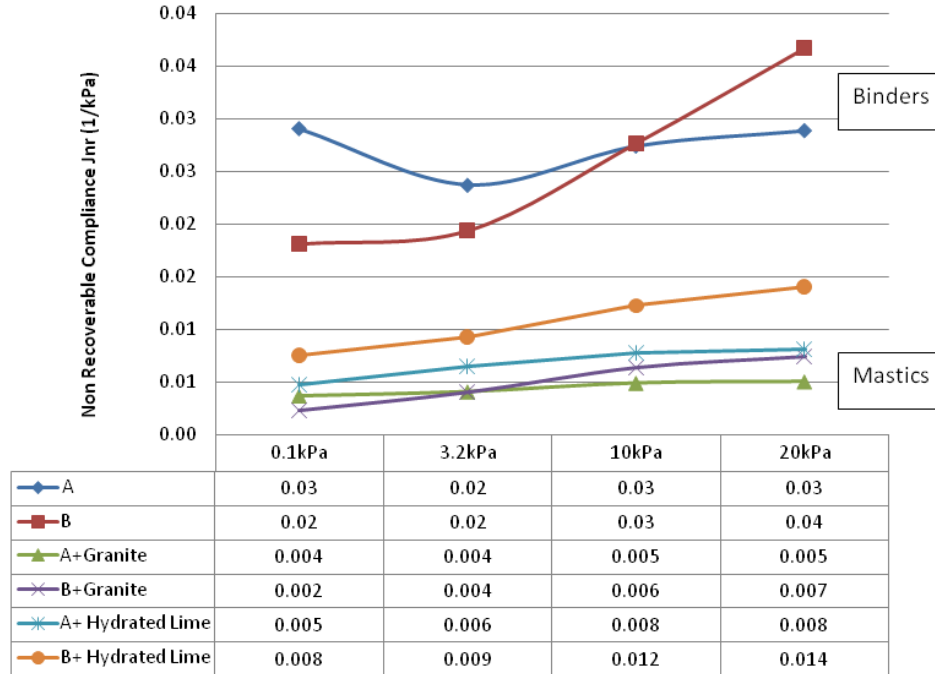


Figure E1b-1.2. Graph. Stress sensitivity of Jnr for binders and mastics at 46 °C.

Figures E1b-1.1 and E1b-1.2 clearly show that the MSCR test can distinguish between binders and mastics. At 64 °C, the elastomer-modified Binder A demonstrates low sensitivity to stress levels compared to the plastomer-modified Binder B. At this temperature, Jnr values of the two binders are very similar, except at a stress level of 10 kPa. Comparing results at 46 °C with those at 64 °C, there is as much as an 80% reduction in the Jnr values. There also appears to be a significant reduction in stress sensitivity, as effects of increased stress show very limited effects. Binder A shows a higher Jnr value than Binder B at the standard MSCR testing stress levels of 0.1 kPa and 3.2 kPa. At 46 °C and a stress level of 10 kPa, Jnr does not allow for clear separation of binders, but this stress level leads to clear differences in binders at 64 °C. At 20 kPa and 46 °C, Binder A has a lower Jnr than Binder B, which was not observed at lower stress levels.

It is important to note that Jnr values for the mastics show very little variation between filler types and binder types upon initial observation. However, closer inspection shows that for both binders, granite filler results in mastics with Jnr values lower than those containing hydrated lime at both 46 °C and 64 °C.

Figures E1b-1.3 and E1b-1.4 show the results of %R. The results show clear distinction between the two binders. At both temperatures, Binder A and the mastics containing Binder A show higher %R than Binder B and mastics containing Binder B, with the exception of results at a stress level of 0.1 kPa. There is also a distinction between stress sensitivity of the recovery for stress level. Binder A and its mastics are much less sensitive to stress than Binder B and its mastics. There is also an effect of filler type on %R, with the granite filler causing higher %R than the hydrated lime in all cases. It is noted that, given a specific binder, addition of granite led

to better performance with respect to lower J_{nr} and higher %R as compared to addition of hydrated lime.

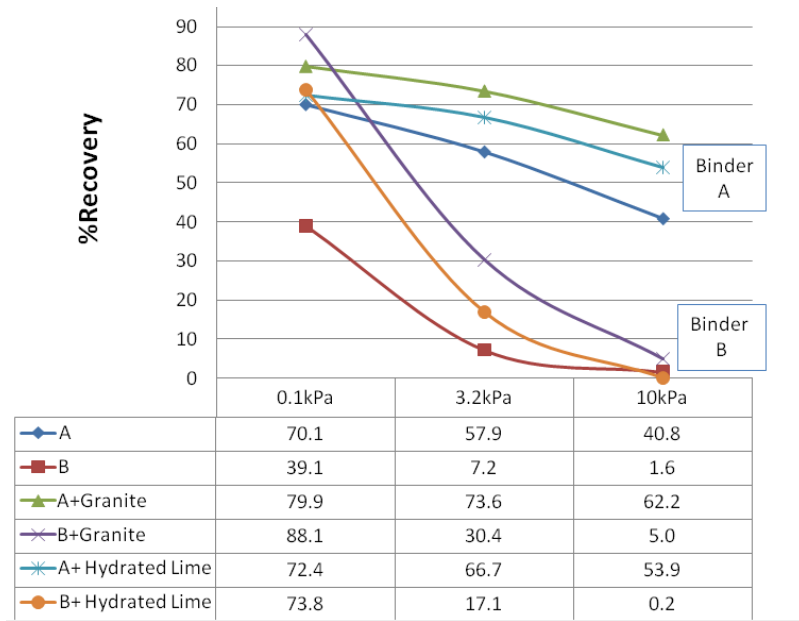


Figure E1b-1.3. Graph. Stress sensitivity of binder and mastic elastic recovery at 64 °C.

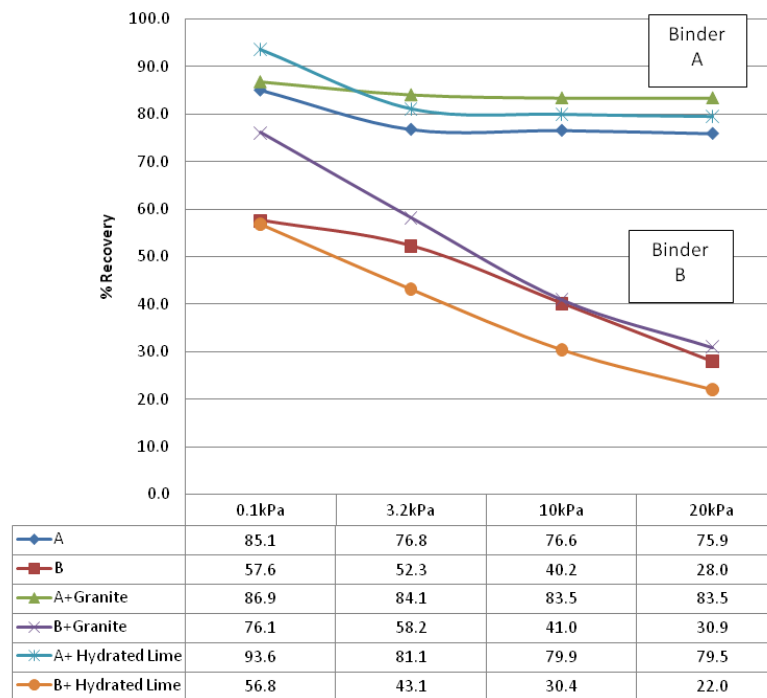


Figure E1b-1.4. Graph. Stress sensitivity of binder and mastic elastic recovery at 46 °C.

Mixture Testing Results

Table E1b-1.1 and figure E1b-1.5 include the FN results of RCR testing performed on mixtures at three stress levels. FN values indicate that mixtures prepared with Binder B show higher values than the mixtures prepared with Binder A for all stress levels, regardless of filler type. In binder/mastic testing, Binder B was found to outperform Binder A based only on Jnr measured at 0.1 and 3.2 kPa at 46 °C. This can lead researchers to believe that mixture behavior is more controlled by mastic performance at lower stresses and that there is no effect of %R on FN values, which are considered the main mixture rutting resistance indicators in the NCHRP 9-33 project.

As for the effects of fillers, mixtures containing the granite filler have higher FNs for a given binder than those containing hydrated lime. In mastic MSCR testing based on %R and Jnr, granite performed better than hydrated lime, which agrees with the mixture testing FN results.

Table E1b-1.1. Mixture FN results.

Binder	Filler	Stress	Replicate		Average	Coefficient of Variation
			1	2		
A	Granite	50	1800	2700	2250	28.3%
		100	680	760	720	7.9%
		150	460	460	460	0.0%
A	Hydrated Lime	50	1600	1850	1725	10.2%
		100	840	500	670	35.9%
		150	480	260	370	42.0%
B	Granite	50	19300	12500	15900	30.2%
		100	1800	1100	1450	34.1%
		150	640	480	560	20.2%
B	Hydrated Lime	50	19300	12900	16100	28.1%
		100	800	1400	1100	38.6%
		150	580	680	630	11.2%

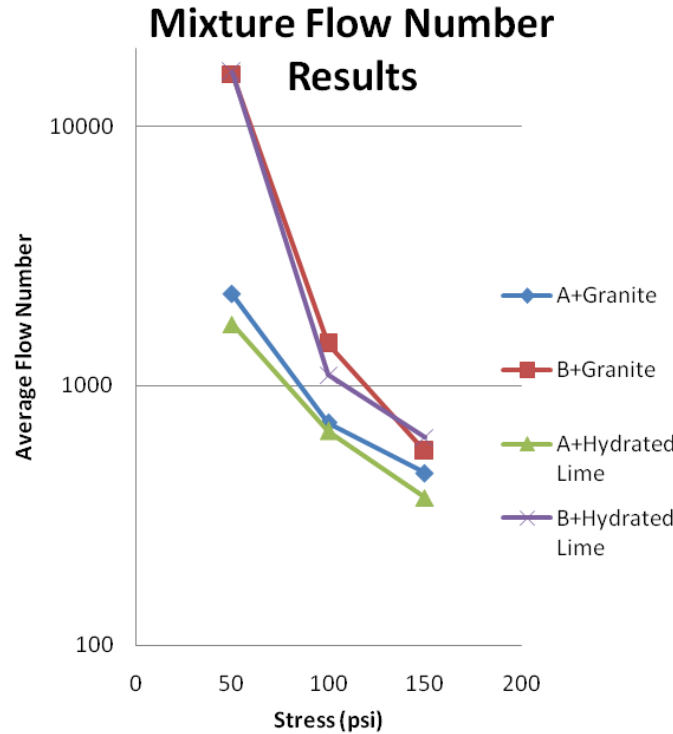


Figure E1b-1.5. Graph. Mixture FN results.

Significant Results

Jnr and %R obtained from MSCR testing allows for distinction between binders and mastics. Temperature, stress level and fillers have significant effects on ranking of the binders and mastics on the basis of Jnr and %R. Granite filler was found to have more favorable effects on binder performance than the hydrated lime for both binders. The plastomer-modified Binder B was found to be more stress-sensitive than the elastomer-modified Binder A.

Mixture FNs obtained from RCR testing were strongly influenced by binder type. The ranking of mixtures on the basis of FN was found to match the ranking of Jnr of the binders contained in those mixtures at binder testing stress levels of 0.1 and 3.2 kPa, when measured at the same temperature as mixture testing. However, since this ranking on the basis of binder Jnr at the same stress levels is reversed at 64 °C, it appears to be critical that binders are tested at the temperature expected in the mixture or pavement. The clearest distinction between binder and filler types was found in the mixture FNs at a stress level of 0.689 MPa (100 psi) in RCR, and in the mastic Jnr at a stress level of 3.2 kPa in MSCR.

Significant Problems, Issues and Potential Impact on Progress

None.

Work Planned Next Quarter

Mixture testing will continue in order to expand the data set. FN testing of fine gradation mixtures will begin. If time permits, dynamic modulus (E^*) testing will also be conducted. Data will be compared to binder and mastic test results and used for further evaluation of the modeling tools currently available.

Subtask E1b-2: Feasibility of Determining Rheological and Fracture Properties of Thin Films of Asphalt Binders and Mastics using Simple Indentation Tests

Work Done This Quarter

The creep compliance of different asphalt binders at room temperature was obtained by means of an indentation test by using a finite-size sample and a spherical indenter, as shown in figure E1b-2.1(a), and the analytical solution proposed by Lee and Radok (1960).

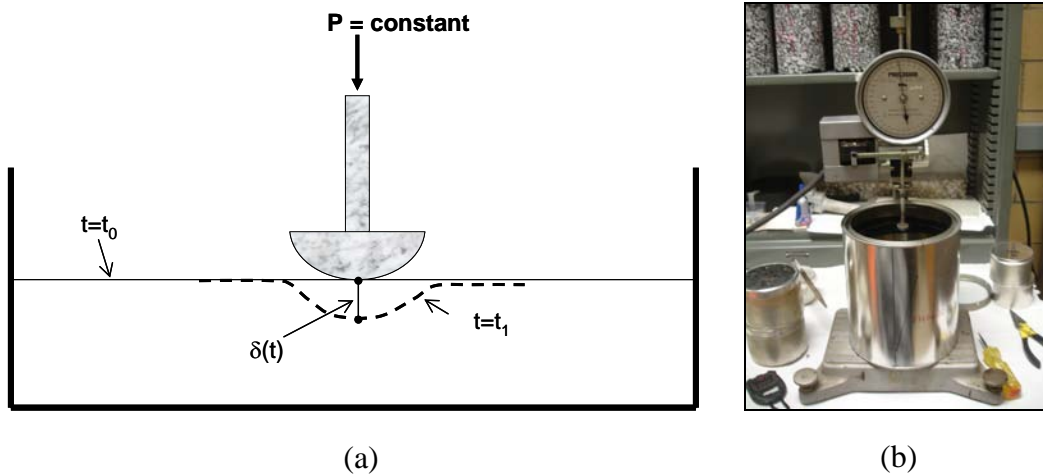


Figure E1b-2.1. Illustration and photo. (a) Schematic of indentation test, and (b) the testing device.

The solution for the creep compliance ($J(t)$) of a viscoelastic half-space for a spherical indenter of radius R , provided that the contact area increases with time, is given by:

$$J(t) = \frac{8R^{1/2}\alpha(t)^{3/2}}{3P(1-\nu)} \quad (\text{E1b-2.1})$$

where

$\mathbf{J(t)}$ = creep compliance

$\delta(t)$ = displacement

\mathbf{R} = radius of indenter

\mathbf{P} = load

ν = Poisson's ratio

The standard penetration test setup was modified, as shown in figure E1b-2.1(b), to run the indentation test with $P = 735$ mN and a spherical indenter of $R = 8.5$ mm. The solution proposed by Lee and Radok is valid only for displacement values that are lower than the radius of the indenter ($\delta(t) < R$).

Three asphalt binders—neat (FH 64-22), elastomer (FH 3% linear styrene-butadiene-styrene (LSBS)), and plastomer (FH 4% CBE)—were used to run preliminary indentation tests. The samples used are cylindrical in shape with fixed radius and heights of 1.7, 3.4 and 5.7 cm. Different specimen heights were used to investigate the influence of the finite sample size on the experimentally obtained creep compliance. The creep compliance obtained from the indentation tests were compared with the compliance obtained from the Dynamic Shear Rheometer (DSR) at two different stress levels: 1 kPa and 10 kPa.

Figure E1b-2.2 shows the results from DSR and indentation tests for the three binders and three specimen sizes. It can be seen from figure E1b-2.2 that the creep compliance from DSR is less stiff compared to that of indentation. There could be many factors responsible for the differences observed. The main contributing factor is that the analytical solution presented in equation E1b-2.1 assumes a semi-infinite medium and the samples used are finite in size. This issue was addressed by predicting the creep compliance for a very large sample (semi-infinite medium) from the creep compliance functions obtained from specimens of three different sizes.

The following approximate method is proposed to take into account the effect of finite specimen size on $J(t)$:

$$\begin{aligned} &\text{By denoting the inverse height of the specimen by } \chi, \\ &\chi = 1/H \end{aligned} \tag{E1b-2.2}$$

where
 H = height of sample.

Then, the creep compliance is a function of time t and χ and hence denoted by $J(t, \chi)$. By replacing H equal to infinity in equation E1b-2.2, the research team obtained that the creep compliance for the viscoelastic half-space is $J(t, 0)$. The idea is to obtain $J(t, 0)$ from the finite thickness samples and, using a Taylor series expansion:

$$J(t, \chi) = J(t, 0) + \frac{\partial J}{\partial \chi}_{\chi=0} \chi + \frac{1}{2} \frac{\partial^2 J}{\partial \chi^2}_{\chi=0} \chi^2 + O(\chi^3) \tag{E1b-2.3}$$

In the present case, the solution exists for the case of heights equal to 1.7, 3.4 and 5.1 cm. Using equation E1b-2.3 for different heights, a set of simultaneous linear equations is obtained in terms of the coefficients. This set is solved for the $J(t, 0)$. This proposed method is used to predict the creep compliance for the three binders tested, as shown in figure E1b-2.3.

Figure E1b-2.3 indicates that this method has promising results. The projected creep compliance from the indentation test is similar to the compliance obtained from the DSR at the 1 kPa stress level. Note that for a stress level of 10 kPa, the material is not in the linear viscoelastic range.

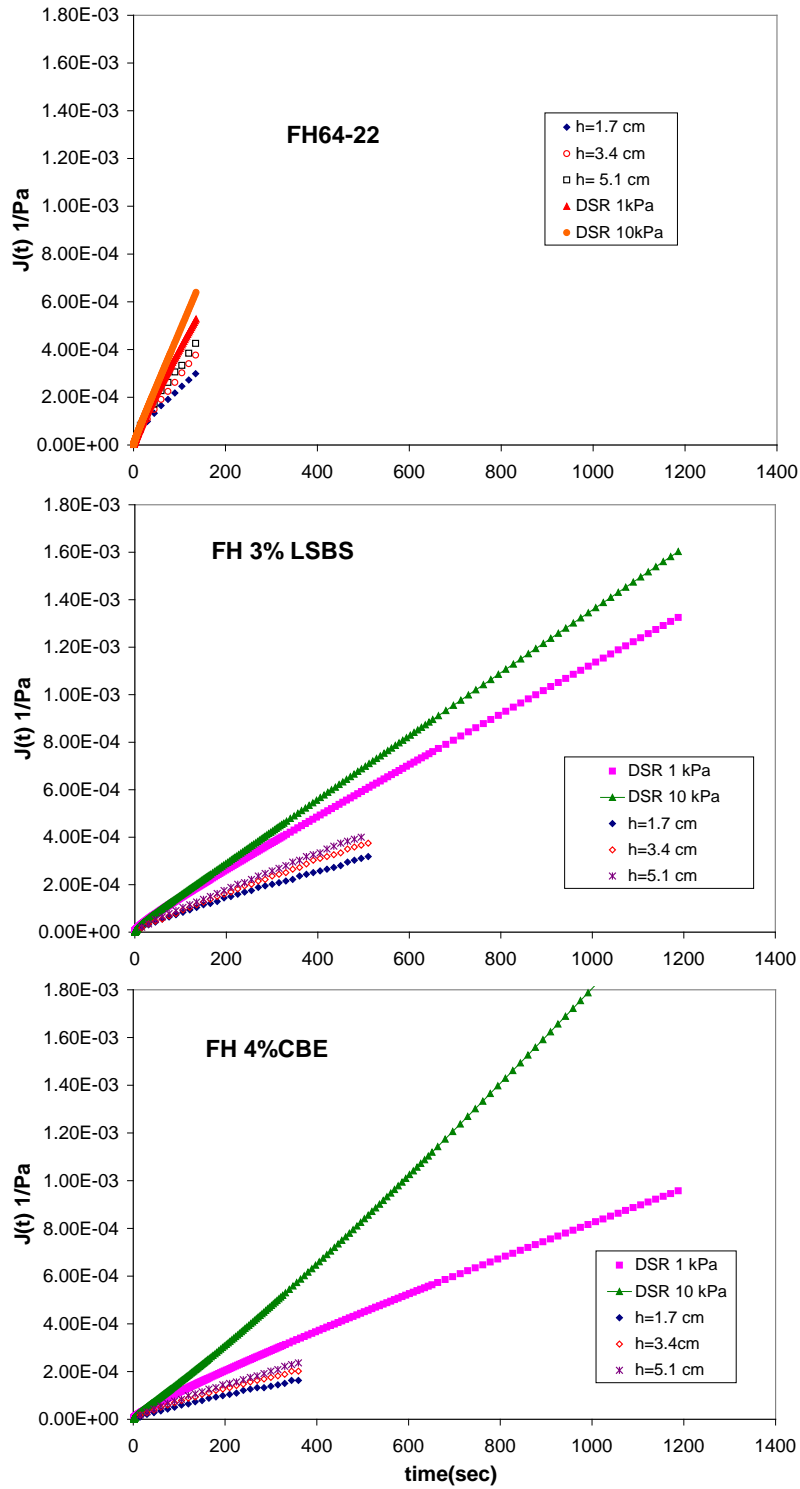


Figure E1b-2.2. Graphs. Creep compliance from indentation test using specimen of different sizes and three binders.

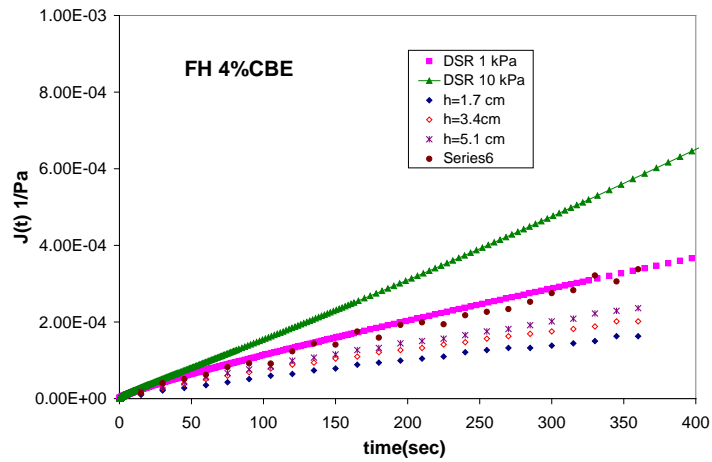
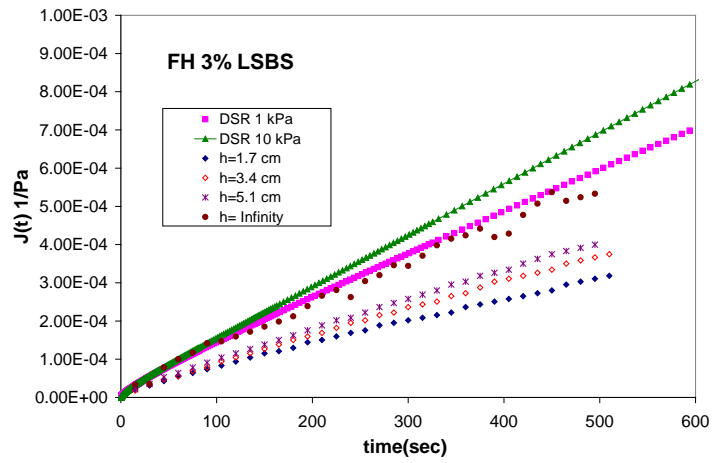
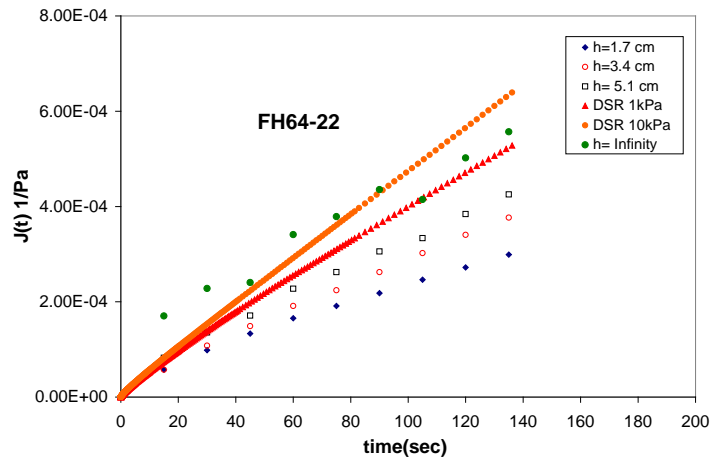


Figure E1b-2.3. Graphs. Creep compliance from indentation test projected to $h = \text{infinity}$.

Additional tests were performed to investigate the effect of the wall thickness on the creep compliance of the material. Tests were run using two 16-ounce cans with different wall thicknesses but with the same material (i.e., FH 4% CBE) and sample height. The wall thickness of the can that contains the testing sample affects the displacement of the indenter and thus the creep compliance obtained from tests quite significantly, as shown in figure E1b-2.4. The sample in the thicker can appears to be stiffer than the sample in the thinner can, which is in agreement with the fact that stiffer walls restrain the deformation more than thinner walls. In both tests, the bottom of the can was kept on the rigid base and therefore may not have a significant effect. However, the lateral walls were unsupported and could deform depending on the force applied to them.

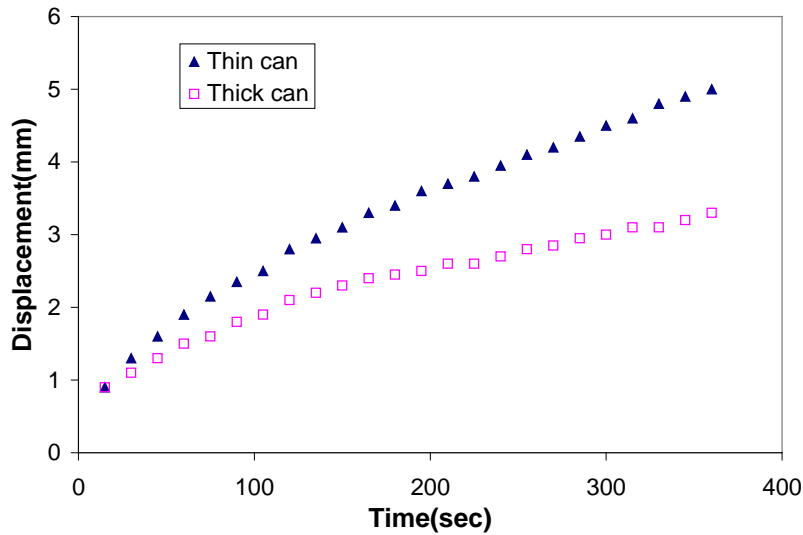


Figure E1b-2.4. Graph. Effect of the wall thickness on the indentation test.

Preliminary tests were performed to investigate the repeatability of the method. Samples of FH 3% LSBS binder with heights equal to 5.1 cm were used to estimate repeatability. Figure E1b-2.5(a) shows that the indentation tests are repeatable. There are no large variations observed for the indentation tests performed on this binder, as shown in figure E1b-2.5(b).

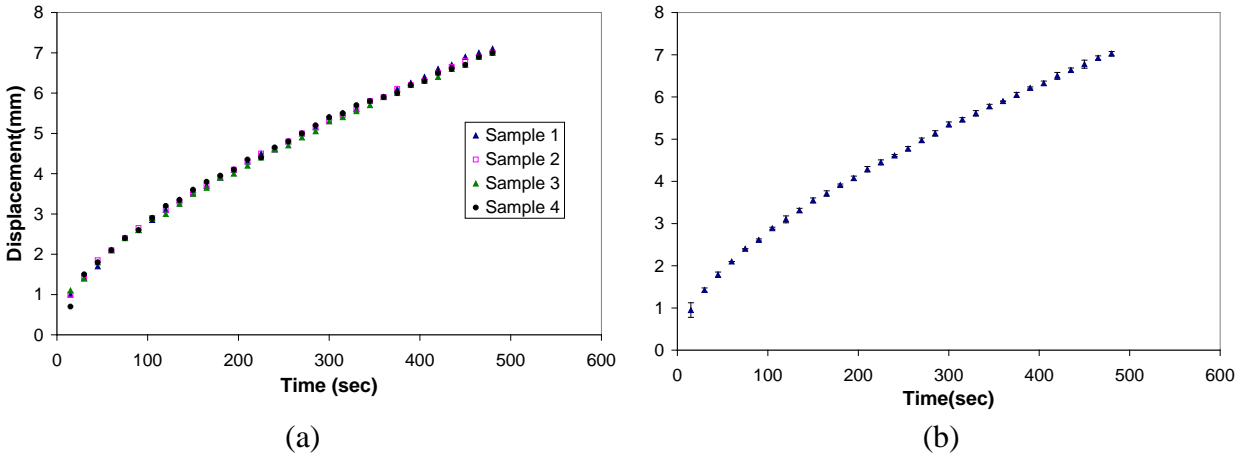


Figure E1b-2.5. Graphs. (a) indentation test of four replicates of FH 3% LSBS binder; (b) average displacement and standard deviation for FH 3% LSBS binder.

In this quarter, the research group at the University of Minnesota started working on the indentation problem at low temperatures. Their objective is to develop a test procedure that estimates the fracture properties of the binder during an indentation test performed in the Bending Beam Rheometer (BBR). The contract for this subtask was recently submitted to the University of Minnesota and is currently being processed.

Significant Results

The indentation test method for asphalt binders is working properly for intermediate temperatures (i.e., room temperature). The method shows excellent repeatability for the creep tests. Further investigation needs to be done to directly obtain the relaxation properties of the binders.

The effect of sample size and wall thickness on creep compliance was successfully investigated in this quarter. Both effects need to be taken into account when estimating the binder's rheological properties from the indentation procedure.

Significant Problems, Issues and Potential Impact on Progress

This test method is intended to be used for rutting characterization. However, testing at higher temperatures (e.g., the high PG limit) is not feasible due to high indentation in soft binders. One approach to solve this problem is to characterize the asphalt at two temperatures for which displacement history can be measured. Researchers can then use numerical methods found in the literature to convert creep compliance into relaxation modulus and build a master curve to predict the behavior at high temperatures.

Relaxation properties from the indentation procedure were investigated, but this highly nonlinear contact problem still results in major theoretical difficulties that are not present during creep loading.

To reflect the actual progress of this research, the Gantt chart has been updated to show later completion dates for subtasks E1b-2.i and E1b-2.ii. The Gantt chart has also been updated to show the planned Draft Report deliverable for subtask E1b-2.iv will be delivered in January 2010 instead of August 2009, and the planned Journal Paper deliverable for subtask E1b-2.iv will be delivered in March 2010 instead of September 2009.

Work Planned Next Quarter

The following points will be investigated in the next quarter:

- The creep compliance will be obtained at other temperatures by constructing a master curve from measurements at two temperatures: 25 °C and 0 °C.
- Appropriate interconversion methods will be investigated to obtain $G^*(\omega)$ and other linear viscoelastic functions from the indentation creep compliance.
- Finite element models will be run to further investigate the effect of the walls and finite sample size on the creep compliance obtained from this procedure.
- Operator sensitivity of the testing device will be analyzed by running tests on the same materials but with different operators.
- Relaxation properties will be investigated with this test methodology by performing a literature review on analytical and approximate models that simulate the changing of the contact area of the indenter during recovery, and also by performing finite element (FE) simulations of the indentation test.
- Continue the work with the research team at the University of Minnesota on fracture properties of binders at low temperatures using indentation tests in the BBR.

Cited References

Lee, E. H., and J. R. M. Radok, 1960, The Contact Problem for Viscoelastic Bodies. *Journal of Applied Mechanics*, 27: 438-444.

Work Element E1c: Warm and Cold Mixes

Subtask E1c-1: Warm Mixes

Work Done This Quarter

Work focused on development and further evaluation of the asphalt lubricity testing that was proposed in the previous quarterly report. Two binder types were tested with and without a warm mix additive. A significant effort was put toward the Manitoba field project, mixes workability for the binder course testing was 75% completed, and a detailed testing plan for pre- and post-construction activities was submitted.

Asphalt binder performance testing and evaluation continued. Work focused on the high-temperature properties, including the Superpave $G^*/\sin(\delta)$ parameter and Multiple Stress Creep and Recovery (MSCR) test results. Asphalt mix workability was evaluated by conducting aggregate coating testing. Gyrotory compaction was also conducted to determine the Construction Force Index (CFI) using the pressure distribution analyzer (PDA), and to determine the number of gyrations to 92% G_{mm} (N92). Two binders—unmodified PG 64 and modified PG 76—and three warm mix additives—Revix, Rediset and Sasobit—were included in the study. In addition, foaming was included as one of the methods for warm mix production.

Significant Results

Asphalt Binder Workability (Lubricity Testing)

The lubricating effect of warm mix asphalt (WMA) additives on asphalt binders was evaluated using the coefficient of friction (μ) measurements obtained from the Asphalt Lubricity Test, which was described in the previous quarterly report. Figure E1c-1.1 summarizes some of the preliminary results. The results indicate that the proposed lubricity test displays sensitivity to material type, as shown by the difference in the values of coefficient of friction between the PG 64-22 and PG 76-22 base and WMA-modified materials.

The PG 76-22 binder shows coefficient of friction values ranging between 17% to 27% higher than the base binder of PG 64-22 grade. This increase is consistent with practical knowledge that, for a given temperature, the workability of a modified PG 76-22 material is significantly lower than that of a PG 64-22 material. The results also show that the warm mix additive Revix results in a noticeable reduction in the coefficient of friction as measured by this new setup.

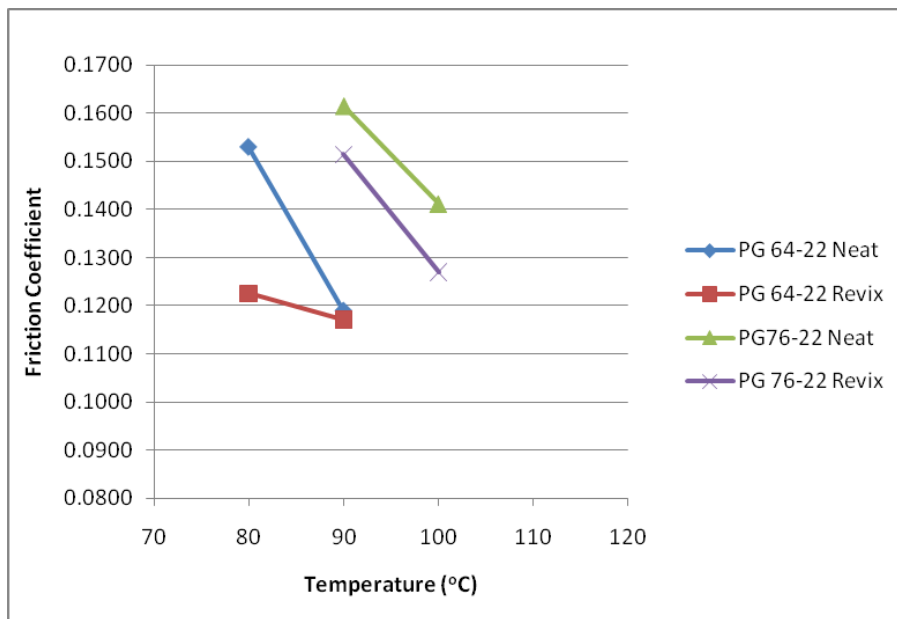


Figure E1c-1.1. Graph. Summary of lubricity test results.

Asphalt Binder Performance

The impacts of WMA additives on binder resistance to permanent deformation were evaluated using the current Superpave rutting parameter ($G^*/\sin(\delta)$) and the proposed MSCR test method to measure nonrecoverable creep compliance (Jnr). Results for the PG 64-22 and PG 76-22 base binders modified with selected WMA additives and processes are shown in figures E1c-1.2 and E1c-1.3, respectively, for the Superpave rutting parameter. Testing of foam binders was conducted immediately after laboratory foaming.

As can be seen in figure E1c-1.2, the addition of 2% Sasobit to the PG 64 binder increased the grade to a PG 70; conversely, the grade of PG 76 binder remained unchanged, as shown in figure E1c-1.3. The surfactant-based additives Rediset and Revix had differing effects on binder properties. Revix reduced the grade of the PG 76 to a PG 70, whereas the WMA-modified Rediset binder remained a PG 76. The WMA Revix also did not cause a change in the grade of the PG 64. In addition, the foamed binder demonstrated no change in high-temperature PG grade relative to the PG 64 and PG 76 base binders.

Results for the Jnr and percent recovery (%R) of the base and WMA-modified PG 64-22 and PG 76-22 binders are provided in figures E1c-1.4 and E1c-1.5, respectively. As shown in figure E1c-1.4, most of the materials meet the 0.4 maximum Jnr proposed specification limit. As expected, results presented in figure E1c-1.5 are drastically different for the neat and polymer-modified base binders. The neat base and WMA Revix materials show negligible %R, which is consistent with expected behavior due to the lack of a polymer modifier to provide elasticity. The PG 64-22 Sasobit material also demonstrated expected behavior, showing %R at 64 °C due to the stiffening effect of the wax additive. The PG 76-22 base and WMA-modified materials all demonstrate recovery after unloading, with the Sasobit providing approximately 10% higher recovery relative to the PG 76 control and surfactant-modified WMAs.

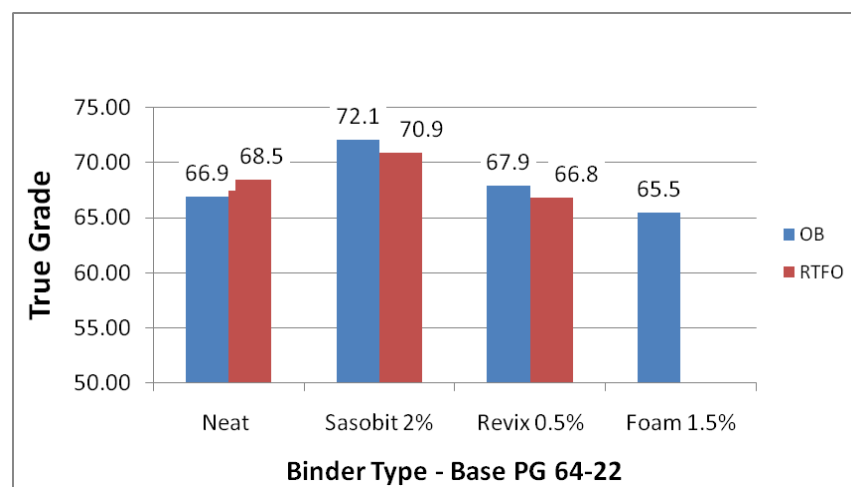


Figure E1c-1.2. Graph. Effect of WMA additives on high-temperature binder grade for base PG 64-22. (OB = original binder; RTFO = rolling thin film oven.)

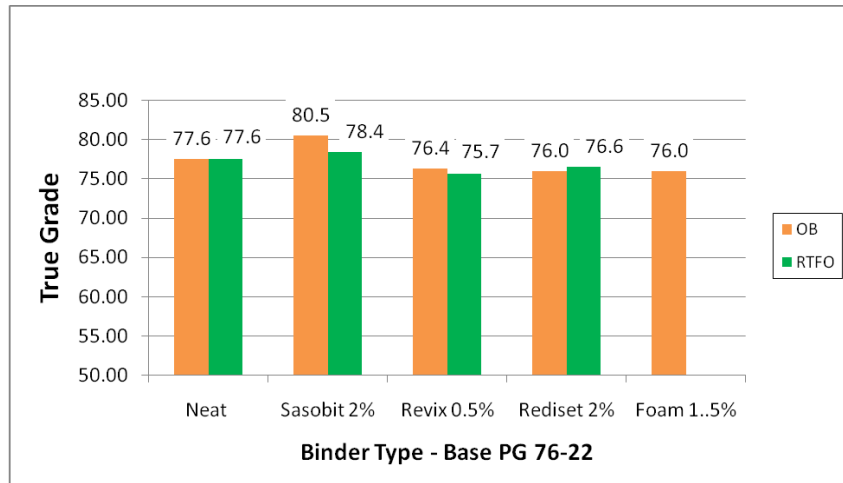


Figure E1c-1.3. Graph. Effect of WMA additives on high-temperature binder grade for base PG 76-22.

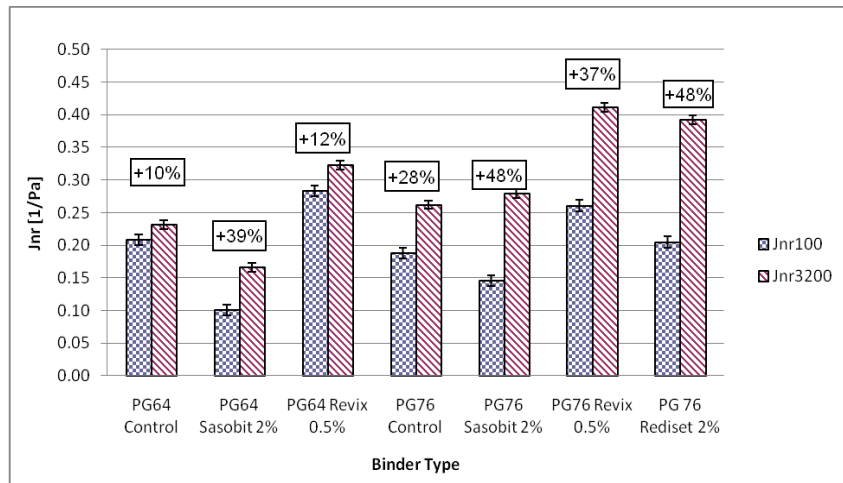


Figure E1c-1.4. Graph. Jnr results from MSCR testing.

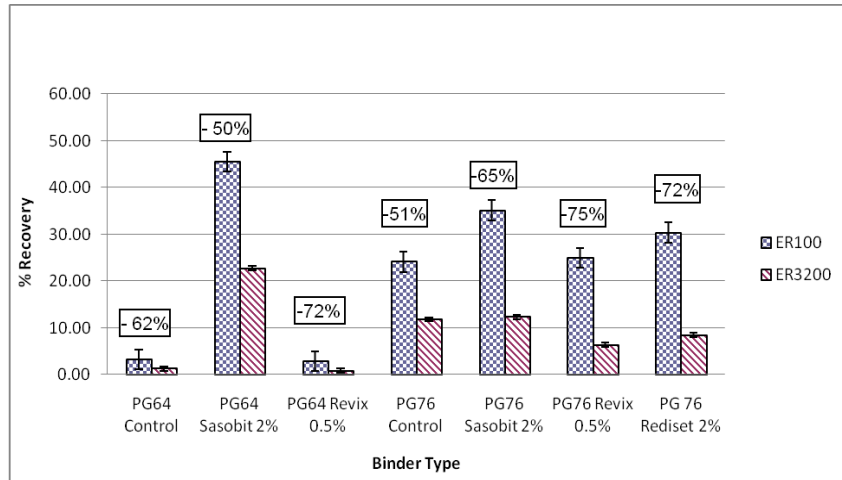


Figure E1c-1.5. Graph. %R results from MSCR testing.

The effect of WMA additives on low-temperature fracture properties was evaluated using the critical cracking temperature measured by the Asphalt Binder Cracking Device (ABCD). Testing was conducted on pressure aging vessel (PAV)-aged material. Results, presented in figure E1c-1.6, demonstrate similar low-temperature fracture performance across both base binder grades. It should be noted that the cracking temperature of all the materials evaluated exceeded that of the intended low-temperature performance grade, -22 °C, by at least 4 °C. In general, the use of Revix caused softening; conversely, use of Sasobit caused increased stiffening and embrittlement. These observations are consistent with data previously presented for standard Superpave testing using the Bending Beam Rheometer (BBR). The use of Rediset with the PG 76 appears to have no significant effects as compared to the base binder.

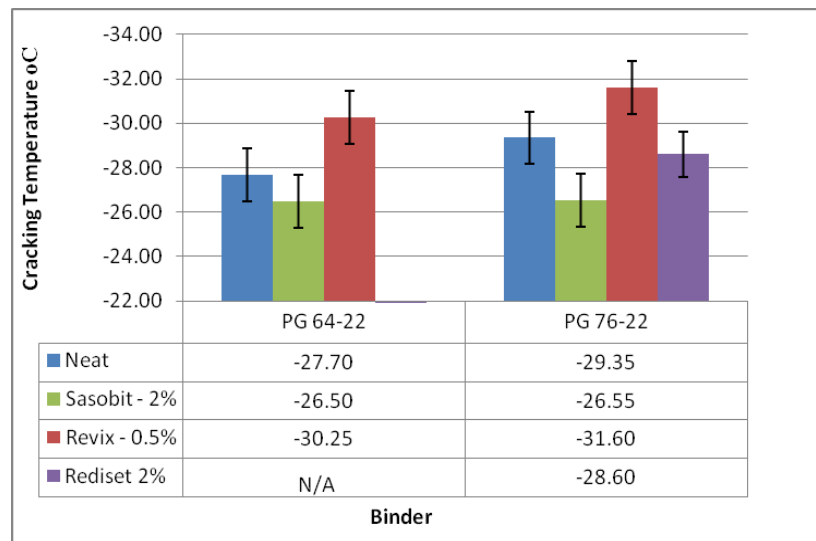


Figure E1c-1.6 Graph. Effect of WMA additives on low-temperature fracture properties using the ABCD test.

Asphalt Mixture Workability

Aggregate coating was evaluated following the AASHTO T 195 procedure. The procedure involves mixing at the prescribed temperature and immediately separating coarse from fine particles on the 3/8-inch sieve. Mixing time was held constant at 1.5 minutes, after which each particle retained on the sieve is examined. A particle is only considered coated if there is no aggregate surface exposed. Percent aggregate coating is expressed as the ratio of coated particles to total particles. Two replicates were conducted for each combination. Results for these tests for the fine gradation mixes are provided in figure E1c-1.7(a) for the PG 64-22 base binder and figure E1c-1.7(b) for the PG 76-22 base binder.

Results for the PG 64-22 base binder demonstrate a clear effect of temperature for both the base binder and WMA-modified materials. Reductions in aggregate coating ranged from approximately 57% to 72% between tests conducted at 150 °C and 105 °C. Conversely, the effect of the WMA processes on aggregate coating is not clear, as there are only minor differences between trends shown in figure E1c-1.7(a). This observation was verified through analysis of variance (ANOVA) analysis, which found the addition of WMA additives to be insignificant with a p-value of 0.900. The adjusted R^2 associated with the analysis for the model was ~93%.

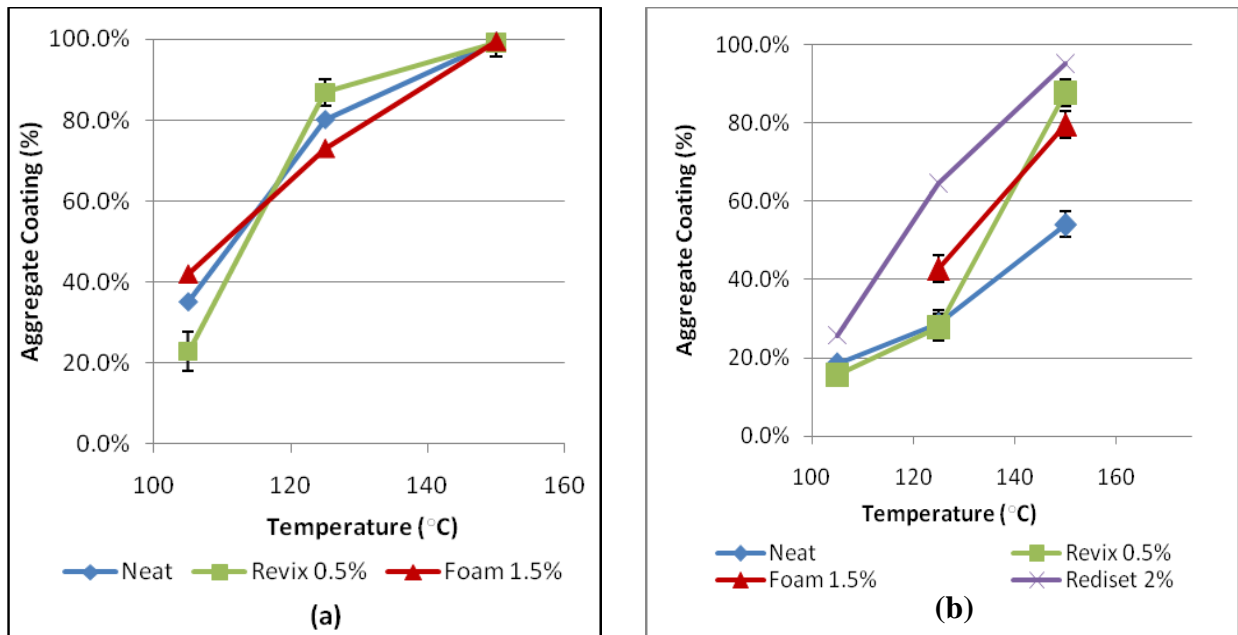


Figure E1c-1.7. Graphs. Aggregate coating versus temperature for granite fine mix:
(a) PG 64-22; (b) PG 76-22.

The PG 76-22 base binder results, however, showed more dependency on temperature and additive type than the PG 64-22 binder. There was less than 50% aggregate coating observed for most mixes below a mixing temperature of 125 °C, with the exception of the binder with the Rediset additive. The < 50% coating unacceptable level of aggregate coating was observed for the 105 °C and 125 °C mixing temperatures for the neat and WMA Revix-modified materials. At 150 °C mixing temperature, the results show that all WMA types improve the coating significantly, from less than 60% for the PG 76 binder to more than 80% with the Revix and Rediset additives.

Asphalt mixture workability at a range of compaction temperatures was evaluated using gyrations required to 92% G_{mm} (N92) and the CFI. The relationship between N92 and CFI for compaction pressures of 300 kPa and 600 kPa for both the coarse and fine mixes across all compaction temperatures is provided in figure E1c-1.8. The results show a strong relationship between N92 and CFI for both compaction pressures, indicating a significant effect of compaction pressure on both workability indices. Furthermore, the effect of gradation is also present for both compaction pressures, with the coarse mix showing less workability as indicated by higher values of N92 and CFI. This effect is more pronounced for the compactions conducted at 300 kPa.

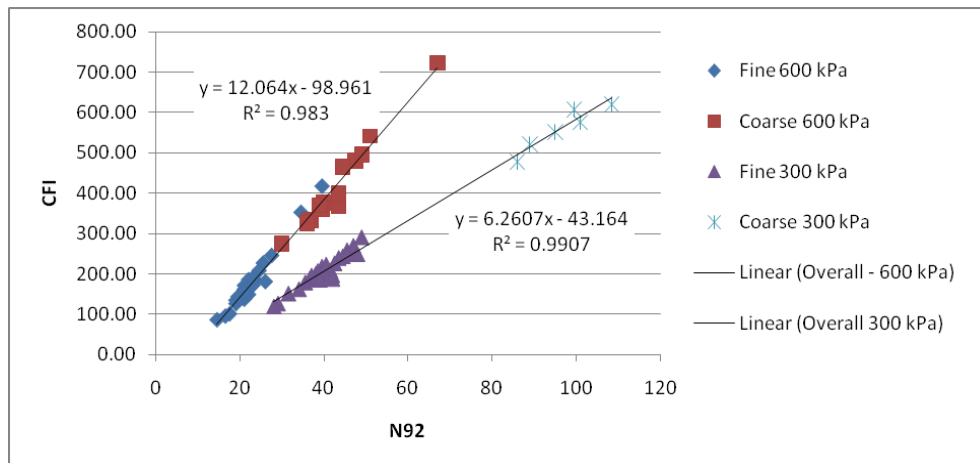
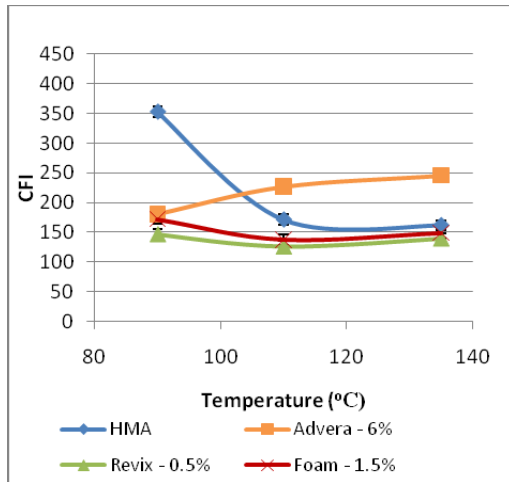
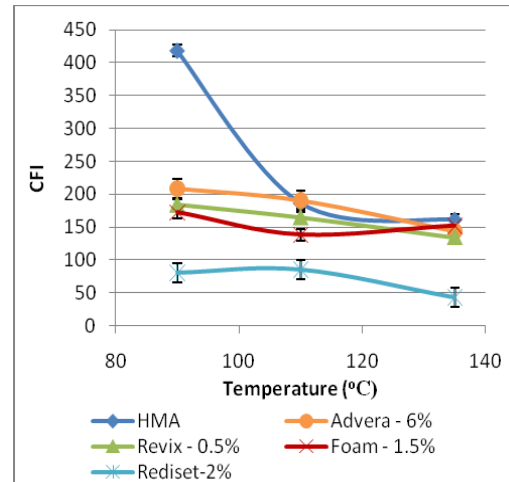


Figure E1c-1.8. Graph. CFI versus N92 as function of compaction pressure.

CFI results for the fine-graded mixtures produced with the PG 64-22 and PG 76-22 binders are provided in figure E1c-1.9. The results demonstrate that the effect of WMA additives is not recognized until compaction temperatures of 90 °C are reached. In addition, the WMA mixes exhibited considerably less temperature sensitivity, as shown by the relatively small change in CFI between compactions at 90 °C and 135 °C. Furthermore, an increase in base binder grade from PG 64-22 to PG 76-22 resulted in only slightly higher values of CFI at lower temperatures. It is seen that at 135 °C, the CFI are almost identical for both binders.



(a)



(b)

Figure E1c-1.9. Graphs. CFI versus temperature for fine mix (600 kPa):
(a) PG 64-22; (b) PG 76-22.

ANOVA analysis was used to identify significant factors and determine if the differences observed at various compaction temperatures and between HMA and WMA are statistically significant. Results of the analysis are presented in table E1c-1.1, which indicates the main effects of WMA additive and compaction temperature along with some two- and three-factor interactions that have a significant effect on CFI. The analysis will continue next quarter to identify critical factors and evaluate the modeling of coating and compaction results as a function of lubricity and viscosity of binders modified by the additives.

Table E1c-1.1. Summary of ANOVA with fine mix at 600 kPa.

Source	DF	Seq Sum of Squares	Adjusted Sum of Squares	Adj Mean Squares	F	P
Additive	3	57492.7	55613.2	18537.7	34.21	0.0000
Binder	1	0.1	103.8	103.8	0.19	0.6670
Compaction Temp	2	53954.2	32409	16204.5	29.91	0.0000
Additive * Binder	3	11709.6	6633	2211	4.08	0.0250
Additive * Compaction Temp	6	71505	74541.4	12423.6	22.93	0.0000
Binder * Compaction Temp	2	6390.7	5026.7	2513.4	4.64	0.0000
Additive*Binder*Compaction Temp	6	3674	3674	612.3	1.13	0.0260
Error	16	8668.9	8668.9	541.8		0.3890
Total	39	213395.3				
R-Squared (adj)	90.1%					

Significant Problems, Issues and Potential Impact on Progress

To reflect the actual progress of this research, the Gantt chart has been updated to show work in Q3 for subtasks i and ii. Also, the planned Journal Paper was written to reflect activities in subtask E1c-1.ii instead of subtask E1c-1.iii.

Work Planned Next Quarter

Work next quarter will focus on the following tasks:

- *Original experimental matrix.* The research team will continue testing binder properties and compacting mixes based on the experimental testing matrix. The focus will be on completing the Pneumatic Adhesion Tensile Testing Instrument (PATTI) and Binder Yield Energy Test (BYET) testing for the binder, and possibly fully grading the foamed binders.
- *Lubricity testing.* A new experiment will be conducted to finalize the newly developed procedure. Three temperatures, four shear rates, and two normal forces will be used on two different binders (PG 64-22 and styrene-butadiene-styrene (SBS)-modified PG 76-22), in addition to testing engine oil to provide a basis for comparison. Once the procedure is finalized, different additives will be incorporated in a full testing plan.
- *Manitoba field project:*
 - Binder testing. This testing will include all binder testing, with viscosity and lubricity testing taking priority.
 - Mixture testing. This testing will include evaluation of mixture workability of surface and binder courses compacted at 600 kPa. A report will be submitted to Manitoba before construction of each lift.

Subtask E1c-2: Improvement of Emulsions' Characterization and Mixture Design for Cold Bitumen Applications

Work Done This Quarter

The research team conducted a literature review to investigate the hypotheses that sweep test results are highly dependent on film thickness and aggregate application rate. The Modified Kearby chip seal design method and the McLeod design method, which are two primary methods used in North America (Lee and Kim 2008; NCHRP 2005), were reviewed in detail. The ASTM sweep test method is a laboratory-based performance test that attempts to measure chip seal performance by simulating the mechanical brooming action experienced by newly constructed chip seals (ASTM 2008; Schuler and Stock 2009). The test is used to determine when the seal can be opened to traffic given aggregate and binder application rates. In practice, contractors typically rely on prior experience or methods that differ from standard methods; some have no formal design method.

Through this review and in conducting the sweep test, two questionable assumptions were identified. The first suggests that the amount of aggregate remains constant, regardless of the

binder type; the second maintains that voids in the aggregate layer must be filled with 70% asphalt binder for adequate performance (Minnesota 2006). When aggregates of different sizes or gradations are used, the voids available to accommodate binder increase or decrease depending on the size and gradation of the aggregates, affecting the amount of binder required to securely retain the aggregates. This is perhaps the greatest deficiency of the current sweep test, in that there is no direct relationship between the aggregate void content and the binder application rate.

The research team also conducted a literature review on rotational viscometry as a method to investigate emulsion drain-out and sprayability. The review suggests that the Brookfield viscometer can be used to evaluate steady-state viscosities of emulsified asphalts, and that these rotational viscosities may be correlated to the Saybolt-Furol viscosities routinely measured at manufacturers' laboratories (Salomon et al. 2004). In the study reviewed, the preparation of emulsified asphalt samples was performed according to the ASTM standard method (ASTM 2004). Brookfield rheometer tests used the 50-50-21 method; that is, emulsion samples were tested at 50 °C and at 50 rpm using the SC4 spindle No. 21 for 30 minutes after an initial temperature acclimation period.

Experimental plans were developed for three promising tests, including the Bitumen Bond Strength (BBS) test, Brookfield rotational viscometer (RV) tests, and the sweep test. The BBS test is being developed as a tool to identify early raveling potential through measurement of cohesion and adhesion between emulsion binders and aggregate plates. The BBS test may also serve as a Dynamic Shear Rheometer (DSR)-surrogate test for investigating emulsion curing based on breaking and setting rates, though further investigation is needed to compare the test methods. The Brookfield RV may be used to evaluate drain-out and sprayability through evaluation of viscosity and low and high shear rates. Sweep testing was conducted to verify experimental results using a performance-based test on the entire chip seal system. These efforts used the ASTM standard method.

Experimental plans for the BBS test were based on recent research findings, as indicated in the previous quarterly report. The CRS-2 samples were retested this quarter using a refined BBS testing protocol and fresher emulsion samples. Factors investigated include aggregate type, curing temperature, curing relative humidity and curing interval. A second BBS experiment focused on comparing a standard CRS-2 emulsion with a modified CRS-2P emulsion. Results from these experiments are given in the "Significant Results" section of this report.

Initial RV testing focused on replicating results given in similar studies and in the literature review (Salomon et al. 2004). Testing protocols were developed using the 50-50-21 method; that is, tests were conducted at 50 °C and 50 rpm (corresponding to a shear rate of 46.5 sec^{-1}) using the SC4 spindle No. 21. Preliminary tests indicate that the RV may relate to Saybolt-Furol seconds (SFS). However, testing must be conducted at different shear rates to determine if the test procedure is able to measure drain-out or sprayability. Subsequent efforts considered three shear rates and three temperatures for a variety of emulsion types and production facilities. Results from these experiments are given in the "Significant Results" section of this report.

An experimental plan was devised for the sweep test to investigate emulsion and aggregate application rates, emulsion type, and aggregate type to investigate the effects on the percent aggregate loss, the response measured in the sweep test. A statistical analysis was conducted to infer which variables have the greatest impact on the percent aggregate loss response variable. The results, presented in greater detail in the “Significant Results” section, will aid the research team in developing an appropriate procedure for chip seal performance testing or improving current design procedures.

Three field projects were selected based on conversations with HG Meigs, a local emulsion supplier. The goal in visiting these field sites was twofold: first, to collect field samples of aggregate chips, emulsion, and when possible, larger rocks from which the chips originated; and second, to gain insight into the chip seal construction process. The materials collected at each field site are given in table E1c-2.1.

Table E1c-2.1. Materials sampled from field sites.

Project Location	Emulsion Type	Aggregate Chip Type	Rock Type
Jefferson County, WI	HFRS-2P	Dolomite	Dolomite
Juneau County, WI	CRS-2	Bottom Ash	-
Lafayette County, WI	HFRS-2P	Slag	-

Materials were collected in late August and will be examined in the next quarter using the battery of current tests. The research team has also acquired a wide variety of emulsion samples to be used in RV and BBS testing. Due to the smaller sample size, sweep testing will not be possible given the significant sample volume needed to run sweep tests.

Testing efforts this quarter focused on evaluating emulsion construction properties. Three tests were used to evaluate emulsion performance, including the BBS test, the sweep test, and the RV test. BBS testing focused on variable screening and redefining the experimental matrix. Sweep testing focused on investigating the effects of aggregate and binder application rates. RV testing focused on correlating Saybolt-Furol viscosities with steady-state viscosities obtained using the Brookfield RV. The research team will continue to investigate a surrogate test for the Bending Beam Rheometer (BBR) using the DSR. Testing is currently on hold while a long-term aging procedure for emulsion residues is finalized.

Strategies for conducting an energy analysis of HMA production facilities are also progressing. Representatives from the research team visited a local HMA production facility to assess standard production methods in an effort to develop a framework for comparing cold mix applications to conventional mixtures. Coordination continues with a prominent automation and systems control company to determine which plant variables can be readily measured, recorded and adjusted to optimize plant efficiency and performance. Establishing a baseline scenario for current HMA production will enable a comparative study of warm and cold mix asphalts. In working to define significant plant variables and analyze plant operational data, the research team is focusing on aggregate moisture content, fuel type and energy distribution throughout the

plant. Significant operational variables may be analyzed once plant operational data has been obtained.

Coordination continues with the Institute for Sustainability (IfS), a division of the American Institute of Chemical Engineers (AIChE). The research team will continue to work with IfS to develop life cycle assessment tools and methods, including the total cost accounting (TCA) methodology. The AIChE Sustainability Index (SI), a benchmarking framework for evaluating holistic sustainability, shows promise at being expanded beyond the chemical industry to include such industries as the pavement construction industry.

The following meetings were held in the last quarter:

- ARC Emulsion Advisory Group Meeting, September 25, conference call.
- University of Stellenbosch, monthly conference call to coordinate BBS testing.
- IfS, monthly conference call to establish a framework for conducting a pavement energy analysis.

Significant Results

Bitumen Bond Strength Test

Two notable experiments were conducted using the BBS test. The first experiment replicated a previous experiment and utilized a fresher CRS-2 emulsion. The effects of experimental factors shown in table E1c-2.2 on the pullout tension response were investigated; results are shown in table E1c-2.3.

Table E1c-2.2. Factors and levels used in the experiment.

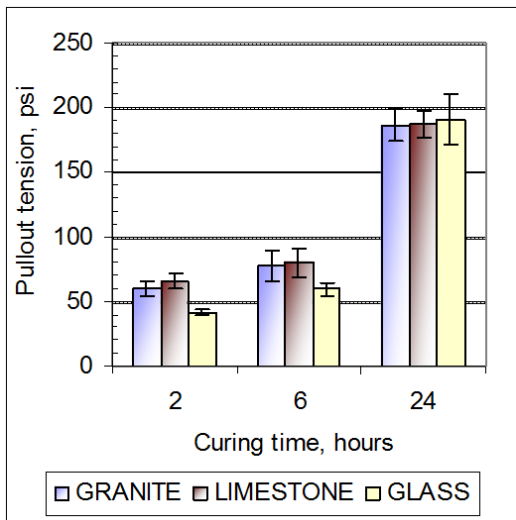
Variable Factors		Level		
		1	2	3
A	Aggregate Type	granite	limestone	glass
B	Curing Temperature, C	35	15	-
C	Curing Relative Humidity, %	70	30	-
D	Curing Interval, hours	2	6	24

Table E1c-2.3. Increase in pullout tension (psi) observed in BBS testing.

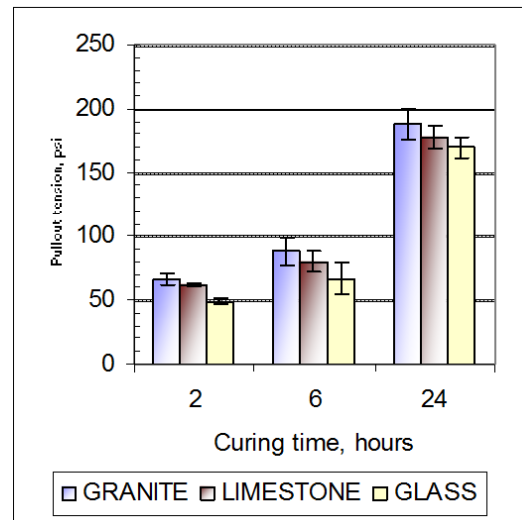
Curing Conditions	Granite		Limestone		Glass	
	2 - 6 HR	6 - 24 HR	2 - 6 HR	6 - 24 HR	2 - 6 HR	6 - 24 HR
35 C - 30 % RH	98.9	43.0	69.6	46.4	46.3	91.5
35 C - 70 % RH	62.6	92.1	51.1	100.4	51.7	101.7
15 C - 30 % RH	21.6	99.2	18.6	97.0	17.4	102.7
15 C - 70 % RH	17.8	109.3	14.3	107.5	18.4	131.0

RH = relative humidity.

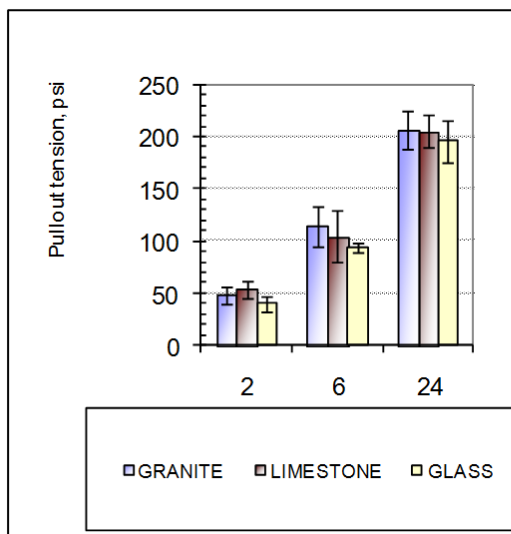
BBS test results are depicted in figure E1c-2.1 for each of four curing condition combinations. Similar tensile strength gains are seen at all combinations in the first two hours of curing for each substrate, with glass performing worse than granite and limestone. Significant strength gains are seen between two and six hours at the higher temperature level. Granite outperforms limestone in three of four curing conditions after six hours. Humidity does not appear to have a significant effect on overall tensile strength, which is confirmed in an analysis of variance (ANOVA). All substrates exhibit similar performance after 24 hours curing, with granite again performing best in three of four curing conditions. Overall, samples tested at 35 °C and 30% RH performed better than samples tested at other curing conditions.



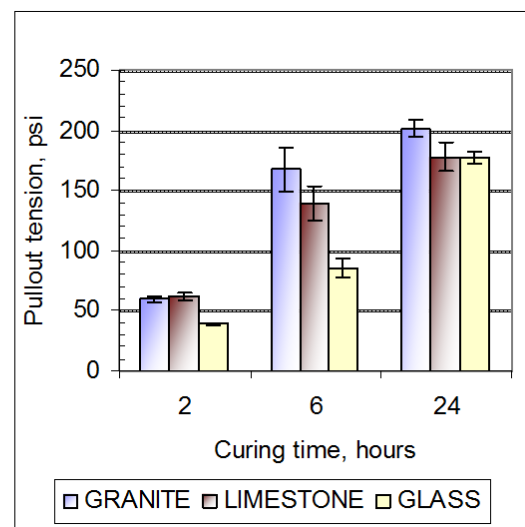
(a)



(b)



(c)



(d)

Figure E1c-2.1. Charts. CRS-2 emulsion cured on selected substrates at (a) 15 °C and 70% RH; (b) 15 °C and 30% RH; (c) 35 °C and 70% RH; and (d) 35 °C and 30% RH.

An ANOVA was prepared to determine the significant effects. Results suggest that at a 95% level of confidence, the main effects of curing interval and curing temperature are statistically significant, while two-way interaction effects are significant for curing temperature–curing interval and curing RH–curing interval. The curing conditions resulting in the greatest initial increase in pullout tension are 35 °C and 30% RH for granite and limestone substrates. The glass substrate demonstrated the highest initial strength gains at conditions of 35 °C and 70% RH. The most significant gains in tensile strength between 6 and 24 hours are seen at curing conditions of 15 °C and 70% RH for all substrates. This suggests that additional moisture in the ambient environment may delay curing.

A second experiment was conducted to compare a modified CRS-2P polymer-modified emulsion to a standard CRS-2 emulsion. The curing conditions for the experiment were 35 °C and 30% RH, conditions screened as ideal in the previous experiment. Table E1c-2.4 summarizes the data collected in this experiment, while figure E1c-2.2 displays the results graphically.

Table E1c-2.4. Average measured pullout tensions for two emulsion types.

Aggregate	Curing time, hours	CRS-2 pullout tension, psi	CRS-2P pullout tension, psi
Granite	2	62.2	42.1
	6	149.4	57.1
	24	186.7	114.3
Limestone	2	57.9	51.1
	6	124.5	73.0
	24	181.9	144.0
Glass	2	39.2	38.9
	6	85.6	47.5
	24	177.0	110.9

From figure E1c-2.2 it can be seen that the pullout tension for the CRS-2 emulsion exceeds that of the CRS-2P emulsion for all substrates at all curing intervals. At all curing intervals, CRS-2 on granite demonstrates the highest pullout tension, with glass demonstrating the lowest pullout tension for both emulsion types. For the CRS-2P emulsion, the highest pullout strengths are observed on limestone substrates. This suggests that particular combinations of emulsions and aggregate types may be more compatible than other combinations.

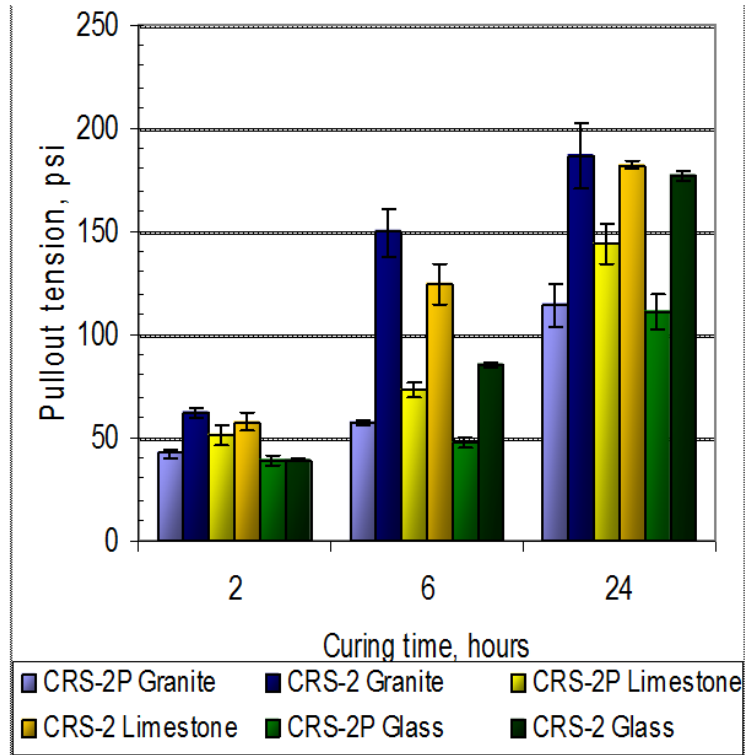


Figure E1c-2.2. Chart. Pullout tensions of CRS-2 and CRS-2P emulsions are compared over time on granite, limestone and glass substrates.

Sweep Test

Sweep testing was conducted to investigate four factors believed to affect total aggregate loss. A full factorial experiment was developed and executed to investigate potentially significant factors. The experimental matrix is shown in table E1c-2.5. Statistical analyses indicate that the aggregate application rate and the emulsion type have the greatest effect on percent aggregate loss at 95% level of confidence. Several two-way interaction effects are also identified as significant. Emulsion application rate appears to be significant at $0.05 < \alpha < 0.10$ values, while aggregate type appears to be the least significant factor. Figure E1c-2.3 depicts the experimental results.

Table E1c-2.5. Factors and levels used in the experiment.

Factor		Levels	
		+	-
A	Aggregate type	granite	limestone
B	Aggregate rate, g	689.0	450.0
C	Emulsion rate, g	115.4	88.5
D	Emulsion type	CRS-2	CRS-2P

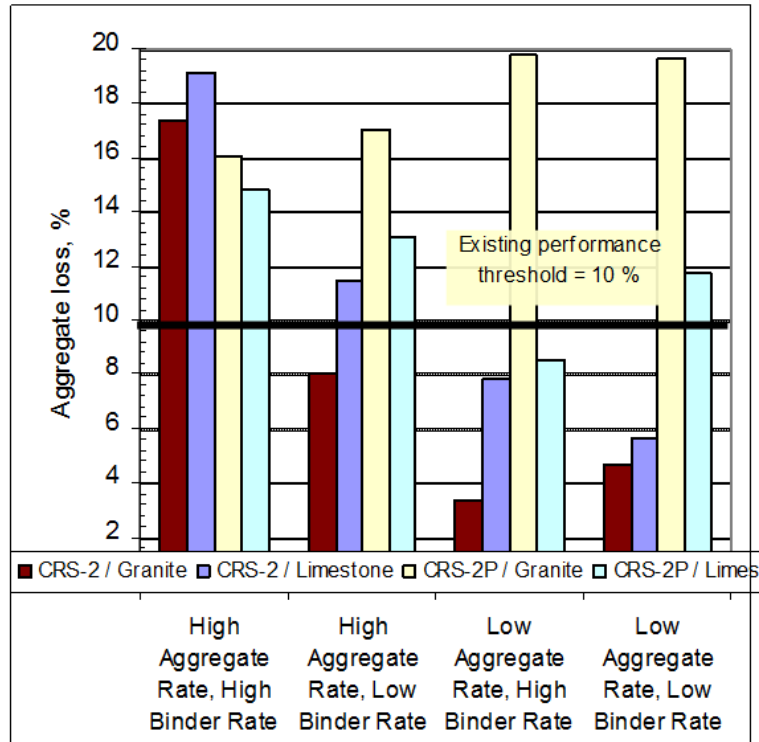


Figure E1c-2.3. Chart. Aggregate loss for CRS-2 and CRS-2P emulsions combined with granite and limestone chips.

Several observations can be made with regard to the data presented in figure E1c-2.3. Aggregate loss is highest for all material combinations (except the CRS-2P/granite combination) at high aggregate and binder levels. The lowest aggregate loss levels are seen in the CRS-2/granite combination at low aggregate levels. In general, applying less aggregate results in less aggregate loss. Aggregate loss levels for the CRS-2P/granite combination are significantly higher at low aggregate application rates, suggesting that these tests should be repeated to ensure their accuracy. With one exception occurring at the combination of high aggregate rate and high binder rate, the CRS-2 emulsion performs better than the CRS-2P emulsion. As with the BBS test, particular combinations of aggregate type and emulsion type may perform better than others. Correlations between the two tests may further define advantageous combinations.

Viscosity Test

The research team initiated viscosity testing this quarter in an effort to investigate drain-out and sprayability construction properties. Using a standard 50 C-50 ROM-21 spindle size test protocol, several emulsion samples were tested. Figure E1c-2.4 displays the correlation between Saybolt-Furol viscosity and steady-state rotational viscosity as measured by the Brookfield RV. By developing strong correlations between the steady-state rotational viscosity and the Saybolt-Furol viscosity, the argument may be made that rotational viscosity measurements, which are easily measured using readily available equipment, may replace Saybolt-Furol viscosity measurements, which are more difficult to measure in practice.

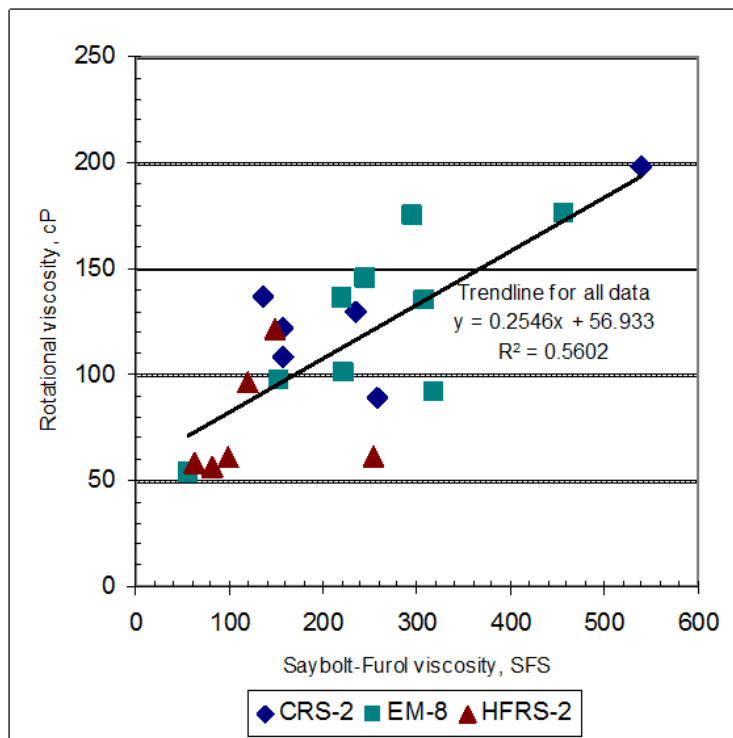


Figure E1c-2.4. Graph. Relationship between Saybolt-Furol viscosity and steady-state rotational viscosity for three emulsion types. Samples were tested using the 50-50-21 test protocol.

Significant Problems, Issues and Potential Impact on Progress

Few notable problems were encountered this quarter. The issues are briefly described below:

- The environmental curing chamber used for curing BBS samples had issues maintaining consistent temperatures and humidity levels. Although the chamber is now working properly, equipment breakdown limited BBS data collection in the second half of the quarter. More results are expected in the following quarter now that the chamber is functioning properly.
- The pavement energy analysis is currently on hold pending additional information from the systems automation company that is responsible for monitoring and recording plant operational data. Information critical to the energy analysis is expected in the next quarter.

Work Planned Next Quarter

Work next quarter will focus on the following tasks:

- *Construction properties of emulsions.* The research team will continue to analyze emulsion construction properties using the BBS test, sweep test and Brookfield RV. BBS testing will focus on testing newly acquired materials over a range of curing intervals. Curing temperatures will also be increased as suggested previously by the emulsion advisory group. Sweep testing will focus on testing the same emulsions and aggregates used in BBS testing so that correlations may be drawn between the two tests. The effect of curing time and emulsion application temperature on total aggregate loss will also be investigated. RV tests will investigate viscosities at a range of temperatures and shear rates. In addition, the research team will initiate an investigation of storage stability.
- *Energy analysis.* Plant operational data will be analyzed to determine the critical factors that can be readily monitored and recorded at HMA production facilities. Establishing a list of measurable variables will enable the research team to begin analyzing operational data.
- *Emulsion residue properties.* The research team will continue evaluating the possibility of using DSR testing protocols as a surrogate for BBR testing at intermediate temperatures.
- *ARC Project Advisory Group and Emulsion Task Force activities.* The research team will continue to hold advisory group meetings and support Emulsion Task Force activities.

Cited References

ASTM, 2004, ASTM D244-04 Standard test methods and practices for emulsified asphalts, American Society of Testing and Materials. West Conshohocken, PA.

ASTM, 2008, ASTM D7000-08 Standard test method for sweep test of bituminous emulsion surface treatment samples, American Society of Testing and Materials. West Conshohocken, PA.

Lee, S., and Y. R. Kim, 2008, Understanding the Effects of Aggregate and Emulsion Application Rates on Performance of Asphalt Surface Treatments. *Transportation Research Record*, 2044:71-78.

Minnesota Seal Coat Handbook, 2006, Manual Number 2006-34. Accessed 4/30/09, <http://www.lrrb.org/pdf/200634.pdf>

NCHRP Synthesis 342, 2005, *Chip Seal Best Practices*, Transportation Research Board, Washington, D.C.

Salomon, D., Zhai, H., Corona, J., and F. Castellanos, 2004, New Tools to Measure Emulsified Asphalt Properties, Idaho Asphalt Supply Inc.

Schuler, S., and A. Stock, 2009, A New Laboratory Test for Predicting Very Early Chip Seal Performance. Presented at the Annual Meeting of the Association of Asphalt Paving Technologists, Minneapolis, Minnesota.

CATEGORY E2: DESIGN GUIDANCE

Work element E2a: Comparison of Modification Techniques (UWM)

Work Done This Quarter

The research team finished collecting the materials needed for this task. The material library for this study includes 17 materials from six sources, including five base binder grades and 12 modified binder grades. The team also began testing the materials following the approved testing matrix. Tests performed to date are Dynamic Shear Rheometer (DSR)-run rheological measurements according to AASHTO TP5 and Multiple Stress Creep and Recovery (MSCR) tests according to ASTM D7405-08a. The collected materials were also subjected to laboratory aging techniques such as rolling thin film oven (RTFO) (AASHTO T240) and pressure aging vessel (PAV) (AASHTO R28).

Significant Results

Table E2a.1 shows the types of modifiers and grades included in the materials database.

Table E2a.1. Types of modifiers and grades received from participating manufacturers.

Material #	Base	Modifier	Class of Modifier	Expected Grade
1	A	None	None	PG 64
2	A	Functionalized PE	Plastomer: Nonreactive	PG 70
3	A	Functionalized PE	Plastomer: Nonreactive	PG 76
4	A	SBS with cross-linking	Elastomer: Reactive	PG 70
5	A	SBS with cross-linking	Elastomer: Reactive	PG 76
6	B	None	None	PG 58
7	B	Terpolymer	Elastomer: Reactive	PG 64
8	B	Terpolymer	Elastomer: Reactive	PG 70
9	C	None	None	PG 58
10	C	PPA	Chemical: Reactive	PG 64
11	C	PPA+SBS+cross-linking	Elastomer: Reactive	PG 70
12	D	None	None	PG 58
13	D	Functionalized PE+SBS	Hybrid: Reactive	PG 64
14	D	Functionalized PE+SBS	Hybrid: Reactive	PG 70
15	E	None	None	PG 70
16	E	SBS with cross-linking	Elastomer: Reactive	PG 76
17	E	SBS with cross-linking	Elastomer: Reactive	PG 82

PE = polyethylene. SBS = styrene-butadiene-styrene. PPA = polyphosphoric acid.

A summary of the $G^*/\sin(\delta)$ and MSCR testing results collected during this quarter is presented in tables E2a.2 and E2a.3.

Table E2a.2. Typical results from DSR testing.

Base	Age	Sample	Temperature (°C)	$G^*/\sin\delta$ (kPa)
A0	OB	1	70	0.5862
			64	1.1563
			65.3	1
		2	70	0.55692
			64	1.1254
			65	1
		3	70	0.54561
			64	1.1053
			64.9	1
A3	OB	1	76	0.57253
			70	1.0461
			70.5	1
		2	76	0.55699
			70	1.036
			70.4	1
		3	76	0.62789
			70	1.1697
			71.5	1
B0	OB	1	64	0.53386
			58	1.077
			58.7	1
		2	64	0.54326
			58	1.0639
			58.6	1
		3	64	0.5247
			58	1.0342
			58.3	1
B1	OB	1	64	1.1263
			70	0.6323
			65.3	1
		2	64	1.0972
			70	0.61001
			65	1
		3	64	1.1841
			70	0.65291
			65.4	1
B2	OB	1	76	0.70549
			70	1.1604
			71.8	1
		2	76	0.71387
			70	1.1535
			71.8	1
		3	76	0.73497
			70	1.17
			72	1

OB = original binder.

Table E2a.3. Typical results from the MSCR test at grade temperature.

Base	Age	Sample	100 Pa Stress		3200 Pa Stress	
			Jnr	% Recovery	Jnr	% Recovery
A0	RTFO	1	2.801	3.520	3.055	1.033
		2	2.651	3.592	2.853	1.108
		3				
B0	RTFO	1	2.686	4.330	2.966	1.210
		2	2.646	4.404	2.894	1.236
		3				
B1	RTFO	1	1.620	32.638	1.946	23.463
		2	1.559	32.542	1.861	23.341
		3	1.569	32.556	1.879	23.414
B2	RTFO	1	0.938	53.209	0.899	51.878
		2	0.989	52.879	0.945	51.659
		3	0.978	53.036	0.940	51.604
C0	RTFO	1	2.830	3.979	3.073	1.090
		2	2.820	4.113	3.090	1.061
		3	2.892	3.923	3.160	1.028
C1	RTFO	1	2.859	9.109	3.466	1.824
		2	2.898	9.103	3.523	1.786
		3	2.774	9.193	3.353	1.830
C2	RTFO	1	0.814	51.828	0.921	44.961
		2	0.784	52.114	0.902	44.784
		3	0.816	51.928	0.931	44.638
D0	RTFO	1	2.102	6.208	2.344	1.944
		2	2.201	6.049	2.428	1.890
		3	2.089	6.172		

Jnr = nonrecoverable creep compliance.

From these preliminary results, very different responses can be clearly observed from the materials tests based on composition, type and level of modification, and base binder. When more data are collected, the research team will be able to better understand how different modification techniques influence the behavior of asphalt binders, and how different modifiers improve different properties from the large spectrum of asphalt binder requirements.

The MSCR test results offer a very good indication of a material's resistance to rutting, as well as good insight into the elastic properties of the binders tested. This type of information, coupled with information collected from fatigue-type tests and direct elastic recovery measurements, will enable the research team to understand the connection, if any, between elasticity and fatigue life of binders.

The research team expresses its gratitude to those who have pledged their support for this work element and looks forward to their continued involvement.

Significant Problems, Issues and Potential Impact on Progress

None.

Work Planned Next Quarter

Next quarter, the research team will continue aging and testing materials included in the database.

Work element E2b: Design System for HMA Containing a High Percentage of RAP Material (UNR)

Work Done This Quarter

This work element is a joint project between University of Nevada, Reno and University of Wisconsin–Madison. The testing and analysis procedure finalized in the previous quarter was used for testing different types of recycled asphalt pavement (RAP) and binder materials. The analysis spreadsheet was further modified to provide estimates of stiffness and m-value of the binder in the RAP rather than only the allowable percentage of RAP in the mix.

The research team also focused on developing testing protocols for measuring the intermediate- and high-temperature properties of the RAP binder using the Dynamic Shear Rheometer (DSR). Initial testing started, and preliminary results are promising.

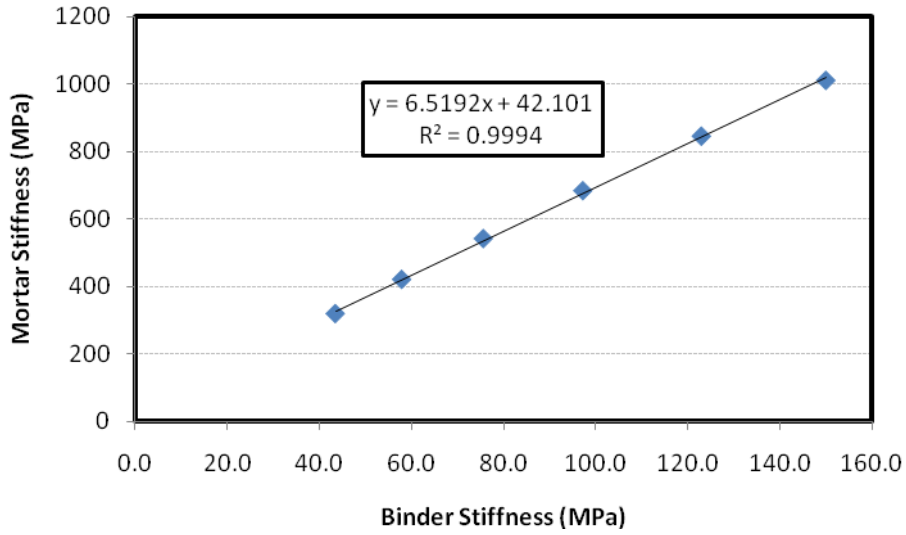
Significant Results

Low-Temperature Testing and Analysis Procedure

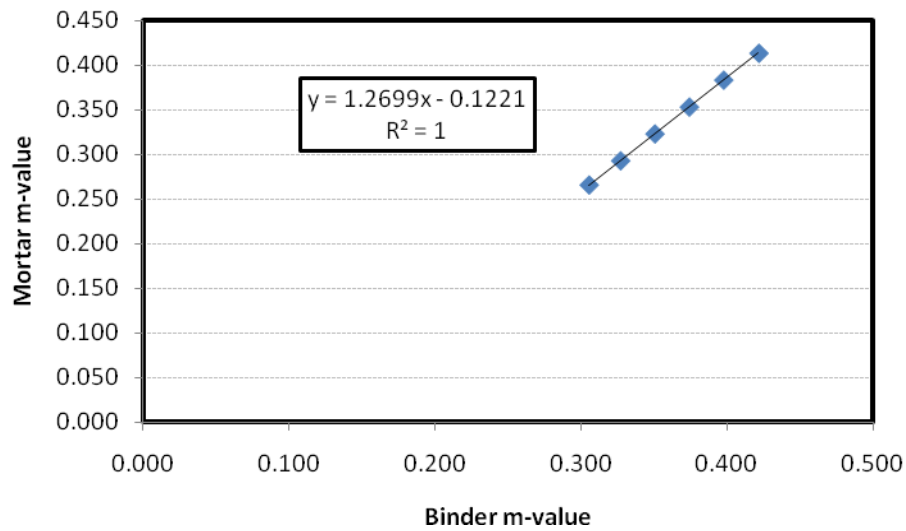
Evaluation of the testing and analysis procedure developed for measuring the low-temperature properties of binder in RAP materials, which was finalized in the previous quarter, continued throughout this quarter. Several tests were conducted on a wide variety of RAP materials. No issues or concerns arose during sample preparation or the testing procedure. The analysis procedure was modified to accommodate estimation of stiffness and m-value for the binder in the RAP. This analysis was incorporated in the spreadsheet using the steps described below.

The first step is to correlate the binder properties to the mortar properties using pressure aging vessel (PAV) binder and PAV RAP (PRAP) mortar, which includes RAP aggregates mixed with PAV binder. This correlation reflects the effect of RAP aggregate on the low-temperature properties of the binder. Figure E2b.1 shows an example of such a correlation for both stiffness and m-value. In the second step, the selective RAP (SRAP) mortar properties, which are measured by testing the RAP mixed with fresh binder, are used to estimate the properties of the RAP-aged binder blended with the fresh binder using the correlations determined from Step 1. Based on the percentage of RAP binder in the SRAP mortar, the aged binder properties in the RAP can be estimated by extrapolating from the known fresh binder properties and the blended

binder properties determined in Step 2. Figure E2b.2 shows the extrapolation for stiffness and m-value.

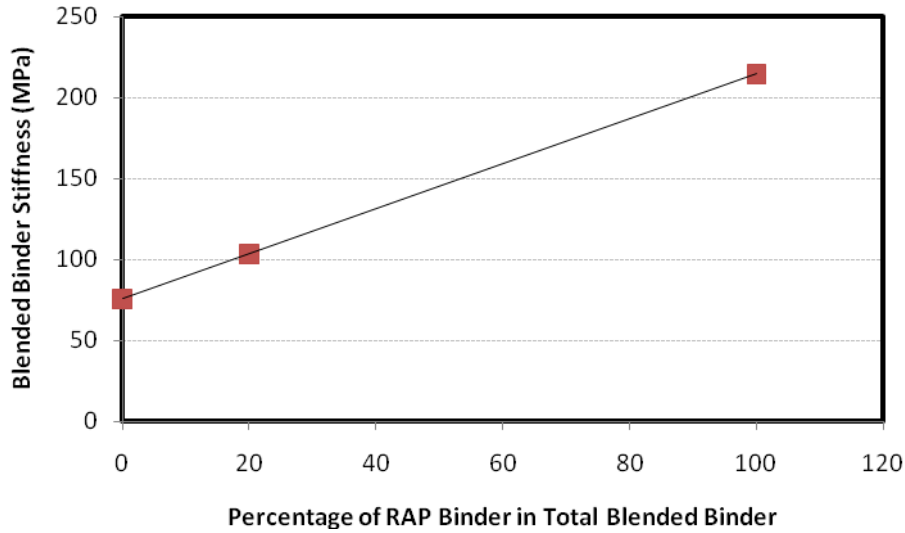


(a)

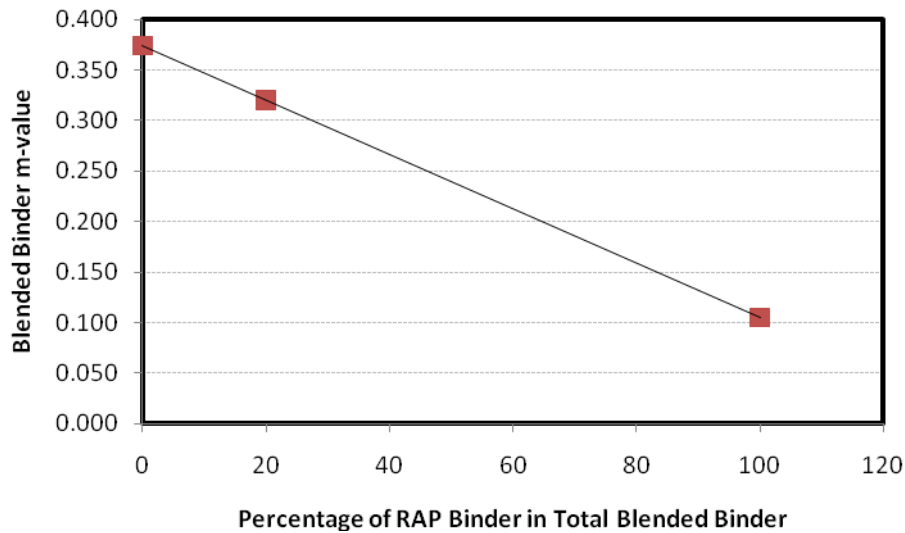


(b)

Figure E2b.1. Graphs. Mortar-binder relationship: (a) stiffness; (b) m-value.



(a)



(b)

Figure E2b.2. Graphs. RAP binder properties by extrapolation: (a) stiffness; (b) m-value.

Intermediate- and High-Temperature Testing and Analysis Procedure

To determine the intermediate- and high-temperature properties of RAP binder, the research team decided to start testing samples in the DSR following the same testing/analysis methodology developed for low-temperature properties. Thus far, one type of RAP material has been tested. The test procedure and material preparation did not indicate any issues or concerns. However, more testing of different materials is needed to identify limitations and recommend the appropriate range for parameters such as testing frequency, testing temperature, sample size modification, if necessary, and percent of RAP binder in the total binder.

Significant Problems, Issues and Potential Impact on Progress

None.

Work Planned Next Quarter

Next quarter, the research team will focus on developing the testing and analysis protocol for intermediate- and high-temperature properties. Spreadsheets will be developed to carry out the analysis procedure. Results of the analysis will include the RAP binder properties and the allowable RAP percentages in asphalt mixes without affecting the fresh binder grading at intermediate and low temperatures.

Work element E2c: Critically Designed HMA Mixtures (UNR)

Work Done This Quarter

Work continued to evaluate the applicability of the recommended deviator and confining stresses for the flow number test. The repeated load flow number testing was performed for the laboratory produced PG64-22 mixture. The flow number was evaluated at three air voids levels: 7, 4, and 2%.

Significant Results

The FN test was conducted for 20,000 cycles using the determined stress conditions at selected temperatures and under a moving truck at 40 mph. At each temperature, the corresponding deviator and confining stresses were determined using the developed equations. The equations require the knowledge of the stiffness of the mix at 2 inches below the pavement surface. Hence, a series of dynamic modulus ($|E^*|$) tests were conducted on the PG64-22 mix at the target air void levels (i.e. 7, 4, and 2%) and the variations of $|E^*|$ were estimated at each of these temperatures using the master curve and shift factors. A loading frequency of 30 Hz was used to determine the representative dynamic moduli values at these temperatures. The loading frequency was selected from the analysis of the deviator stress pulse time at the corresponding temperature and vehicle speed. Using the determined $|E^*|$ along with the corresponding temperature and the vehicle speed (40 mph), deviator and confining stresses were determined. Table E2c.1 summarizes the testing conditions for the PG64-22 mix at the various air voids level and temperatures. Overall, the deviator stress varied between 74 and 77 psi as a function of temperature while the confining stress varied between 40 and 59 psi as a function of temperature. At each air void level, the confining stress was found to decrease with the increase in temperature.

Two replicates were conducted at each temperature. The flow number was calculated using the three stage permanent deformation method (Zhou et al. 2004), the stepwise increase method (Goh and You 2008), and the Francken model (Biligiri et al. 2007). Table E2c.1 summarizes the test results for all three air void levels. Figure E2c.1 shows the flow number as a function of

temperature for all three air-void levels. The FN was found to be sensitive to the FN analysis method. Comparable results for the FN were found between the three-stage and the stepwise analysis methods. Overall the Francken model resulted in lower FN values when compared to the three-stage and stepwise approaches.

The PG64-22 mix at 7% air voids exhibited a tertiary stage at a temperature greater than 35°C. On the other hand, the PG64-22 mix at 4% and 2% air voids exhibited a tertiary stage at a temperature greater than 40°C. The data indicate the existence of a critical temperature between 35 and 40°C for the PG64-22 mix at 7% air voids and a critical temperature between 40 and 45°C for the PG64-22 mix at both 4% and 2% air voids. However the critical temperature of the PG64-22 mix at 2% air voids was observed at a higher number of load repetitions (i.e. FN) when compared to the critical temperature of the PG64-22 mix at 4% air voids.

Figure E2c.1 shows the flow number as a function of air-voids level at the various testing temperatures. The data shows an increase in the flow number with the decrease in air voids.

Table E2c.1 Flow number testing conditions and results.

Testing Temp (°C)	Dynamic Modulus (psi)	Deviator Stress (psi)	Confining Stress (psi)	Rep	Flow Number (3 Stage Approach)		Flow Number (Stepwise Increase)		Flow Number (Francken Model)	
					Results	Average	Results	Average	Results	Average
PG64-22 Mix at 7% Air Voids										
35	536,355	77	54	1	No FN*	No FN*	No FN*	No FN*	No FN*	No FN*
				2	No FN*		No FN*			
40	370,573	76	49	1	10,600	10,300	10,297	9,748	4,795	5,045
				2	9,999		9,198		5,295	
45	250,272	76	44	1	4,499	3,750	4,095	3,995	2,895	2,495
				2	3,000		3,895		2,095	
50	168,416	76	40	1	1,998	1,948	1,999	1,948	1,095	1,045
				2	1,897		1,896		995	
PG64-22 Mix at 4% Air Voids										
40	439,407	76	52	1	No FN*	No FN*	No FN*	No FN*	No FN*	No FN*
				2	No FN*		No FN*			
45	314,857	75	48	1	7,999	7,497	7,495	6,947	6,095	5,446
				2	6,995		6,398		4,795	
50	226,523	75	44	1	4,696	4,747	4,895	4,797	4,095	3,845
				2	4,798		4,699		3,595	
PG64-22 Mix at 2% Air Voids										
40	551,586	75	59	1	No FN*	No FN*	No FN*	No FN*	No FN*	No FN*
				2	No FN*		No FN*			
45	399,534	75	53	1	13,699	12,097	15,598	13,197	12820	13,148
				2	10,495		10,796		13477	
50	290,276	74	48	1	8,796	7,847	9,795	8,695	8,595	7,745
				2	6,897		7,595		6,895	

* A flow number was not found

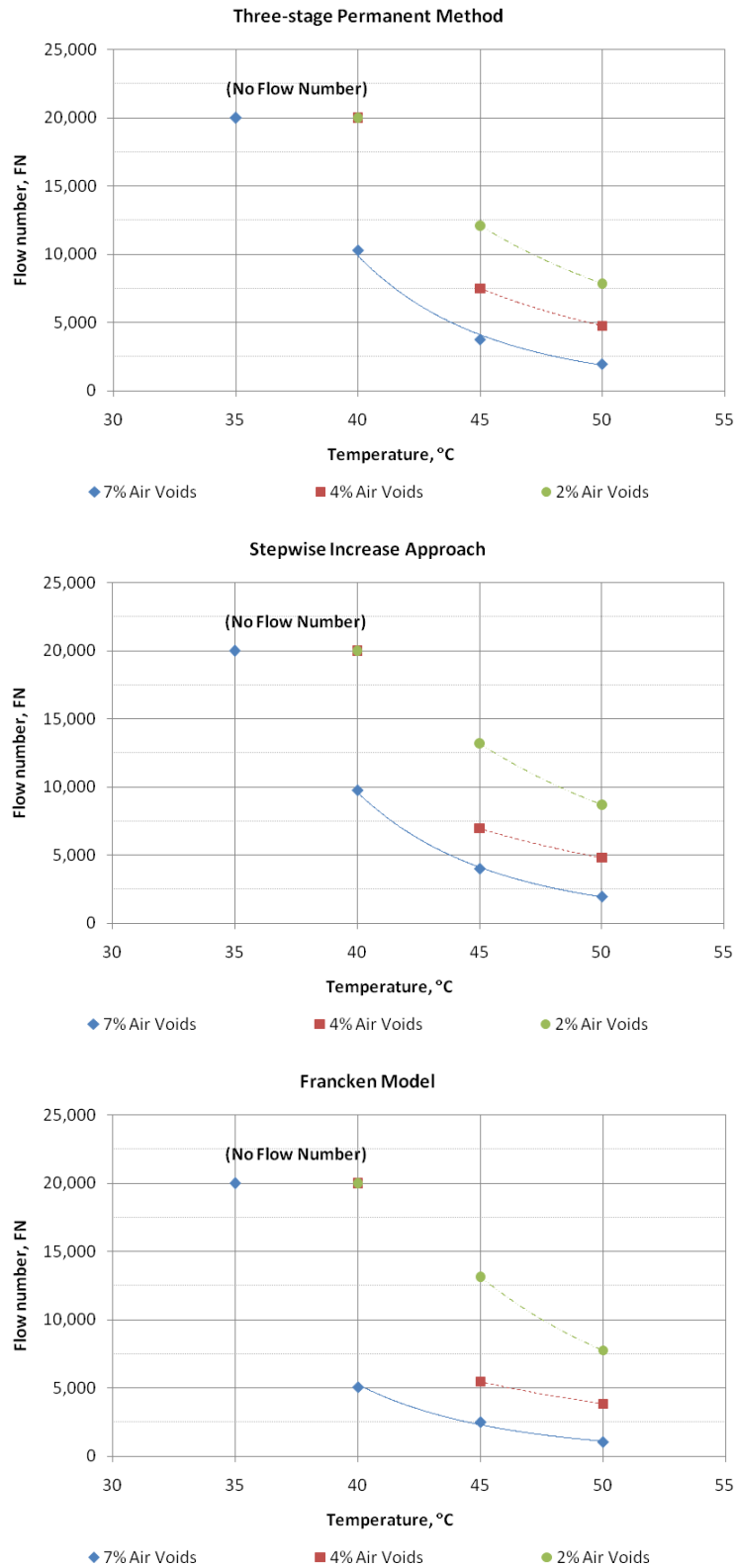


Figure E2c.1. Flow number versus temperature for 7, 4, and 2% air voids.

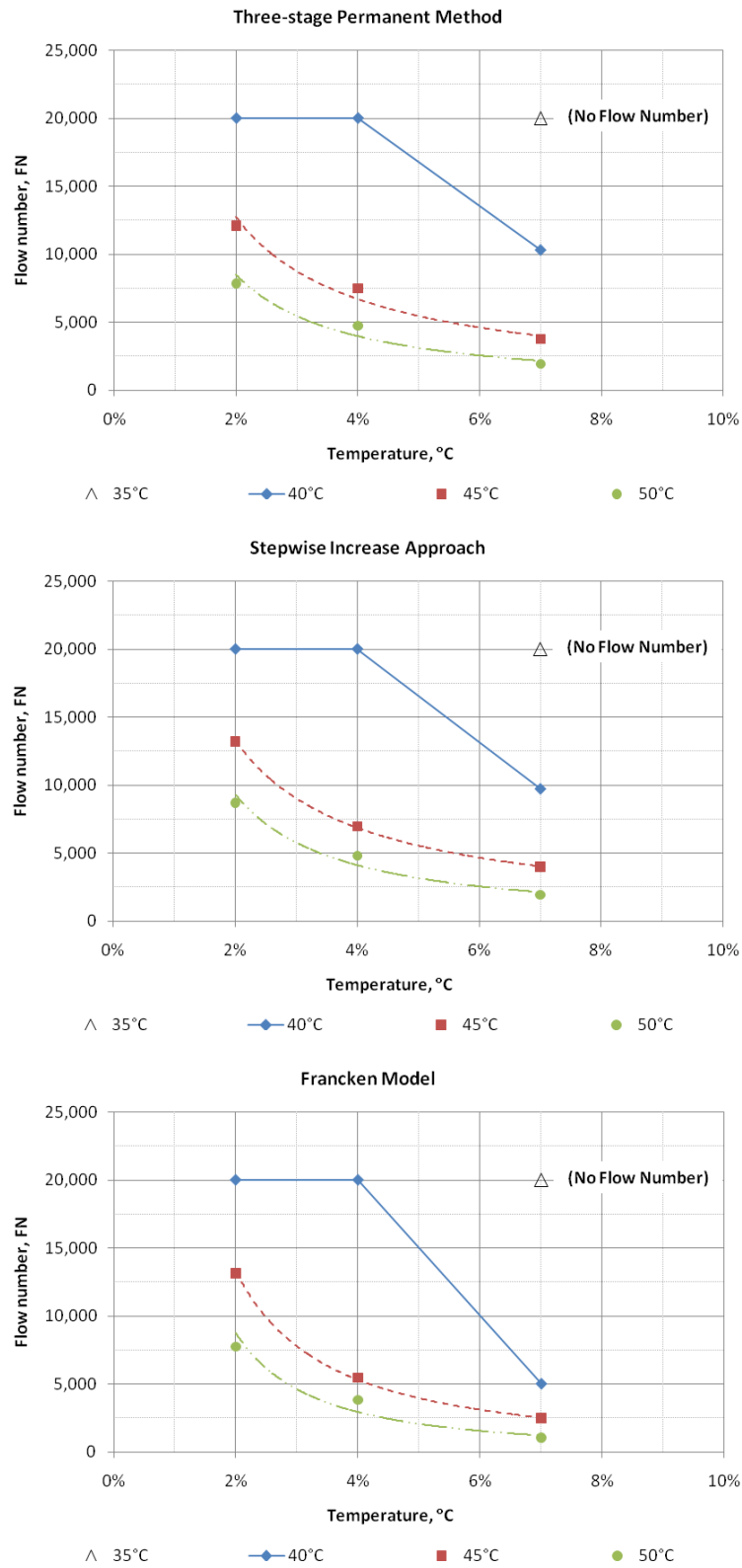


Figure E2c.2. Flow number versus air-void levels for different testing temperatures.

Significant Problems, Issues and Potential Impact on Progress

The 3D-Move runs are taking more time than what was anticipated because of limitations in the number of computers that can be used. Delay is expected to complete all the runs described in the experimental plan of this work element.

Work Planned for Next Quarter

The calculations of the 3D-Move model will continue to cover all the loading conditions that were described in the experimental plan for this work element.

Evaluate field mixtures with known rutting performance in the laboratory for permanent deformation characteristics under the repeated load triaxial test.

Cited References

Biligiri, K., K. Kaloush, M. Mamlouk, and M. Witzak, 2007, Rational Modeling of Tertiary Flow for Asphalt Mixtures. *Transportation Research Record*, TRB, Washington, D.C.

Goh, S.W., and Z. You., 2008, A Simple Method to Determine the Tertiary Flow in the Repeated Load Test. *Proc.*, Mid-Continent Transportation Research Forum, University of Wisconsin-Madison, Madison, Wisconsin.

Zhou, F., T. Scoullion, Pellinen, and L. Sun, 2004, Verification and Modeling of Three-stage Permanent Deformation Behavior of Asphalt Mixes. *Journal of Transportation Engineering*, ASCE.

Work element E2d: Thermal Cracking Resistant Mixes for Intermountain States (UNR & UWM)

Work Done This Quarter

This work element is a joint project between University of Nevada Reno and University of Wisconsin–Madison. Efforts at UNR this quarter include parts of Subtask E2d-1, “Identify Field Sections,” and Subtask E2d-3, “Identify an Evaluation and Testing System.” These are described below.

The UNR team has been writing a draft report summarizing the work completed under Subtask E2d-1 that is related to the analyses of the air and pavement temperature profiles data from the LTPP Seasonal Monitoring Program (SMP) and Westrack pavement sections. The draft report was supposed to be submitted for review by the end of this quarter but the analysis included a significant amount of figures that delayed the completion of the report until the next quarter.

The long-term oven aging process continued for the binders as described in the experimental plan for this work element. Table E2d.1 shows the work progress for the binder aging. Additionally, the completed aged binders are under testing for their rheological properties.

Table E2d.1. Binder aging matrix.

Aging Temp (°C)	Aging Period Unit	Aging Period	Binder Grade/Type				
			PG64-22	PG64-28NV	PG64-22 +10%Lime	PG64-22 +20%Lime	PG64-22+3% SBS
135	hours	8	AC	AC	AC	AC	AC
		15	AC	AC	AC	AC	AC
		30	AC	AC	AC	AC	AC
		44	AC	AC	AC	AC	AC
100	hours	44	AC	AC	AC	AC	AC
		90	AC	AC	AC	AC	AC
		150	AC	AC	AC	AC	AC
		240	AC	AC	AC	AC	AC
85	days	7.5	AC	AC	AC	AC	AC
		15	AC	AC	AC	AC	AC
		25	AC	AC	AC	AC	AC
		40	AC	AC	AC	AC	AC
60	days	30	AC	AC			
		60	AC	AC			
		100	AC	AC			
		160	AC	AC			
50	days	60	AC	AC			
		120	AC	AC			
		200	AC	AC			
		320	AC	AC			
AC =	Aging Completed						

The experimental plan to evaluate the impact of aggregate absorption and aggregate gradation on the long-term aging properties of the binder in the HMA mix is undergoing. Current progress of the aggregate absorption portion of this subtask was focused around developing mix designs for the materials recently received (California and WesTrack). Significant progress was continued in sample production and aging. The entire E* samples for two sources (Nevada and Colorado) have been prepared and are currently in the aging process (3, 6, and 9 months). The unaged and some 3 months aged E* samples have been tested and are ready for the binder extraction process (wrapped in plastic and are in the freezer). Some of the binder extraction process has just recently begun. The material from California has been received and is in the mix design process.

Thus all the aggregate sources have been received for both tasks (Aggregate, Absorbition and Mix Characteristics).

Further progress has been made in the E*-tension area, however final results and methods are still not yet determined. Contrary to last quarter, it does appear that full E*-tension master curves may be possible. New research by Luo and Lytton of TAMU (ASCE 2009) suggests that E* curves may be developed by a greatly simplified procedure. It is too early to determine if this method can in fact be conducted on the equipment at UNR, however exploration is underway.

Similar to the aggregate absorption subtask, this mixture characteristics subtask has seen significant progress in the area of sample preparation and E* testing. Currently Nevada, Utah, and about half of WesTrack have been prepared and are in the aging process for both intermediate (coarse for WesTrack) and Fine gradations at all applicable air void levels (4, 7, and 11%). Similar to the aggregate absorption subtask, progress in the completion of E* testing includes unaged and some of the 3 month samples.

Efforts at UW–Madison this quarter include parts of Subtask E2d-2, “Identify the Causes of the Thermal Cracking,” and Subtask E2d-3, “Identify an Evaluation and Testing System.” The work performed on each device for thermal-cracking characterization is described below.

Glass Transition Temperature (T_g) Binder

Improvements to the dilatometric testing system for binders were performed in this quarter. The software and data acquisition system for the T_g machine are working properly. All software issues known to date were addressed and solved. Alcohol leaking in the dilatometric chambers was eliminated. However, the influence of the contraction properties of the Buna rubber o-ring used for sealing the top and bottom of the chamber can represent a potential problem during the analysis of the thermo-volumetric binder data, as observed in figure E2d.1. The calibration curve for the dilatometric cell shows a bilinear dependency with temperature.

Harder o-rings were used to remove the bilinear trend from the calibration curve of the cell. Figure E2d.2 shows the results from calibration tests using aluminum specimens after one and two cycles of thermal loading. The observed calibration curve for the hard o-ring is linear. However, leaking was observed when two cycles were used. Further, closing the cells with this type of o-ring was difficult to perform.

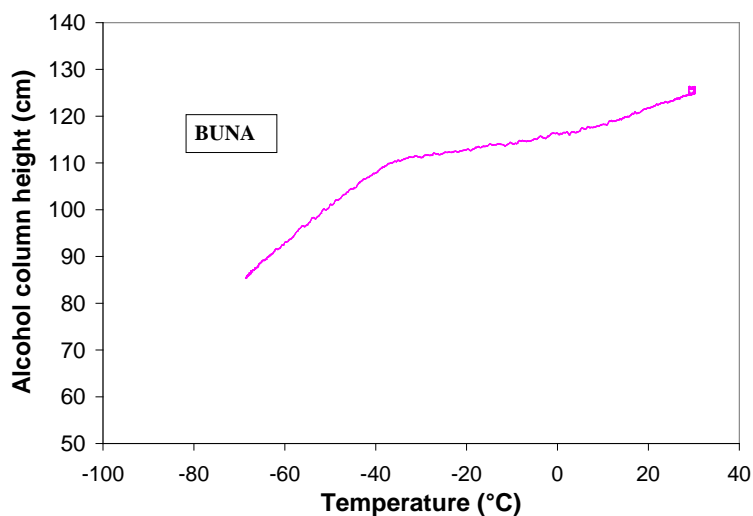


Figure E2d.1. Graph. T_g calibration with Buna o-ring.

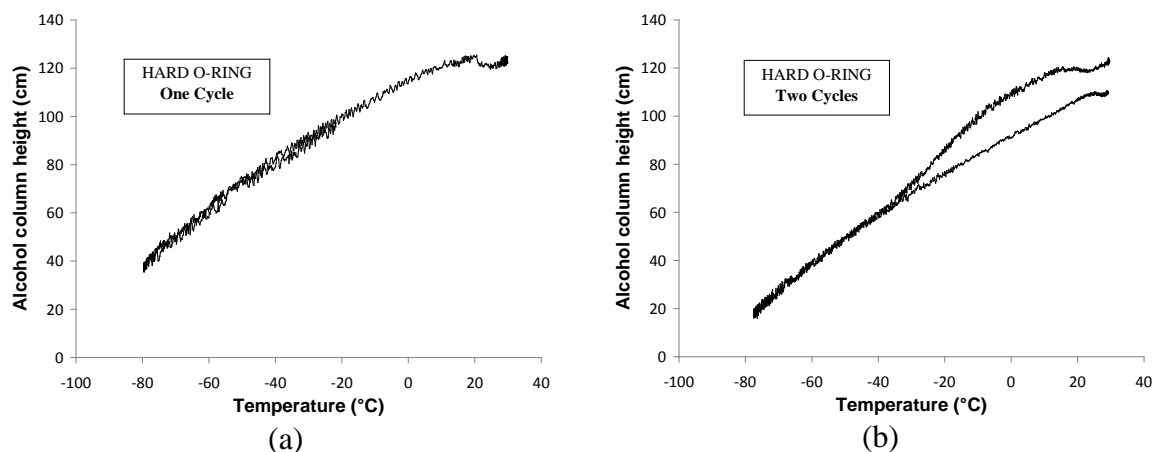
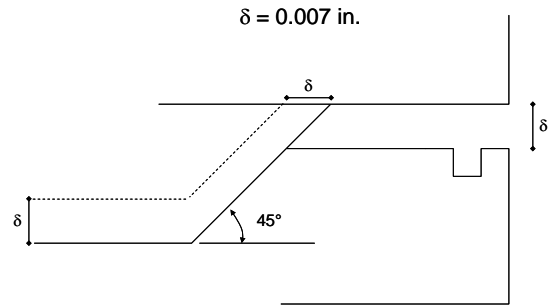
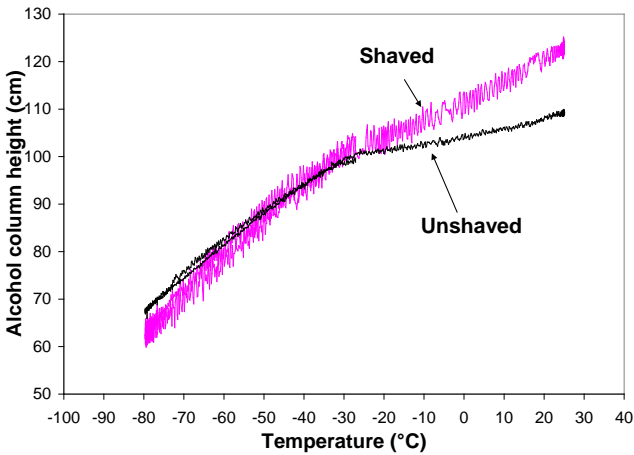


Figure E2d.2. Graphs. T_g calibration with hard o-ring: (a) after one cycle; (b) after two cycles.

Another approach taken by the research team was to change the geometry of the top part of the dilatometric cell, as reflected in figure E2d.3(b), so that the deformation of the rubber o-ring during testing is reduced. Figure E2d.3(a) shows that the calibration curve for the modified cell tends to be a single line. A problem with this approach is that the amount of alcohol is increased. The capillary tubes used in the T_g system are expensive and have a height limitation due to bending. More alcohol in the system implies taller capillary tubes; therefore, the amount of alcohol is restricted by the current height of capillary tubes.



(a)

(b)

Figure E2d.3. Graph and Illustration. Calibration of dilatometric cells: (a) before and after removing material in cell; (b) schematic of material removed.

A simple one-dimensional numerical model was built to understand the influence of the o-ring deformation on the thermo-volumetric response of the system and to determine if the response observed in figure E2d.3 represents the physical experiment or the results of operator and device errors. The dilatometric cell is treated as a one-dimensional system made of two components in a series: alcohol and rubber. The material is subjected to a reduction of temperature with time, as shown in figure E2d.4.

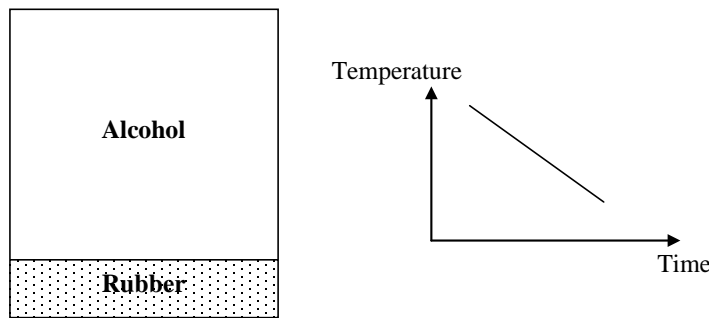


Figure E2d.4. Illustration. Simplified one-dimensional model of dilatometric cell.

A simple linear thermo-volumetric relation is assumed for both alcohol and rubber:

$$\frac{\Delta V}{V_0} = \alpha \Delta T \quad (\text{E2d.1})$$

The volume of the cell can be calculated by

$$V_{system}(T) = V_0 - \Delta V_{alcohol} + \Delta V_{rubber} \quad (E2d.2)$$

The volume of the cell (system) can be calculated by replacing equation E2d.1 in equation E2d.2:

$$V_{system}(T) = V_0 - \alpha_{alcohol}(T - T_0)V_{0_alcohol} + \alpha_{rubber}(T - T_0)V_{0_rubber} \quad (E2d.3)$$

Equation E2d.3 can be used to simulate volume changes of the dilatometric cell as a function of temperature. Typical values for the coefficient of thermal contraction of alcohol and rubber are used for the simulation values presented in figure E2d.5.

The modeled results have similar trends in comparison to the experimental results shown in figure E2d.5. This observation indicates the important effect that the o-ring has in the dilatometric cell response to temperature changes.

Based on these observations and analyses, the dilatometric cells were redesigned to minimize the effect of the rubber o-ring on the thermal response of the system. The new design is shown in figure E2d.6. Dilatometric testing with the new cell will be performed next quarter.

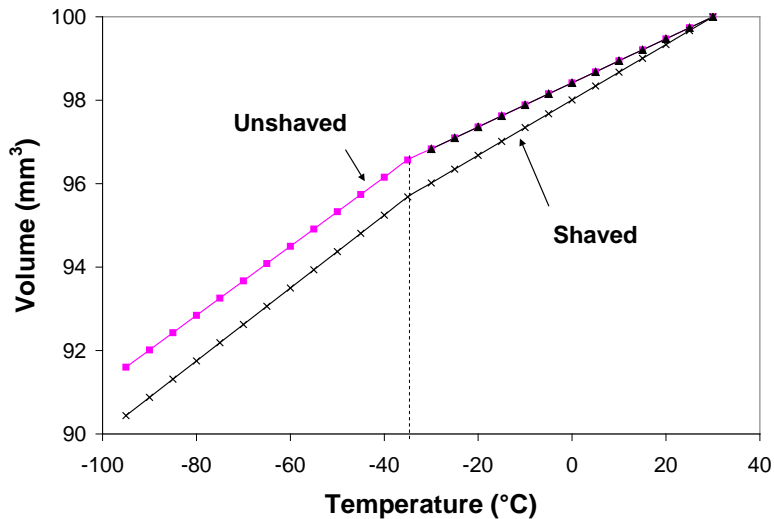


Figure E2d.5. Graph. Results from simulation of thermal contraction of cells.



Figure E2d.6. Photographs. New dilatometric cell for T_g testing of binders.

T_g Mixtures

A new procedure for testing the thermal expansion and contraction coefficients for asphalt mixtures was implemented. The goal is to obtain mixture samples from cores extracted from gyratory-compacted cylinders. These cores will be glued in a single specimen for T_g testing. The main concern of this approach is the use of an epoxy that may affect the measured coefficient of thermal contraction/expansion and the T_g .

To determine the influence of the epoxy on the response of the sample in the T_g test, a beam sample of $65 \times 65 \times 375$ mm was tested first and then cut into three pieces, glued together and retested, as shown in figure E2d.7.



Figure E2d.7. Photograph. T_g mixture sample after gluing.

Figure E2d.8 shows that no significant differences are observed between the thermal response of the asphalt mixture before and after gluing. This result is encouraging, but further testing on cylindrical specimens extracted from gyratory-compacted samples needs to be performed.

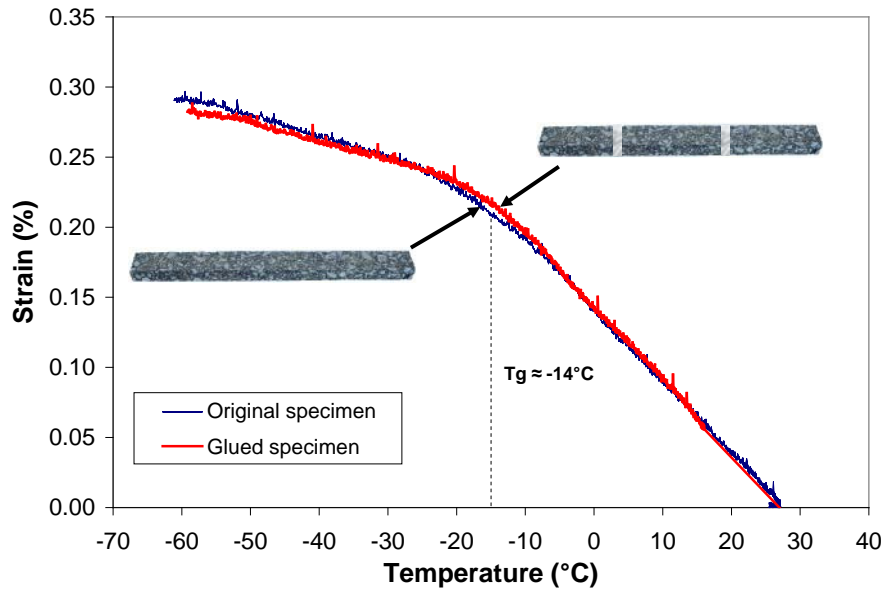


Figure E2d.8. Graph. T_g mixture results for unglued and glued specimens.

Single-Edge Notched Bending (SENB)

The torque of the step motor of the SENB device was increased by changing some configuration parameters. The difficulty in maintaining the displacement rate observed in previous quarters was solved with these changes. Figure E2d.9 shows SENB results of a PG 64-22 binder tested at -6°C before and after changes of the torque configuration. Smoother load-displacement curves are obtained with the new configuration of the step motor.

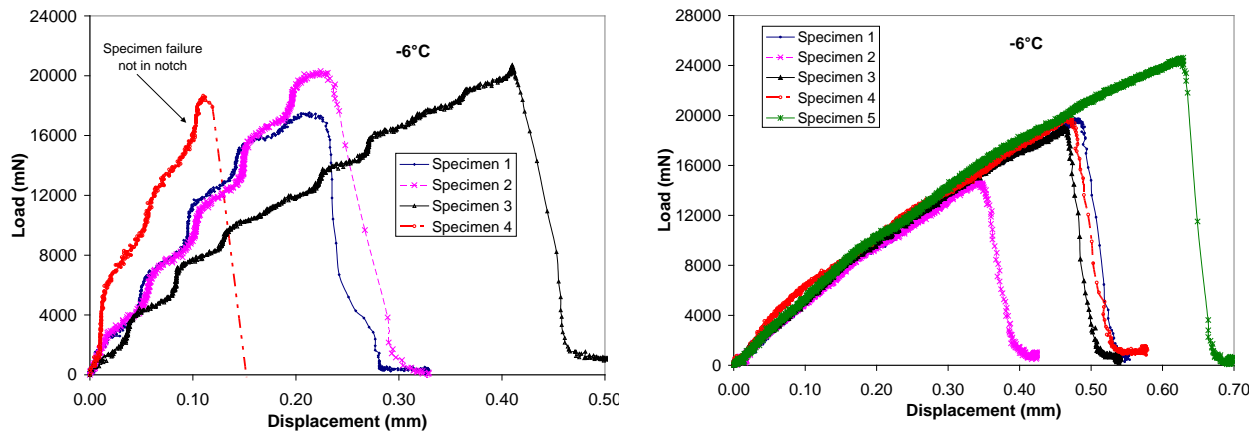


Figure E2d.9. Graphs. Asphalt binder SENB test results for two configurations of step motor.

Figure E2d.10 shows that the applied displacement rate is constant throughout the binder SENB tests with the new configuration.

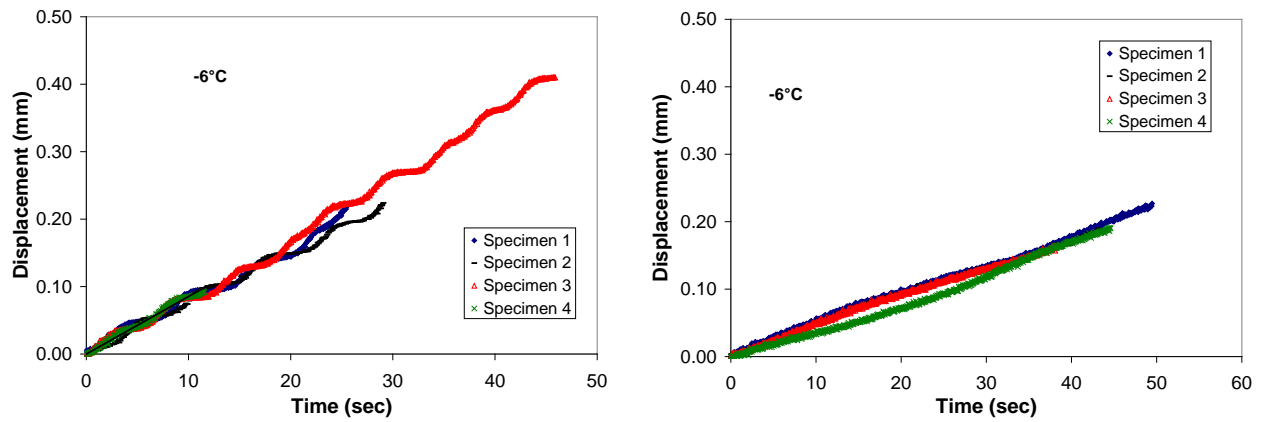


Figure E2d.10. Graphs. Displacement history of binder specimens tested in SENB with two configurations of the step motor.

There is reasonably good repeatability of the SENB test results for binders. For the majority of the tests, failure of the specimens happened at the notch, as shown in figure E2d.11.

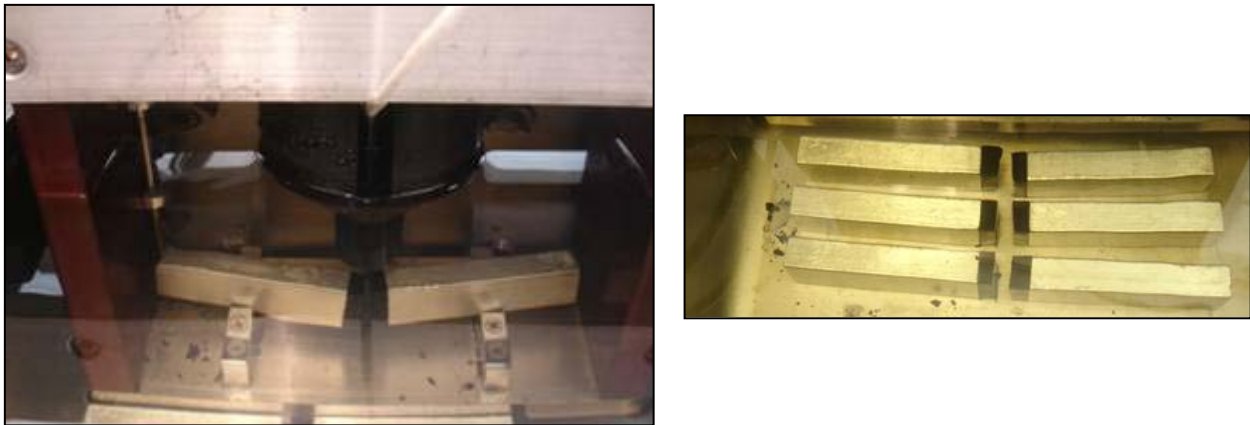


Figure E2d.11. Photographs. SENB samples after testing.

Significant Results

A new SENB testing system with an independent cooling bath is nearly completed, as shown in figure E2d.12. The SENB system was successfully implemented for testing fracture properties of asphalt binders. The ductile-to-brittle transition behavior of asphalt binders at low temperatures can be detected with the new SENB system, which is shown in figure E2d.13. A PG 64-22 binder was tested at three temperatures (-6 °C, -12 °C and -18 °C). It was observed how the

ductility of the binder was significantly reduced from the test at -6°C to the test at -18°C . Further work needs to be conducted to improve the testing system for mastics. Currently, the step motor used does not provide enough torque to maintain a constant displacement rate. Therefore, a change in the geometry of mastic samples to produce more compliant specimens will be investigated.

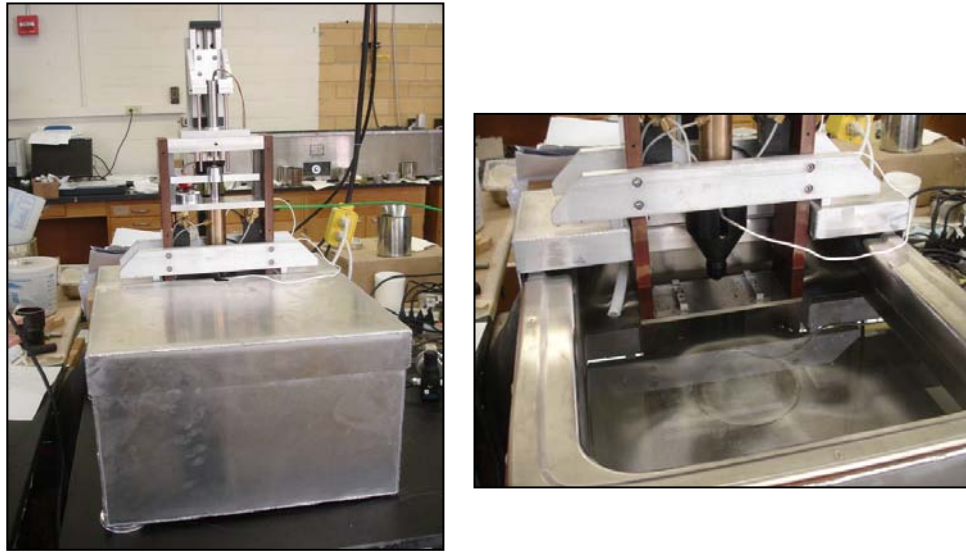


Figure E2d.12. Photographs. SENB testing system.

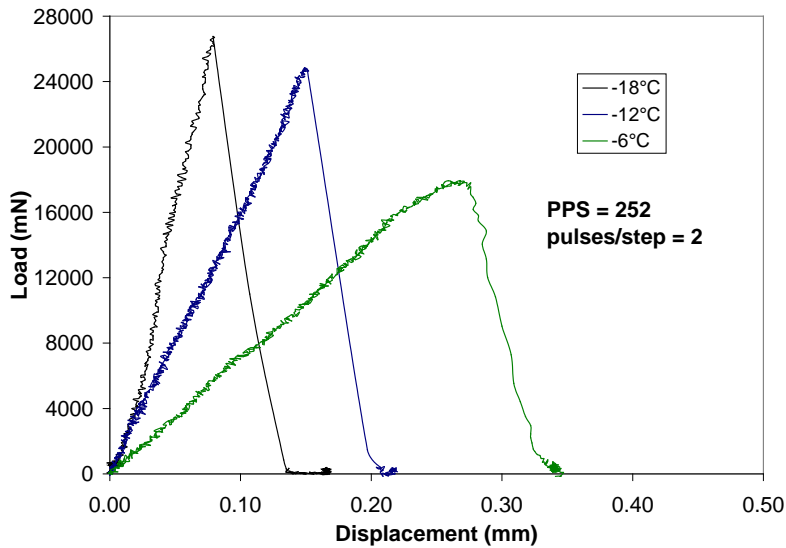


Figure E2d.13. Graph. SENB testing of asphalt binder PG 64-22 at three temperatures. (PPS = pulses per second.)

Preliminary results, shown in figure E2d.14, indicate that the SENB system can be used to run fracture tests of asphalt mixtures at low temperatures. Asphalt mixtures prepared with granite and limestone were successfully tested with the system. Specimens were obtained by cutting Bending Beam Rheometer (BBR)-size specimens from slab-compacted samples.

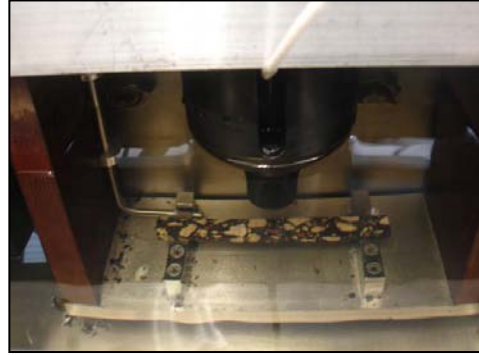
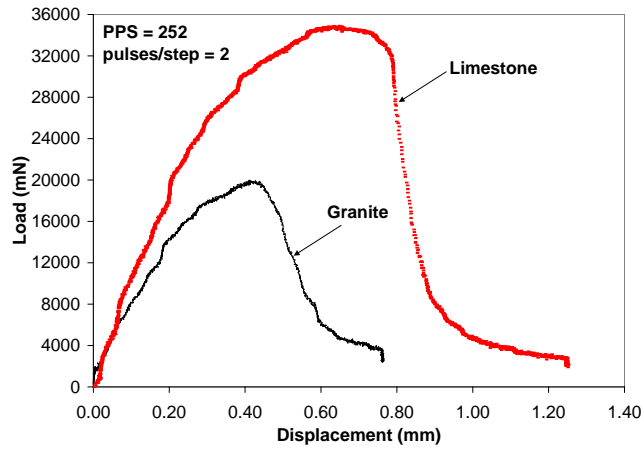


Figure E2d.14. Graph and Photograph. (a) SENB test for two asphalt mixtures; (b) limestone asphalt mixture in SENB device.

Based on preliminary results, the approach of gluing asphalt mixture specimens to measure T_g and coefficient of linear expansion/contraction is promising. Further testing needs to be performed to validate this methodology.

Significant Problems, Issues and Potential Impact on Progress

Completion of the experimental plan for T_g of binders is expected to be delayed due to delays in delivery of the newly designed dilatometric cell.

For the SENB device, results to date show strong potential of the system. The research team was able to establish the appropriate system control parameters to eliminate problems previously noted in binders. The next step is to run SENB with larger, more compliant mastic beams. The current configuration of the SENB system presents some internal friction in the loading shaft. This problem will be corrected by improving the alignment of system components.

To reflect the actual progress of this research, the Gantt chart has been updated to show the planned draft report deliverable for subtask E2d-1 will be delivered in November 2009 instead of September 2009. Additionally, the Gantt chart has been updated to show the planned Journal Paper deliverable for subtask E2d-3 will be delivered in March 2010 instead of August 2009.

Work Planned Next Quarter

Continue the aging process of binders and continue measuring the properties of the aged binders.

Continue the work on the impact of aggregate absorption and gradation on the aging of the asphalt binder.

The research team plans to begin and complete the testing matrix for the T_g and thermal expansion/contraction of both binders and mixtures. Adjustments to the SENB procedure will be made to run tests on mastic specimens. The team also plans to start implementing the Thermal Stress Restrained Specimen Test (TSRST) system for characterization of asphalt mixtures. Preliminary testing using the TSRST is planned next quarter, and the methodology of using glued specimens of asphalt mixtures for T_g testing will be further investigated.

Work element E2e: Design Guidance for Fatigue and Rut Resistance Mixtures (AAT)

Work Done This Quarter

Dr. Christensen gave a presentation at the P3 symposium in Laramie in July. The title of the talk was “Accounting for Age Hardening and Climate Variability in Field Studies of Rutting in HMA Pavements.” This presentation dealt with how to address age hardening and climate variability when calibrating rutting models using field data. More specifically it described in detail how these issues were accounted for when developing the resistivity/rutting model which is being further refined as part of this work element.

Also during the past quarter Dr. Christensen further refined the reduced loading cycles/endurance limit approach to continuum damage fatigue analysis (CD-RC/EL). The improved model now addressing damage tolerance—that is, the amount of damage that an HMA mixture can sustain before localization occurs. This improvement was based on data collected during NCHRP Projects 9-25/31 that had not been previously analyzed in detail. The damage ratio at localization for a large number of mixes was tabulated and analyzed statistically and graphically and a model developed for predicting damage tolerance as a function of modulus. This model was then incorporated into the more general CD-RC/EL model. A preliminary simple means for incorporating healing into the model was also developed although at this time there is no data for calibrating the healing model.

A useful feature of the CD-RC/EL approach to fatigue analysis is that it can be used to develop relatively simple fatigue damage functions that can easily be incorporated into existing layered elastic analysis (LEA) pavement design programs to provide improved prediction of fatigue performance. Although this is only an approximate approach and is not nearly as rigorous as finite element analysis, it has the advantage that it can be quickly implemented as represents a useful interim step between existing pavement design approaches and rigorous finite element analysis incorporating continuum damage concepts. During the past quarter, Dr. Christensen developed such a damage function which is based on the CD-RC/EL model, including damage tolerance and healing. Dr. Nelson Gibson of the Federal Highway Administration (FHWA) has

forwarded to Dr. Christensen a copy of the Excel Spreadsheet EVERSTRESS, which is an LEA pavement design and analysis program implemented as a spreadsheet. The spreadsheet was developed by Dr. Nadarajah Sivaneswaran, also of the FHWA. It should be possible to incorporate the CD-RC/EL damage function into EVERSTRESS and develop plots showing damage evolution in HMA pavements as predicted using this simplified continuum damage approach.

Dr. Christensen, along with other ARC researchers Y. Richard Kim, Dallas Little, Eyad Masad and Yong-Rak Kim, wrote a white paper on continuum damage analysis for presentation at the San Antonio Models Expert Task Group (ETG) meeting in September. The title of the paper is “Practical Approaches to Continuum Damage Fatigue Analysis.” Dr. Christensen attended the ETG meeting to participate in the discussion of this white paper and the possibility of a continuum damage workshop to be held in the spring of 2010. It appeared that the ETG felt additional work was needed prior to holding such a workshop. Dr. Bonaquist participated in the Mixtures and Construction ETG meeting also held in San Antonio in September.

Significant Results

A comprehensive CD-RC/EL model was developed. A damage function was developed based on this model that can be easily implemented in LEA pavement design software was developed.

Significant Problems, Issues and Potential Impact on Progress

None.

Work Planned Next Quarter

As experimental data is gathered in laboratory fatigue testing, the CD-RC/EL model will be evaluated and refined as needed. The CD-RC/EL damage function will be put into EVERSTRESS and plots of damage evolution for typical HMA pavement structures developed to determine if this approach produces reasonable results.

Engineered Materials Year 3	Year 3 (4/2009-3/2010)												Team
	4	5	6	7	8	9	10	11	12	1	2	3	
(1) High Performance Asphalt Materials													
E1a: Analytical and Micro-mechanics Models for Mechanical behavior of mixtures													TAMU
E1a-1: Analytical Micromechanical Models of Binder Properties												JP	
E1a-2: Analytical Micromechanical Models of Modified Mastic Systems													
E1a-3: Analytical Models of Mechanical Properties of Asphalt Mixtures			JP	P	JP(2)				P(2)			M&A	
E1a-4: Analytical Model of Asphalt Mixture Response and Damage				P	JP(2)				P(3)				
E1b: Binder Damage Resistance Characterization													UWM
E1b-1: Rutting of Asphalt Binders													
E1b-1-1: Literature review													
E1b-1-2: Select Materials & Develop Work Plan													
E1b-1-3: Conduct Testing					JP						P		
E1b-1-4: Analysis & Interpretation					JP						F		
E1b-1-5: Standard Testing Procedure and Recommendation for Specifications													
E1b-2: Feasibility of determining rheological and fracture properties of asphalt binders and mastics using simple indentation tests (modified title)													UWM
E1b-2i: Literature Review													
E1b-2ii: Proposed SuperPave testing modifications							P						
E1b-2iii: Preliminary testing and correlation of results										D			
E1b-2iv: Feasibility of using indentation tests for fracture and rheological properties										D	P	JP	
E2a: Comparison of Modification Techniques													UWM
E2a-1: Identify modification targets and material suppliers					DP								
E2a-2: Test material properties												P	
E2a-3: Develop model to estimate level of modification needed and cost index													
E2a-4: Write asphalt modification guideline/report on modifier impact over binder properties													
E2c: Critically Designed HMA Mixtures													UNR
E2c-1: Identify the Critical Conditions					JP			D				F	
E2c-2: Conduct Mixtures Evaluations												D	
E2c-3: Develop a Simple Test													
E2c-4: Develop Standard Test Procedure													
E2c-5: Evaluate the Impact of Mix Characteristics													
E2d: Thermal Cracking Resistant Mixes for Intermountain States													UWMUNR
E2d-1: Identify Field Sections									D				
E2d-2: Identify the Causes of the Thermal Cracking													
E2d-3: Identify an Evaluation and Testing System	DP	D						DP		D		JP	
E2d-4: Modeling and Validation of the Developed System													
E2d-5: Develop a Standard													
E2e: Design Guidance for Fatigue and Rut Resistance Mixtures													AAT
E2e-1: Identify Model Improvements													
E2e-2: Design and Execute Laboratory Testing Program											P		
E2e-3: Perform Engineering and Statistical Analysis to Refine Models													
E2e-4: Validate Refined Models													
E2e-5: Prepare Design Guidance													
(2) Green Asphalt Materials													
E2b: Design System for HMA Containing a High Percentage of RAP Material													UNR
E2b-1: Develop a System to Evaluate the Properties of RAP Materials	D				JP				F	P			
E2b-2: Compatibility of RAP and Virgin Binders											D		
E2b-3: Develop a Mix Design Procedure													
E2b-4: Impact of RAP Materials on Performance of Mixtures													
E2b-5: Field Trials													
E1c: Warm and Cold Mixes													UWM
E1c-1: Warm Mixes													
E1c-1-i: Effects of Warm Mix Additives on Rheological Properties of Binders													
E1c-1-ii: Effects of Warm Mix Additives on Mixture Workability and Stability						JP					P	DP	
E1c-1-iii: Mixture Performance Testing													
E1c-1-iv: Develop Revised Mix Design Procedures													
E1c-1-v: Field Evaluation of Mix Design Procedures and Performance Recommendations													
E1c-2: Improvement of Emulsions' Characterization and Mixture Design for Cold Bitumen Applications													UWMUNR
E1c-2-i: Review of Literature and Standards	D1						D3						
E1c-2-ii: Creation of Advisory Group													
E1c-2-iii: Identify Tests and Develop Experimental Plan	D1									D5			
E1c-2-iv: Develop Material Library and Collect Materials													
E1c-2-v: Conduct Testing Plan						JP			D4		P		
E1c-2-vi: Develop Performance Selection Guidelines													
E1c-2-vii: Validate Performance Guidelines						D2							
E1c-2-viii: Develop CMA Mix Design Guidelines													
E1c-2-ix: Develop CMA Performance Guidelines													

Deliverable codes
D: Draft Report
F: Final Report
M&A: Model and algorithm
SW: Software
JP: Journal paper
P: Presentation
DP: Decision Point

Deliverable Description
Report delivered to FHWA for 3 week review period.
Final report delivered in compliance with FHWA publication standards
Mathematical model and sample code
Executable software, code and user manual
Paper submitted to conference or journal
Presentation for symposium, conference or other
Time to make a decision on two parallel paths as to which is most promising to follow through

Work planned
Work completed
Parallel topic

Engineered Materials Year 2 - 5	Year 2 (4/08-3/09)				Year 3 (4/09-3/10)				Year 4 (04/10-03/11)				Year 5 (04/11-03/12)				Team
	Q1	Q2	Q3	Q4	Q1	Q2	Q3	Q4	Q1	Q2	Q3	Q4	Q1	Q2	Q3	Q4	
(1) High Performance Asphalt Materials																	
E1a: Analytical and Micro-mechanics Models for Mechanical behavior of mixtures																	TAMU
E1a-1: Analytical Micromechanical Models of Binder Properties				P, JP	JP	P	P	JP	M&A	D	F, SW						
E1a-2: Analytical Micromechanical Models of Modified Mastic Systems				P, JP	JP	P	P		M&A	JP	D	F, SW					
E1a-3: Analytical Models of Mechanical Properties of Asphalt Mixtures	P	P, JP		P, JP	JP	P	P	M&A		D	SW, JP	F					
E1a-4: Analytical Model of Asphalt Mixture Response and Damage				P, JP	JP	P	P		M&A	D	F, JP	SW					
E1b: Binder Damage Resistance Characterization																	UWM
E1b-1: Rutting of Asphalt Binders																	
E1b-1-1: Literature review																	
E1b1-2: Select Materials & Develop Work Plan	DP, P			P													
E1b1-3: Conduct Testing																	
E1b1-4: Analysis & Interpretation				JP	P		JP	P			JP						
E1b1-5: Standard Testing Procedure and Recommendation for Specifications										P		DP	P	D	JP	F	
E1b-2: Feasibility of Determining rheological and fracture properties of asphalt binders and mastics using simple indentation tests (modified title)																	
E1b-2i: Literature Review																	
E1b-2ii: Proposed SuperPave testing modifications or new testing devices							P										
E1b-2iii: Preliminary testing and correlation of results									D								
E1b-2iv: Feasibility of using indentation tests for fracture and rheological properties									D, P, JP		F						
E2a: Comparison of Modification Techniques																	UWM
E2a-1: Identify modification targets and material suppliers				DP			DP										
E2a-2: Test material properties									P								
E2a-3: Develop model to estimate level of modification needed and cost index																	
E2a-4: Write asphalt modification guideline/report on modifier impact over binder properties																	
E2c: Critically Designed HMA Mixtures																	UNR
E2c-1: Identify the Critical Conditions				JP		D, F		JP	D	F							
E2c-2: Conduct Mixtures Evaluations									D	D, F	JP						
E2c-3: Develop a Simple Test														D, F	JP		
E2c-4: Develop Standard Test Procedure														D, F			
E2c-5: Evaluate the Impact of Mix Characteristics																D, F	
E2d: Thermal Cracking Resistant Mixes for Intermountain States																	UWM/UNR
E2d-1: Identify Field Sections				D, F	D, F			D									
E2d-2: Identify the Causes of the Thermal Cracking					D					D, F	JP						
E2d-3: Identify an Evaluation and Testing System					DP	JP	DP, D						D, F	JP			
E2d-4: Modeling and Validation of the Developed System																D, F	
E2d-5: Develop a Standard																D, F	
E2e: Design Guidance for Fatigue and Rut Resistance Mixtures																	AAT
E2e-1: Identify Model Improvements									P								
E2e-2: Design and Execute Laboratory Testing Program																	
E2e-3: Perform Engineering and Statistical Analysis to Refine Models										JP		P, D, F					
E2e-4: Validate Refined Models														JP			
E2e-5: Prepare Design Guidance															M&A	P, D, F	
(2) Green Asphalt Materials																	
E2b: Design System for HMA Containing a High Percentage of RAP Material																	UNR
E2b-1: Develop a System to Evaluate the Properties of RAP Materials				JP		P	D	JP	F	P					D, F	JP	
E2b-2: Compatibility of RAP and Virgin Binders															D, F	JP	
E2b-3: Develop a Mix Design Procedure										D					D, F	JP	
E2b-4: Impact of RAP Materials on Performance of Mixtures																D, F	
E2b-5: Field Trials																D, F	
E1c: Warm and Cold Mixes																	UWM
E1c-1: Warm Mixes																	
E1c-1i: Effects of Warm Mix Additives on Rheological Properties of Binders																	
E1c-1ii: Effects of Warm Mix Additives on Mixture Workability and Stability				P	D	F, DP		JP									
E1c-1iii: Mixture Performance Testing										P, DP							
E1c-1iv: Develop Revised Mix Design Procedures											JP	P					
E1c-1v: Field Evaluation of Mix Design Procedures and Performance Recommendations														JP	D	P, F	
E1c-2: Improvement of Emulsions' Characterization and Mixture Design for Cold Bitumen Applications																	UWM
E1c-2i: Review of Literature and Standards				JP, P, D	F		D1	D3									
E1c-2ii: Creation of Advisory Group																	
E1c-2iii: Identify Tests and Develop Experimental Plan					P, DP		D1	D5									
E1c-2iv: Develop Material Library and Collect Materials																	
E1c-2v: Develop Testing Plan								JP	D4	P							
E1c-2vi: Develop Performance Selection Guidelines										JP	D	P, F					
E1c-2vii: Validate Guidelines								D2						JP	P		
E1c-2viii: Develop CMA Mix Design Procedure												P					
E1c-2ix: Develop CMA Performance Guidelines														JP	D	F	

Deliverable codes
D: Draft Report
F: Final Report
M&A: Model and algorithm
SW: Software
JP: Journal paper
P: Presentation
DP: Decision Point

Deliverable Description
Report delivered to FHWA for 3 week review period.
Final report delivered in compliance with FHWA publication standards
Mathematical model and sample code
Executable software, code and user manual
Paper submitted to conference or journal
Presentation for symposium, conference or other
Time to make a decision on two parallel paths as to which is most promising to follow through



PROGRAM AREA: VEHICLE-PAVEMENT INTERACTION

CATEGORY VP1: WORKSHOP

Work element VP1a: Workshop on Super-Single Tires

This work element is complete.

CATEGORY VP2: DESIGN GUIDANCE

Work element VP2a: Mixture Design to Enhance Safety and Reduce Noise of HMA (UWM)

Work Done This Quarter

Work focused on continuing the measurements of surface macrotexture and microtexture (friction properties) of laboratory-prepared gyratory specimens using the sand-patch method and the British Pendulum Skid Resistance Tester, respectively. Measurements were conducted for approximately 140 samples. The samples covered a wide range of mix variables, such as aggregate gradation, aggregate type, design equivalent single axle loads (ESALs), compaction pressure and compaction temperature. A parametric/statistical analysis to identify the relationship between asphalt surface properties and the different mix variables was completed.

A preliminary procedure for the abrasion/polishing of asphalt mix specimens using a circular rotating abrasion device was developed. Two new samples were tested in manner similar to the sample tested in the previous quarter.

Significant effort was put toward selecting an appropriate laser profilometer and noise absorption measuring device. Several samples were shipped to the University of Pisa for surface profile measurements and absorption coefficient as part of the collaboration between the University of Wisconsin–Madison and the asphalt research group at the University of Pisa.

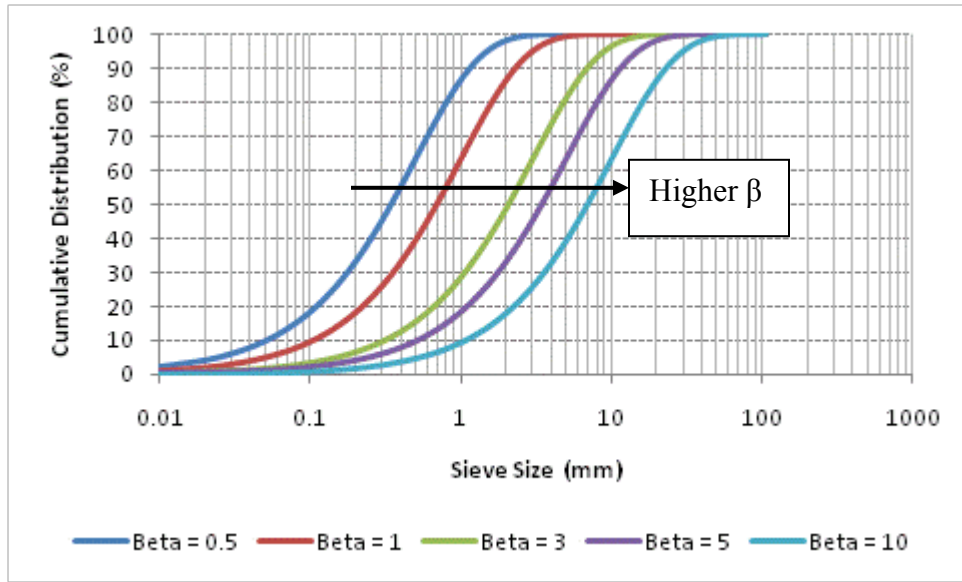
Significant Results

Macrotexture and Microtexture Correlations

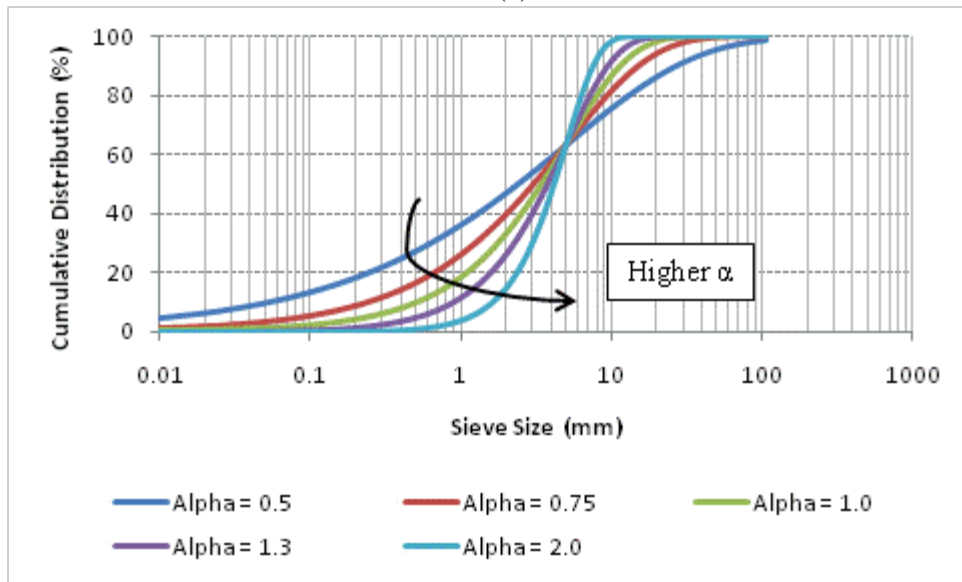
The asphalt mix sample measurements from the previous quarter, along with measurements conducted this quarter, were statistically analyzed to identify relationships between macrotexture and microtexture surface properties with the following mix and aggregate properties: fine aggregate angularity (FAA), percent crushed aggregates, flat-to-elongated ratio, gradation, air voids, compaction temperature and compaction pressure. The Weibull cumulative distribution function was used to fit the mix gradations. The function is expressed mathematically in equation VP2a.1 and has two parameters: α and β .

The behaviors of this function for different α and β values are shown in figure VP2a.1. Figure VP2a.1(a) shows the function plots for a constant value of α equal to 1 and variable values of β , while figure VP2a.1(b) shows the function plots for a constant β value of 5 and variable α values. The effect of changing the value of β shifts the gradation curve horizontally, and thus it represents the fineness, or coarseness, of the aggregate gradation. Higher β values indicate a coarser mix. On the other hand, the value of α defines the slope of the gradation curve, and thus it defines the density of the mix. For the mix gradations used in this study, the function was fitted to all the different gradations, and the obtained R^2 values were all equal to or higher than 0.95.

$$F(x, \alpha, \beta) = 1 - e^{-(x/\beta)^\alpha} \quad (\text{VP2a.1})$$



(a)



(b)

Figure VP2a.1. Graphs. Weibull function behavior for different α and β values (aggregate): (a) variable β values ($\alpha = 1$); (b) variable α values ($\beta = 5$).

The analysis was performed by sorting the data multiple times, with each time based on one of the factors listed above. For different ranges of the sorting factor, averages of the other factors were correlated with the mean texture depth (MTD) and British Pendulum Number (BPN) values. These averages are then used to investigate the effect of each of the aggregate or mixture compaction factors on the asphalt mix BPN and MTD values, as indicators of microtexture and macrotexture. Table VP2a.1 summarizes the factors that were found to significantly correlate ($R^2 > 0.60$) with each of the two properties; the R^2 values are shown in parentheses. The second

column in table VP2a.1 includes the number of levels for each sorting factor, and the center point of each level. Figures VP2a.2 and VP2a.3, respectively, show the macrotexture and microtexture properties correlation with the aggregate gradation.

Table VP2a.1. Significant factors affecting BPN and MTD measurements.

Sorting Factor	Levels Included in Analysis	Correlations with BPN	Correlations with MTD
Gradation	Six Levels: 3, 4, 5, 6, 7 and 8	None	Gradation (0.72) and Temperature (0.77)
FAA	Five Levels: 43, 44, 45, 46 and 47	Gradation Beta Index (0.83) and Superpave Flat and Elongated (0.67)	Gradation (0.95) and Temperature (0.80)
% Crushed Faces	Five Levels: 75, 80, 85, 90 and 95	Gradation Beta Index (0.64) and Pressure (0.88)	Gradation (0.85), Temperature (0.97) and Air Voids (0.61)
Flat/Elongated	Six Levels: 0.4, 1.1, 1.8, 2.5, 3.2 and 3.9	Gradation Beta Index (0.84), Pressure (0.92) and Temperature (0.63)	Gradation (0.93) and Temperature (0.77)

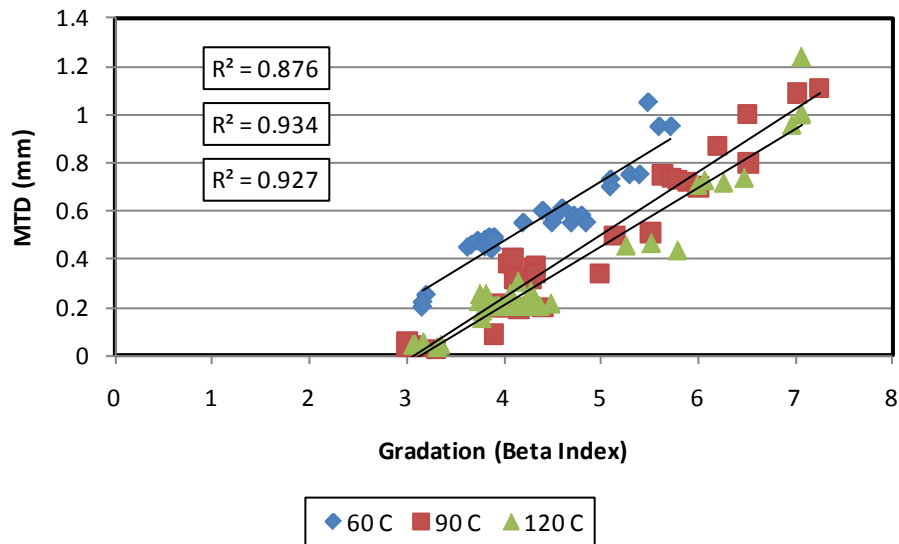


Figure VP2a.2. Graph. MTD correlation with gradation at different mixing temperatures.

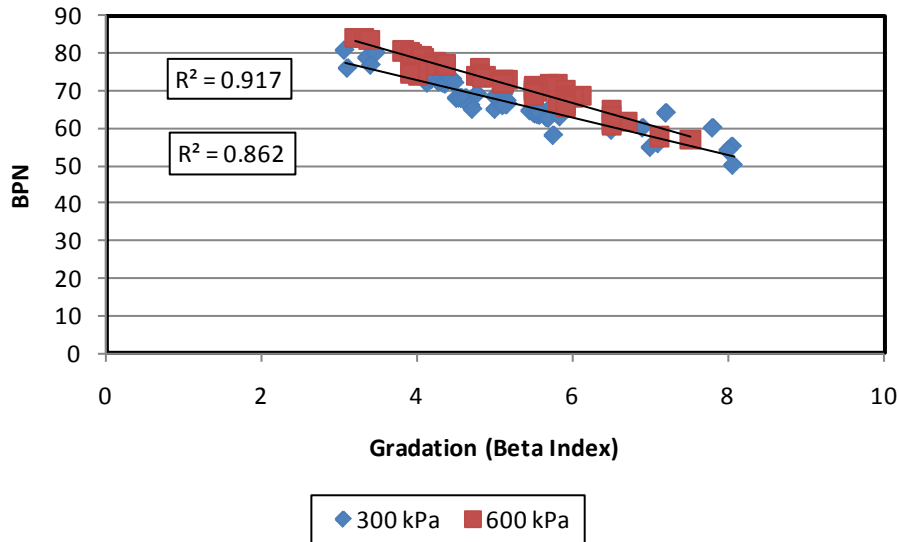


Figure VP2a.3. Graph. BPN correlation with gradation at different compaction levels.

The main findings from the analysis indicate that the newly developed protocol for measuring MTD and BPN is sensitive to aggregate and mixture properties, and there are statistically important correlations between the measured responses of mixture properties. This is encouraging, as it indicates the potential of the methods to be used as part of a mixture design process to estimate and control surface characteristics related to safety and friction of pavements.

Laboratory Polishing of Asphalt Mixes

Polishing of asphalt pavements due to traffic was simulated using an abrasive rotating disk applied on the surface of the gyratory samples. A commercially available abrasive rotating disk—3M Quick Change Disk No. 9140-9143—was used in this study. The disk was rotated at nominal constant rotation speed of 600 rpm using a No. 7144 Type 3 Black and Decker drill. The approach proposed for measuring the polishing of the samples is to measure the BPN before any polishing, then polish the sample for 9 minutes at 30-second intervals. The BPN is measured after each 30-second interval. Figure VP2a.4 shows the percent change in the BPN values with the polishing time for three samples selected to evaluate and develop this procedure. The two dashed lines are the 2% increase and decrease bounds for BPN values. As figure VP2a.4 shows, after about 6 minutes of polishing, all the changes are less than 2%. Polishing for 9 minutes is proposed as a sufficient time of polishing to reach a stable condition.

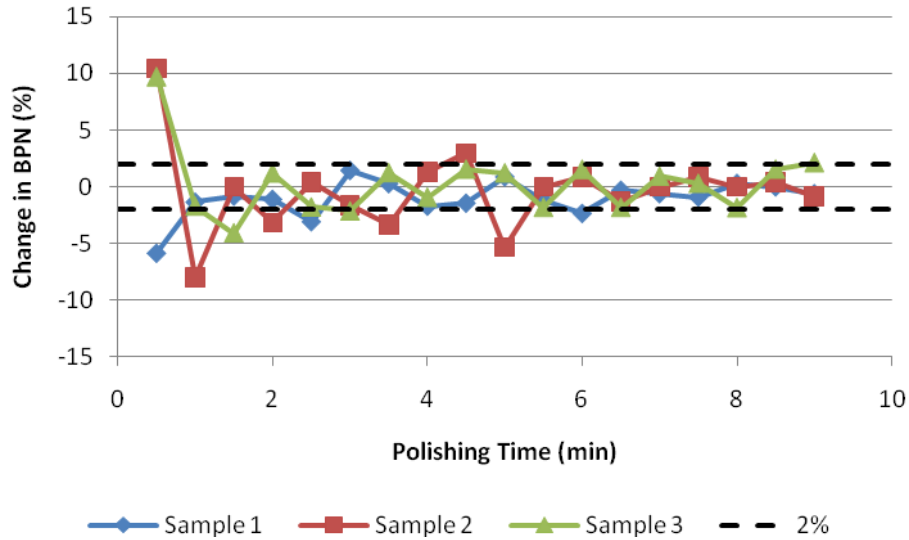


Figure VP2a.4. Graph. Percent change in BPN measurements as function of polishing time.

Laser Profilometer and Noise Absorption Measurement

The research team at UW–Madison initiated the process of purchasing a laser profilometer and an impedance tube for measuring the noise absorption of asphalt mixes. As part of a collaborative effort with Professor Massimo Losa of the University of Pisa, Italy, asphalt samples were shipped to Professor Losa’s lab for testing and evaluation of surface macrotexture using the laser profilometer and a noise absorption device using the impedance tube.

A presentation was given to the Modeling ETG during their September meeting to update the group on the research team’s activities. The research team will follow up on useful feedback received during that meeting. The first set of surface texture data as measured by the laser equipment at the labs of Professor Losa was received and analysis has started. The development of software to determine the texture spectrum is under way and active exchange of ideas is taking place between the research team and a few collaborators.

Significant Problems, Issues and Potential Impact on Progress

The waveguide sound absorption device developed at UW–Madison was a main concern during this quarter. Based on communication with Professor Losa, the research team decided to purchase a commercially available impedance tube, as the current device had a significant amount of noise in the data collected due to isolation issues.

To reflect the actual progress of this research, the Gantt chart has been updated to show the planned Model and Algorithm deliverable for subtask VP2a-4 will be delivered in March 2010 instead of September 2009.

Work Planned Next Quarter

Next quarter, the research team will focus on measuring the noise absorption properties and the surface macrotexture properties using the laser profilometer. Samples will be selected to cover a wide range of mix properties such as gradation and air voids. The research team will also review the literature and consult with the research group at the University of Pisa to decide if additional gradations should be considered.

Effort will also be directed to finalizing the polishing procedure for laboratory-compacted asphalt samples. Once the procedure is finalized, several samples will be polished to quantify their terminal friction properties.

CATEGORY VP3: MODELING

Work element VP3a: Pavement Response Model to Dynamic Loads (UNR)

Work Done This Quarter

Continued the work on the 3D-Move model to make it a menu-driven software to integrate the Non-Highway” vehicles in the 3D-Move model. Started the testing of the alpha-version of the 3D-Move model.

Significant Results

One of the important inputs to 3D-Move is the axle configuration and corresponding pavement contact stress distribution. Our recent work has focused on extending the application of 3D-Move to “Non-Highway” vehicles. The types of vehicles that have been included are: End Dump Truck, Fork Lift, Log Handler, Reach Stacker, Straddle Carrier, and Wheel Loader. For each of these vehicles, there are many options (or Product ID) and these vehicles are marketed by many different manufactures. The variable nature of these vehicle types and corresponding axle configurations requires that an innovative procedure be implemented to match the user’s design case under consideration. The procedures adopted in the software development are illustrated using windows presented below. For example, figure VP3a.1 shows that once the End Dump Truck and BELAZ have been selected as the Vehicle Type and Manufacturer, respectively, the available choices for Product ID along with a picture of the vehicle are displayed on right. In addition, a complete manufacturer’s specifications of the vehicle data can be viewed by clicking on “Table of Vehicle Specification” (see top right). For the vehicle selected, a sketch of the corresponding axle configuration along with the spacing will be displayed as shown. The subsequent input selection is “Tire Data,” which provides information on type of tire and contact area. The contact area is available from the manufacturer’s input, once the tire type is known. As shown in figure VP3a.1, once the option of GoodYear 33.00-51 is selected, the corresponding contact area of 0.6226 m² (from Manufacture’s specifications) is displayed directly below.

Option E : Special Non-Highway Vehicles

Vehicle Type <input type="checkbox"/> End Dump Truck <input type="checkbox"/> Fork Lift <input type="checkbox"/> Log Handler <input type="checkbox"/> Reach Stacker <input type="checkbox"/> Straddle Carrier <input type="checkbox"/> Wheel Loader	Manufacturer <input type="checkbox"/> BELAZ <input type="checkbox"/> Caterpillar <input type="checkbox"/> Komatsu <input type="checkbox"/> Terex <input type="checkbox"/> User Defined	Product ID <input type="checkbox"/> BELAZ-7513 Series <input type="checkbox"/> BELAZ-7530 Series <input type="checkbox"/> BELAZ-7540 Series <input type="checkbox"/> BELAZ-7547 Series <input type="checkbox"/> BELAZ-7555 Series (For User Defind Case , Enter ID here) <input type="text"/> <input type="button" value="Click for Table of Vehicle Specification"/>
--	--	---

Vehicle Configuration

Front Axle:
 Rear Axle:

L1: m
 S1: m

Tire data

Tire Type:
 Loaded Area: sq.m

Load Distribution

Front Tire Load (When Empty): kN
 Rear Tire Load (When Empty): kN
 Pay Load (Max Pay Load is 1275 kN): kN

	Front Axle	Rear Axle
Load Distribution As Percentage	<input type="text" value="33"/>	<input type="text" value="67"/>
Load Distribution as Load Value (kN)	<input type="text" value="676"/>	<input type="text" value="1374"/>


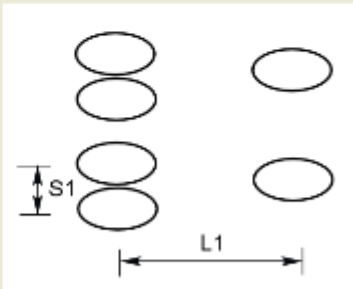



Figure VP3a.1. Main window for the input of data for non-highway vehicles

The next input information deals with Load Distribution. The load distribution to axles when empty is again extracted from the manufacturer's specification. The user can change these default empty tire loads and is prompted to specify a Pay Load. An additional control on the tire load distribution is provided through the use of the Load Distribution option. This option provides an opportunity to assign the loads carried by the tires. For the example, the case shown in figure VP3a.1, the total gross load of the vehicle is the sum of the front axle (267 kN/tire) load, rear axle load (129 kN/tire), and pay load, giving a grand total of 2050 kN. This total

vehicle load is then distributed to Front and Rear Axle according the specified distribution rate of 33% and 67%, respectively. The final Load Distribution to the axles calculated according to these input is provided at the bottom of the window.

The next step is to select the contact stress distributions under the tires (figure VP3a.2). This undertaking requires initially inputting a choice for the axle for analysis and then providing information for friction coefficient (needed for contact shear stress distribution) and shape of the loaded area. From the tire load and contact area assigned in figure VP3a.1, the contact pressure is determined internally and is displayed near the middle of the window. The sizing for the contact area, depending on the shape selected from the bottom of the window, is calculated internally along with the entire contact stress distribution for the axle (one side of axle). This stress distribution is assigned to the 3D-Move model.

The screenshot shows a software window titled "Option E : Special Non-Highway Vehicles". The window contains several input fields and sections:

- Axle to be Analyzed:** A dropdown menu set to "Rear Axle".
- Type of Vehicle:** A text box containing "End Dump Truck".
- Manufacturer:** A text box containing "BELAZ".
- Tire Type:** A text box containing "Goodyear 33.00-51".
- Tire Load:** A text box containing "343" with "kN" to its right.
- Friction Coefficient:** A section with two radio buttons: "Bracking Friction" (selected) with a value of "0.5" in a text box, and "Rolling Friction" with an empty text box.
- Uniform Contact Pressure Distribution:** A section with a "Tire Pressure" text box containing "551" and "kPa" to its right.
- Geometry of Loaded Area:** A section with three radio buttons: "Circle" (selected), "Ellipse", and "Rectangle". To the right is a diagram of a circle with a radius line labeled "R". Further right is the formula:
$$R = \sqrt{\frac{\text{Tire Load}}{\pi \times (\text{Tire Pressure})}}$$
 Below the formula is a "Calculated R" text box containing "0.44513" and "m" to its right.

At the bottom of the window are four buttons: "Back", "Next", "Cancel" (with a red X icon), and "OK" (with a green checkmark icon).

Figure VP3a.2. Input of friction and shape of contact area.

In addition, to provide flexibility to the users, a choice of Tire Type other than those specified by the manufacturer is also allowed. For example, as in figure VP3a.3 if the option “Other” is selected, this option unlike the previous case requires the input of area of contact. The user-defined contact area can be specified using the text box found directly below.

The alpha version of 3D-Move model is under testing at UNR. The 3D-Move model is being tested under a variety of loading conditions and material properties.

Option E : Special Non-Highway Vehicles

Vehicle Type End Dump Truck Fork Lift Log Handler Reach Stackler Straddle Carrier Wheel Loader	Manufacturer BELAZ Caterpillar Komatsu Terex User Defined	Product ID BELAZ-7513 Series BELAZ-7530 Series BELAZ-7540 Series BELAZ-7547 Series BELAZ-7555 Series	(For User Defind Case , Enter ID here) <input type="text"/> <input type="button" value="Click for Table of Vehicle Specification"/>
---	---	--	--

Vehicle Configuration

Front Axle: Single Axle - Single Tire

Rear Axle: Single Axle - Dual Tire

L1: 5.30 m

S1: 1.42 m

Tire data

Tire Type: Other

Loaded Area: sq.m


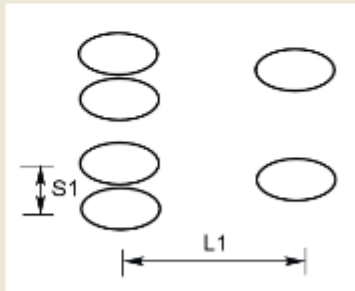
Load Distribution

Front Tire Load (When Empty): 267 kN

Rear Tire Load (When Empty): 129 kN

Pay Load (Max Pay Load is 1275 kN): 1000 kN

Load Distribution As Percentage	Front Axle: 33	Rear Axle: 67
Load Distribution as Load Value (kN)	676	1374

Back Next

Figure VP3a.3 Flexibility of assigning user-defined tire type

Significant Problems, Issues and Potential Impact on Progress

There has been a short unexpected delay in the development of the windows for Non-Highway Vehicles. This was mainly caused by the time consuming effort needed in the assembling of the manufacturer's specifications and software development associated with the data generation for contact stress distribution for any-shape loaded area.

Bugs were encountered during the testing of the 3D-Move alpha version which delayed the release of the beta-version of 3D-move.

To reflect the actual progress of this research, the Gantt chart has been updated to show the planned beta version deliverable for subtask VP3a-3 will be delivered in January 2009 instead of September 2009.

Work Planned Next Quarter

Continue working on the 3D-Move model to make it a menu-driven software. Evaluate the beta version for 3D-Move.

Vehicle-Pavement Interaction Year 3	Year 3 (4/2009-3/2010)												Team	
	4	5	6	7	8	9	10	11	12	1	2	3		
(1) Workshop														
VP1a: Workshop on Super-Single Tires														UNR
(2) Design Guidance														
VP2a: Mixture Design to Enhance Safety and Reduce Noise of HMA														UWM
VP2a-1: Evaluate common physical and mechanical properties of asphalt mixtures with enhanced frictional skid characteristics														
VP2a-2: Evaluate pavement macro- and micro-textures and their relation to tire and pavement noise-generation mechanisms														
VP2a-3: Develop a laboratory testing protocol for the rapid evaluation of the macro and micro-texture of pavements														
VP2a-4: Run parametric studies on tire-pavement noise and skid response					JP									M&A,D
VP2a-5: Establish collaboration with established national and international laboratories specialized in transportation noise measurements. Gather expertise on measurements and analysis														
VP2a-6: Model and correlate acoustic response of tested tire-pavement systems														
VP2a-7: Proposed optimal guideline for design to include noise reduction, durability, safety and costs														
(3) Pavement Response Model Based on Dynamic Analyses														
VP3a: Pavement Response Model to Dynamic Loads														UNR
VP3a-1: Dynamic Loads														
VP3a-2: Stress Distribution at the Tire-Pavement Interface														
VP3a-3: Pavement Response Model								SW, v, β						
VP3a-4: Overall Model														

Deliverable codes

- D: Draft Report
- F: Final Report
- M&A: Model and algorithm
- SW: Software
- JP: Journal paper
- P: Presentation
- DP: Decision Point

Deliverable Description

- Report delivered to FHWA for 3 week review period.
- Final report delivered in compliance with FHWA publication standards
- Mathematical model and sample code
- Executable software, code and user manual
- Paper submitted to conference or journal
- Presentation for symposium, conference or other
- Time to make a decision on two parallel paths as to which is most promising to follow through

 Work planned
 Work completed
 Parallel topic

Vehicle-Pavement Interaction Years 2 - 5	Year 2 (4/08-3/09)				Year 3 (4/09-3/10)				Year 4 (04/10-03/11)				Year 5 (04/11-03/12)				Team
	Q1	Q2	Q3	Q4	Q1	Q2	Q3	Q4	Q1	Q2	Q3	Q4	Q1	Q2	Q3	Q4	
(1) Workshop																	
VP1a: Workshop on Super-Single Tires																	UNR
(2) Design Guidance																	
VP2a: Mixture Design to Enhance Safety and Reduce Noise of HMA																	UWM
VP2a-1: Evaluate common physical and mechanical properties of asphalt mixtures with enhanced frictional skid characteristics				DP													
VP2a-2: Evaluate pavement macro- and micro-textures and their relation to tire and pavement noise-generation mechanisms				DP													
VP2a-3: Develop a laboratory testing protocol for the rapid evaluation of the macro and micro-texture of pavements		M&A		P													
VP2a-4: Run parametric studies on tire-pavement noise and skid response			JP			JP		M&A, D									
VP2a-5: Establish collaboration with established national laboratories specialized in transportation noise measurements. Gather expertise on measurements and analysis																	
VP2a-6: Model and correlate acoustic response of tested tire-pavement systems									JP	D	F						
VP2a-7: Proposed optimal guideline for design to include noise reduction, durability, safety and costs										D	P, F						
(3) Pavement Response Model Based on Dynamic Analyses																	
VP3a: Pavement Response Model to Dynamic Loads																	UNR
VP3a-1: Dynamic Loads			JP							D, F	JP						
VP3a-2: Stress Distribution at the Tire-Pavement Interface										D, F	JP						
VP3a-3: Pavement Response Model						SW, v. 6							SW, JP				
VP3a-4: Overall Model													D	F			

Deliverable codes

D: Draft Report
F: Final Report
M&A: Model and algorithm
SW: Software
JP: Journal paper
P: Presentation
DP: Decision Point

Deliverable Description

Report delivered to FHWA for 3 week review period.
Final report delivered in compliance with FHWA publication standards
Mathematical model and sample code
Executable software, code and user manual
Paper submitted to conference or journal
Presentation for symposium, conference or other
Time to make a decision on two parallel paths as to which is most promising to follow through



PROGRAM AREA: VALIDATION

CATEGORY V1: FIELD VALIDATION

Work element V1a: Use and Monitoring of Warm Mix Asphalt Sections (Year 1 start)

Work Done This Quarter

The Yellowstone National Park warm-mix and control hot-mix sections were monitored in late August. As occurred last year, the Park Service allowed the acquisition of small samples of pavement that were obtained by using a ½ inch masonry drill bit. The pavement samples were obtained from the shoulder of the pavement near the beginning of each of the nine monitoring sections. The nine monitoring sections are comprised of three from each of the three materials, control hot-mix, Advera additive, and Sasobit additive. The small samples obtained are for assessment of the aging that has occurred in the pavement. These samples are unconventional in the sense that they are not typical 4 or 6-inch pavement cores, however, the research team at WRI is investigating if accurate aging data can be obtained from small samples. If this is successful, it will be a very rapid and inexpensive method to obtain samples from in service pavements for assessing aging, both near the surface and with depth.

There was no distress noted in any of the monitoring sections which is what was expected of pavement sections that have been in service for only two years.

Significant Results

None.

Significant Problems, Issues and Potential Impact on Progress

None.

Work Planned Next Quarter

No work planned.

Work element V1b: Construction and Monitoring of additional Comparative Pavement Validation sites (Year 1 start)

Work Done This Quarter

A journal paper was prepared and submitted to Road Materials and Pavement Design for possible acceptance to the European Asphalt Technology Association meeting in Parma, Italy in June 2010. The title of the paper is “Comparative Field Performance Using Asphalts from

Multiple Crude Oil Sources”, authored by P. Michael Harnsberger, Michael J. Farrar, Shin-Che Huang, and Raymond E. Robertson. Add this reference to TT1c also.

The ARC and Manitoba Infrastructure & Transportation collaborated to plan and construct two new comparative pavement performance sites in the province of Manitoba, Canada. One site was planned to use two different amounts of RAP and the second site was planned to use warm-mix additives. Construction on the RAP comparative pavement performance site began in late September and finished in early October. The RAP site is on provincial highway 8 about 10 km north of Gimli. The total project length is about 28 km (17 miles) but the ARC sections were placed in about 5 km (3.1 miles) of the project. The existing pavement was milled in the Fall of 2008 and stored for use this year.

The ARC sections at the RAP project were constructed using two 50 mm lifts with conventional hot-mix, 15% RAP, 50% RAP with no grade change for the new asphalt (150/200 pen), and 50% RAP with a grade change (200/300 pen). Over 400 5-gallon buckets, representing about 32,000 pounds, of construction material samples were obtained during construction. The samples were obtained for ARC research at the University of Nevada Reno, Western Research Institute, North Carolina State University, and for storage at the FHWA MRL in Sparks, Nevada. North Carolina State University will also use the samples for a separate contract between NCSU and FHWA.

After completion of construction, WRI personnel planned and established two 500 foot performance monitoring sections in each of the four different pavement sections. The eight monitoring sections will be used to acquire detailed performance monitoring data annually using LTPP protocols. Areas outside of the monitoring sections can be used to obtain core samples as the pavement ages in service.

The second comparative performance project site using warm-mix additives was begun in early October. The bottom 50 mm lift (of two total lifts) of one hot-mix control section and a section using Advera were constructed before adverse weather forced the project to be stopped for the winter. ARC representatives and Manitoba officials will have future discussions on the possible effects of the partial construction and on possible alternatives.

Significant Results

A new comparative pavement performance site using high RAP content, moderate RAP content, and conventional hot-mix was constructed in Manitoba, Canada. This site should provide valuable performance data, especially on the effect of RAP on low temperature properties.

Significant Problems, Issues and Potential Impact on Progress

Partial construction of the warm-mix site in Manitoba Canada was not as planned. The effect of the comparison of materials is to be determined.

Work Planned Next Quarter

It is planned to begin laboratory work on samples from the Manitoba RAP sections.

CATEGORY V2: ACCELERATED PAVEMENT TESTING

Work element V2a: Accelerated Pavement Testing including Scale Model Load Simulation on Small Test Track (Later start)

Work Done This Quarter

No activity this quarter.

Significant Results

None.

Significant Problems, Issues and Potential Impact on Progress

None.

Work Planned Next Quarter

No accelerated (field) testing is planned.

Work element V2b: Construction of Validation Sections at the Pecos Research & Testing Center (Later start)

This work element is included to indicate that this may be a possibility for accelerated pavement testing for ARC research because it is a facility in the TAMU system.

CATEGORY V3: R&D VALIDATION

Work element V3a: Continual Assessment of Specifications (UWM)

Work Done This Quarter

Cooperation with the Western Cooperative Testing Group (WCTG) for assessment of the binder testing procedures used by the group began, and a number of conference calls with the group's advisory board have taken place. Work this quarter focused on testing binders used in building pavements during this construction season. A standard binder test report was finalized that will

be used to compile test results from each sample. The testing battery includes conventional Superpave and PG Plus tests.

The University of Wisconsin–Madison received the first two binders from WCTG and began testing them in accordance with the WCTG binder test report. UW–Madison is scheduled to receive eight more binders—one per month—to be tested as part of WCTG’s round-robin testing program.

The long-term purpose of these tests is to establish a database that will allow for comparison between laboratory test results and results of pavement performance in the field. This information can then be used to determine which tests better predict actual field performance and are therefore more appropriate for use as a standard test.

Work also continued on development of the Single-Edge Notched Bending (SENB) testing system. Modifications were made on the loading rate and an independent cooling bath is nearly complete. The SENB was successfully used to test fracture properties of asphalt binders, and preliminary testing of asphalt mixtures was also performed.

Significant Results

The WCTG binder test report, shown in figures V3a.3 and V3a.4 at the end of this report, was finalized to include the following battery of standard Superpave tests:

- G^* and δ (AASHTO T315) at high PG on original binder.
- Rotational viscosity (AASHTO T316).
- Rolling thin film oven (RTFO) loss on heating (AASHTO T240).
- G^* and δ (AASHTO T315) at high PG on RTFO-aged binder.
- G^* and δ (AASHTO T315) at high PG -6 °C on RTFO-aged binder.
- G^* and δ (AASHTO T315) at 22 °C on pressure aging vessel (PAV)-aged binder.
- Bending Beam Rheometer (BBR) (AASHTO T313) one-hour conditioning.
- Direct tension (AASHTO T314).

In addition to the above tests, the binder test report includes the following PG Plus tests:

- Ductility (AASHTO T351) at 4 °C on original binder.
- Toughness and tenacity (ASTM D 5801) on original binder.
- Multiple Stress Creep and Recovery (MSCR) (ASTM D 7405) at high PG on RTFO-aged binder.
- MSCR (ASTM D 7405) at high PG -6 °C on RTFO-aged binder.
- Ductility (AASHTO T51) at 4 °C on RTFO-aged binder.
- BBR (AASHTO T313) 24-hour conditioning.

Testing of the first two WCTG round-robin samples is nearly complete using the above battery of tests.

The new SENB system detected the brittle transition behavior of asphalt binders at low temperatures. Figure V3a.1 shows a PG 64-22 binder that was tested at -6 °C, -12 °C and -18 °C. Results show a clear reduction in the ductility of the binder as the temperature decreases.

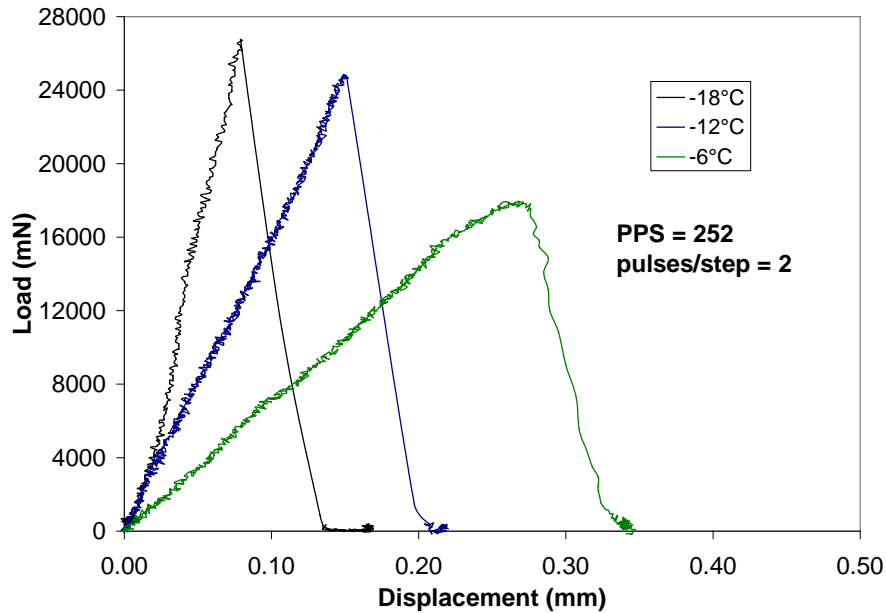


Figure V3a.1. Graph. SENB testing of asphalt binder PG 64-22 at three temperatures. (PPS = pulses per second.)

The SENB system was also used to test fracture properties of asphalt mixtures at low temperatures. Preliminary testing of mixtures containing granite and limestone was successful. Specimens were obtained by cutting BBR-sized specimens from slab-compacted samples. The results from these tests, shown in figure V3a.2, demonstrate a significant difference in the fracture properties of limestone mixtures versus granite mixtures.

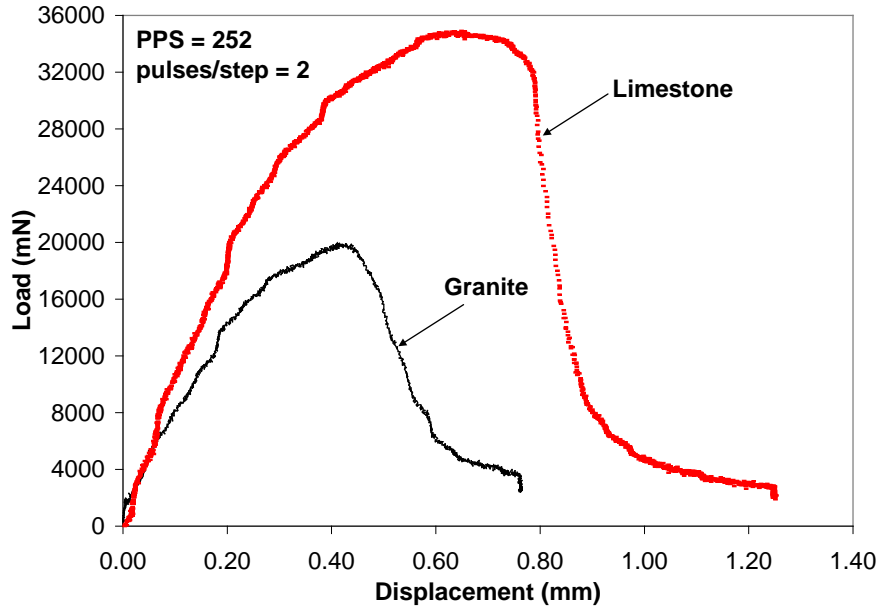


Figure V3a.2. Graph. SENB test for two asphalt mixtures.

Significant Problems, Issues and Potential Impact on Progress

None.

Work Planned Next Quarter

Round-robin testing will continue on specimens received from WCTG. Samples 508A (Mountain States), 509A (Terry Asphalt), and 510A (Valero) are scheduled to be tested next quarter.

Further work on the SENB system will be conducted to improve the testing system for mastics. The step motor does not provide enough torque to maintain a constant loading rate, so a change in geometry of the mastics samples will be investigated.

Test results from the BBR, the SENB, and the Asphalt Binder Cracking Device (ABCD) will be compared to determine which is most suitable as a new PG Plus test.

WESTERN COOPERATIVE TEST GROUP
PG BINDER TEST REPORT (Updated 8/15/2009)

Date Shipped: _____ Sample No.: _____ Results Due By: _____
 Grade: _____ Submitted By: _____
 Contact Name/Phone #: _____

TESTS ON ORIGINAL BINDER

Rotational Viscosity at 135°C @ 20 RPM (T316), (nearest 0.01 Pa-s)
 Note: 1 cP = 0.001 Pa-s
 Spindle # 21 Shear Rate 18.6 _____
 Rotational Viscosity at 135°C @ 1 RPM (T316), (nearest 0.01 Pa-s)
 Note: 1 cP = 0.001 Pa-s
 Spindle # 21 Shear Rate 0.93 _____

Dynamic Shear at High PG °C, 25 mm plate, 1 mm gap (T315)
 Complex Shear Modulus, G* (nearest 0.01 kPa) _____
 Phase Angle, δ (nearest 0.1 degree) _____
 G*/sinδ (nearest 0.01 kPa) _____
 Actual Stress _____ (kPa) or Strain ____ (%) level used

Ductility, **4.0°C** (39.2°F), 5cm/min, cm (T51) (nearest 0.1 cm) _____

Toughness, inch-lbs (nearest 0.1 inch-lbs) (D 5801) _____

Tenacity, inch-lbs (nearest 0.1 inch-lbs) (D 5801) _____

TESTS ON AGED MATERIAL, RTFO (T240)

Loss on heating (T240) (nearest 0.001%)
 RTFO Loss X Gain _____

Dynamic Shear at **High PG** °C, 25 mm plate, 1 mm gap (T315)
 Complex Shear Modulus, G* (nearest 0.01 kPa) _____
 Phase Angle, δ (nearest 0.1 degree) _____
 G*/sinδ (nearest 0.01 kPa) _____
 Actual Stress _____ (kPa) or Strain ____ (%) level used

MSCR, D 7405 : Test at High PG °C, 25 mm plate
 Creep Compliance, Jnr_3.2kPa (nearest 0.1) _____
 Percent difference in non-recoverable creep compliance
 ((Jnr3.2 - Jnr0.1)x 100)/Jnr0.1, nearest 1% _____
 Creep Compliance, Jnr_10kPa (nearest 0.1) (New Specimen) _____
 Average percent recovery @ 0.1 kPa (nearest 0.1%) _____
 Average percent recovery @ 3.2 kPa (nearest 0.1%) _____
 Average percent recovery @ 10 kPa (nearest 0.1%) (New Specimen) _____

Dynamic Shear at **High PG-6** °C, 25 mm plate, 1 mm gap (T315)
 Complex Shear Modulus, G* (nearest 0.01 kPa) _____
 Phase Angle, δ (nearest 0.1 degree) _____
 G*/sinδ (nearest 0.01 kPa) _____
 Actual Stress _____ (kPa) or Strain ____ (%) level used

Company / Lab: _____

Figure V3a.3. Form. WCTG test report, page 1.

WESTERN COOPERATIVE TEST GROUP

Page 2:

Sample No.: _____

Grade: _____

MSCR, D 7405 : Test at **High PG -6** °C, 25 mm plate
Creep Compliance, Jnr_3.2kPa (nearest 0.1) _____
Percent difference in non-recoverable creep compliance _____
((Jnr3.2 - Jnr0.1)x 100)/Jnr0.1, nearest 1% _____
Creep Compliance, Jnr_10kPa (nearest 0.1) (New Specimen) _____
Average percent recovery @ 0.1 kPa (nearest 0.1%) _____
Average percent recovery @ 3.2 kPa (nearest 0.1%) _____
Average percent recovery @ 10 kPa (nearest 0.1%) (New Specimen) _____

Ductility, 4.0°C (39.2°F), 5cm/min, cm (T51) (nearst 0.1 cm) _____

Elongation Recovery, % (25°C)(T301) _____

TESTS ON PAV RESIDUE (R28) - PAV AT 100 °C

Dynamic Shear at **22** °C, 8 mm plate, 2 mm gap (T315)
Complex Shear Modulus, G* (nearest kPa) _____
Phase Angle, δ (nearest 0.1 degree) _____
G*.sinδ (nearest kPa) _____
Actual Stress _____ (kPa) or Strain ____ (%) level used _____

BBR: 1hour conditioning (T313)

BBR Creep Stiffness at **Low PG +10** _____ °C, 60 s, (MPa, 3 significant figures) _____
BBR Slope, m-value, at **Low PG +10** _____ °C, 60 s, (nearest 0.001) _____

BBR: 24hour conditioning (T313)

BBR Creep Stiffness at **Low PG +10** _____ °C, 60 s, (MPa, 3 significant figures) _____
BBR Slope, m-value, at **Low PG +10** _____ °C, 60 s, (nearest 0.001) _____

Direct Tension (T314)

DT Failure Stress , at **Low PG +10** _____ °C, 1 mm/min. (T314), (nearest 0.01 MPa) _____
DT Failure Strain, at **Low PG +10** _____ °C, 1 mm/min. (T314), (nearest 0.01%) _____

Tested by: _____
Reported by: _____

Company / Lab: _____
Phone #: _____

Submit to: Carol Crawford W.C.T.G.
Wyoming Department of Transportation
PO Box 1708, Cheyenne, Wyoming 82003-1708

PHONE (307) 777-4076
FAX (307) 777-4481

Figure V3a.4. Form. WCTG test report, page 2.

Work element V3b: Validation of the MEPDG Asphalt Materials Models Using New MEPDG Sites and Selected LTPP Sites (UNR, UWM)

Subtask V3b-1: Design and Build Sections (Start Year 1, Year 2, and Year 3)

Work Done This Quarter

None.

Significant Results

None.

Significant Problems, Issues and Potential Impact on Progress

Only three agencies have committed to the construction of MEPDG sites: the Washoe RTC in northern Nevada in 2008, The South Dakota DOT in 2009/2010, and the Wisconsin DOT in 2009. The researchers are facing significant hesitation from the DOTs to use the MEPDG to design and construct HMA pavements. The level of this work element may have to be reduced.

Work Planned Next Quarter

Continue discussions with the states to select field sections for the MEPDG validation sites.

Subtask V3b-2: Additional Testing (Start Year 2, Year 3, and Year 4)

Work Done This Quarter

This work element is to provide additional testing for states (or others) that commit to MEPDG validation sites.

Significant Results

None.

Work Planned Next Quarter

None planned at this time.

Subtask V3b-3: Select LTPP Sections (Start Year 1 thru Year 5)

Work Done This Quarter

The research group focused on continuing Binder Yield Energy Test (BYET) testing of the LTPP binders listed in table V3b-3.1. Selected materials were sent to Turner-Fairbank Highway Research Center (TFHRC) for evaluation using the Double-Edge Notched Tension (DENT) test. Plans for the testing the binders using the Linear Amplitude Sweep test discussed in work element F2e have been developed.

Table V3b-3.1. LTPP binders used for validation of new binder testing procedures.

SHRP ID	PG High Temperature [°C]	PG Low Temperature [-°C]	Climate	Fatigue Cracking (m²)
04-B901	76	10	DN	328
09-0902	64	28	WF	0
09-0961	58	34	WF	2.1
34-0901	64	22	WF	49.5
34-0961	78	28	WF	178.8
35-0902	64	22	DN	32
37-0962	76	22	WN	0
89-A902	52	40	WN	6.7

DN = dry and no freeze. WF = wet and freeze. WN = wet and no freeze.

Significant Results

Preliminary results presented in figure V3b-3.1 indicate a fairly good correlation between the yield energy (YE) obtained from the BYET test and the fatigue performance of the pavements. The full set of LTPP binders needs to be tested to draw conclusions about the correlation of the BYET test and pavement performance. As it is observed in figure V3b-3.1, there are two apparent outliers in the data set. However, a statistical analysis of the complete experimental plan needs to be performed to determine if those points are outliers.

Significant Problems, Issues and Potential Impact on Progress

None.

Work Planned Next Quarter

The research group plans to finish the testing of the LTPP binders listed in table V3b-3.1 using the BYET and amplitude sweep procedures. Experimental results from the DENT tests performed at TFHRC are expected to be completed.

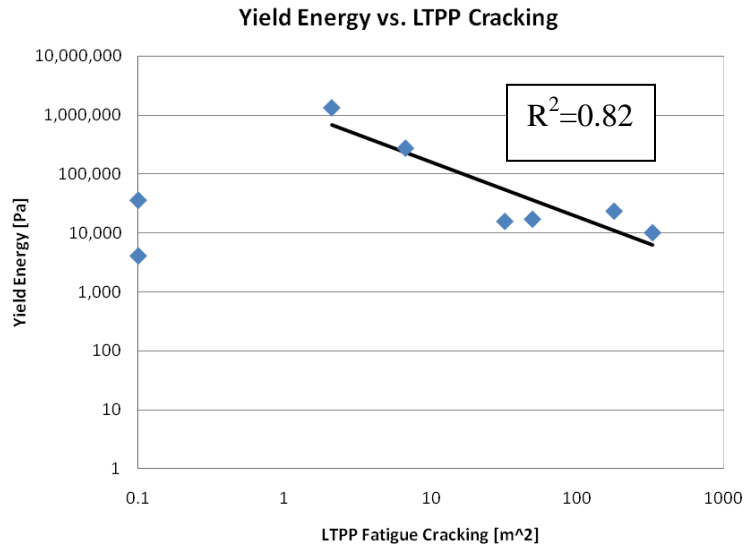


Figure V3b-3.1. Graph. Comparison between fatigue performance and YE from BYET test of LTPP binders.

Subtask V3b-4: Testing of Extracted Binders from LTPP Sections (Start Year 1)

Work Done This Quarter

No work planned.

Subtask V3b-5: Review and Revisions of Materials Models (Start Year 2, Year 3, Year 4, and Year 5)

Work Done This Quarter

No work planned.

Subtask V3b-6: Evaluate the Impact of Moisture and Aging (Start Year 3, Year 4, and Year 5)

No activity to date.

Validation Year 3	Year 3 (4/2009-3/2010)												Team
	4	5	6	7	8	9	10	11	12	1	2	3	
(1) Field Validation													
V1a: Use and Monitoring of Warm Mix Asphalt Sections													WRI
V1b: Construction and Monitoring of additional Comparative Pavement Validation sites													WRI
(2) Accelerated Pavement Testing													
V2a: Accelerated Pavement Testing including Scale Model Load Simulation on small test track (This work element will include all accelerated pavement testing)													WRI
V2b: Construction of validation sections at the Pecos Research & Testing Center													WRI
(3) R&D Validation													
V3a: Continual Assessment of Specification													UWM
V3a-1: Evaluation of the PG-Plus practices and the motivations for selecting the "plus" tests.													
V3a-2: Detailed analysis of all PG-Plus tests being proposed or in use today, documentation of benefits and costs of these tests, and comparison with new tests			D										
V3a-3: Development of protocols for new binder tests and database for properties measured					JP								
V3a-4: Development of specification criteria for new tests based on field evaluation of construction and performance						D					P		
V3a-5: Interviews and surveys for soliciting feedback on binder tests and specifications													
V3b: Validation of the MEPDG Asphalt Materials Models and Early Verification of Technologies Developed by ARC using new MEPDG Sites and Selected LTPP sites													UNR/UWM/WRI
V3b-1: Design and Build Sections													UNR
V3b-2: Additional Testing (if needed)													
V3b-3: Select LTPP Sites to Validate New Binder Testing Procedures							DP				P		UWM
V3b-4: Testing of Extracted Binders from LTPP Sections													
V3b-5: Review and Revisions of Materials Models													
V3b-6: Evaluate the Impact of Moisture and Aging													

Deliverable codes

- D: Draft Report
- F: Final Report
- M&A: Model and algorithm
- SW: Software
- JP: Journal paper
- P: Presentation
- DP: Decision Point

Deliverable Description

- Report delivered to FHWA for 3 week review period.
- Final report delivered in compliance with FHWA publication standards
- Mathematical model and sample code
- Executable software, code and user manual
- Paper submitted to conference or journal
- Presentation for symposium, conference or other
- Time to make a decision on two parallel paths as to which is most promising to follow through

-  Work planned
-  Work completed
-  Parallel topic

Validation Years 2 - 5	Year 2 (4/08-3/09)				Year 3 (4/09-3/10)				Year 4 (04/10-03/11)				Year 5 (04/11-03/12)				Team
	Q1	Q2	Q3	Q4	Q1	Q2	Q3	Q4	Q1	Q2	Q3	Q4	Q1	Q2	Q3	Q4	
(1) Field Validation																	
V1a: Use and Monitoring of Warm Mix Asphalt Sections																	WRI
V1b: Construction and Monitoring of additional Comparative Pavement Validation sites																	WRI
(2) Accelerated Pavement Testing																	
V2a: Accelerated Pavement Testing including Scale Model Load Simulation on small test track																	WRI
V2b: Construction of validation sections at the Pecos Research & Testing Center																	WRI
(3) R&D Validation																	
V3a: Continual Assessment of Specification																	UWM
V3a-1: Evaluation of the PG-Plus practices and the motivations for selecting the "plus" tests.		P	D,F														
V3a-2: Detailed analysis of all PG-Plus tests being proposed or in use today, documentation of benefits and costs of these tests, and comparison with new tests				P	D												
V3a-3: Development of protocols for new binder tests and database for properties measured						JP			P								
V3a-4: Development of specification criteria for new tests based on field evaluation of construction and performance					D		P	P			JP	P		JP			
V3a-5: Interviews and surveys for soliciting feedback on binder tests and specifications								P		JP		P		D	F		
V3b: Validation of the MEPDG Asphalt Materials Models and Early Verification of Technologies Developed by ARC using new MEPDG Sites and Selected LTPP sites																	UNR/UWM
V3b-1: Design and Build Sections									D, F								
V3b-2: Additional Testing (if needed)																	
V3b-3: Select LTPP Sites to Validate New Binder Testing Procedures						DP		P		JP		P			D	F	
V3b-4: Testing of Extracted Binders from LTPP Sections																	
V3b-5: Review and Revisions of Materials Models																D, F	
V3b-6: Evaluate the Impact of Moisture and Aging																D, F	

Deliverable codes

D: Draft Report
 F: Final Report
 M&A: Model and algorithm
 SW: Software
 JP: Journal paper
 P: Presentation
 DP: Decision Point

Deliverable Description

Report delivered to FHWA for 3 week review period.
 Final report delivered in compliance with FHWA publication standards
 Mathematical model and sample code
 Executable software, code and user manual
 Paper submitted to conference or journal
 Presentation for symposium, conference or other
 Time to make a decision on two parallel paths as to which is most promising to follow through

 Work planned
 Work completed
 Parallel topic

PROGRAM AREA: TECHNOLOGY DEVELOPMENT

Work element TD1: Prioritize and Select Products for Early Development (Year 1)

Work Done This Quarter

None. This work element has been completed.

Significant Results

Six early technology development projects have been identified and all have received favorable ratings from the ETGs.

Work element TD2: Develop Early Products (Year 3)

Work Done This Quarter

AAT has not yet received the final version of the uniaxial fatigue test software for the AMPT from Interlaken Technology Corporation (ITC), although ITC has assured AAT that the software is very near completion. Uniaxial fatigue testing to further refine the CD-RC/EL model cannot take place until this software is in place and fully functional.

Significant Results

As discussed in the progress report for work element E2e, additional refinements in the continuum damage-reduced cycles/endurance limit fatigue model have been made which potentially will allow implementation of a simplified approach to continuum damage fatigue analysis in layered elastic pavement design software.

Significant Problems, Issues and Potential Impact on Progress

None.

Work Planned Next Quarter

The test method and equipment will be applied to fatigue data from several mixtures. A ruggedness testing plan for the simplified continuum damage fatigue test will be developed.

Work element TD3: Identify Products for Mid-Term and Long-Term Development (Years 2, 3, and 4)

Work Done This Quarter

The research team continued to review interim research products to identify potential mid-term and long-term development projects.

Significant Results

None.

Significant Problems, Issues and Potential Impact on Progress

The research team with continue to review interim research products to identify potential mid-term and long-term development projects.

Work Planned Next Quarter

The research team with continue to review interim research products to identify potential mid-term and long-term development projects.

Work Element TD4: Develop Mid-Term and Long-Term Products (Years 3, 4, and 5)

This activity is planned for later in the project.

PROGRAM AREA: TECHNOLOGY TRANSFER

CATEGORY TT1: OUTREACH AND DATABASES

Work element TT1a: Development and Maintenance of Consortium Website (Duration: Year 1 through Year 5)

Work Done This Quarter

The ARC website was maintained and updated. The ARC quarterly technical progress report, Apr 1- Jun 30, was uploaded to the ARC website.

Significant Results

None

Significant Problems, Issues and Potential Impact on Progress

None

Work Planned Next Quarter

Continue maintaining and updating the ARC website.

Work element TT1b: Communications (Duration: Year 1 through Year 5)

Work Done This Quarter

The fifth ARC Newsletter was published in September 2009.

Significant Results

None

Significant Problems, Issues and Potential Impact on Progress

None

Work Planned Next Quarter

None

Work element TT1c: Prepare Presentations and Publications

Presentations

Greenfield, M. L., Petersen Conference (Laramie, WY; July 2009): fundamental approaches to rheology modeling and its connections to chemo-mechanics.

Greenfield, M. L., Models ETG meeting (San Antonio; September 2009): molecular contributions to chemo-mechanical properties of asphalts (presentation specifically requested by ETG).

Greenfield, M. L., International Workshop on Chemo-Mechanics (Delft, the Netherlands; June 2009 in prior quarter): molecular contributions to chemo-mechanical properties of asphalts (*costs not charged to this project*).

Greenfield, M. L., Thermodynamics 2009 (London, UK; September 2009): contributions of individual molecules to overall asphalt relaxation and viscosity (*costs not charged to this project*).

Mahmoud, E., and H. U. Bahia, "Mixture Design to Enhance Safety and Reduce Noise of HMA," Modeling Expert Task Group, San Antonio, Texas, September 18, 2009.

Miller, T., "Engineering Sustainable Asphalt Pavements," American Society of Civil Engineers, Wisconsin Section Meeting, Oconomowoc, Wisconsin, September 11, 2009.

Pauli, Troy, and James Beiswenger, "ASTM D 4124-09: Standard Test Method for Separation of Asphalt into Four Fractions" presented at the Binder Expert Task Group Meeting, San Antonio, TX, September 16, 2009.

Pauli, Troy, A. Beemer, J. Miller, W. Grimes, J. Beiswenger, and J. F. Branthaver, "Physical Chemistry of Asphalt" presented at the Models Expert Task Group, September 17, 2009, NuStar, San Antonio, TX.

Prapaitrakul, Nikornpon, Rongbin Han, Xin Jin, and Charles J. Glover. "Transport Model Calculations of Asphalt Binder Oxidation in Pavements," presented at the 46th Annual Petersen Asphalt Research Conference, Laramie, Wyoming, July 14, 2009.

Prapaitrakul, Nikornpon, Rongbin Han, Xin Jin, and Charles J. Glover, "A Transport Model of Asphalt Binder Oxidation in Pavements," presented at the 3rd International Conference on Asphalt Materials, Qingdao, Shandong Province, China, August 6, 2009.

Publications

Arega, Z., Miller, T., and H. U. Bahia, 2009, "Correlating Rheological Properties of Emulsion Residue to Early Chip Seal Performance." *Transportation Research Board 89th Annual Meeting*, submitted.

Caro, S., E. Masad, A. Bhasin, D. Little, and M. Sanchez-Silva, 2009a, Probabilistic Modeling of the Effect of Air Voids on the Mechanical Performance of Asphalt Mixtures Subjected to Moisture Diffusion. *Journal of the Association of Asphalt Paving Technologists (AAPT)* (submitted for evaluation).

Caro, S., E. Masad, M. Sanchez-Silva, and D. Little, 2009b, Stochastic Micromechanical Modeling of Asphalt Mixtures Subjected to Moisture Diffusion Processes. *The International Journal for Numerical and Analytical Methods in Geomechanics* (submitted for evaluation).

Darabi, M., R. Abu Al-Rub, E. Masad, C. W. Huang, and D. Little, 2009, A Thermo-Viscoelastic-Viscoplastic-Viscodamage Constitutive Model for Asphaltic Materials. *International Journal of Solids and Structures* (In Review).

Greenfield, M. L., 2009, Bitumen at the Molecular Level: Molecular Simulations and Chemo-Mechanics, submitted to *Proceedings: International Workshop on Chemo-Mechanics of Bituminous Materials*, Delft, the Netherlands.

Hanz, A., Arega, Z., and H. U. Bahia, 2009, "Rheological Behavior of Emulsion Residues Produced by an Evaporative Recovery Method." *Transportation Research Board 89th Annual Meeting*, submitted.

Harnsberger, P. Michael, Michael J. Farrar, Shin-Che Huang, and Raymond E. Robertson. "Comparative Field Performance Using Asphalts from Multiple Crude Oil Sources," prepared and submitted to *Road Materials and Pavement Design* for possible acceptance to the European Asphalt Technology Association meeting in Parma, Italy in June 2010.

Huang, C. W., R. Abu Al-Rub, E. Masad, and D. Little, 2009, Three-Dimensional Simulations of Asphalt Pavement Permanent Deformation Using a Nonlinear Viscoelastic and Viscoplastic Model. *Journal of Materials in Civil Engineering*, ASCE (Accepted for Publication).

Luo, R., and R.L. Lytton, 2009, Characterization of the Tensile Viscoelastic Properties of an Undamaged Asphalt Mixture. *Journal of Transportation Engineering, American Society of Civil Engineers (ASCE)*, Accepted for Publication.

Masad, E., J. Howson, A. Bhasin, S. Caro, and D. Little, 2009, Relationship of Ideal Work of Fracture to Practical Work of Fracture: Background and Experimental Results. *Journal of the Association of Asphalt Paving Technologists (AAPT)* (submitted for evaluation).

Miller, T., and H. U. Bahia, 2009, "Establishing a Framework for Analyzing Asphalt Pavement Sustainability." *Enviroad 2009 Conference*, accepted.

Prapaitrakul, Nikornpon, Rongbin Han, and Charles J. Glover, 2009, A Transport Model of Asphalt Binder Oxidation in Pavements. *Road Materials and Pavement Design*, 10 (Special Issue): 95-113.

Rongbin Han, Xin Jin, and Charles J. Glover. "Modeling Pavement Temperature for Use in Binder Oxidation Models and Pavement Performance Prediction," submitted July 2009 to *Journal of Materials in Civil Engineering*.

Zhang, Y., R. Luo, and R.L. Lytton, 2009, Anisotropic Viscoelastic Properties of Undamaged Asphalt Mixtures under Compressive Loading. *Journal of Transportation Engineering, American Society of Civil Engineers (ASCE)*, Submitted for review.

Work element TT1d: Development of Materials Database (Duration: Year 2 through Year 5)

Work Done This Quarter

Development continued on the ARC database project this quarter. The version of SQL Server was upgraded from SQL Server 2005 to SQL Server 2008 because of significant performance improvements. Development and testing of the database also continued this quarter. Several new forms have been added to manage validation sections, perform user and role management, and upload and download files.

Significant Results

Development and testing continued on the Material Editing Form, Material Browser form, and Material Properties form. The interface for entering property measurements has been implemented. This includes automatic validation features using min/max and valid value lists created by users for each property. Validation values can be overridden, if necessary.

The database has been expanded to provide a detailed record of validation section information and field samples, linking them with the existing materials and properties. Material properties can now be assigned field measurements in addition to lab measurements. Field measurements can record information about the core or slab sample, along with the location and layer of the material. A prototype form has been created to manage validation sections as shown in Figure TT1d.1.

The database now has the ability to search and filter both laboratory and field measurement records by numerous factors, such as validation section, field sample, date of record, standard procedure, user who entered record, and the organization of the user. The user interface for these features is currently being implemented. Factors can be applied in any combination. Ability to view records created by all users can be modified based on access level of requester.

A role-based security system has been implemented and testing is underway. The following five roles have been defined.

- Administrator – Administrative users will have full access to the system. Administrative users are allowed to add new users and assign access rights to those users.
- FullAccess – FullAccess users are allowed to use all parts of the system with the exception of user management and role management.

- ConsortiumAccess – ConsortiumAccess users can view all data stored in the system. ConsortiumAccess users can change data as designated by the project coordinator.
- LimitedAccess – LimitedAccess users can view all data but cannot make changes to that data.
- AnonymousAccess – Anonymous access users can view limited data as designated by the project coordinator.

The user interface for role management has been completed and appears in figure TT1d2.

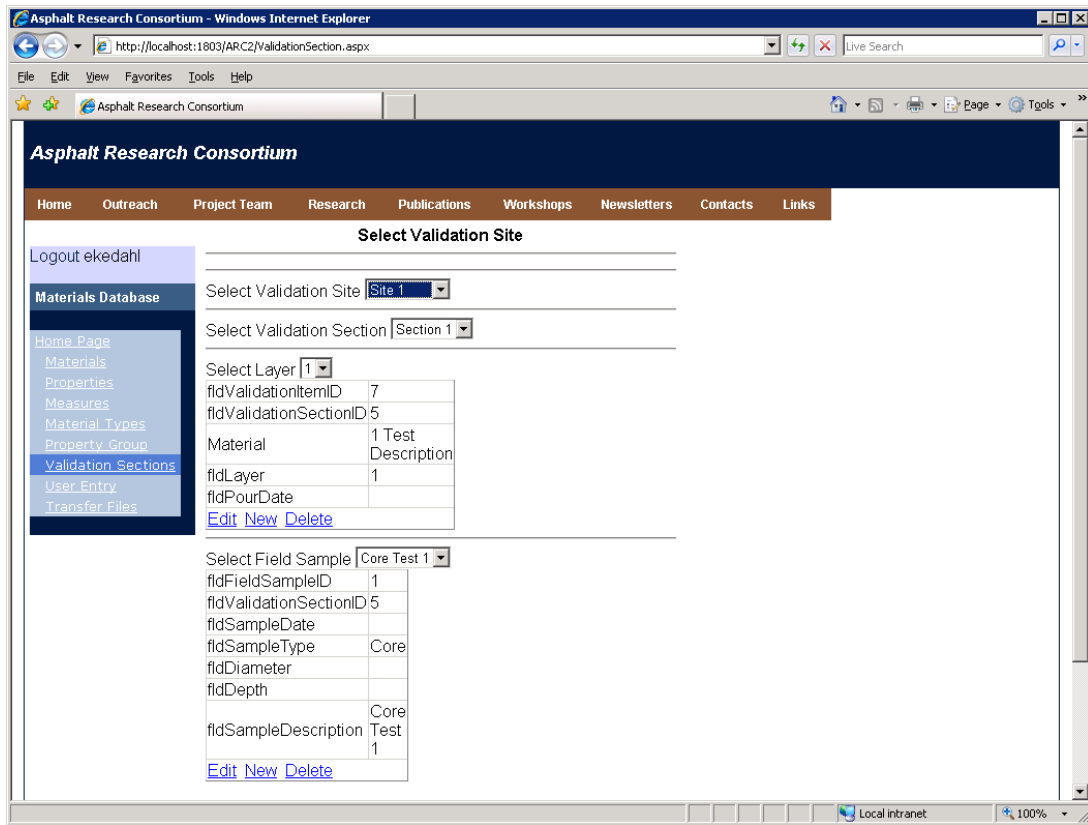


Figure TT1d.1. Validation Site form.

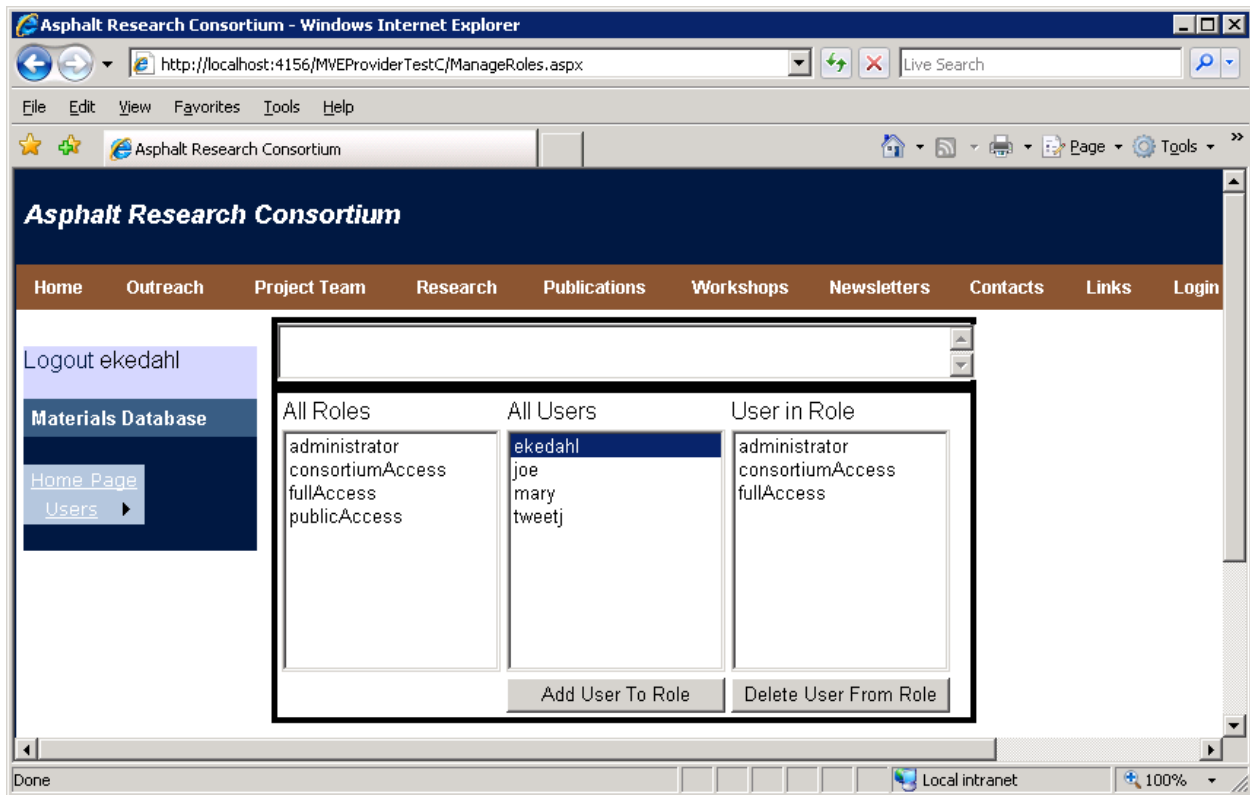


Figure TT1d.2. Role Management Form

An authentication database has been created to store user information. The authentication database has the following characteristics:

- Passwords are stored in the database using a 1-way hash for additional security.
- The authentication database has a failed attempt counter. Accounts are locked after three failed login attempts. Only users in the Administrator role can unlock a locked account.
- Strong passwords are enforced
- All authenticated users can change their passwords and password question and answer.
- Users designated as Administrator can create new users and assign roles to users.

Figure TT1d.3 shows the form to add, change, and delete users. Finally, authenticated users can update their own personal information as shown in Figure TT1d.4.

A prototype system to upload and download research reports and other files has been completed. Authenticated users can upload files from to the ARC database and download files to their home computer. Figure TT1d.5 shows the Upload / Download form.

Asphalt Research Consortium - Windows Internet Explorer

http://localhost:4156/MVEProviderTestC/ManageUsers.aspx

File Edit View Favorites Tools Help

Asphalt Research Consortium

Asphalt Research Consortium

Home Outreach Project Team Research Publications Workshops Newsletters Contacts Links Login

Logout ekedahl

Materials Database

Home Page

Users

MESSAGES

Username found.

USER INFORMATION

User Name (Login):

E-Mail:

Password: Confirm Password:

Password Question:

Password Answer:

PERSONAL INFORMATION

Account Approved User is Online Account Locked

Comment:

Title: First Name:

Last Name:

Address: City:

State: Zip Code:

Telephone: Extension:

Cell Phone:

HISTORY

Last Activity: Last Login:

Password Changed: Creation Date:

Last Locked Out Date:

Failed PW Count: Failed PW Window:

Failed PW Ans Count: Failed PW Ans Start:

Notes:

Local intranet 100%

Figure TT1d.3. Add / Change / Delete user form.

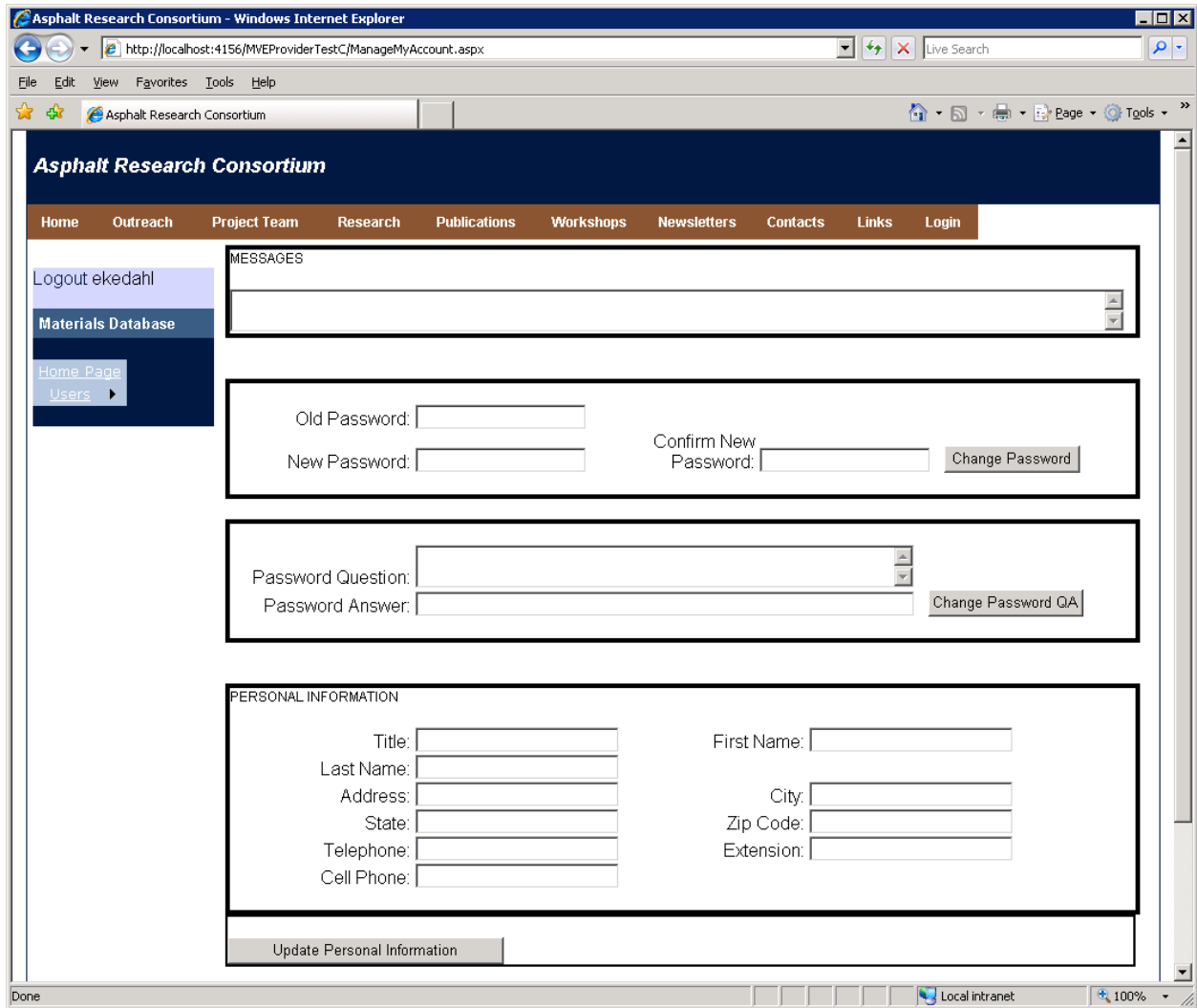


Figure TT1d.4. Update User Information form.

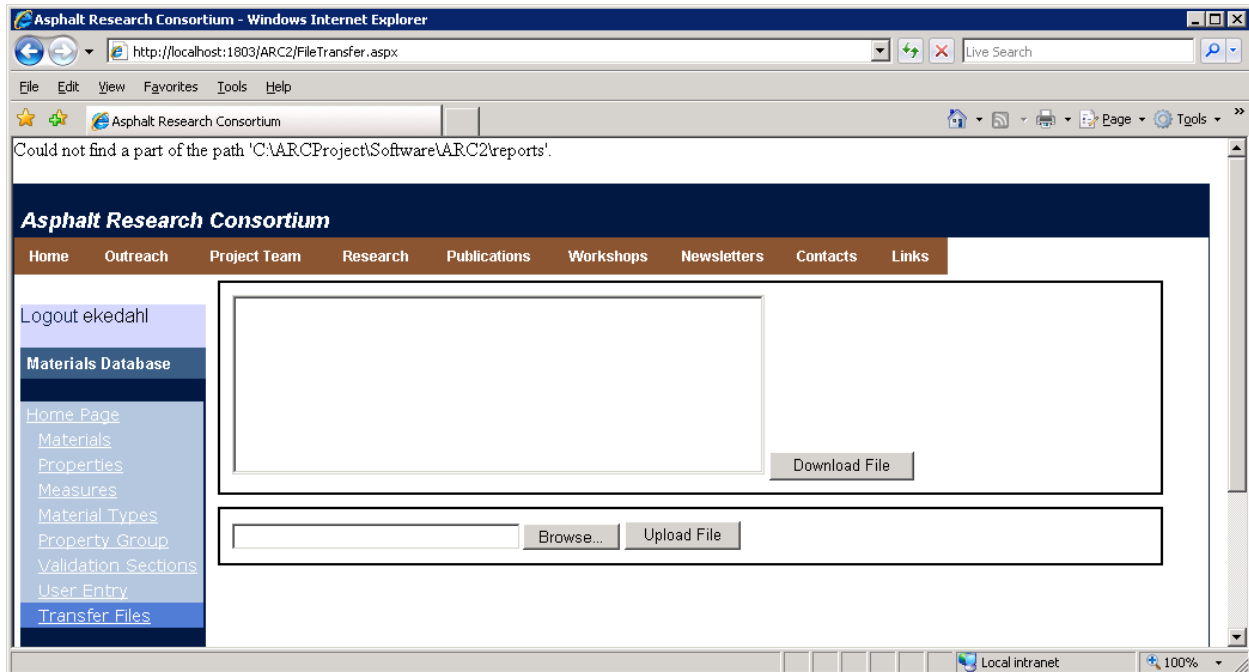


Figure TT1d.5. Upload / Download form.

Significant Problems, Issues and Potential Impact on Progress

None

Work Planned Next Quarter

- Continued development of property measurement interface.
- Creation of the framework and user interface to enter material source records.
- Creation of a graphical navigator for validation second grid to aid visualization and ease of use.
- Using the role-based infrastructure already created, restrict access to specific forms and functions as defined by the project coordinator.
- Complete transactional logging system.

Work element TT1e: Development of Research Database (Duration: Year 2 through Year 5)

Work Done This Quarter

Uploaded the quarterly technical progress report to the ARC website.

Significant Results

None

Significant Problems, Issues and Potential Impact on Progress

None

Work Planned Next Quarter

Upload the ARC quarterly technical progress report to the ARC website.

Work Element TT1f: Workshops and Training

Work Done This Quarter

No activity this quarter.

Significant Results

None

Significant Problems, Issues and Potential Impact on Progress

None

Work Planned Next Quarter

No activities are planned for the next quarter.

Technology Transfer Year 3	Year 3 (4/2009-3/2010)												Team	
	4	5	6	7	8	9	10	11	12	1	2	3		
(1) Outreach and Databases														
TT1a: Development and Maintenance of Consortium Website														UNR
TT1b: Communications														UNR
TT1c: Prepare presentations and publications														UNR
TT1d: Development of Materials Database														UNR
TT1d-1: Identify the overall Features of the Web Application														
TT1d-2: Identify Materials Properties to Include in the Materials Database														
TT1d-3: Define the Structure of the Database														
TT1d-4: Create and Populate the Database									SW, v. β			SW		
TT1e: Development of Research Database														UNR
TT1e-1: Identify the Information to Include in the Research Database														
TT1e-2: Define the Structure of the Database														
TT1e-3: Create and Populate the Database														
TT1f: Workshops and Training														UNR

Deliverable codes

- D: Draft Report
- F: Final Report
- M&A: Model and algorithm
- SW: Software
- JP: Journal paper
- P: Presentation
- DP: Decision Point

Deliverable Description

- Report delivered to FHWA for 3 week review period.
- Final report delivered in compliance with FHWA publication standards
- Mathematical model and sample code
- Executable software, code and user manual
- Paper submitted to conference or journal
- Presentation for symposium, conference or other
- Time to make a decision on two parallel paths as to which is most promising to follow through

 Work planned
 Work completed
 Parallel topic

Technology Transfer Years 2 - 5	Year 2 (4/08-3/09)				Year 3 (4/09-3/10)				Year 4 (04/10-03/11)				Year 5 (04/11-03/12)				Team
	Q1	Q2	Q3	Q4	Q1	Q2	Q3	Q4	Q1	Q2	Q3	Q4	Q1	Q2	Q3	Q4	
(1) Outreach and Databases																	
TT1a: Development and Maintenance of Consortium Website																	UNR
TT1b: Communications																	UNR
TT1c: Prepare presentations and publications																	ALL
TT1d: Development of Materials Database																	UNR
TT1d-1: Identify the overall Features of the Web Application																	
TT1d-2: Identify Materials Properties to Include in the Materials Database																	
TT1d-3: Define the Structure of the Database																	
TT1d-4: Create and Populate the Database								SW, v. β	SW								
TT1e: Development of Research Database																	UNR
TT1e-1: Identify the Information to Include in the Research Database																	
TT1e-2: Define the Structure of the Database																	
TT1e-3: Create and Populate the Database																	
TT1f: Workshops and Training																	UNR

Deliverable codes

D: Draft Report
 F: Final Report
 M&A: Model and algorithm
 SW: Software
 JP: Journal paper
 P: Presentation
 DP: Decision Point

Deliverable Description

Report delivered to FHWA for 3 week review period.
 Final report delivered in compliance with FHWA publication standards
 Mathematical model and sample code
 Executable software, code and user manual
 Paper submitted to conference or journal
 Presentation for symposium, conference or other
 Time to make a decision on two parallel paths as to which is most promising to follow through

 Work planned
 Work completed
 Parallel topic